DURBAN UNIVERSITY OF TECHNOLOGY
INYUVESI YASETHEKWINI YEZOBUCHWEPHESHE

Microalgae Growth in Industrial Wastewater for the Production of Hydrocarbons

Submitted in fulfilment of the requirements for the degree of Doctor of Engineering: Chemical Engineering in the Faculty of Engineering and the Built Environment (FEBE) at the Durban University of Technology

Donald Tyoker Kukwa

Supervisor: Prof. Manimagalay Chetty

2025

DECLARATION

I confirm that this thesis is composed of my original work and contains no material previously submitted to the Durban University of Technology or any other institution for academic qualifications. The content of the thesis consists of work I have carried out since the commencement of my PhD research. All information utilised and their sources have been duly acknowledged.

Signature: **Date:** 07 February 2025

Donald Tyoker Kukwa

ABSTRACT

Microalgae have demonstrated unique abilities to photosynthesise the conversion of biodegradable organic materials and inorganic carbon to value-added biomass because dissolved nitrogen and reactive phosphate are present in the cultivation medium. The absence of a breakthrough in biomass production that would enable it to meet and exceed the existing fossil energy demand has elicited research into technologies and protocols that would yield competing energy output. The financial and energy implications associated with the technology employed for biomass harvesting would significantly contribute to the overall cost of the process. Would the microalgae strains that exhibit high growth rates and lipid content, as well as accommodate culture conditions, enhance biomass and lipid productivity?

The goal of this study was to provide microalgae with nutrients from industrial wastewater while also producing hydrocarbon compounds that could have positive social effects. A tailored airlift-raceway photobioreactor was utilised to grow microalgae in industrial wastewater after the wastewater was characterised and the optimum conditions for microalgae development were investigated. The resulting production of hydrocarbon derivatives was optimised. Wastewater from the sugar refinery, brewing industry, and dairy industry was characterised by its physical, chemical, mineral, and biological properties using conventional methods. The different industrial wastewater sources were tested for microalgal growth rate and biomass output. The generated biomass was assayed for carbohydrates, lipids, and protein contents of the microalgae strains, and the wastewater that gave the highest biomass and lipid yields was used for advanced cultivation techniques. After careful consideration, the brewery wastewater was found to be the most effective wastewater

for microalgae growth and was thus selected for this investigation. Using a novel airlift-raceway photobioreactor system, *Scenedesmus sp.* biomass was produced in brewery wastewater using optimised conditions. Also, the biomass of a microalgae consortium, native to Durban, South Africa, was produced, leading to hydrocarbons and hydrocarbon derivatives using nutrient-enriched brewery wastewater.

This study investigated these capabilities to sequester heavy metals and other pollutants from brewery wastewater and sparged carbon dioxide gas. The light was sourced from 40 W fluorescent tubes, which were powered by a 210 V supply and used at different electromagnetic frequencies ranging from red to blue in a novel airlift-raceway system for microalgae cultivation. The microalgal biomass, which was harvested by filtration, was freeze-dried and the surface morphology was analysed using the scanning electron microscope (SEM). The microalgal lipid was extracted with a hexane-methanol solvent system by the soxhlet technique. The morphology of the extracted biomass was analysed using SEM, and the composition of the microalgae oil was analysed using gas chromatography-mass spectrometry (GC-MS).

Investigations revealed that the sugar wastewater (SWW) used did not support microalgal growth. However, dairy wastewater (DWW) only supported microalgal growth to some extent, while brewery wastewater (BWW) was best suited for the growth of *Scenedesmus sp.* and the microalgae consortium. The BWW was nutrients enriched through the oxidation pond, thus raising the influent NO_3^--N (4.98±0.13 mg/L), PO_4^{3-} (13.34±0.48), BOD (35±19), and COD (3979±3) to NO_3^--N (15.98±0.91), PO_4^{3-} (39.93±1.83), BOD (279±10), and COD (5855±4), respectively. GC-MS analysis of the oil extract of the microalgae biomass showed the presence of saturated, monounsaturated (MU), and polyunsaturated (PU) fatty acids in both *Scenedesmus sp.* and the microalgae consortium, and the presence of an isolated C_4

and C_8-C_{38} hydrocarbons and hydrocarbon derivatives, mostly fatty acid esters, in the microalgal oils.

Nutrient enrichment of the brewery wastewater enables microalgal growth sustainably, thus encouraging lipid accumulation. Using the novel airlift-raceway photobioreactor in this study changed the mass transfer dynamics due to the enhanced hydrodynamics of the novel reactor. Because of this, it was simpler for light and nutrients to reach every area equitably, which is what propels the formation of biomass. The dominance of fatty acid esters in the microalgal oil demonstrates that the protocols adopted in this study can serve to save on the cost of the transesterification step in the production of biodiesel and other useful bio-products. This serves as a major contribution to the body of knowledge on this subject.

DEDICATION

To my wife, Erdoo

ACKNOWLEDGEMENTS

First, I thank the Department of Higher Education (DHE), South Africa, and the Durban University of Technology for their financial contributions to this program. I would also like to express my gratitude to the Department of Biotechnology and the Institute of Water and Wastewater Technology (IWWT) for providing the framework for my initial training and laboratory investigation execution. These short certificate courses gave me the confidence I needed to approach the research. This program offered me the opportunity to attend courses, conferences, workshops, seminars, retreats and visit several wonderful locations across South Africa and Europe, and most importantly, meet fellow researchers, research Scientists, and Engineers.

I thank my supervisor, Prof. Maggie Chetty, not only for building the career-transforming Research Team but also for her focused guidance during the development of this research. Her support and trust gave me the confidence with which I approached the challenges as they emerged during the program. I appreciate Prof Yusuf Makarfi Isa, who was my Head of Department for most of this program, for the financial and moral support interventions at times of need.

I owe everything I've accomplished in my life to God Almighty and my family. I am grateful to my beautiful, loving, and lovely wife, Dr Rose Erdoo Kukwa, for accompanying me on this adventure. Her unwavering moral, emotional, and material support, dedication, and love were my fuel throughout these years, and it would not have been possible without her steadfast dedication. I thank God for our daughter, Princess Favour Iwueseter, for being my inspiration, because watching her grow up from the cradle was all I needed to keep going.

I value my colleagues in the Green Engineering and Sustainability (GES) research group, particularly Dr Edward Kwaku Armah, Jeremiah Adebisi Adedeji, and Boldwin Mutsvene whose interaction and assistance with information dissemination was unparalleled. I also thank my colleagues who worked under different supervisors but contributed significantly to the successful completion of this arduous journey. In this regard, I express my gratitude to Dr Martha Chollom, Dr Emmanuel Kweinor Tetteh, Smarte Ifeanyi Anekwe, and Dr Felicia Omolara Afolabi.

To conclude, I appreciate everyone who, by omission or commission, has not been recognised earlier, but has contributed significantly to the success of this research. In this category, I appreciate the safety officer of the faculty and the Chief Technician of the Department, Mr Roderick Terence Christy, whose intervention located the organisation that constructed the raceway part of the reactor that was designed and built for this research.

The National Research Foundation (NRF) BRICS (BRIC190321424123) provided a good percentage of the funding for this research, courtesy of the Institute for Water and Wastewater Technology (IWWT), DUT.

TABLE OF CONTENTS

LIST OF FIGURES

LIST OF TABLES

RESEARCH OUTPUT

Output in research is an outcome of a research process and it can take many forms. It is what the researcher or system has learned or produced. This can be expressed in the following categories: measurable research outputs, national and/or international acclaim for the research, exploitability of research outputs and effects of research results.

a). Measurable research output: There are various names for different sorts of measurable output. Among them are the following: original research papers, short reports or letters, review articles, case studies, conference presentations or proceedings, book chapters, datasets, and books or theses.

(i) Original Research papers: scholarly journal papers that have undergone peer review. This research produced and published two research papers, and three other papers were under review for publication.

(ii) Short Reports or Letters: Also known as Brief Communications, they are condensed versions of original research publications that fall beyond the length range of scholarly articles. Their purpose is to promptly update researchers and academics on the latest procedures within a particular field of study.

(iii) Review Articles: A review paper provides an overview of the current status of research in a discipline or on a specific subject. This kind of article might tell readers about topics like ongoing discussions on a subject, notable researchers or contributors, knowledge gaps, or it may even forecast the future course of a field. It frequently quotes a large number of experts to provide a broad perspective. This research produced a review article, which was under review for publication.

(iv) Case Studies: Case studies are in-depth analyses of a specific individual, location, organisation, or circumstance within a given time frame. Case studies aim to investigate and elucidate the fundamental ideas, incidental connections, and effects a case subject has within its actual environment.

(v) Conference Presentations or Proceedings: Researchers come together to present and discuss their work in conferences, which are structured events typically focused on a single field or topic. Before a conference, speakers usually submit abstracts, which are summaries of their work, and a committee of organisers chooses which scholars will speak. After they are delivered, conference presentations are often written up, published, and transcribed. This research appeared at four conferences and made four paper presentations as listed hereunder.

(vi) Book Chapters: Books typically consist of several chapters, each authored by a different person. These publications are typically arranged according to a subject, with each author providing a different point of view or argument in a chapter. Many times, one or more authors—who may also write a chapter or foreword themselves, curate and arrange books with chapters written by themselves. This research published six book chapters, which are listed hereunder.

(vii) Datasets: In the course of their job, researchers frequently generate or work with vast volumes of data, which they then collect into datasets. Datasets can include details on a broad range of subjects, such as demographics and generic codes. After that, these datasets might be published separately or in conjunction with another academic work, like an article. Researchers are now required by many scientific grants and journals to publish datasets. This research produced so much data but did not publish any data.

(viii) Books and/or Thesis: Books are the research product of researchers across all fields and disciplines. This means that, although books can differ greatly in terms of content, length, form, and style, they frequently offer a more comprehensive overview of a subject than shorter research outputs like articles or conference proceedings. Books can have one author or multiple writers, and researchers can work on a book in a variety of ways: they can write a foreword, gather and arrange previously published works into an anthology, or create the entire book. A thesis is a written report that summarises the research findings. Data, analysis, conclusions, and any other material gleaned from the study done for the thesis may be included. This is a Doctoral Thesis in Chemical Engineering.

b). National and/or international acclaim for the research: The technique of capturing carbon dioxide emissions from fossil fuel-burning industrial processes, wildfires, and internal combustion engines is known as carbon capture. There are two main methods of capturing carbon dioxide from the atmosphere: biological carbon capture and storage, which uses the natural environment's resources like forests, seas, algae, and trees to sequester CO_2 from the atmosphere, and artificial/geological carbon capture and storage, which stores CO_2 emissions from man-made processes in enormous subterranean facilities. Microalgae can sequester CO_2 through carbon storage and metabolism. When it comes to producing carbon-neutral bioproducts including food supplements, nutraceuticals, biofuels, bioplastics, and fertilisers, microalgal biomass provides a powerful renewable feedstock. The development of biohydrocarbon resources to supply bioproducts is the primary goal for sustainability, displacing fossil resources. Since microalgae are a worldwide resource, biodiesel made from their oil has good emission qualities and is readily renewable. As it incorporates pollution mitigation, this study is environmentally friendly, cost-effective, and

promotes a safer environment following the Kyoto Protocol of December 1997, which went into force in February 2005.

c). Exploitability of research outputs: To exploit research is to assign a value to it apart from its current one. This refers to putting information, abilities, and research findings to use or making them marketable. Despite expressing interest in producing biofuels since 2005, South Africa lacked policies to support this ambition. According to a recent instruction from the Energy Department of South Africa, by 2015, all petroleum manufacturers were required to incorporate a minimum of 5% biodiesel into their production. As one of the first developing nations, South Africa must discover sustainable ways to meet its energy needs without using fossil fuels. In the short term, biodiesel is a viable and cost-effective way to meet South Africa's energy needs.

d). Effects of research results: Effects of research findings refers to how the study affects the engineering and/or scientific communities. The results of the study, as presented in publications and this thesis, might influence further studies that employ the special method to cultivate microalgae. The h-index and i10-index of Google Scholar show that researchers are already taking notice of the work.

LIST OF JOURNAL PAPERS

1. **Kukwa, D. T.** and Chetty, M. 2022. Biomass Production and Simultaneous Minerals Sequestration from Brewery Wastewater with Concomitant Lipid Accumulation Using Algae. *Chemical Engineering Transactions (CET),* 96: 475-480.

   Kukwa, D. T. and Chetty M. 2023. Potential for Corroborative Microalgal Energy Storage from Brewery Wastewater, *Chemical Engineering Transactions (CET),* 106, 31-36 DOI:10.3303/CET23106006

2. **Kukwa, D. T.** and Chetty M. Characterisation of lipid from microalgae mixotrophically cultivated in brewery wastewater with different initial nutrient configurations (Manuscript ready for submission).
3. **Kukwa D. T.** and Chetty M. Kinetics and thermodynamics of lipid and hydrocarbon accumulation as the Microalga *Scenedesmus sp.* cells are cultivated in CO_2-sparged brewery wastewater (Manuscript ready for submission).
4. **Kukwa D. T.** and Chetty M. The development of photobioreactors for biological treatment of industrial wastewater for environmental gains and energy recovery: A review (Manuscript ready for submission).

LIST OF BOOK CHAPTERS

1. **Kukwa**, D. T. and Chetty, M. 2020. Microalgae: The Multifaceted Biomass of The 21st Century, in *Biotechnology Applications for Biomass*, IntechOpen 29 DOI: 10.5772/intechopen.94090.
2. Armah, E. K., Chetty, M., Adedeji, J. A. and **Kukwa, D. T.** 2020. Valorization of Lignocellulosic and Microalgae Biomass, in *Biotechnology Applications for Biomass* IntechOpen online http://dx.doi.org/10.5772/intechopen.93654
3. Armah, E. K., Chetty, M., Bakare, B. F., Adedeji**,** J. A., **Kukwa D. T**, Mutsvene, B., and Shabangu, K. P. 2020. Emerging trends in wastewater treatment technologies: the current perspective, in *Promising Technologies for Wastewater Treatment and Water Quality Assessment,* IntechOpen, London: 28 *DOI:* 10.5772/intechopen.93898.

4. **Kukwa**, D. T., Chetty, M., Anekwe, I., Adedeji, J. 2022. Conversion of Agricultural and Forest Wastes into Water Purifying Materials, in *Agricultural and Kitchen Waste*. CRC Press, 19.
5. **Kukwa, D. T.,** Chetty, M., Tshemese, Z., Estrice, D. and Duma, N. 2022. Resource reclamation for biogas and other energy resources from household and agricultural wastes, in Abhomorha, A. E.-F. and Salama, E.-S. (Eds.), *Biogas: Basics, Integrated Approaches and Case Studies*. London, UK: IntechOpen, 29-56.
6. **Kukwa, D. T.,** Afolabi, F. O., Tetteh, E. K., Anekwe, I. M. S., & Chetty, M. (2022). Bioremediation of Hazardous Wastes, in R. B. Jeyakumar, K. Sankarapandian, & Y. K. Ravi (Eds.), *Hazardous Waste Management*. IntechOpen. https://doi.org/10.5772/intechopen.102458

CONFERENCE PRESENTATIONS

1. **Donald T, Kukwa,** Maggie Chetty (2019). Brewery Wastewater and the Potential for Corroborative Microalgal Energy Storage. Oral presentation at DUT 4th Interdisciplinary Research and Innovation Conference: Global Trends and Challenges in Research and Innovation, held at Hilton Hotel, Durban, South Africa, 17-20 September 2019.
2. **Donald T. Kukwa**, Maggie Chetty (2020). Kinetics and thermodynamics of lipid and hydrocarbon accumulation as the microalga *Scenedesmus sp.* is cultivated in CO_2-sparged brewery wastewater. Online presentation via MS Teams at DUT 5th Interdisciplinary Research and Innovation Virtual Conference, 15-17 September 2020.

3. **Donald Tyoker Kukwa**, Maggie Chetty (2022). Biomass Production and Simultaneous Minerals Sequestration from Brewery Wastewater with Concomitant Lipid Accumulation Using Algae. Oral presentation at the 7th International Conference on Industrial Biotechnology, held in Napoli, Italy 5-8 June 2022.

4. **Donald T, Kukwa,** Maggie Chetty (2023). Brewery Wastewater and the Potential for Corroborative Microalgal Energy Storage. 9th International Conference on Low Carbon Asia (ICLCA2023), held in Okayama, Japan 17 and 18 October 2023

RESEARCH GAPS

Despite advancements in biodiesel production from microalgae, several research gaps remain, particularly in the economic, technical, and environmental aspects of using *Scenedesmus* sp. cultivated in brewery wastewater with a hybrid airlift-raceway photobioreactor and blue light manipulation. Addressing these gaps can enhance process efficiency, scalability, and economic feasibility.

TECHNICAL RESEARCH GAPS

a. Optimization of Lipid Productivity Under Blue Light Manipulation

Current Status: Studies show blue light enhances lipid accumulation, but the optimal intensity, duration, and spectral composition for maximizing FAME-rich lipid yields remain unclear.

Research Gap:

(i) How does blue light modulation affect long-term biomass productivity?

(ii) What is the optimal light-dark cycle for maximizing both biomass and lipid yields?

b. Efficiency of Hybrid Airlift-Raceway PBRs at Scale

Current Status: Hybrid PBRs combine benefits of raceway ponds (low cost, large scale) and airlift reactors (efficient gas exchange). However, scale-up data are limited.

Research Gap:

(i) How do hydrodynamics, mass transfer, and light penetration affect productivity in larger-scale systems?

(ii) What are the optimal reactor configurations for energy-efficient mixing and CO_2 utilization?

c. Improved Harvesting and Extraction Methods

Current Status: Solvent-based extraction is common, but alternatives like ionic liquids, microwave-assisted extraction, and supercritical CO_2 are being explored.

Research Gap:

(i) Which non-toxic, low-cost, and scalable extraction method is most suitable for FAME-rich microalgae lipids?

(ii) Can bio-flocculation or low-energy dewatering methods further reduce costs?

d. Direct Purification of FAME-Rich Lipids

Current Status: Since FAMEs dominate the lipid profile, transesterification can be bypassed, requiring only purification.

Research Gap:

(i) What is the best low-cost purification strategy to meet ASTM D6751 and EN 14214 biodiesel standards?

(ii) Can membrane separation, adsorption, or fractional distillation be optimized for microalgal FAME purification?

ECONOMIC AND FEASIBILITY RESEARCH GAPS

a. Full Life Cycle Assessment (LCA) and Technoeconomic Modeling

Current Status: TEA models exist but comprehensive LCAs comparing this process with traditional biodiesel pathways are rare.

Research Gap:

(i) How does the carbon footprint and energy return on investment (EROI) compare to fossil fuels and first-generation biodiesel?

(ii) What is the economic breakeven point for different production scales?

b. Policy and Incentives for Industrial Adoption

Current Status: Government incentives exist for biofuels, but microalgae-based systems are not widely incentivized.

Research Gap:

(i) What regulatory barriers exist for direct FAME production from microalgae?

(ii) How can carbon credit policies make microalgal biodiesel more competitive?

c. Integration of Wastewater Treatment with Brewery Industries

Current Status: Brewery wastewater is rich in nutrients, making it ideal for microalgal growth. However, there is limited industrial collaboration in large-scale applications.

Research Gap:

(i) What are the economic trade-offs between brewery wastewater treatment and biodiesel production?

(ii) How can co-product valorization (e.g., residual biomass for animal feed) improve profitability?

ENVIRONMENTAL AND SUSTAINABILITY RESEARCH GAPS

a. Long-Term Impacts of Wastewater-Derived Lipids on Fuel Quality

Current Status: Nutrient variations in wastewater impact lipid composition, potentially affecting biodiesel stability and combustion properties.

Research Gap:

(i) Does seasonal variability in wastewater composition alter FAME profiles?

(ii) How can biochemical monitoring ensure fuel quality consistency?

b. Water and Energy Footprint Optimization

Current Status: Although brewery wastewater recycling improves sustainability, the net water and energy balance is unclear.

Research Gap:

(i) How much water and energy is saved by using wastewater compared to freshwater cultivation?

(ii) What energy recovery strategies (e.g., anaerobic digestion of biomass residues) can improve sustainability?

c. End-of-Life and Byproduct Utilization Strategies

Current Status: Residual biomass is often discarded or used in low-value applications like composting.

Research Gap:

(i) Can microalgal biomass be upgraded for higher-value applications (e.g., protein supplements, bioplastics)?

(ii) How does residual biomass compare to soybean meal or fishmeal in animal feed trials?

SCALE-UP AND COMMERCIALIZATION RESEARCH GAPS

a. Industrial-Scale Production Bottlenecks

Current Status: Most studies focus on lab or pilot-scale production, with limited commercial success.

Research Gap:

(i) What are the major barriers (logistics, infrastructure, cost) to scaling up this system?

(ii) How can process automation and AI-based monitoring improve scalability?

b. Supply Chain and Logistics for Large-Scale Deployment

Current Status: Transporting, processing, and distributing microalgal biodiesel at scale is complex.

Research Gap:

(i) What are the best decentralized production models to reduce transportation costs?

(ii) How can mobile biorefineries be designed for localized production?

SYMBOLS, ABBREVIATIONS AND ACRONYMS

Alias	Introducing distortion or error
μ	Specific growth rate
μm	Micrometre
BD	Blue Drop
BOD	Biochemical oxygen demand
BWW	Brewery Wastewater
COD	Chemical oxygen demand
DO	Dissolved oxygen
DW_0	Dry weight at time t_0
DW_1	Dry weight at time t_1
DWW	Dairy Wastewater
EC	Electrical Conductivity
GD	Green Drop
HRAP	High-rate algal pond
IWW	Industrial Wastewater
LC-PUFA	Long-chain polyunsaturated fatty acid
M_1	Dry biomass at time t_1
M_2	Dry biomass at time t_2
MUFA	Monounsaturated Fatty Acids
NH_4^+	Ammonium
NH_4-N	Ammonium-nitrogen
OD	Optical density
P	Biomass productivity

PBR	Photobioreactor
PUFA	Polyunsaturated Fatty Acids
SWW	Sugar Wastewater
t	Time
T_2	Doubling time
TDS	Total Dissolved Solids
TN	Total nitrogen
TOC	Total organic carbon
TP	Total phosphorous
TS	Total Solids
TSS	Total Suspended Solids

CHAPTER 1

Introduction

1.0 Background

The composition, concentration and condition of wastewater differ widely depending on the origin, time, season and weather conditions; and can be diluted by rainwater runoff. Wastewater from residences and institutions, carrying bodily wastes (primarily faeces and urine), washing water, food preparation wastes, laundry wastes, and other waste products of normal living, are classed as domestic or sanitary sewage. Wastewater from stores and service establishments serving the immediate community termed commercial wastewater, adds up to the sanitary or domestic sewage category if its characteristics are similar to household wastewater flows. Wastewater that results from industrial processes such as the production or manufacture of goods is classed as industrial wastewater, not as sewage (Kulkarni, Wanjule and Shinde 2018).

The characteristics of industrial wastewater and factory effluents depend on the types of products that are manufactured. In the effluents of some factories, including those related to mining, steel making and chemical production, most of the foreign particles are mineral ores; while in some other factories, such as those related to food products and starch manufacture, organic matter constitutes most of the foreign materials (Jebrail 2016; Ramanna 2015). Also producing wastewater are agricultural operations. Cleansing water from animal farms; animal faeces carried by precipitation runoff; harvest products and equipment washed; chemical fertilisers (like calcium ammonium nitrate, calcium nitrate, calcium sulphate, ammonium thiosulfate, ammonium nitrate, diammonium phosphate, and monocalcium phosphate), and pesticides (such as

fungicides, herbicides, and insecticides: specific synthetic chemical pesticides are glyphosate, acephate, deet, propoxur, metaldehyde, boric acid, diazinon, dursban, DDT, malathion, etc.) constitute the bulk of agricultural wastewater. Consequently, they are a potential source of freshwater pollution (Jebrail 2016).

Surface runoff, also known as storm flow or overland flow, is a portion of precipitation that runs rapidly over the ground surface to defined channels. Precipitation absorbs gases and particulates from the atmosphere, dissolves and leaches materials from vegetation and soil, suspends matter from the land, washes spills and debris from urban streets and highways, and carries all these pollutants as wastes in its flow to a collection point (Jebrail 2016; Kumar 2016).

Consequently, due to the diverse pollutant composition of wastewater, it can be categorised into physical, chemical and biological pollutants: The physical and chemical pollutants include macro-solids such as sanitary napkins, nappies/diapers, condoms, needles, children's toys, dead animals or plants, etc.; Heavy metals including mercury, lead and chromium; Organic particles such as faeces, hairs, food, vomit, paper fibres, plant material, humus, etc.; soluble organic material such as urea, fruit sugars, soluble proteins, drugs, pharmaceuticals, etc.; Inorganic particles such as sand, grit, metal particles, ceramics, etc.; soluble inorganic material such as ammonium, road-salt, sea-salt, cyanide, hydrogen sulphide, thiocyanates, thiosulphates, etc.; gases such as ammonia, hydrogen sulphide, carbon dioxide, methane, etc.; emulsions such as paints, adhesives, mayonnaise, hair colorants, emulsified oils, etc.; toxins such as pesticides, poisons, herbicides, etc.; pharmaceuticals and hormones and other hazardous substances; thermal pollution from power stations, and industrial manufacturers (Jebrail 2016; Kumar 2016; Martonen 2017).

Biological pollutants are born from wastewater that contains human and animal faeces, coupled with microbes-infested waste food as is the case for sewage, then it may also contain pathogens in the form of bacteria (such as *Salmonella, Shigella, Campylobacter, Vibrio cholerae*), viruses (such as hepatitis A, rotavirus, enteroviruses), protozoa (such as *Entamoeba histolytica*, *Giardia lamblia, Cryptosporidium parvum, Trypanosoma, Balantidium coli, Trichomonas vaginalis, Plasmodium, Sarcodina*) and parasites such as helminths and their eggs (e.g. *Ascaris* (roundworm), *Ancylostoma* (hookworm), *Trichuris* (whipworm)) (Turgeon *et al.* 2018). It can also contain non-pathogenic bacteria and other organisms such as insects, arthropods, and small fish (Hodgkinson *et al.* 2017; Kim *et al.* 2018).

In typical wastewater, 75 % of the suspended solids and 40 % of the dissolved materials are organic. The dissolved organic materials are a mixture of proteins (65 %), carbohydrates (25 %), fats (9 %) and detergents (1 %). There are substantial inorganic compounds which include sodium, calcium, magnesium, chlorine, sulphates, phosphates, bicarbonates, nitrates, ammonium and heavy metals in trace amounts (Hani, Qasaimeh and Qasaimeh 2012). The most significant of these are chlorides (100 - 200 gm^{-3}) and sulphides (0.1 - 0.7 gm^{-3}). Sulphides, despite their low concentrations, are of greater concern than chlorides because they impart a very foul-smelly odour even at this level.

The main essence of wastewater-treatment systems is to (1) remove floating and suspended substances from wastewater (2) oxidise unstable organic compounds in the wastewater and convert them to stable materials such as nitrates, sulphates and phosphates and then settle and separate them (3) separate soluble and insoluble toxic substances like heavy metals (4) disinfect and eliminate pathogenic microorganisms in wastewater (Jebrail 2016; Krustok 2016).

Four stages generally used in the course of wastewater treatment include preliminary, primary, secondary and tertiary. The preliminary treatment removes debris and grit while the primary treatment removes the suspended solids (40 – 60 %), which flocculate easily and reduces the biochemical oxygen demand (BOD_5) by about 25 – 35 %. Secondary treatment substantially degrades the organic material and reduces the BOD_5 by about 75 – 95 % and the tertiary treatment provides the final treatment stage to raise the quality of the treated wastewater before it is discharged to the receiving environment, which may be a river, lake, sea, or ground. More than one tertiary treatment process may be used at any treatment plant.

Microalgae have been used for tertiary treatment of wastewater due to their capacity to assimilate nutrients. Microalgae strains are generally sensitive to different types of wastewater due to imbalance in the nutrient profile, deficiency of some important trace elements, and the presence of inhibiting and/or toxic compounds in wastewater streams, and the only limited number of strains within a few species (such as *Chlorella sp*. and *Scenedesmus sp.*) could adapt well in different wastewater environments. After treating rice mill effluent using the algae species *Oedogonium* and *Chara sp.*, Sahoo and Baweja (2015) measured some metrics, including BOD_5, COD, ammonia, nitrogen, and phosphate; and observed percentage reduction rates as 53.97 (COD) and 59.61 (BOD5). Several species of algae have been tested under CO_2 concentrations of over 15 %, such as *Chlorococcum littorale* which could grow under 60 % CO_2 using the stepwise adaptation technique.

1.1 Problem Statement

Microalgae are known to be pollutant scavengers for a broad category of chemicals released from the domestic, industrial and agricultural sectors. Aside from the usual

chemical compounds present in wastewater such as nitrates, phosphates, sulphates and ammonium, microalgal cells can also assimilate and break down more persisting molecules such as hydrocarbons, antibiotics, pharmaceutical and personal care products (PPCPs), endocrine disrupting compounds (EDCs) and heavy metals (Delrue *et al.* 2016).

Microalgae produce biomass, an embodiment of stored chemical energy with great potential for the sustainable production of fuels and other goods with added value, as they scavenge nutrients from the medium (Shukla and Kumar 2018; Subhash *et al.* 2017). Several microalgae-based products are already well established in some high-value markets such as pigments, antioxidants, nutraceuticals, fertilizer and animal feeds (Lima *et al.* 2018; Udaiyappan *et al.* 2017). While bioremediation of nutrients in wastewater by microalgae has been extensively documented over many years (Piligaev *et al.* 2018; Zhimiao *et al.* 2016; Caporgno *et al.* 2015;), research is intensified to establish processes and technologies for the conversion of microalgae biomass to liquid fuels at the industrial scale. Despite the encouraging attention algae have received in the research world coupled with the interest attracted in the commercial sector, industrial production of liquid biofuel from algae has not started (Singh *et al.* 2015). One major factor is that the breakthrough in biomass production to meet and surpass the current demand has not been achieved (Rashid, Park, and Selvaratnam 2018).

Another factor to overcome is the cost and energy requirement for biomass harvesting technique, which should not add substantially to the cost of the process (Fazal *et al.* 2018). It is necessary to have productive strains and optimal culture conditions that can produce biomass with a high growth rate and lipid content at the same time. (Kube *et al.* 2018). Nevertheless, considerable advances in the field of biology and substantial

processing improvements are required to achieve economic, environmental, and energetic sustainability in the production of microalgae biofuels (Rastogi *et al.* 2018). The shift from pilot-scale to industrial-scale operations frequently exposes microalgae cells to unfavourable and hostile environments, which lowers output yields. (Klinthong *et al.* 2015). This research seeks to bridge the gap between pilot-scale and industrial-scale microalgal biomass production accounting for both the kinetic and thermodynamic models and to foster the production of hydrocarbons and their derivatives.

1.2 Justification of the study

Microalgae can assimilate organic and inorganic pollutants from wastewater into cellular constituents such as lipids, protein and carbohydrates, thus achieving pollutant reduction in an environmentally friendly way. Nutrients absorbed can be removed from wastewater via biomass harvest. Moreover, since microalgae can fix CO_2 and release O_2, their use leads to a decrease in the harmful emissions of CO_2. The use of fossil fuels accumulates greenhouse gases (GHG) above what the cycle of the individual gases (NO_x, CO_2) can accommodate, thereby causing the greenhouse effects. Biofuels have more friendly emission properties to both man and the environment.

Wastewater carries with it diverse pollutants that are not just detrimental to human and animal health but both terrestrial and aquatic ecosystems. Algae that were hitherto a menace to the environment, causing discomfort as they bloom, are now seen as valuable assets. The use of algae to treat wastewater and a means to mitigate atmospheric CO_2, therefore, should receive the accolade and be promoted/encouraged. The use of algae biomass to produce biofuel has removed the stress imposed on food crops for such purposes thereby improving food security issues, particularly in the

developing world, where already more than 800 million people (excluding China) suffer from hunger and malnutrition (Zhu 2014). This study would encourage Governments worldwide to encourage the development of microalgae biodiesel resources.

1.3 Objectives of the study

This research aimed to investigate the feasibility of cultivating hydrocarbon-producing microalgae in industrial wastewater, optimizing growth conditions, and evaluating hydrocarbon yields. The research objectives were outlined as follows:

- To a**ssess** the suitability of industrial wastewater for microalgae cultivation by analyzing its physicochemical properties and screening.
- To identify and optimize key parameters (e.g., nutrient concentration, pH, temperature, and light intensity) that enhance microalgal growth and hydrocarbon production.
- To evaluate the hydrocarbon yield and composition of selected microalgal strains grown in different wastewater sources.
- To develop a bioremediation model to assess nutrient removal efficiency and wastewater treatment potential using airlift-raceway reactor.
- To perform techno-economic and life cycle assessments to determine the viability of integrating microalgal biofuel production with industrial wastewater treatment.

1.5 Thesis Framework / Outline

This thesis is made up of eight (8) chapters and appendices, which are outlined below:

Chapter 1: Introduction

In Chapter 1, the research's focus is set. It provides a summary of the issue, explains the research's purpose and goals, and establishes the thesis's structure.

Chapter 2: Literature Review

Chapter 2 provides an overview of the research on techniques for managing water and wastewater resources, covering their sources, characteristics, and treatments. The overview also covered the selection of photosynthetic microalgal strains for this study, as well as cultivation methods, lighting schemes, harvesting methods, and their uses in biotechnology; microalgae biomass production, including CO_2 biofixation; photosynthesis; photobioreactors; and the extraction and characterization of microalgae lipids.

Chapter 3: Materials and Methods

This chapter describes the sampling methods for the wastewater for the various analyses. It also presents a vivid description of the techniques adopted to characterise industrial wastewater as enshrined in the standard methods, except where there was a need for modification, and it was so stated.

Chapter 4: Characterisation and Screening of Industrial Wastewater

The characteristics of industrial wastewater were reported and discussed in this chapter. The different wastewater sources were screened for nutrient availability and the amount, and these were used with other cogent parameters as the basis for choosing the wastewater source that was used in this research.

Chapter 5: Cultivation of Microalgae in Industrial Wastewater

Microalgae were cultivated at the desktop level in scotch bottles and a three-litre bubble column photobioreactor. The Design-Expert version 11 statistical software was used to model the experiment. The Design of Experiment DOE) provided the number

of experimental runs that could average adequately and the conditions that would produce the optimum yield of microalgal biomass with a scale-up scenario. The chapter also reports the effect of CO_2 gas sparging rate, and initial nutrient concentration, on biomass production.

Chapter 6: Hydrocarbons and Lipid Profiling of *Scenedesmus sp.* Grown in Brewery Wastewater Using a Novel Airlift-Raceway Photobioreactor

This chapter reports the production of microalgal biomass in a novel airlift-raceway photobioreactor. It monitors the flow regime of the broth in the bioreactor and the CO_2 sparging rate. The chapter also presents bio-hydrocarbon profiling of microalgal lipids; highlighting the enrichment of hydrocarbons and hydrocarbon derivatives in microalgal biomass and the subsequent extraction of hydrocarbon- and hydrocarbon derivative-rich bio-oil. Gas chromatography-mass spectroscopy (GC-MS) analysis of the microalgal bio-oil and scanning electron microscopy (SEM) analysis of the biomass were also reported in this chapter.

Chapter 7: Techno-economic and Life Cycle Analyses of Microalgae-Based Bio-hydrocarbon Production

This chapter attempts to present a techno-economic analysis (TEA) of the process by the research and typically evaluates the feasibility, costs, and potential profitability of the process. The dominance of fatty acid methyl esters (FAMEs) in the microalgae-oil extracts suggests that the traditional transesterification step could be bypassed in favour of a purification step. This modification reduces chemical and processing costs while simplifying the biodiesel production process. The chapter also presents a life-cycle assessment (LCA), which examines the environmental impacts of everything that occurs during the life cycle of a bio-based hydrocarbon and hydrocarbon derivative product, process, or service. From the moment raw materials are discovered

and processed to the manufacture, distribution, and usage of the product, to the recycling or disposal of the materials that make it up, environmental implications are considered.

Chapter 8: Summary, Conclusion and Recommendations

This chapter presents the summary of this research findings; the conclusion is drawn from the findings and highlights the recommendations for future research.

References: This section provides the list of all citations in the body of this thesis. Except for standards and standard methods, all citations in this thesis are works that were published within the last ten years.

Appendices: This section provides supplementary information, which may help provide a more comprehensive understanding of some sections of this thesis.

CHAPTER 2

Literature Review

2.1 Background

In addition to discussing cultivation systems, lighting strategies, harvesting techniques, and their applications in biotechnology, this chapter covers topics related to water, wastewater and wastewater treatment, microalgae, microalgae biomass production, and the strain chosen for this study. Other topics covered include CO_2 biofixation, an explanation of photosynthesis, extraction, and characterization of microalgae oils. The chapter delves into the function of photobioreactors in the process of producing biomass.

2.2 Water and Wastewater

2.2.1 Water resources in South Africa

Water availability in South Africa varies greatly by region and season, making it a country that is considered to be water-scarce. Rainfall in the eastern and southeastern areas of the country can reach 1,000 mm per year, while the western parts receive as little as 100 mm. An estimated 43 to 48 km^3 of surface runoff occurs annually, however, because of flood spillage losses, only roughly 14 km^3 are usable each year. Additionally, groundwater supplies are scarce, with an estimated annual flow of only 1 km^3 (Molobela and Sinha, (2011).

Numerous factors are putting tremendous strain on South Africa's water resources, such as climate change, which has caused key dams to have lower water levels and groundwater levels to decline as a result of increased extraction and saltwater intrusion

in coastal areas. Additionally, the Department of Water and Sanitation is finding it difficult to carry out its job due to pervasive corruption and bad governance, which has made water shortages worse.

In response to these challenges, microalgae-based bioremediation has emerged as a promising and sustainable solution for wastewater treatment in South Africa. Microalgae possess the ability to remove contaminants, including nitrogen, phosphorus, and heavy metals, from wastewater through mechanisms such as accumulation, adsorption, and metabolism.

Implementing microalgae-based wastewater treatment systems can help alleviate water scarcity by enabling the reuse of treated water for agricultural or industrial purposes, thereby reducing the demand for freshwater resources. Moreover, the biomass generated from microalgae-based bioremediation can be utilized in various industries, including biofuel production, animal feed, and fertilizers, contributing to economic development and sustainability. However, challenges such as the need for specific microalgal strains and the optimization of operational conditions must be addressed to fully realize the potential of microalgae in wastewater treatment.

While South Africa faces significant water resource challenges, the application of microalgae-based bioremediation offers a viable strategy to enhance water availability and quality. By integrating such innovative solutions, the country can work towards meeting the growing water demands and ensuring sustainable water management for the future.

Existing water sources in South Africa are becoming increasingly stressed as a result of rising global water demand and a lack of enough precipitation. The measurement of water withdrawal to meet the needs of the agricultural, industrial, and municipal sectors is known as water demand. Cape Town was impacted hard by the drought in

southern Africa, with the dramatic pronouncement of Day Zero on July 7, 2018, when the taps were to be shut off (Naidoo 2018). This event came after severe droughts in the greater southern African region, which were described as the worst in 20 years (Naidoo, 2018). Although large drought episodes have continued in South Africa and its neighbours, indicating a shift in weather patterns, water augmentation plans (massive new water supply infrastructure) have not taken other eventualities into account. The continued conservatism of the current global establishment, according to Naidoo (2018), is one of the primary difficulties in addressing water scarcity in Africa, and indeed the decreasing water security worldwide; in trying to solve 21st-century problems, African leaders use 20th-century technology and solutions, with 19th-century operating rules, standards, and guidelines. The second problem is Cape Town's excessive reliance on traditional surface water supplies, with little investment in a long-term groundwater strategy or other augmentation possibilities such as desalination. In the early 2000s, the water demand management strategy fell significantly short of what was needed to provide water security through 2022. Third, South African institutions and their international partners are hesitant to accept a variety of innovative ideas and technologies. Cape Town and other South African towns are well-known for having some of the world's best water utilities, which is a crucial reason why South Africa has managed to maintain water security in the world's 30th driest country (Naidoo 2018).

South Africa is a water-scarce country with an average yearly rainfall of less than 60 % of the world average. As a result, it's critical to urge businesses to reduce their water use and, where possible, recycle and reuse water and wastewater. South Africa has made it mandatory to treat wastewater to suitable standards and return it to the watercourse from which it was originally acquired in 1956, thanks to the South African

Water Act (Act 54 of 1956). Wastewater and sewage treatment plants became increasingly stressed as water demand increased as a result of economic expansion and population growth. As a result of this predicament, water and sanitation officials have been under pressure to discover solutions to maintain the quality of water resources. The East Rand Water Care Company (ERWAT) was founded in 1992 as a Section 21 company with the mission of providing a cost-effective wastewater treatment service to local governments in the Gauteng province of South Africa, with catchment areas including the Ekurhuleni Metropolitan Municipality, Johannesburg Metropolitan Municipality, and Lesedi Local Municipality. The organization controls the entire spectrum of wastewater in the region through consolidation. Twelve Water Services Authorities in Gauteng supply wastewater services through an infrastructure network of 56 wastewater collectors and treatment systems, serving over 2000 companies and 3.5 million people. The 56 treatment facilities receive a total flow of 2579 ML/day, with a combined hydraulic design capacity of 2595 ML/day (as ADWF). This means that the operating flows have used 99.38 % of the design capacity, leaving no excess to fulfil future demand without adding new capacity.

The DWA passed two incentive-based regulations on September 11, 2008, which targeted two programs: the Blue Drop Certification Programme for Drinking Water Quality Management Regulation and the Green Drop Certification Programme for Wastewater Quality Management Regulation. This campaign was designed to help water and wastewater managers gradually improve their operations so that they don't have a detrimental influence on the water bodies into which they discharge their waste. The goal of the system was to give water service authorities Blue and/or Green Drop Status if they followed DWS's drinking water and wastewater legislation as well as other best practices (DWS 2017).

The countrywide microbiological compliance for South African tap water was measured at 93.3 % against the National Standard in the first Blue Drop Report in 2009 (SANS 241). Table 2.1 shows the microbial determinants in the blue drop regime during the time stipulated. The 2012 Blue Drop Report showed that this incentive-based regulation method was having a beneficial influence on the South African water sector, with a score of 97.3 %. Overall, municipalities are taking their Blue Drop status seriously, with Ekurhuleni and the City of Johannesburg at the top of the rankings, closely followed by eThekwini and the City of Cape Town (DWS 2017). Table 2.2 gives the macrodeterminants limits in the blue drop regime, while Table 2.3 gives the limits for microdeterminants and Table 2.4 presents the limits for organic determinants.

Table 2.1: Microbiological determinants of potable water (SANS 241: 2011)

Determinant	Risk	Unit	Standard
E. coli[a] or faecal coliforms[b]	Acute health	Count per 100 mL	Not detected
Cytopathogenic viruses[c]	Acute health	Count per 10 L	Not detected
Protozoan Parasites[d]			
Cryptosporidium spp	Acute health	Count per 10 L	Not detected
Giardia spp	Acute health	Count per 10 L	Not detected
Total coliforms[e]	Operational	Count per 100 mL	≤ 10
Heterotrophic plate count[f]	Operational	Count per mL	≤ 1 000
Somatic coliphages[, g]	Operational	Count per 10 mL	Not detected

[a] Definitive, preferred indicator of faecal pollution.

[b] Indicators of unacceptable microbial water quality could be tested instead of *E. coli* but is not the preferred indicator of faecal pollution. Also provides information on treatment efficiency and after-growth in distribution networks.

[c] Confirms the risk of human infection and faecal pollution and also provides information on treatment efficiency. The detection of selected viruses confirms faecal pollution of human origin.

[d] Confirms a risk of infection and faecal pollution and also provides information on treatment efficiency. The detection of selected protozoan parasites confirms a human health risk.

[e] Indicates potential faecal pollution and provides information on treatment efficiency and after-growth.

[f] Process indicator that provides information on treatment efficiency, after growth in distribution networks and adequacy of disinfectant residuals.

[g] Process indicator that provides information on treatment efficiency.

Table 2.2: The Blue Drop limits for macro-determinants (DWS, 2017)

Determinant	Unit	SANS 241: 2006		SANS 241: 2011		WHO: 2014	
		Risk	Std	Risk	Std	Risk	Std
NO_3^--nitrogen	mg/L	-	-	Acute Health	≤11		≤10
NO_2^--nitrogen	mg/L	-	-	Acute Health	≤0.9		≤1
NO_3 + NO_2 as N	mg/L	health	<10	-	-		-
Potassium as K^+	mg/L	-	-	-	-		≤30
Sodium as Na^+	mg/L	-	-	Aesthetic	≤200		≤200
Sulphate as SO_4^{2-}	mg/L			Health (acute)	≤500		≤250
Chloride as Cl^-	mg/L						≤250
Fluoride as F^-	mg/L						≤1.5
Ammonium as NH_4^+	mg/L						0.75
Phosphate as PO_4^{3-}	mg/L						0.3
Calcium as Ca^{2+}	mg/L						≤200
Magnesium as Mg^{2+}	mg/L						≤150
Zinc as Zn^{2+}	mg/L	-	-	Aesthetic	≤5	-	-
pH							6.5-8.5
Alkalinity as $CaCO_3$	mg/L						≤200
Total dissolved solids	mg/L						≤1000
Total hardness	mg/L						≤500

Conductivity	μS/cm	≤1000
Turbidity	NTU	≤5
Colour	Hz	≤15

Table 2.3: The Blue Drop limits for micro-determinants

Determ't	Unit	SANS 241: 2006		SANS 241: 2011		WHO: 2014	
		Risk	Std	Risk	Std	Risk	Std
Al	μg/L			Operational	≤300		
Sb	μg/L	-	-	Health(chronic)	≤20		
As	μg/L	Health	<10	-	-		
Cd	μg/L	health	<5	-	-		
Cr	μg/L	health	<100	-	-		
Co	μg/L	health	<500	-	-		
Cu	μg/L	-	-	Health(chronic)	≤2000		
CN^-	μg/L	-	-	Health (acute)	≤70		
Fe	μg/L	-	-	Aesthetic	≤300		≤300
Pb	μg/L	Health	<20	-	-		
, Mn^{2+}	μg/L	Aesthetic	<100	-	-		≤400
Hg	μg/L	-	-	Health(chronic)	≤6		
Ni	μg/L	health	<150	-	-		
Se	μg/L	Health	<20	-	-		
U	μg/L	-	-	-	-		
V	μg/L	Health	<200	-	-		

Table 2.4: The Blue Drop limits for organic chemical determinants

Determinant	Unit	SANS 241: 2006		SANS 241: 2011		WHO: 2014	
		Risk	Std	Risk	Std	Risk	Std
DOC	μg/L	Health	<10	-	-		
TOC	μg/L	-	-	Health (chronic)	≤10		
Trihalomethanes (total)	μg/L	Health	<200	-	-		
Chloroform	μg/L	-	-	Chronic health	≤300		
Bromoform	μg/L	-	-	Chronic health	≤100		
Dibromochloromethane	μg/L	-	-	Chronic health	≤100		
Dichlorobromomethane	μg/L	-	-	Chronic health	≤60		
Microcystin as LR	μg/L	-	-	-	-		
Phenols	μg/L	-	-	Aesthetic	≤10		

2.2.2 Wastewater

Wastewater is used water from any combination of domestic, industrial, commercial or agricultural activities, surface runoff or stormwater, and any sewer inflow or sewer infiltration. Therefore, wastewater is a by-product of domestic, industrial, commercial or agricultural activities (Jebrail 2016; Mostafa, Elshafei and Peters 2015). The characteristics of wastewater vary depending on the source. Figure 2.1 gives a broad view of sources of wastewater.

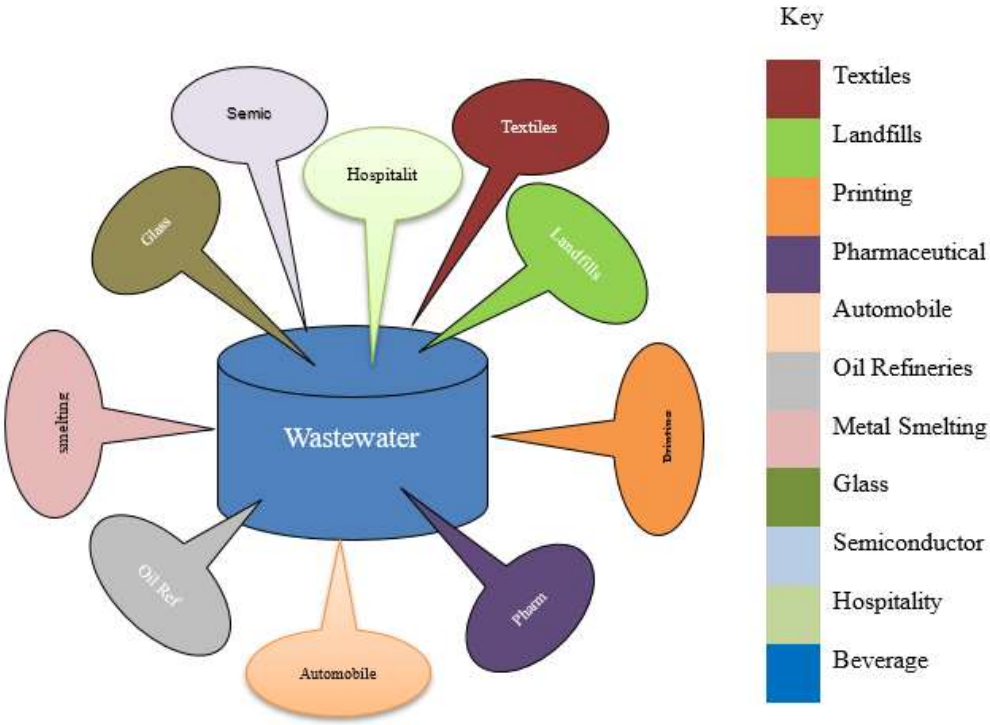

Figure 2.1 Sources of wastewater

According to Kwaku *et al*. (2021), there are three different types of wastewater: industrial wastewater from industrial activities, municipal wastewater from communities (also known as sewage), and domestic wastewater from households. Pollutants of the chemical, biological, and physical types may be present in wastewater.

2.2.2.1 Wastewater Physical characteristics

The concentration of all solids in wastewater, which includes colloidal, floating, settleable, and materials in solution, is its most significant physical feature. Particle size distribution, turbidity, colour, transmittance, temperature, electrical conductivity, density, specific gravity, and weight are further significant physical attributes (Mostafa, Elshafei, and Peters 2015).

a. Solids in Wastewater

It is customary to remove coarse elements from the sample before analysing it for particles when characterising wastewater. Table 2.5 lists and identifies the several classes of solids in water and wastewater. Since a filter is used to separate the TSS from the TDS, the TSS test is somewhat arbitrary, depending on the pore size of the filter paper used for the test. Filters with nominal pore sizes varying from 0.45 μm to about 2.0 μm have been used for the TSS tests. More TSS will be measured as the pore size of the filter used is reduced. Thus, it is important to note the pore size of the filter paper used when comparing reported TSS values. It is also important to note that the TSS test itself has no fundamental significance. The principal reasons that the test lacks a fundamental basis are the following: (1) the measured values of TSS are dependent on the type and pore size of the filter paper used in the analysis; (2) depending on the sample size used for the determination of TSS, auto filtration, where the suspended solids that have been intercepted by the filter also serve as a filter, can occur (Mostafa, Elshafei, and Peters 2015). The measured TSS value will appear to be higher than the real amount due to auto filtration; (3) Adsorption of small particles to the material already retained by the filter can remove them, depending on the properties of the particulate matter; (4) Since the number and size distribution of the particles that make

up the observed value is unknown, TSS is a lumped parameter. However, TSS test findings are frequently used to evaluate the effectiveness of traditional treatment methods and the necessity of effluent standards, which are used to evaluate treatment plant performance for regulatory control purposes.

a(i) Total dissolved solids (TDS) in Wastewater

By definition, the solids contained in the filtrate that passes through a filter with a nominal pore size of 2.0 μm or less are classified as dissolved. Yet it is known that wastewater contains a high fraction of colloidal solids. The size of colloidal particles in wastewater is typically in the range of 0.001 to 1.0 μm as stated in Table 2.5.

a(ii) Volatile solids and fixed solids in Wastewater

Material that can be volatilized and burned off when ignited at 500$\pm$50^{o}C is classified as volatile (Table 2.5). In general, volatile solids (VS) are presumed to be organic matter, although some organic matter will not burn, and some inorganic solids break down at high temperatures. Fixed solids (FS) comprise the residue that remains after a sample has been ignited. Thus TS, TSS, and TDS are comprised of both FS and VS. The ratio of VS to FS is often used to characterise the wastewater for the amount of organic matter present (Jubb 2015).

a(iii) Turbidity of Wastewater

Turbidity is a metric for the ability of water to transmit light. It is one of the test criteria used to show the amount of colloidal and residual suspended matter present in natural waterways and wastewater discharges. The intensity of light scattered by a sample and a reference suspension under identical conditions are compared to determine the turbidity of the sample (Macdonald 2015). The main reference standard is in the form of formazin suspensions. The units used to report turbidity measurement results are nephelometric turbidity units (NTU). Normally, light would not be able to pass through

colloidal particles because they would scatter or absorb it. Air bubbles in the fluid would change its refractive index, introducing misleading light transmission and, consequently, causing estimates of turbidity to be inaccurate. Turbidity and total suspended particle content in untreated wastewater typically don't correlate.

Table 2.5: Solids found in wastewater

Test	Description
Total solids (TS)	The residue remaining after a wastewater sample has been evaporated and dried at a special temperature (103 – 105°C)
Total volatile solids (TVS)	Those solids that can be volatilized and burned off when the TS is ignited (500±50 °C)
Total suspended solids (TSS)	After being dried at a specific temperature(105 °C), a fraction of TS is measured and kept on a filter with a specific pore size.
Volatile suspended solids (VSS)	Those solids that can be volatilized and burned off when TSS are ignited (500±50 °C)
Fixed suspended solids (FSS)	The residue that remains after TSS is ignited (500±50 °C
Total dissolved solids (TDS) = (TS – TSS)	After passing through the filter, those solids are dried and evaporated at a predetermined temperature. Keep in mind that dissolved and colloidal solids are included in the measurement of TDS. Typically, colloids range in size from 0.001 to 1 μm.
Total volatile dissolved solids (VDS)	The solids that burn off and volatilize at 500±50 °C when the TDS ignites
Fixed dissolved solids (FDS)	The residual left over after igniting TDS at 500±50 °C
Settleable solids	Milligrams per litre of suspended solids will settle out of suspension in a predetermined amount of time.

However, for the settled and filtered secondary effluent from the activated sludge process, there is a decent link, Equation (2.1), between turbidity and total suspended solids (Kainth 2015; Macdonald 2015; Karki 2016).

$$TSS\ (mg/L) = TSS_f(T) \quad (2.1)$$

where TSS = total suspended solids, (mg/L); TSS_f = factor used to convert turbidity readings to total suspended solids, (mg/L TSS)/NTU; T = turbidity, NTU.

The factor's particular value varies depending on the biological treatment process's parameters and is unique to a particular treatment plant.

a(iv) Temperature of Wastewater

The temperature of wastewater is commonly higher than that of the local water supply, because of the addition of warm water from households and industrial activities. As the specific heat of water is much greater than that of air, the observed wastewater temperatures are higher than the local air temperatures during most of the year and are lower only during the hottest periods (Maxil 2015; Jebrail 2016; Martonen 2017). Because it affects aquatic life, chemical reactions and reaction rates, and the water's appropriateness for useful applications, water temperature is a crucial characteristic. Generally speaking, the species of fish that can live in the receiving body of water can alter due to the rising temperature (De Klein *et al.* 2017). Compared to cold water, warm water has less oxygen soluble in it. When the temperature rises, the pace of biological reactions increases. This, along with the decrease in oxygen levels in surface waters, can lead to a significant reduction in dissolved oxygen (DO) concentrations during the hot months of the year (Jebrail 2016; De Klein *et al.* 2017).

The optimum temperatures for microorganism activity are in the range of 25 to 35ºC. Aerobic digestion and nitrification of bacteria stop when the temperature rises to 50ºC. At about 15ºC, the methane-producing bacteria practically deactivate and at about 5ºC,

the autotrophic nitrifying bacteria cease to function. At 2°C even the chemoheterotrophic bacteria acting on carbonaceous material become essentially dormant (Newinger 2015; Sigdel 2017). The Van't Hoff-Arrhenius equation, which describes the temperature dependency of the rate and equilibrium constants as provided in Equation (2.2), characterises the temperature effect on reaction rates.

$$\frac{d(lnk)}{dt} = \frac{E}{RT^2} \tag{2.2}$$

where k = reaction rate constant; T = Thermodynamic temperature, measured in kelvin (K); E = a constant that is characteristic of the reaction (such as activation energy), measured in $Jmol^{-1}$; R = ideal gas constant, 8.314 $Jmol^{-1}K^{-1}$.

When the same reaction is carried out at two different temperatures T_1 and T_2, integration of Equation (2.2) over these temperatures gives Equation (2.3).

$$ln\frac{k_2}{k_1} = \frac{E(T_2 - T_1)}{RT_1T_2} = \frac{E}{RT_1T_2}(T_2 - T_1) \tag{2.3}$$

Equation (2.3) can be used to evaluate k_2 if k_1 is known for a particular temperature and if E is known. The majority of wastewater treatment procedures and operations are carried out at ambient temperature or slightly above it, thus it is reasonable to assume that the quantity, $\frac{E}{RT_1T_2}$ is a constant. If this quantity is denoted by the letter C, Equation (2.3) becomes Equation (2.4), and finally Equation (2.5).

$$ln\frac{k_2}{k_1} = C(T_2 - T_1) \tag{2.4}$$

$$\frac{k_2}{k_1} = e^{C(T_2 - T_1)} = \theta^{(T_2 - T_1)} \tag{2.5}$$

where the temperature coefficient, denoted by θ, can be utilised to modify the operative rate constant value of a particular reaction in response to temperature variations. Despite the assumption that its value remains constant, θ frequently varies with

temperature. It is therefore important to exercise caution while choosing suitable values for θ across various temperature ranges.

a(v) Electrical conductivity (EC) of Wastewater

The EC of water is a measure of the ability of the water to conduct an electric current. Electrical current is transported by ions in solution, and conductivity increases as the ions increase. The measured EC is therefore an indirect measure of the TDS concentration. When assessing if water is suitable for irrigation, one factor to take into account is its EC. The salinity of treated wastewater to be used for agriculture is determined by its EC measurement. Equation (2.6) gives the SI units of EC in millisiemens per meter (mS m^{-1}) and micromhos per centimetre (μmho cm^{-1}).

$$1 \text{ mS } m^{-1} = 10 \text{ μmho } cm^{-1} = 1 \text{ μS } cm^{-1} \quad (2.6)$$

The relationship between EC and TDS is not directly linear, however, since the conductive mobility of ionic species is variable. Univalent cations such as Na^+ and K^+ are more mobile than multivalent ions such as Ca^{2+} and Al^{3+}. Similarly, univalent anions such as Cl^- and NO_3^- are more mobile than multivalent anions such as SO_4^{2-} and CO_3^{2-}, which are in turn more mobile than charged humic substances. Thus, stream water with Na^+ and Cl^- as its dominant dissolved species will have a higher conductivity than one dominated by Ca^{2+} and SO_4^{2-} if the pH and electrolyte strength are the same. Electrical conductivity is proportional to the sum of cations and anions, and roughly equivalent to total dissolved solids (TDS) in water. The relationship between EC and TDS is expressed by Equation (2.7) (Taylor, Elliott & Navritsky, 2018).

$$\text{TDS (mg } L^{-1}) = \text{EC (μS } cm^{-1}) \times 0.65 \quad (2.7)$$

Since the movement of ions under an electrostatic potential increases with increasing temperature, EC values are temperature-dependent. Most EC data are corrected to

25°C and the values are then technically referred to as specific electrical conductivity (SEC). An arbitrary constant is commonly used for temperature compensation assuming that the relationship between EC and temperature is linear; for example, a 2% increase in EC per 1°C (Qureshimatva *et al.* 2015; Lukubye and Andama 2017). Electrical conductivity is widely used for monitoring the mixing of fresh and saline water, for separating stream hydrographs and for geophysical mapping of contaminated groundwater. Distilled water should typically have an EC of less than 0.3 µS cm^{-1}. For groundwater, EC values greater than 500 µS cm^{-1} indicate that the water may be polluted, although values as high as 2000 µS cm^{-1} may be acceptable for irrigation water. In Europe, the EC of drinking water should be no more than 2500 µS cm^{-1}. Water with a higher TDS may have water quality problems and be unpleasant to drink (Lukubye and Andama 2017).

a(vi) Density, Specific gravity and Specific weight

In SI terms, density ρ is defined as mass per unit volume, represented as g L^{-1} or kg m^{-3}. Due to the possibility of density currents forming in sedimentation tanks, chlorine contact tanks, and other treatment units, density is a crucial physical property of wastewater. When it comes to density, home wastewater (which doesn't contain a lot of industrial waste) is about the same as water at the same temperature. Specific gravity S_w is frequently employed in wastewater engineering instead of density. By definition, specific gravity is expressed as given in Equation (2.8).

$$s_w = \frac{\rho_w}{\rho_o} \tag{2.8}$$

where ρ_w is the density of the wastewater; and ρ_o is the density of water.

Wastewater's specific gravity and density are both temperature-dependent and change depending on the amount of total solids present. A fluid's weight per unit volume is

known as its specific weight (γ). It is expressed as kN m^{-3} in SI units and given by Equation (2.9).

$$\gamma = \rho g \tag{2.9}$$

where g is the acceleration due to gravity, which is 9.81 ms^{-2} in SI units.

2.2.2.2 Inorganic chemical characteristics of wastewater

Inorganic chemical constituents of concern include nutrients, non-metallic constituents, metals, and gases. The sources of inorganic non-metallic and metallic constituents in wastewater derive from the background levels in the water supply and the additions resulting from domestic use, from the addition of highly mineralised water. Inorganic non-metallic constituents of importance include pH, nitrogen, phosphorus, alkalinity, chlorides, sulphur, gases and odours (Tan, Zhang and Liu 2022).

a. pH and Alkalinity

The pH is an important quality parameter of both natural water and wastewater. As a chemical component of the wastewater, pH has a direct influence on wastewater treatability, regardless of whether treatment is physical/chemical or biological. The decomposition of organic matter may lower the pH, while the presence of industrial wastewater may cause degrees of fluctuations. Generally, the pH of raw sewage falls between 5.5 and 9.0 (Lin, Nguyen & Lay 2017; Mujtaba & Lee 2017).

The presence of hydroxides (OH^-), carbonates (CO_3^{2-}), and hydrogen carbonates (HCO_3^-) of calcium, magnesium, sodium, potassium, and ammonia causes wastewater to become alkaline. The most common are calcium and magnesium hydrogen carbonates. Borates, silicates, phosphates, and similar chemical species can also contribute to alkalinity. The alkalinity in wastewater helps to resist changes in pH

caused by the addition of acids. Wastewater is normally alkaline, receiving its alkalinity from the water supply, the groundwater, and the materials added during domestic use. The measure of alkalinity in wastewater is necessitated by the chemical and biological treatment of the wastewater (Kumar 2016) in biological nutrient removal and ammonia removal by air stripping (Samy *et al.* 2022). Titrating against a standard acid yields the alkalinity. The outcomes, shown in mg/L of $CaCO_3$, are as follows:

$$CaCO_3 + 2H^+ \longrightarrow Ca^{2+} + CO_2 + H_2O \quad (2.10)$$

$$Ca \rightleftharpoons Ca^{2+} + 2e^-$$

$$\text{Alkalinity}, \frac{equivalent}{m^3} = \frac{milliequivalent}{L} = C_{HCO_3^-} + C_{CO_3^{2-}} + C_{OH^-} - C_{H^+} \quad (2.11)$$

$$1 \text{ milliequivalent mass of } CaCO_3 = \frac{100\ mg/mmole}{2\ meq/mmole} = 50\ mg/meq \quad (2.12)$$

b. Chlorides

Natural water contains chlorides due to the leaching of mineral rocks and soils containing chloride and from saltwater intrusion in coastal locations. Furthermore, the wastewater discharged to surface water bodies by home, agricultural, and industrial sources contains chlorides. Higher than normal chloride concentrations can be interpreted as a sign that a water body is being utilised for trash disposal because traditional wastewater treatment techniques do not significantly remove chloride. High levels of sulphates and chlorides may also come from groundwater seeping into sewers next to seawater.

c. Nitrogen

Nitrogenous substances derived from plants and animals, atmospheric nitrogen, and sodium nitrate are sources of nitrogen compounds. One common example of nitrogen derived from decomposing plant matter is ammonia, which is obtained by the

distillation of bituminous coal. There is a mineral deposit of sodium nitrate. Since there isn't much naturally occurring $NaNO_3$, atmospheric nitrogen is biologically fixed by a mediated process, with the majority of nitrogen coming from biological sources in soil and groundwater. Depending on the specifics of the biochemical reaction, nitrogen might be in a positive or negative oxidation state; the reaction can also be aerobic or anaerobic.

Biological nitrogen fixation (BNF) occurs when atmospheric nitrogen is converted to ammonia by an enzyme called nitrogenase, which is given in Equation (2.13).

$$N_2 + 8H^+ + 8e^- \rightarrow 2NH_3 + H_2 \quad (2.13)$$

Equation (2.14) shows the process coupled to the hydrolysis of 16 equivalents of ATP and is accompanied by the co-formation of one molecule of H_2 (James, 2017) and 16 equivalents of ADP.

$$N_2 + 8H+ + 8e- + 16ATP \rightleftarrows 2NH_3 + H_2 + 16ADP \quad (2.14)$$

Enzymes responsible for nitrogenase action are often very susceptible to destruction by oxygen. For this reason, many bacteria cease production of the enzyme in the presence of oxygen. Many nitrogen-fixing organisms exist only in anaerobic conditions (James 2017). In an aqueous solution, ammonia nitrogen can exist as either the ammonium ion (NH_4^+) or as ammonia gas (NH_3), contingent upon the pH level of the solution:

$$NH_4^+ \rightleftarrows NH_3 + H^+ \quad (2.15)$$

Total Kjeldahl Nitrogen (TKN) is the sum of organic nitrogen and ammonia. In the simplified TKN method, inorganic and organic nitrogen are oxidized to nitrate by digestion with peroxodisulphate. The nitrate ions react with 2,6-dimethylphenol in a solution of sulphuric and phosphoric acid to form a nitrophenol. Oxidized forms of nitrogen in the original sample (nitrite + nitrate due to sample preservation) are

determined in the second test vial and then subtracted, which results in TKN (Hicks *et al.* 2022).

High levels of oxidisable organic substances (COD) affect the reagent colour. This test procedure is therefore advised for wastewater only when the COD level is less than 500 mg/L (Phanwilai *et al.* 2020). No cumulative effects or influences of other ions were found. Wastewater samples that are purported to have high COD values are necessarily diluted to achieve highly accurate determinations. Dilution ratios are therefore employed to obtain the actual COD values. Table 2.6 shows the determinant concentrations that do not cause interference.

d. Phosphorus

The usual forms of phosphorus in an aqueous solution are orthophosphates, polyphosphates, and organic phosphates. Without additional breakdown, the orthophosphates (OP), also known as reactive phosphates (RP), such as PO_4^{3-}, HPO_4^{2-}, $H_2PO_4^-$, and H_3PO_4, are available for biological metabolism. Polyphosphate (PP) is a general term for several linked water-soluble phosphate molecules. The molecules are linked to each other by oxygen atoms, which determine the molecule's chemical properties and stability (Kullberg 2016). In an aqueous solution, PP hydrolyzes to produce the OP forms, however, this process is often extremely sluggish.

The OPs such as ATP (Adenosine Triphosphate) are formed primarily by biological processes. ATP is a chemical compound that breaks down to release energy in the body. OPs enter sewage via human waste and food residues and can be formed from orthophosphates in biological treatment processes or by receiving water biota.

Table 2.6: Determinants and their levels below which interference would not occur for TKN

Interfering determinant	Interference level
Cd^{2+}	50 mg/L
Ca^{2+}	50 mg/L
Cl^{-}	500 mg/L
Cr^{6+}	5 mg/L
Co^{2+}	10 mg/L
Cu^{2+}	50 mg/L
Fe^{2+}	10 mg/L
Fe^{3+}	50 mg/L
Pb^{2+}	50 mg/L
Ni^{2+}	50 mg/L
NO_2^{-}	2 mg/L
K^{+}	500 mg/L
Ag^{+}	100 mg/L
Na^{+}	500 mg/L
Sn^{2+}	50 mg/L
Zn^{2+}	50 mg/L

e. Sulphur

Sulphur is needed for the synthesis of proteins and is released during their degradation; it is reduced biologically under anaerobic conditions to sulphide, which can then combine with hydrogen to form hydrogen sulphide, according to the reactions in Equations (2.16) and (2.17). The sulphate ion is found naturally in most freshwater and is also present in wastewater (Lin *et al.* 2018).

$$\text{Organic matter} + SO_4^{2-} \xrightarrow{bacteria} S^{2-} + H_2O + CO_2 \quad (2.16)$$

$$S^{2-} + 2H^{+} \xrightarrow{bacteria} H_2S \quad (2.17)$$

A typical example is the presence of lactic acid as the precursor organic chemical matter, which reduces sulphate to sulphide as expressed in equation (2.18).

$$2CH_3CH(OH)COOH + SO_4^{2-} \xrightarrow{bacteria} 2CH_3COOH + S^{2-} + 2H_2O + 2CO_2 \quad (2.18)$$

When H_2S gas diffuses into the headspace above wastewater in sewers, it tends to gather and build up at the pipe's crown. The Biological oxidation of H_2S to sulphuric acid, H_2SO_4, (Equation 2.19) leads to corrosion of the concrete sewer pipes.

$$H_2S + 2O_2 \xrightarrow{bacteria} H_2SO_4 \quad (2.19)$$

The corrosive effect of the H_2SO_4 is referred to as “crown rot” (Suwarno & Nasir 2020).

f. Gases

Gases that are commonly associated with wastewater are N_2, O_2, CO_2, H_2S, NH_3 and CH_4. N_2, O_2 and CO_2 are gases that are commonly found in the atmosphere and waters that are exposed to air have them dissolved in them to varying degrees (Koh and Shaw 2017). H_2S, NH_3 and CH_4 are products of the degradation of organic matter present in wastewater.

2.2.2.3 Metallic composition of wastewater

Most waterways include trace levels of various metals, including mercury (Hg), nickel (Ni), zinc (Zn), cobalt (Co), cadmium (Cd), chromium (Cr), copper (Cu), iron (Fe), lead (Pb), and manganese (Mn). Metals such as Cd, As, Cu, Pb, Hg, Ni, and Zn are classified as priority pollutants, while Cu, Fe, Mn, and Zn are necessary growth agents for biological life such as algae (Sunday, Henrietta and Monday 2017). For healthy

growth, all living things need different levels of metals like Fe, Cr, Cu, Zn, and Co. These same metals can pose a danger when their presence is above threshold levels. Tables 2.7 and 2.8 present minerals and their potential applications in wastewater. With the increased use of treated wastewater effluent for horticulture, landscape irrigation, and agriculture, a study is required to prevent any unfavourable outcomes. The determination of the sodium adsorption ratio (SAR), a crucial component in evaluating the appropriateness of treated wastewater for agricultural applications, depends on the presence of calcium (Ca), magnesium (Mg), and sodium (Na).

Groundwater infiltration, commercial and industrial emissions, and residential discharges are some of the sources of trace metals in wastewater. Industrial effluent frequently contains cadmium, chromium, lead, and mercury. Wastewater from industries that manufacture electronics frequently contains the hazardous anion fluoride. Instrumental techniques such as flame atomic absorption, electro-thermal atomic absorption, inductively coupled plasma, or ICP-mass spectrometry are commonly used to identify the presence of these metals in wastewater. Metals in wastewater fall into four categories:

(1) The presence of dissolved metals in samples of unacidified wastewater that go through a 0.45 μm membrane filter;

(2) Metals suspended in unacidified wastewater and trapped on a 0.45 μm membrane filter are known as suspended metals;

(3) Total metals is a metric that quantifies the combined amount of suspended and dissolved metals, or the concentration of metals on an unfiltered wastewater sample following digestion; and

(4) Metals in solution that remain after treating an unfiltered wastewater sample with a hot, diluted mineral acid are known as acid-extractable metals.

Table 2.7 Minerals and their potential applications in wastewater

Metal	Nutrients for growth		Threshold concentration. of inhibitory effect on heterotrophic organisms (mg/L)	Used to determine SAR for land application of effluent	Used to determine if bio-solids are suitable for land application
	Macro	Micro			
Arsenic (As)			0.05		✓
Cadmium (Cd)			1.0		✓
Calcium (Ca)	✓			✓	
Chromium (Cr)		✓	1.0		
Cobalt (Co)		✓			
Copper (Cu)		✓	1.0		✓
Iron (Fe)	✓				
Lead (Pb)		✓	0.1		✓
Magnesium (Mg)	✓	✓		✓	
Manganese (Mn)		✓			
Mercury (Hg)			0.1		✓

Table 2.8: Minerals and their potential applications in wastewater

Determinant	Nutrients for growth		Threshold concentration of inhibitory effect on heterotrophic organisms	Used to determine SAR for land application of effluent	Used to determine if bio-solids are suitable for land application
	Macro	Micro	mL		
Molybdenum (Mo)		✓			✓
Nickel (Ni)		✓	1.0		✓
Potassium (K)	✓				
Selenium (Se)		✓			✓
Sodium (Na)	✓			✓	
Tungsten (W)		✓			
Vanadium (V)		✓			
Zinc (Zn)		✓	1.0		✓

2.2.2.4 Organic constituents

Most organic compounds are composed mainly of carbon, hydrogen and oxygen, and in some cases, nitrogen or sulphur. In wastewater, the organic matter consists of carbohydrates (25 – 50 %), lipids (8 – 12 %), and proteins (40 – 60 %). Human and animal urine contains urea, which is an organic compound, and is present in only fresh wastewater because it rapidly degrades to other products, and it is seldom found in stale wastewater. Other organic chemicals are also present in wastewater. According

to Kim *et al*. (2022), the organic content of wastewater is ascertained by quantifying individual organic molecules and utilising aggregate organic matter, which consists of certain organic elements with comparable features that are indistinguishable from one another.

To measure aggregate organic matter in wastewater, whose concentration is greater than 1.0 mg/L, methods commonly used include (1) biochemical oxygen demand, BOD_5, (2) chemical oxygen demand, COD, and (3) total organic carbon, TOC. Gas chromatography and mass spectroscopy are used to determine trace organic material with trace concentrations in the range of 10^{-12} to 10^{0} mg/L (Kim *et al*. 2022; Kabdash, Sunay, and Orhon 2022).

a). Biochemical oxygen demand (BOD_5)

Measuring the dissolved oxygen (DO), which microbes employ in the metabolic oxidation of organic materials, takes five days to complete. When assessing the risk of oxygen depletion in a particular water or wastewater system, this metric is crucial. The aerobic biological breakdown of organic matter will proceed until all of the materials are consumed when oxygen is available. Complete oxidation (combustion) of organic materials yields identical products no matter what the organic starting material is. Equations (2.20) and (2.21) are general forms.

$$C_nH_aO_bN_c + O_2 \rightarrow CO_2 + H_2O + NH_3 \quad (2.20)$$

$$C_nH_aO_bN_c + \left(\frac{n+a}{4} - \frac{b}{2} - \frac{3c}{4}\right) O_2 \rightarrow nCO_2 + \left(\frac{a}{2} - \frac{3c}{2}\right) H_2O + cNH_3 + \text{energy} \quad (2.21)$$

In the presence of bacteria, thermal oxidation is subdued, and the bacteria biologically oxidise the organic matter in aerobic digestion; but the reaction takes a longer time duration. Equation (2.22) demonstrates the bacterial activity.

$$C_nH_aO_bN_c+\left(\frac{n+a}{4}-\frac{b}{2}-\frac{3c}{4}\right)O_2+\text{bacteria}\rightarrow nCO_2+\left(\frac{a}{2}-\frac{3c}{2}\right)H_2O+cNH_3+\text{energy} \quad (2.22)$$

If cell tissue is represented by the empirical formula, $C_5H_7NO_2$, the bacteria trap the energy released in Equation (2.22) as they use oxygen and organic matter to build new cell tissues. Equation (2.23) is a typical demonstration of this.

$$C_nH_aO_bN_c+\left(\frac{n+a}{4}-\frac{b}{2}-\frac{3c}{4}\right)O_2+\text{bacteria}+\text{energy}\rightarrow C_5H_7NO_2 \quad (2.23)$$

Equation (2.24) is the endogenous respiration.

$$C_5H_7O_2N+5O_2\rightarrow 5CO_2+NH_3+2H_2O \quad (2.24)$$

If only the oxidation of organic carbon present in wastewater is considered, the ultimate BOD is the oxygen to complete the three reactions (2.20), (2.21) and (2.22). This is oxygen requirement, also known as the Ultimate Carbonaceous or First-stage BOD (uBOD). Under anoxic conditions, endogenous respiration occurs, a situation in which living organisms oxidize some of their cellular mass instead of new organic matter they adsorb or absorb from their environment (Li, Song and Visvanathan 2019).

Endogenous respiration is an energy requirement for organism maintenance, where a fraction of the active organism mass is oxidized to provide energy for the maintenance of the mass remaining. The mass of organisms that "disappears" is directly equated to the oxygen consumption for endogenous respiration. An unbiodegradable fraction remains and accumulates as an endogenous residue (van der Merwe *et al.* 2018). The modelling of the endogenous decay rate in Equation (2.25) is a first-order process for the active heterotroph biomass concentration (Ezechi *et al.* 2015).

$$\frac{dZ_{BH}}{dt}=-b.Z_{BH} \quad (2.25)$$

Z_{BH} = Active heterotroph biomass concentration (mgCOD/L), b = Specific endogenous decay rate (d^{-1}).

A fraction (*f*) of the mass that disappears remains as an endogenous residue; the rate of accumulation is given in Equation (2.26).

$$\frac{dZ_E}{dt} = f.b.Z_{BH} \quad (2.26)$$

Z_E = Endogenous residue concentration (mgCOD/L), f = Endogenous residue fraction. The net organism mass that disappears (mgCOD/L/d) is the oxygen consumed for endogenous respiration, which is expressed in Equation (2.27).

$$O_E = (1 - f).b.Z_{BH} \quad (2.27)$$

O_E = Oxygen consumed during endogenous respiration (mgO/L/d).

The endogenous decay rate parameter, *b*, is determined experimentally by aerating a batch of mixed liquor for several days while monitoring the oxygen uptake rate (OUR) (Ezechi *et al.* 2015).

The endogenous decay consumes the oxygen of nitrate in the denitrification step represented in Equation (2.28).

$$C_5H_7O_2N + 5NO_3^- \rightarrow 5CO_2 + 3\frac{1}{2}H_2O + NO + 4N_2 \quad (2.28)$$

b). Chemical oxygen demand (COD)

This is the measure of the oxygen-equivalent organic matter in wastewater that can be oxidised chemically using dichromate or permanganate in an acid solution (Dhanjal *et al.* 2019). Equation (2.29) shows that organic nitrogen selects the dichromate when it is in the reduced state (oxidation number = -3).

$$C_nH_aO_bN_c + dCr_2O_7^{2-} + (8d+c)H^+ \longrightarrow nCO_2 + (\frac{a+8d-3c}{2})H_2O + cNH_4^+ + 2dCr^{3+} \quad (2.29)$$

where $d = \frac{2n}{3} + \frac{a}{6} + \frac{b}{3} + \frac{c}{2}$

The chemical oxygen demand (COD) is a measure of water and wastewater quality. Utilising the COD test to track water treatment plant efficacy is common. COD is the

amount of oxygen consumed to chemically oxidize organic water contaminants to inorganic end products. High COD/BOD levels in stormwater runoff are caused by the residual food and beverage waste from cans/bottles, antifreeze, and emulsified oils from industrial food processing and agricultural activities. As most forms of COD are water-soluble, this pollutant spreads easily via stormwater to waterways.

c). Fat, Oil and Grease (FOG)

The generation of oily wastewater during the extraction of oil and gas is a serious problem in the petroleum industry due to the high volume generated and the chemical nature (toxicity and solubility) of the contaminants contained in this wastewater. Large volumes of heavily contaminated water are also generated during oil refining. The oil present in these wastewaters is classified as free, dispersed, emulsified or dissolved FOG. In untreated wastewater, the total FOG concentration can vary between 100 to 2,000 ppm (Cirne *et al.* 2016). The concentration of dispersed FOG is an important parameter for water quality and safety. FOG in water can cause surface films and shoreline deposits leading to environmental degradation and can induce human health risks when discharged in surface or groundwater sources. Additionally, FOG may interfere with aerobic and anaerobic biological processes and lead to decreased wastewater treatment efficiency. FOG analyses attempt to quantify compounds that have greater solubility in an organic solvent than in water. The main constituents of FOG are fats, soaps, fatty acids, hydrocarbons, waxes, and oils. The contribution of each of these substances will depend upon the origin of the wastewater being analysed and the type of extracting solvent used (Robillard, Gabriel and Williams 2018).

d). Surfactants

Large organic molecules that are slightly soluble in water and cause foaming in wastewater treatment plants and surface water are referred to as surfactants or surface-active agents. The most frequent component of surfactants is a very hydrophobic group, usually a hydrocarbon radical (R) with ten to twenty carbon atoms in it. There are two kinds of hydrophobic groups used: those that are ionising in water and those that are not. Negatively charged anionic surfactants are $(RSO_3N)^-Na^+$, while positively charged cationic surfactants are $(RMe_3N)^+Cl^-$. Surfactants that are non-ionizing, or non-ionic, usually have a polyoxyethylene hydrophilic group $ROCH_2CH_2OCH_2CH_2$…often written as Re_n, where n is the average number of -OCH_2CH_2 units in the hydrophilic group, is a common acronym for OCH_2OCH_2OH (Palmer and Hatley 2018). Surfactants tend to gather where the hydrophilic group in the water and the hydrophobic group in the air meet at the air-water interface. These substances accumulate on the surface of the air bubbles in wastewater during aeration, resulting in the formation of a very stable foam.

2.2.2.5 Biological characteristics

Wastewater contains bacteria, archaea, protozoa, fungi, viruses, algae, rotifers, helminths and nematodes. Sources are the soil (through infiltration) and human intestines. Table 2.9 gives an estimated biological composition of wastewater.

Table 2.9: Biological composition of wastewater

Organism	Description
Bacteria	- Unicellular organisms - Present in various forms and sizes - Main organisms responsible for the stabilisation of organic matter - Some bacteria are pathogenic, causing mainly intestinal diseases
Archaea	- Similar to bacteria in size and basic cell components - Different from bacteria in their cell wall, cell material and RNA composition - Important in anaerobic processes
Algae	- Autotrophic photosynthetic organisms, containing chlorophyll - Important in the production of oxygen in water bodies and some sewage treatment processes - In lakes and reservoirs, they can proliferate in excess, deteriorating the water quality
Fungi	- Predominantly aerobic, multicellular, non-photosynthetic, heterotrophic organisms - Also, of importance in the decomposition of organic matter - Can grow under low pH conditions
Protozoa	- Usually, unicellular organisms without a cell wall - Majority is aerobic or facultative - Feed themselves on bacteria, algae and other microorganisms - Essential in biological treatment to maintain an equilibrium between the various groups - Some are pathogenic

Viruses	- Parasitic organisms, formed by the association of genetic material (DNA or RNA) and a protein structure - Pathogenic and frequently difficult to remove in water or wastewater treatment
Helminths	- Higher-order animals - Helminth eggs present in sewage can cause illnesses
Rotifers	- microscopic aquatic animals of the phylum Rotifera, also called wheel animalcule -
Nematodes	- Commonly parasitic on humans - Examples include ascarids (Ascaris), filaria, hookworms, pinworms (Enterobius), and whipworms (*Trichuris trichiura*). -The species Trichinella spiralis, commonly known as the 'trichina worm', occurs in rats, pigs, and humans - They are responsible for the disease trichinosis.

Controlling diseases brought on by pathogenic bacteria and other organisms with human origins depends critically on the biological properties of wastewater (Litvinov *et al*. 2022).

2.2.2.6 Antibiotics

The environment's constant supply of antibiotics and their unchecked proliferation both contribute to disease resistance. As a result, drugs, including antibiotics, become less effective against germs and cause continual changes and the rise of new infections that are resistant to them. Abramova *et al.* (2020) categorised antibiotic detection techniques and based these techniques on the way antibiotics develop with various

wastewater effluents. The classification emphasised the detection techniques, which include using solid-state polarography to analyse the antibiotic concentration of dust. The improper disposal of pharmaceutical and personal care products (PPCPs) into the environment raises significant concerns regarding the possible negative effects on the health of both humans and animals. Osuoha, Anyanwu and Ejileugha (2023) reported these contaminants in surface water, groundwater, and wastewater treatment facilities at varying amounts. Most PPCPs are hazardous to living things, both acutely and over time. They harm the feeding, mating, metabolic processes, and reproductive habits of fish, invertebrates, and higher vertebrates, including humans. They also negatively affect the structure and function of the algal community. Another health risk is the development of antibiotic resistance in bacterial populations as a reaction to PPCP pollution. There is increasing awareness regarding the effect of antibiotics on various organisms in the ecosystem even though they may occur at relatively low concentrations. Thus, their concentration needs quantification precisely in various matrices including groundwater, surface water, and municipal wastewater. The use of liquid chromatography together with high-resolution mass spectrometry (HR-LC-MS/MS) has enhanced the reliability, accessibility, and accuracy of detecting antibiotics. Mohapatra, Padhye and Mukherji (2018), developed an HR-LC-MS/MS-based method for four antibiotics (ciprofloxa+cin, norfloxacin, azithromycin, and sulfamethoxazole). The effect of solution pH, drying time of cartridge, and solvent used in the concentration step on the recovery of antibiotics during solid-phase extraction (SPE) was also evaluated. Subsequently, the recovery of antibiotics from influent and effluent wastewater samples, obtained from a wastewater treatment plant (WWTP) in India, was determined based on the matrix spike method. The results revealed that for these wastewater samples, even the use of structurally

similar, isotopically labelled (deuterated) standards could not adequately improve the recovery of target antibiotics.

Zhang *et al.* (2023) emphasised the prospects, obstacles, and future paths for microalgae-based methods to eliminate antibiotics from wastewater because of their special advantages, which include cost-effectiveness and environmental friendliness. In three significant wastewater treatment facilities in Finland, Kortesmäki *et al*. (2020) reported the concentrations of several antibiotics and their metabolites that belong to five different antibiotic families. For the extraction and analysis of the chemicals, the researchers used an online solid-phase extraction-liquid chromatography-tandem mass spectrometry approach. The environmental risk assessment underscored the significance of utilising technology in the efficient elimination of xenobiotics from wastewater.

2.2.2.7 Wastewater Pre-treatment

Using sophisticated wastewater treatment with microalgae cultivation to produce biomass and lipids for microalgae-based biofuel requires careful selection of the wastewater, robust microalgal species, and pre-treatment techniques. The majority of laboratories choose to sterilise materials by wet heat, or autoclaving, which involves heating the item under pressure with steam. Autoclaving and dry heating (baking and flaring) differ significantly in one important way. Radiation, solvents, and filtration are more techniques.

a). Autoclaving

In most laboratories, autoclaving, heating the material to be sterilised using pressured steam, is the preferred method of sterilisation. This approach is quite effective in killing all microorganisms, spores, and viruses; nevertheless, it is necessary to utilise

high temperatures or incubation times for certain specific bugs. By effectively hydrolyzing and coagulating cellular proteins in the presence of water, autoclaving eliminates microorganisms. Steam is the source of the tremendous heat. Pressured steam has a high latent heat, holding seven times as much heat at 100 ºC as water does at that same temperature. The release of this heat occurs when it comes into contact with the sterilisable material's cooler surface, facilitating quick heat delivery and effective penetration of thick materials (Leitzen *et al.* 2021).

Water is quite effective at hydrolyzing proteins at high temperatures, making those bugs virtually impossible to kill. The best conditions for autoclave sterilisation are ones in which the microorganisms are either directly touched by the steam or kept in a tiny amount of aqueous (mostly water) liquid. Steam at a pressure of roughly 15 psi under these circumstances will kill all organisms and their endospores in about 15 minutes when the temperature reaches 121 ºC. One of the fundamental laws of chemistry is that a gas's temperature rises according to its pressure. As in the case of free-flowing steam that is 100 ºC in temperature and 1 atmosphere above sea level pressure. The temperature increases to 121 ºC at a pressure of roughly 15 psi. By raising the pressure to 20 psi, the temperature rises to 126 ºC. Table 2.10 illustrates the link between temperature and pressure. In this sense, steam, being a gas, gains temperature in a closed system when its pressure increases. The penetration of water molecules in steam increases significantly with increasing energy. This idea shortens the time needed for autoclave sterilisation and cooking in a home pressure cooker. It is crucial to remember that moist heat, not pressure, is the sterilising agent.

Sterilisation of culture media, instruments, dressings, syringes, transfusion equipment, applicators, solutions, and many more items resistant to high pressure and temperatures is accomplished via autoclaving. To sterilise bacteriological media and

eliminate pathogenic cultures, the laboratory technician uses it. A microbiological laboratory's initial instrument order is usually the autoclave, which is equally helpful for glass and metalware. Large-scale industrial usage of autoclaves is another application.

Table 2.10 The relationship between pressure and temperature of steam at sea level

Pressure (psi above atm pressure)	Temperature (^{o}C)
0	100
5	110
10	116
15	121
20	126
30	135

The term "retort" refers to large industrial autoclaves, but the same idea also applies to ordinary pressure cookers used for food canning at home. Table 2.11 illustrates how the autoclave-sterilization time varies with container size.

Table 2.11 Effect of container size on autoclave sterilisation time for liquid solutions

Container size	Liquid volume (mL)	Sterilization time (min)
Test Tube (18x150 mm)	10	15
Erlenmeyer Flask (125 mL)	95	15
Erlenmeyer Flask (2000 mL)	1500	30
Fermentation Bottle (9000 mL)	6750	70

It is possible to determine whether heat treatment has succeeded in sterilising using some commercially available techniques. Devices to track internal temperature and maintain appropriate pressure are included in modern autoclaves. Even if such a device is present, the operator needs to regularly check pressure and maintain the proper pressure. Chemical reactions occur when the right temperatures and times are met, causing an indicator to change colour. Some designs include the words "autoclaved" or "sterile" printed on tapes or wrappings. The lack of information regarding the duration of suitable conditions maintained makes these recordings partially untrustworthy. Large packages should have tapes or other sterilisation indications placed inside and close to the middle to check if heat seeped through. Another technique involves melting a pellet within a glass container. Impregnated paper strips with preparations of specific species of bacterial endospores, including Bacillus stearothermophilus, are a commonly used test. A soft plastic vial contains an ampule of the medium and the spore strip. The vial is autoclaved after being positioned in the middle of the material that needs to be sterilised. One can aseptically inoculate these into culture media after autoclaving them. Growth in the culture medium suggests that the endospores are surviving and that the processing was insufficient. Some designs employ endospore suspensions that can be heated and then released into a culture medium that surrounds them inside the same vial.

b). Dry Heating (Flaming, Baking)

Dry heating differs from autoclaving in one very important way. Protein hydrolysis is not possible since there is no water present. Rather, the oxidation of biological components caused by dry heat tends to destroy microorganisms. Higher temperatures are necessary for effective sterilisation by dry heat since this needs more energy than

protein hydrolysis. For instance, autoclaving at 121 ºC can often achieve sterilisation in 15 minutes, while dry heating would typically require a temperature of 160 ºC to achieve sterility in a comparable length of time (Rashed *et al*. 2020).

c). Filtration

Filtration is a great way to quickly sterilise solutions without heating. Filters, of course, work by passing the solution through a filter with a pore diameter that is too small for microbes to pass through. Filters can be sintered glass funnels made from heat-fused glass particles or, more commonly these days, membrane filters made from cellulose esters. For the removal of bacteria, filters with an average pore diameter of 0.2 μm are normally used. But viruses and phages can pass through these filters, so filtration is not a good option if these are a concern (Bani-Melhem *et al.* 2023).

d). Solvents

Commonly employed as a disinfectant, ethanol is probably not the best choice because isopropanol works better as a solvent for fat. Both require dilution to 60–90 % in water for optimal activity, as they denaturize proteins through a mechanism that necessitates water. It's crucial to remember that while ethanol and IPA are effective in eliminating microorganisms, they do not affect spores (Acharya and Chaudhuri 2021).

e). Radiation

Electromagnetic radiation such as UV, x-rays, and gamma rays may cause significant harm to DNA, which is why they are effective for sterilisation. Their penetration is the primary distinction between them in terms of efficacy. Sterilisation only happens in a short region surrounding the lamp due to UV's limited ability to penetrate the air. It is, nevertheless, reasonably safe and helpful for sterilising small spaces, such as laminar

flow hoods. Due to their greater penetration, gamma and X-rays are more hazardous but also very effective when used for large-scale cold sterilisation of plastic products (such as syringes) during the production process (Yuan et al. 2023).

2.3 The Algae

Algae represent a large group of different organisms from different phylogenetic groups, representing many taxonomic divisions. They are plant-like organisms that are usually photosynthetic and aquatic but do not have true roots, stems, leaves, or vascular tissue and have simple reproductive structures. They are distributed worldwide in the sea, in freshwater and moist areas on land. Most are microscopic, but some are quite large, such as some marine seaweeds that can exceed 50 m in length. Also, depending on their origin, algae are referred to as terrestrial algae, snow algae, seaweeds, phytoplankton and "pond scums" (which are composed of stringy masses of cyanobacteria), as well as true algae such as Spirogyra (Jyothi, Krishna and Mohan 2016).

Algae are morphologically simple, chlorophyll-containing organisms that range from microscopic and unicellular (single-celled) to very large and multicellular. The algal body is relatively undifferentiated and there are no true roots or leaves. Algae are typically autotrophic, deriving their nutrients, or energy, from their surroundings in the form of sunlight. They play an important role in food chains and in maintaining the oxygen supply on our planet. Algae are sometimes considered plants and sometimes considered postists (a grab-bag category of generally distantly related organisms that are grouped based on not being animals, plants, fungi, bacteria, or archaeans).

Multicellular marine algae, or seaweeds, are plant-like organisms that generally live attached to rocks or other hard substrata in coastal areas. They belong to three different

groups, recognized since the mid-nineteenth century based on thallus colour: red algae (phylum Rhodophyta), brown algae (phylum Ochrophyta: class Phaeophyceae), and green algae (phylum Chlorophyta: classes Bryopsidophyceae, Chlorophyceae, Dasycladophyceae, Prasinophyceae, and Ulvophyceae). As a result of modern investigations (ultrastructural and biochemical studies and, more recently, phylogenetic analyses based on DNA sequencing), we now know that the differences among these three groups run beyond the colour differences suggested by their names. The three seaweed groups differ considerably in many ultra-cultural and biochemical features, including what photosynthetic pigments they contain, what chemical compounds they use for energy storage, the composition of their cell walls, the presence/absence of flagella, details of mitosis, the types of connections between adjacent cells, and the fine structure of the chloroplasts (Wall, Dumont and Murphy 2018).

Some of the larger brown algae known as kelps, such as the giant kelp (also known as giant bladder kelp) *Macrocystis pyrifera*, exhibit translocation (internal transport of organic materials and nutrients) and a similar process have been shown to occur in the green Charophytes, but translocation is not seen in most algal groups. In general, however, algae have little need for transporting nutrients through their bodies because they are, at some stage, surrounded by water and individual cells can therefore exchange materials directly with their surroundings.

2.3.1 Varieties of algae

Diatoms, Chlorophyta, Euglenophyta, Dinoflagellata, Chrysophyta, Phaeophyta, Rhodophyta, and Cyanobacteria are the principal phylogenetic families of algae. Below are the paragraphs that discuss each of these groups:

i. Diatoms

These are unicellular members of the kingdom Protista, distinguished by their frequently exquisite and intricately sculpted silica shells. While some diatoms combine to form colonies, most diatoms exist alone. In freshwater and saltwater, moist soil, and on the damp surface of plants, they are typically yellowish or brownish. Because of the availability of both light and (winter-regenerated) nutrients, fresh-water and marine diatoms are most abundant early in the year, a phenomenon known as the Spring Bloom. They divide their cells asexually to reproduce. As aquatic diatoms die, their shells fall to the bottom where they accumulate in the ooze and eventually become diatomaceous earth since they are not vulnerable to decomposition. Figure 2.2 shows the different shapes and types of diatom.

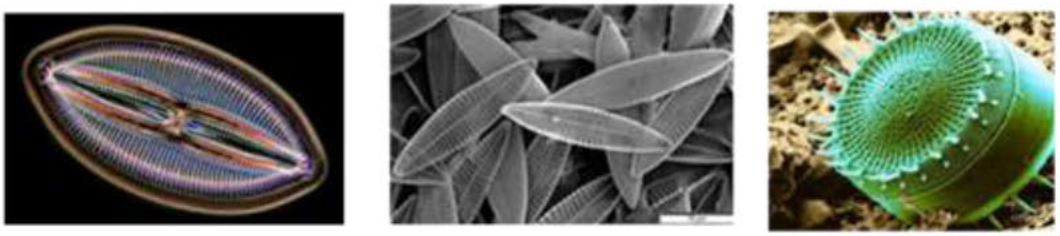

(a) (b) (c)

Figure 2.2 Shapes and morphology of diatoms: (a) Simply identified as Diatom (b) Lyrella sp. (c) Freshwater diatom

Diatoms can also exist in a more compact form than diatomite, a soft, chalky, and light rock. Diatomite is used to make dynamite and other explosives, filters, abrasives, and similar items, as well as an insulator against sound and heat. The majority of the limestone on Earth was accumulated by diatoms, and diatoms are the source of most petroleum. Diatoms are nearly always present in the surface mud of a lagoon, ditch, or pond (Goessling 2017).

ii. Chlorophyta

This group of organisms, which goes by the name "green algae," is a subclass of the kingdom Protista. Algae come in a wide variety of forms and environments, but green algae are the most diversified. Like plants, they are green in colour because they have pigments called chlorophyll. However, under unfavourable weather, some also show up in red. Whereas chlorophyll-b absorbs reddish-blue light, chlorophyll-a absorbs blue-violet light. Greenlight is either reflected or transmitted by chlorophyll, so it appears green even though neither chlorophyll-a nor chlorophyll-b can absorb it.

Figure 2.3 Chlorophyta at different magnifications

Green algae come in a variety of morphologies, including bag-like colonies, spherical colonies, flagellated and motile forms, long filament and thread-like forms, and multicellular and unicellular species that contain several nuclei in a single cell. Figure 2.3 presents Chlorophyta in different magnifications. While some green algae can also be found in coastal habitats, such as Ulva, the majority of green algae are found in freshwater, and wet soil, and adhered to rocks and tree bark. Green algae can photosynthesize. But unlike red algae, they absorb red light, which has a lower energy wavelength. These algae are found adhering to rocks in low-tide places because red light cannot travel very far below the surface of the ocean. Certain green algae exhibit symbiotic relationships with lichens and fungi.

iii. Euglenophyta

Eclypteran eukaryotes, or excavated eukaryotes, belong to the small phylum Euglenophyta, also called Eugenides or Euglenoids, which is a phylum of the Kingdom Protista and largely consists of unicellular aquatic algae. While some euglenoids are heterotrophic and able to absorb or consume their food, others have chloroplasts with pigments used in photosynthetic processes. Cells divide longitudinally during reproduction.

Figure 2.4 Euglenaphyta structure and shapes

The majority are freshwater creatures. Common in ponds and pools, the most distinctive genus is Euglena, which becomes more apparent when runoff from fertilizer-treated lawns or fields contaminates the water. About a thousand species of euglenoids exist.

iv. Dinoflagellata

There are many flagellate protists in this group. While many species are photosynthetic and possess chlorophyll, some are heterotrophic. There's a chance that other pigments will cover up these chlorophylls' green colour. Other species are crucial to the biology of coral reefs as endosymbionts of protozoa and marine mammals. A few types of dinoflagellates are parasitic, whereas others are colourless predators of other protozoa. The majority of dinoflagellates reproduce asexually by dividing their cells simply after

going through mitosis. Because they are significant components of plankton, dinoflagellates serve as the main food supply in warmer oceans. Figure 2.5 shows the structure and shape of *Dynoflagella.* Numerous types exhibit phosphorescence, which

(a) (b) (c)

Figure 2.5 Dinoflagellata: (a) Dinoflagellates algae (b) The fire algae (plantlet) (c) Freshwater dinoflagellate (Ceratium hirundinella)

is mostly what makes tropical seas phosphorescent at night. Dinoflagellates come in over 2000 different species.

v. Chrysophyta

Mostly found in freshwater, Chrysophyta is a broad category of eukaryotic algae also known as golden algae. They were once thought to comprise all such forms, except for diatoms and multicellular brown algae, but they have now been separated into some distinct families according to factors such as pigmentation and cell shape. Numerous chrysophytes have cell walls made primarily of cellulose and silica in significant amounts. Figure 2.6 has different presentations of the golden algae, courtesy,

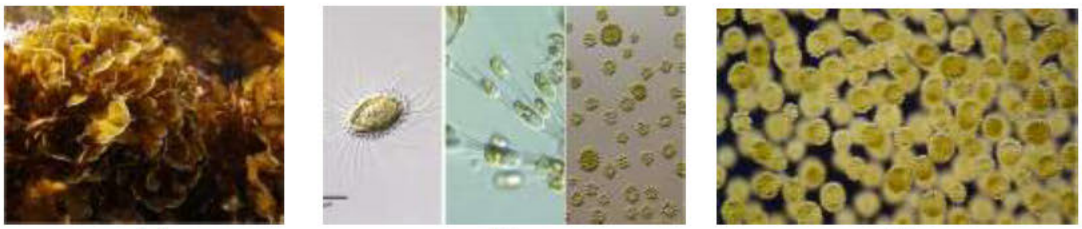

(a) (b) (c)

Figure 2.6 Chrysophyta: (a) Golden algae (b) Rocky mountain lake algae (c) Synura uvella

They have the photosynthetic pigments chlorophyll a and c, which were once considered to be characteristics of plants. They can reproduce sexually in certain situations, although cell division is the most common method.

vi. Phaeophyta

The organisms typically referred to as brown algae belong to this phylum within the kingdom Protista. Members of Phaeophyta include many of the well-known seaweeds found worldwide. Similar to chrysophytes, fucoxanthin, a dominant xanthophyll pigment, gives brown algae their colour by hiding other xanthophylls like beta-carotene, chlorophyll-a and -c (as there is no chlorophyll-b), and other colours. The appearances of Phaeophyta in Figure 2.7 presents different brown algae.

(a) (b) (c)

Figure 2.7 Phaeophyta (brown algae): (a) Brown algae (b) Phaeophyceae (c) Hormosira banskii

Generally, food reserves consist of higher alcohols, sugars, and complex polysaccharides. Brown algae, with very few exceptions, are marine plants that thrive in the world's coldest waters. Many of them do so in the tidal zone, where they are constantly under stress from waves, while others grow in deep water (Din *et al*. 2022). Phaeophyta has roughly 1500 species.

vii. Rhodophyta

This is the kingdom Protista's phylum, which includes the photosynthetic creatures known as red algae. Auxiliary pigments known as phycobilins give members of this

division their distinctive clear red or purplish colour. The multicellular red algae have a high degree of branching without the ability to differentiate into complex tissues. This group includes the majority of seaweeds found worldwide. All oceans include red algae, although warm-temperate and tropical temperatures are home to the majority of red algae populations, which may exist at depths greater than those of any other photosynthetic creature. This is the proper home for the majority of coralline algae, which release calcium carbonate and are essential to the development of reefs. Oriental cuisine traditionally includes red algae. Figure 2.8 presents different species of Rhodophyta.

(a) (b) (c)

Figure 2.8 Rhodophyta (Red algae): (a) Plocamium telfairiae (b) Schmitzia japonica (c) Griffiunsia subcylindrica

Four thousand species of red algae are known to exist in the ocean; a few also exist in freshwater. Machín-Sánchez, Gil-Rodríguez, and Haroun (2018) examined the red algal Laurencia complex (Rhodomelaceae, Rhodophyta) in South Africa and emphasised the value of the South African flora when discussing distribution patterns and biogeographic relationships within this diverse assemblage of red algae, as well as the significance of incorporating South African and SWIO floras when assessing global diversity in the Laurencia complex.

viii. Cyanobacteria

In contrast to the other algal groups, which are all eukaryotes, cyanobacteria, also known as cyanophyta, cyanophyceae, cyanoprokaryota, or blue-green algae, are a prokaryotic group of Gram-negative bacteria that are the major microorganism phyla. They obtain their energy through photosynthesis. The most prevalent and morphologically varied group of organisms in habitats, cyanobacteria can take the shape of filamentous, unicellular, planktonic, benthic, or colonial (coccoid) forms. Contrary to their name, filamentous colonies can develop into three different cell types: red, brown, or yellow. The Red Sea got its name from red species blooms, which are dense masses on the water's surface (Liu *et al.* 2015). Figure 2.9 showcases the cynobacterial boom, species and cell structure.

(a) (b) (c)

Figure 2.9 Cyanobacteria (Blue-green algae): (a) Cyanobacteria boom (b) Spirulinaceae (c) Cell structure

There are two primary types of pigmentation: most cyanobacteria have a characteristic blue-green to greyish-brown hue due to the presence of chlorophyll-a and a variety of proteins known as phycobilins. Some genera, on the other hand, are vivid green because they have both chlorophyll-a and chlorophyll-b instead of phycobilins. In contrast to bacteria, which are heterotrophic decomposers of garbage and other species' bodies, cyanobacteria are pigment-containing organisms that can undertake

photosynthesis because they possess the green pigment chlorophyll along with other pigments. Therefore, cyanobacteria make their food by autotrophic means using basic raw resources. Only carbon dioxide and nitrogen are required for nitrogen-fixing cyanobacteria to survive. These bacteria can fix nitrogen gas, which plants are unable to absorb, into ammonia (NH_3), nitrites (NO_2^-), or nitrates (NO_3^-), which plants can then absorb and use to produce protein and nucleic acids (Helliwell *et al*. 2016). Certain cyanobacteria species create toxins that are harmful to both people and animals. Drinking or bathing in tainted water can expose people to cyanobacterial toxins (Liu *et al.* 2015). An evolutionary varied group known as cyanobacteria and eukaryotic algae can adapt to microhabitats by having changeable genomes that may express different genes in response to different environmental factors.

2.3.2 Microalgae

The unicellular microscopic algae are known as microalgae. Microalgae are also commonly called phytoplankton. Many microalgae are autotrophs, which use photosynthesis to produce food. Some heterotrophic microalgae can grow in the dark by utilizing sugars. A few microalgae grow by combining both nutritional modes and they are called mixotrophic algae (Martonen 2017). Diatoms and dinoflagellates are the two types of microalgae. Diatoms can be spheres, triangles, ellipticals or stars. A silica shell serves as the cell wall of diatom cells, protecting the cells. Many dinoflagellates comprise two flagella for their movement through the water. Both diatoms and dinoflagellates comprise oils in their cells, helping them to swim. Both diatoms and dinoflagellates can grow very quickly and cause algal blooms.

Microalgae is a promising source of renewable biofuels, and the optimization and control of the biomass growth stage can make techno-economic improvements. Algae

do not compete with traditional food crops for space and resources (Bleakley and Hayes 2017). Among all varieties of algal organisms, microalgae are the most abundant in different environments. The cell size of unicellular eukaryotic algae typically is 3–30 μm and cyanobacteria are as small as 0.2–2 μm (Krustok 2016).

Microalgae biomass consists mainly of lipids, proteins, carbohydrates and pigments and the product range is very versatile as presented in Table 2.2 (Klinthong *et al.* 2015; Najafabadi *et al.* 2015)**.** These products range from high-value nutraceuticals, healthy food components and cosmetics to the lower-value commodities biofuels, food, fertiliser and application in wastewater treatment (Klinthong *et al.* 2015; Subhash *et al.* 2017).

Jyothi, Krishna and Mohan (2016) posited that algal species dominance of lakes occurs in response to changes in season, temperature, wind, precipitation patterns, and nutrient cycles. They have a short life span and respond quickly to environmental changes. Microalgae are a very useful tool for the biomonitoring of a water body about its pollution status. However, their unattended growth may pose serious consequences to other aquatic resources.

Different kinds of microalgae have been used in wastewater treatment. Wastewater characteristics and seasonal environmental conditions are some of the factors that affect the characteristics and the predominance of microalgae. Different researchers (Krustok 2016; Van Wagenen *et al.* 2016) examined the characterisations of algae species that are present in wastewater oxidation ponds and found that algae, consisting primarily of *Chlorella* and *Scenedesmus*, composed approximately 80 % of the solids inventory during the study period. *Chlorella* species are reported to be tolerant and adaptive and can survive under different wastewater physical and biochemical conditions (Van Wagenen *et al.* 2016). Figure 2.10 presents three different species of

microalgae, namely, *Chlorela vulgaris*, *Scenedesmus obliquus* and *Botryococcus braunii*.

(a) (b) (c)

Figure 2.10 Microalgae: (a) Chlorela vulgaris (b) Scenedesmus obliquus (c) Botryococcus braunii

Depending on the method of sludge separation, Mahmoud, Wang, and He (2022) used centrate as an initial source of water and nutrients for microalgal growth of *Chlorella sorokiniana*, *Encyonema caespitosum, Nitzschia thermalis, Scenedesmus sp., Synechocystis sp.,* and *Limnothrix sp*. mostly isolated from the habitats influenced by municipal wastewater. Two green algae were eligible. In the laboratory, the green algae *C. sorokiniana* and *Scenedesmus sp*. grew in the media composed of centrate or algal residue faster than in the mineral medium BG11, optimised for algal growth.

The enhanced productivity is mainly attributed to the photosynthesis known for the mixotrophic process and the presence of organic carbon in the wastewater, which serves as an extra source of energy. In the case of *C. sorokiniana*, an unusually high optimum temperature between 32 and 35°C was also an attributing factor to the enhanced productivity of algae. Besides, this study examines the variations in the lipid content of algae, which affects the overall oil productivity at biofuel plants. The results demonstrated that lipid content is a dynamic property, negatively correlated to the growth rate.

A variety of objectives are necessary to consider when choosing an algae species for emissions remediation. One main concern is economic practicability; it is important to evaluate if valuable co-products can come from the mass cultivation of algae (Mehta *et al.* 2018). Also, the level of tolerance to CO_2 is necessary to consider with the ultimate goal being to maximize CO_2 mitigation. Temperature tolerance is another limiting variable that must be considered. Most thermal power stations discharge gases at 120°C. Therefore, it is important to identify which algae strains can tolerate high temperatures to decrease cooling costs. These variables have been considered for many different types of algae including *Chlorella*, *Dunaliella*, *Spirulina* and *Scenedesmus*. Table 2.12 gives the average composition of some microalgae species (Klinthong *et al.* 2015). The physiological response of the different microalgae strains subjected to different growth conditions is an important step in screening microalgae for various applications. Lee *et al*. (2015) isolated three strains of the green microalga *Botryococcus braunii*: JJS, KCM, and KJD from different water bodies in Korea and grew them in batch cultures in the laboratory. The researchers investigated the effects of different growth media and temperatures on the growth rate of the strains, as well as the influence of temperature on the total lipid content and lipid profile. All three strains exhibited the highest growth rates in the BG-11 medium at 25 °C. The JJS strain had optimum lipid production (g L^{-1}) at 30 °C, while the KCM and KJD strains expressed optimal lipid production at 25 °C. However, on a dry weight basis, all three strains produced the highest percentage of total lipids at 15°C and had the lowest percentage at 25 °C. The most common fatty acids in all three strains were oleic acid, linolenic acid, and behenic acid (docosanoic acid), which is a cholesterol-raising saturated fatty acid in humans. However, the three strains exhibited considerable variation in their fatty acid profiles at different culture temperatures.

Table 2.12 Microalgae species and their composition

Microalgae species	Protein (%)	Carbohydrate (%)	Lipid (%)
Anabaena cylindrical	43 – 56	25 – 30	4 – 7
Aphanizomenon flos-aquae	62	23	3
Arthrospira maxima	60 – 71	13 – 16	6 – 7
Botryococus braunii	8 – 17	8 – 20	21
Chlamydomonas rheinhardii	48	17	21
Chlorella pyrenoidosa	57	26	2
Chlorella vulgaris	51 – 58	12 – 17	14 – 22
Dunaliella bioculata	49	4	8
Dunaliella salina	57	32	6
Euglena gracilis	39 – 61	14 – 18	14 – 20
Isochrysis sp.	31 – 51	11 – 14	11 – 20
Neochloris oleoabundans	20 – 60	20 – 60	35 – 54
Porphyridium cruentum	28 – 39	40 – 57	9 – 14
Prymnesium parvum	28 – 45	25 – 33	22 – 38
Scenedesmus obliquus	50 – 56	10 – 17	12 – 14
Spirogyra sp.	6 – 20	33 – 64	11 – 21
Spirulina maxima	60 – 71	13 – 16	6 – 7
Spirulina platensis	46 – 63	8 – 14	4 – 9
Synechococcus sp.	63	15	11
Tetraselmis maculate	52	15	3

Srirangan *et al.* (2015) investigated the marine microalgae *Dunaliella spp* for their great potential as feedstocks for renewable liquid transportation fuels because they could replace petroleum-derived fuels without competing for resources like land or

freshwater required for food and feed production at a variety of different temperatures and found *Dunaliella*'s optimal cell division temperature to be 20 °C (Srirangan *et al.* 2015; Wu *et al.* 2016). Using both Soerensen and McIlvain buffers, results supported the finding that *Dunaliella*'s optimal pH is in the range of 6.0 and 6.2 (Nielsen 2015). The approximate maximum CO_2 concentration in this species is 15 %. *Dunaliella* also proves to be suitable for more than just CO_2 mitigation. Depending on growth conditions *Dunaliella tertiolecta* can remove between 51 and 96 % of nitric acid present at 15 % CO_2 and 1000 ppm of NO (Sutherland *et al.* 2015). *Dunaliella* also provides useful by-products, such as β-carotene, which help with economic barriers to mass production. *Dunaliella spp*. grows in media containing an extremely wide range of NaCl concentrations from 0.05M to 5.5 M NaCl. The ability of *D. salina* to produce high levels of carotenoids made it commercially viable as a nutritional supplement. In contrast to *D. salina*, *D. viridis* does not accumulate large amounts of β-carotene but produces oxygenated carotenoids. *Dunaliella spp.* lacks a cell wall, which enables the extraction of lipids by osmotic shock in freshwater as one of the most inexpensive and environmentally friendly techniques to extract lipids from microalgae cultures. The techno-economic analysis identified microalgae lipid content and growth rates as the two top cost modifiers of fuel production (Srirangan *et al.* 2015).

Spirulina is another species that has demonstrated the potential for carbon capture. *Spirulina* has an optimal temperature range between 30 and 35°C (Klinthong *et al.* 2015). The optimal pH for *Spirulina* was found to be in a wide range between 8 and 11. *Spirulina* is not just used for CO_2 mitigation: as a result of its high protein content, *Spirulina* has been used for the production of food products and aquaculture nutrition (Bleakley and Hayes 2017). *Scenedesmus* is a strain that appears to be a reasonable option for mitigating large amounts of CO_2 emissions. Recent research showed that

Scenedesmus sp. has an optimal temperature of 27 °C with a growth rate of 0.0284 L/h (Hamouda *et al*., 2016). *Scenedesmus sp.* can also tolerate a high maximum CO_2 concentration, estimated to be 80 %. Based on previous results within the overall research project, *Scenedesmus* was selected as the algae to investigate further (Bleakley and Hayes 2017).

Bleakley and Hayes (2017) carried out batch experiments using the alga *Cladophora glomerata* to determine its growth rate in wastewater, nutrient removal potential in wastewater, and biofuel potential. Specific growth rates were highest in the effluent wastewater sample, with 0.115 grams of algae growth per gram algae per day (day^{-1}) and 0.159 day^{-1}. Nutrient concentrations in wastewater-grown *Cladophora glomerata* were determined to be approximately 0.0136 g phosphorus per dry weight (DW) gram of algae and 0.0415 g nitrogen per DW gram of algae. The predicted methane yield from *Cladophora glomerata* was calculated at 0.289 – 0.578 L CH_4/g DW algae.

Botryococcus braunii is a colonial *Trebouxyophiceae* (green microalgae) commonly associated with fresh and brackish water bodies. The potential of *Botryococcus braunii* as a renewable source of chemical feedstock or fuel has been explored and Rinna *et al.* (2017) evaluated the effect of wastewater as a nutrient source for two *Botryococcus braunii* strains, UTEX LB 572 and IBL C116. The fatty-acid composition was used to estimate the quality of the derived biodiesels. Both strains were compared based on their bioremediation efficiency. Both microalgae were cultivated under constant temperature (25 ± 1° C) and agitation (90 bpm), with enriched aeration (2.5 % CO_2 supplementation), and under a photoperiod of 12:12 h light: dark cycles (intensity at 174 μE m^2 s^{-1}). Wastewater effluent was used as a growth medium, and the standard growth medium (CHU-13) was also used as a control. The experiments were carried out in triplicates using 1 L borosilicate Pyrex flasks (0.6 L working volume). Their

goal was to identify which conditions would be more appropriate to generate the best biodiesel. Biodiesel quality is dependent on the FAME (fatty-acids-methyl-esters) molecular structure, which is responsible for the fuel properties of the generated biodiesels. Thus, algal biodiesels will have different fuel qualities, according to the diversity of fatty acid composition. The fuel quality is indicated mainly by parameters related to ignition, lubricating quality and oxidation stability; all can be evaluated by the following parameters: (i) Cetane Number (CN), which estimates the delay of ignition and combustion performance; the high the CN is, the best in the ignition quality; (ii) Iodine Value (IV), representing the total unsaturation within a mixture of FAME; (iii) the Saponification Value (SV), which represents the average molecular weight of all FA present in the oil; (iv) the Oxidation Stability (OS) estimates the biodiesel's susceptibility to deterioration, and is mainly related to the content of double-bonds in the mixture of FAME. The higher the polyunsaturated methyl ester content, the higher the biodiesel oxidation potential.

Krustok (2016) looked at the species, metabolic pathways and growth dynamics of both algae and bacteria. He used municipal wastewater, which was inoculated with algae and compared to non-inoculated reactors. The dominant algae in the tested systems belonged to the genera *Scenedesmus, Desmodesmus* and *Chlorella.* In addition to algae, the systems contained a large number of bacteria, mostly from the phyla *Proteobacteria* and *Bacteroidetes*. The bacteria found in the systems were shown to be involved in the synthesis of vitamins essential for algae growth such as vitamin B12, suggesting cooperation between the bacteria and algae. Microalgae and bacteria systems under autotrophic and mixotrophic growth have removed >95 % of NH_4^+ and >90 % of P. Under heterotrophic conditions, the nutrient levels also decreased, but not

as efficiently as during autotrophic growth. The harvesting of the microalgae grown in wastewater also provides a way for the nutrients, most importantly P, to be recycled. Several studies have reported that N or P deficiency or limitation during microalgae cultivation can improve lipid accumulation and transformation for most species. In practice, microalgae are cultured in full media with enough nutrients in the early stages, while in later stages nutrient deficiency or limitation needs to be designed to improve the lipid content. Nitrogen deficiency conditions could cause a decrease in amino acids in algal cells to 1/20 the amount or less, while the quantities of neutral lipids increased greatly (Morales-Sánchez *et al.* 2020) as the stored carbohydrates from the growth phase might channel towards the formation of triacylglycerides (TAGs), leading to an efficient composition for biodiesel production.

2.4 Photosynthesis

Algae are a very diverse group of predominantly aquatic photosynthetic organisms that account for almost 50 % of the photosynthesis that takes place on Earth. Algae have a wide range of antenna pigments to harvest light energy for photosynthesis giving different types of algae their characteristic colour. Photosynthetic microalgae are autotrophic organisms that fix carbon dioxide from the atmosphere to grow; they are actively under consideration for large-scale biodiesel production since, under the right conditions, some strains of algae produce high levels of lipid that are suitable for conversion to biodiesel (González *et al.* 2015). There are two stages of photosynthesis: in the first, light-dependent processes, also known as light reactions, use light energy to create the energy-storing molecules NADPH and ATP (Klinthong *et al*. 2015). Equation (2.28) illustrates how the light-independent reactions employ these products to absorb and decrease carbon dioxide during the second stage.

$$CO_2 + 2H_2O \xrightarrow{photons} [CH_2O] + O_2 + H_2O \quad (2.28)$$

Cancelling n water molecules from each side yields the overall Equation (2.29), which highlights the fact that water is both a reactant in the light-dependent reaction and a product of the light-independent reaction. The typical free energy in this reaction is 2,870 kJ/mol for the production of glucose (Chaudhry and Varacall 2018).

$$CO_2 + H_2O \xrightarrow{photons} [CH_2O] + O_2 \quad (2.29)$$

One molecule of the pigment chlorophyll absorbs one photon and loses one electron in light-dependent processes. This electron travels through pheophytin, a modified version of chlorophyll, and then to a quinone molecule. This initiates the electron's journey along an electron-transport chain, which ultimately reduces NADP to NADPH. This produces a gradient of energy (photons) across the chloroplast membrane, which ATP synthase uses to synthesise ATP. After splitting a water molecule in a process known as photolysis, which releases an oxygen (O_2) molecule as a waste product, the chlorophyll molecule eventually regains the electron it lost (Klinthong *et al*. 2015).

$$2H_2O + 2NADP^+ + 3ADP + 3P_i \xrightarrow{light} 2NADPH + 2H^+ + 3ATP + O_2 \quad (2.30)$$

Not all light wavelengths are suitable for photosynthesis. The kind of accessory pigments present determines the photosynthetic action spectrum. For example, in green plants, the action spectrum resembles the absorption spectrum of carotenoids and chlorophylls, which has peaks for red and violet-blue light. The blue end of the spectrum is used by red algae to develop in deeper waters that block out the longer wavelengths (red light) that are utilised by green plants above ground. This is possible since red algae's action spectrum is blue-green light. What gives photosynthetic organisms (such as green plants, red algae, and purple bacteria) their colour is the non-

absorbed portion of the light spectrum, which is also the least useful for photosynthesis in those particular organisms (Máté 2016).

The enzyme RuBisCO (also called RuBP carboxylase) is involved in light-independent (or "dark") reactions. It takes CO_2 from the atmosphere and uses the newly formed NADPH to release three-carbon sugars, which are then combined to form sucrose and starch. This process is known as the Calvin-Benson cycle (Máté 2016). Equation (2.31) represents the general formula for the light-independent processes in green plants.

$$3CO_2 + 9ATP + 6NADPH + 6H^+ \rightarrow$$
$$C_3H_6O_3\text{-phosphate} + 9ADP + 8P_i + 6NADP^+ + 3H_2O \qquad (2.31)$$

The Calvin-Benson Cycle uses the energy transformed by light reactions along with carbon dioxide to produce organic compounds. The intermediate three-carbon sugar product is created by carbon fixation and is subsequently transformed into the final carbohydrate products. After photosynthesis, the simple carbon sugars are utilised to form other organic compounds, like cellulose, which is a building block, the precursor for the biosynthesis of lipids and amino acids, or as fuel for cellular respiration, which happens in both plants and animals when plant energy is transferred through a food chain (Máté 2016).

Atmospheric carbon dioxide is constantly being fixed into sugars (and other macromolecules), which, in turn, are oxidized back into CO_2. This relationship, on a global scale, is termed the ‘carbon cycle’. Through the burning of fossil fuels, CO_2 is generated at a faster rate than plants can fix back into sugars and other carbon molecules (Klinthong *et al*. 2015).

2.5 Microalgae Cultivation Techniques

Microalgae cultivation is the sum of procedures and techniques to produce feedstock biomass that subsequently is refined to obtain valuable products. Therefore, prospecting, selecting or developing a strain (by genetic and metabolic engineering) together with microalgae cultivation, and growth medium preparation belongs to the upstream part of the entire process; biomass harvesting, de-watering, extraction of valuable compounds, transformation and purification belong to the downstream part of the process.

In the cultivation of microalgae, it is important to know the right amount of CO_2 concentration that is suitable for the different types of microalgae. Different species have various CO_2 tolerances. High CO_2 concentration may result in growth inhibition while lower concentration could limit microalgae cell growth (Jyothi, 2016). Atmospheric CO_2 of 0.0387 % v/v is too low for microalgae growth, therefore requiring supplementing with carbon sources. The carbon sources include CO_2, H_2CO_3, HCO_3^-, and CO_3^{2-}, but for the cultivation of microalgae only CO_2 and HCO_3^- are used. Although high CO_2 concentrations can cause a narcotic effect, some species can tolerate CO_2 concentrations greater than 15 %. Typically, microalgae's optimal temperature range is between 20 and 30 °C. Flue gas from a coal-fired power plant is released at a high temperature; therefore, it is important to consider the algae's tolerance to high temperatures because it can help reduce cooling costs. Temperature is, therefore, an important consideration in choosing algae growth locations because of variability in weather conditions.

Microalgae cultivation using sunlight energy can be carried out in open or covered ponds or closed photobioreactors, based on a tubular, flat plate or other designs. Closed

systems are much more expensive than ponds, and present significant operating challenges (overheating, fouling). The cultivation of algae can be done in various ways depending on algal species selection and the structure used to grow the organisms. In all cases, the algae's cultivation involves exposure to light and access to nutrients and carbon dioxide. Algal growth is impacted by factors such as sun exposure, temperature, and pH (Rupiper, 2016).

2.5.1 Open systems

The open systems are outdoor facilities consisting of ponds, lagoons, deep channels, shallow circulating units and others. Open ponds have been used for large-scale microalgae cultivation considering their simple construction and easy operation. The cultivation systems can be classified as (1) natural waters (e.g., lakes, lagoons, ponds, etc.) and (2) artificial water systems (e.g., artificial ponds, tanks, and containers). The shapes, sizes and types (agitated, inclined, etc.) of open systems depend on the applications. There are various types of ponds, including unstirred, raceway and circular ponds (Klinthong *et al*., 2015). Unstirred ponds are the most economical due to their simple management and construction. Commercial unstirred ponds are built in natural water ponds of less than half a meter in depth. Unstirred ponds are commercially used for some microalgae species, such as *Dunaliella salina* (Costa *et al*., 2019). However, this type of pond is very limited in its applications, given that microalgae are not able to grow under frequently poor growth conditions and competitive growth with contaminating protozoa, bacteria and viruses.

Raceway ponds (or stirred paddle wheel open ponds) are the most famous open systems in current use. Raceway ponds are usually shallow, between 15 and 25 cm in depth. These ponds are normally constructed as either a single channel or groups of

channels that are built by connecting individual raceway ponds. According to Costa *et al*. (2019), biomass productivity in the raceway pond ranges from 60 to 100 mg dry weight/L/day. The oldest open ponds used for large-scale algae farming are circular ponds. These ponds are about 25-30 centimetres deep. Typically, microalgae are produced in 45-meter-diameter concrete circular ponds that are agitated by spinning paddles. Paddle wheels are continuously moving beneath a 20-30 cm thick layer of inorganic fertiliser solution containing algae that is exposed to sunshine and CO_2 bubbles.

Variables affecting high-rate pond performance include hydraulic retention time, pond depth, nutrient concentration, light intensity, pH and temperature. Control of wastewater pond operation and treatment performance is limited by natural variables such as microalga species growth and reduced biomass yields from predator organisms. Elevated pH values resulting from consumption of inorganic carbon during algae cell growth may be controlled by CO_2 addition to maintaining a pH of 7.5 to 8.5, an optimal range for algae and bacteria. CO_2 addition can also lead to the manipulation of nutrient removal mechanisms by reducing pH, therefore preventing ammonia volatilization or auto-flocculation. In comparison to energy-intensive conventional treatment systems, HRAPs with CO_2 supplementation abate GHG emissions by 100-400 kg of CO_2/mL treated. According to Kinthong *et al*. (2015), open systems have the following drawbacks: (1) low cell light consumption; (2) evaporative losses; (3) limited CO_2 diffusion from the atmosphere; (4) large land area requirement; and (5) susceptibility to contamination by undesired bacteria, mould, and algae.

2.5.2 Closed systems

You can cultivate microalgae in a closed system with regulated parameters including light usage, area needed, and carbon dioxide. There are certain issues with open systems that the closed system can help with. A form of closed pond system called a photobioreactor (PBR) is used to cultivate microalgae because it can minimise water evaporation, control temperature, remove carbon dioxide losses, and lessen the possibility of contamination with unwelcome algae, mould, and bacteria (Klinthong *et al*. 2015). It is important to remember that while photobioreactors greatly inhibit the growth of algal weeds that compete with one another, they are unable to completely stop the growth of pollutants.

There are numerous sizes, forms, and designs for photobioreactors. The most popular PBRs are the tubular varieties, which are constructed of transparent materials (either glass or PVC) and are installed outdoors in facilities that receive sunlight (Rupiper 2016). The main reactor is connected to gas exchange vessels that supply CO_2, air, and nutrients to remove O_2. (Razzak *et al*. 2023). To optimise the exposure of microalgae to sunlight, a wide surface area per unit volume is necessary for the design of these cultivation vessels. To preserve sunlight permeability, the tubes typically have a diameter of less than 10 cm. A common tubular microalgae growing system involves rotating the medium through the tubes so that photosynthesis can occur in the presence of sunlight.

A mechanical pump or an airlift pump is used to circulate the medium back to a reservoir. The purpose of the pump is to help maintain a highly turbulent flow within the reactor to prevent the flocculation of microalgal biomass (Klinthong *et al*. 2015). Transparent polythene bags, also known as plastic bag photobioreactors, are used to

cultivate microalgae. These bags are hung or placed in a cage under sunlight irradiation, and the microalgae are mixed with air in the bottom of the bags. To prevent cell settling, transparent polyethene sleeves with a conical seal at the bottom are used. Numerous kinds of microalgae are mass-cultivated in Airlift photobioreactors. Made of acrylic glass, they make up the dark (also known as the riser) and irradiated zones of airlift photobioreactors. According to Kinthong *et al*. (2015), airlift photobioreactors are thought to fulfil the requirements for the new generation of photobioreactors, which include minimum contamination, high light penetration and biomass production, and ease of maintenance. With high medium cycling between the irradiation and dark zones, vertical bubble columns and airlift cylinders can achieve a significantly higher radial fluid circulation. High mass transfer, good mixing with minimal shear stress, low energy consumption, relatively simple operation under sterile conditions, good immobilisation of algae on moving particles, and reduced photoinhibition and oxidation are some of the benefits of these units.

Nonetheless, there are a few drawbacks to these units: (1) high expenses for production and upkeep; (2) lower radiation per unit surface area; (3) more complex building materials; (4) increased shear stress on microalgal cultivations; and (5) a greater number of units required to build a commercial plant (Razzak *et al*. 2023).

Flat plate photobioreactors are a highly efficient method for growing microalgae biomass. These photobioreactors have an easy-to-scale-up modular architecture and a high surface area-to-volume ratio for lighting. With a mixing rate that can provide the culture with the right quantity of CO_2, eliminate surplus oxygen, and intensify the flashing effect, the biomass production of microalgae grows quickly. According to Kinthong *et al*. (2015), flat plate photobioreactors are quite inexpensive, useful for immobilising algae, and ideal for both indoor and outdoor cultivation. Long-lasting,

effectively operating machines with a volume capacity of 1000–2000 L can accept vertical flat plates. PBRs provide more control over variables such as light, temperature, gases, and the selection of uncontaminated algae strains (Pruvost *et al*. 2015; Rupiper 2016). PBRs come in the following shapes and forms: plastic bags submerged in water ponds; vertical and horizontal thin films in greenhouses; horizontal and vertical tubular and plate in greenhouses; vertical annular; and vertical plastic bags in greenhouses (Wagenen *et al.* 2016).

2.6 Effects of Cultivation Conditions on Microalgal Oil Production

The growth and composition of microalgae, as outlined in the subsequent sections, are greatly influenced by the growing conditions.

2.6.1 pH

Most microalgae species thrive in a pH range of 8.2 to 8.7, however, some are highly tolerant of extremely acidic or basic environments. Maintaining pH in an ideal range is crucial since it has a significant impact on every facet of media biochemistry (Sakarika and Kornaros 2016). pH has a significant impact on both the cell's metabolic biochemistry and the media's ionic absorption. These two elements have a profound impact on algal cultures because they can neutralise the effects of external buffering agents.

2.6.2 Temperature

Equation (2.32) utilises the Arrhenius formula for the temperature to determine the optimal rate of biomass production (Castro-Tapia, Dibildox-Alvarado, and Soria-Guerra 2022).

$$\mu = Ae^{\frac{-E_a}{R}\frac{1}{T}} \quad (2.32)$$

where A is the maximal growth rate (per day), μ is the first-order growth rate (per day), R is the universal gas constant (kJ mol^{-1} K^{-1}), T is the temperature (K), and E_a is the approximate activation energy for photosynthesis (kJ mol^{-1}).

2.6.3 Light

The energy source for the photosynthetic conversion of carbon dioxide to carbohydrates is photosynthetically active radiation or PAR. PAR is described as radiation with wavelengths ranging from 400 to 700 nm, which accounts for roughly 43 % to 45 % of the radiation that enters the system. In theory, PAR can transform up to 27 % of its mass into carbohydrates (Nzayisenga *et al*. 2020). The geometry of the algal growth area should be considered to determine the total amount of light accessible to algae.

Seasonal variations in available solar flux limit the quantity of sunlight that algae may absorb in ponds. As light enters the algae tank and moves across its surface, microalgae absorb or scatter it. The light continues to get weaker and more scattered as the optical path length (such as the depth of the pond) increases. Furthermore, when algae densities increase, the effects of shade become more noticeable and reduce PAR levels. It has been suggested that the maximal PAR conversion efficiency in photosynthesis is reduced to 10 % by the combined effects of photon absorption restrictions, optical transfer losses, and energy expenditure for the algae's life-supporting processes; in open ponds, the PAR conversion efficiency is reported to be 3.7 %.

When algae concentrations are low (less than 10 g/L), overexposure to light can cause photoinhibition, which is more significant for the entire algal population. The effect of photoinhibition (for algae) typically begins at roughly 10 % of the full sun intensity at

midday, though it varies depending on the species (Ogbonna *et al*. 2021). Equation (2.33) provides a rough approximation for the biomass yield of an algal farm.

$$Y = \frac{QT\eta}{E_c(1-L)+E_lL} \tag{2.33}$$

where Q is the month-average PAR energy per day (kWh m^{-2} day^{-1}), T is time (number of days in the month), η is the theoretical final PAR conversion efficiency (10%), Ec is the energy necessary for building one gram of carbohydrate (17 kJ g^{-1}), E_l is the energy necessary for synthesizing one gram of lipid (38 kJ g^{-1}), and L is the lipid content ($\frac{g\ lipid}{g\ alga}$) of the algae by dry weight.

2.6.4 Nitrogen

In microalgal wastewater treatment procedures, assimilation to algal cells is the primary mechanism for nitrogen removal. Nitrogen can make up more than 10 % of the biomass and is the second most essential nutrient after carbon (Wagenen 2016). There are various types of nitrogen, but the two most frequently digested by microalgae are nitrate (NO_3^-) and ammonium (NH_4^+). Ammonium is the preferred molecule, and no other nitrogen sources will be digested while this is available. When wastewater contains less ammonium (NH_4^+), microalgae may begin to absorb nitrate (NO_3^-) as a source of nitrogen for their cells (Yaakob *et al.* 2021). It is not advisable to use high ammonium concentrations (>20 mg NH_4-N L^{-1}), though, as this might cause ammonia toxicity in cells when combined with high pH levels. As sources of nitrogen, urea ($(NH_2)_2CO$) and nitrite (NO_2^-) could be employed in addition to ammonium and nitrate. However, it is less practical due to nitrite's toxicity in larger quantities. To synthesise proteins and nucleic acids, algae need nitrogen (Maltsev, Kulikovskiy, and Maltseva 2023). Nitrate (NO_3^-) and ammonium (NH_4^+) are more easily obtainable for algae to utilise than atmospheric nitrogen (N_2), which is not as

readily available as carbon dioxide. Nitrogen deprivation causes lipid production in microalgae to increase dramatically at the expense of a slower rate of overall development (Shrestha, Dandinpet, and Schneegurt 2020).

2.6.5 Phosphorus

Phosphorus is the second essential nutrient for microalgae. It is an important element that comprises 1 % of the cell's dry weight. However, microalgae can uptake more than what they need through their ability to synthesize and accumulate polyphosphate in their cells. Phosphorous plays several roles in microalgae as a constituent of phospholipids (for cell membranes) and adenosine triphosphate (to carry energy for cell functions), among other functions. The phosphate ion, PO_4^{3-}, is perhaps the most bioavailable form of phosphorous, as phosphorous bound to metal ions is not as easily accessed (Maltsev, Kulikovskiy and Maltseva 2023).

2.6.6 Carbon dioxide

When microalgae photosynthesise, they take up inorganic carbon from the water. The inorganic carbon species normally used by microalgae are carbon dioxide (CO_2), bicarbonate (HCO_3^-) and carbonate (CO_3^{2-}), the bicarbonate requires the enzyme carbonic anhydrase to convert it to CO_2. When bicarbonate is used as a carbon source, the pH in the medium increases due to the reaction in Equation (2.34) (Wu *et al.* 2019).

$$HCO_3^- \rightarrow CO_2 + OH^- \quad (2.34)$$

This pH increase, which can elevate the pH in algal cultures to values above 11, strongly affects the water chemistry. Carbon dioxide capture and utilization (CCU), a concept of turning greenhouse gas into a useful feedstock, has been gaining much attention in recent years (Jajesniak *et al.* 2015). Increasing CO_2 emission into the

atmosphere, from fossil fuel combustion and other anthropogenic activities, has challenged researchers to source more sustainable and economical routes of chemical syntheses. Instead of developing new chemical catalysts and CO_2-based chemistry, we should perhaps learn from Nature. Despite the advances made in utilizing CO_2 as a chemical feedstock, large-volume CO_2 conversion is currently limited. Impressive industrial use of CO_2 includes the production of urea, inorganic carbonates and pigments, methanol, salicylic acid and propylene carbonate (Klinthong *et* al. 2015).

Photosynthetic organisms convert huge amounts of carbon into biomass annually. In other words, Nature has evolved highly sophisticated mechanisms for carbon fixation and utilization; a resource that remains largely untapped and could potentially be a disruptive technology in CCU (Eloka-Eboka and Inambao 2017).

Linthong *et al*. (2015) investigated the effects of CO_2 on microalgae growth and lipid induction using ambient and 15 % CO_2 concentrations and light intensities of 35 and 140 μmol m^{-2} s^{-1}. The method employed involved cultivating microalgal *Chlorella protothecoides* in a 250 mL Erlenmeyer flask with an inoculation of 1×10^5 cells/mL under cool, white fluorescent light at room temperature. Some researchers (Eloka-Eboka and Inambao 2017) were able to identify the ideal growing parameters for green microalgae to generate high biomass and lipids using these settings. The hydrophobic fluorescent probe Nile red dye was employed to identify the increased intracellular lipids. Additionally, the closed continuous loop system of gas chromatograph-mass spectrometry (GC-MS) was utilised to ascertain the CO_2 contents in every culture flask. The intention was to investigate how the microalgae were utilising the 15 % CO_2 concentration during the cultivation process. After cultured *Chlorella protothecoides* for 9 to 10 days in both open and closed systems, the results showed that the conditions of high light intensity of 140 μmol $m^{-2}s^{-1}$ with 15 % CO_2 concentration acquired high

cell concentration of 7 x 10^5 cells mL^{-1}. Fluorescence intensity with 1.3 to 2.5 times the CO_2 reduction released by power plants was used to determine a higher lipid content. When *Chlorella protothecoides* were cultivated under similar conditions (140 μmol $m^{-2}s^{-1}$ with 15 % CO_2 concentration), the cells also induced lipid accumulation, which led to an increase in particle size.

2.6.7 Photoautotrophic cultivation

Light is the primary energy source and inorganic carbon, such as CO_2, is the carbon source in the photoautotrophic culture mode. The range of lipid content in microalgae during photoautotrophic cultivation is 5-68 %, depending on the species. In general, a nitrogen- or nutrient-limiting condition might cause microalgae to increase in their lipid content. Still, some research has demonstrated that poorer biomass production is associated with higher lipid content (Wagenen *et al*. 2016). Finding the right growth elements is crucial to achieving the ideal growing conditions. For example, it is more appropriate to quantify lipid productivity to assess the capacity of microalgae to produce oil. This variable reflects the interaction between lipid content and biomass output. According to literature reports (Jajesniak *et al.* 2015), Chlorella sp. exhibits the highest lipid productivity during photoautotrophic cultivation, with an approximate value of 179 mg $L^{-1}d^{-1}$.

2.6.8 Heterotrophic cultivation

In heterotrophic cultivation, microalgae use organic carbon as a source of carbon and energy while it's dark outside. An alternate approach to resolving the issue of light limitation in large-scale photobioreactors may be this culture condition. Certain microalgae species showed higher lipid content during the heterotrophic development stage. For example, *Chlorella protothecoides*'s lipid content rose by up to 40 % when

the culture conditions shifted from phototrophic to heterotrophic. Microalgae can grow by assimilating a wide range of organic carbon sources (Klinthong *et al.* 2015). Thus, research has been done on accessing less expensive sources of organic carbon to replace sugars, including maize powder.

2.6.9 Mixotrophic cultivation

When grown in a mixotrophic environment, microalgae can obtain their carbon via photosynthesis by utilising both organic components and inorganic carbon, or carbon dioxide. As a carbon source, microalgae use carbon dioxide and organic compounds; in phototrophic environments, they use the CO_2 extracted during respiration. The generation of microalgae oil under phototrophic and heterotrophic settings is more common than under this sort of growing circumstance. Nielsen (2015) tested the ability of the microalgae species *Scenedesmus dimorphus* and *Selenastrum minutum,* under mixotrophic growth, to remove dissolved organic carbon (DOC), nitrogen (N), and phosphorus (P) from municipal and industrial wastewater. Other factors that may affect algae growth and nutrient removals such as bacteria, the quality of the DOC, the concentration of the DOC in wastewater, and the addition of flue gas were also investigated. He posited that bacteria were responsible for the majority of the DOC removal. Also, Nielsen (2015) averred that under mixotrophic growth in industrial wastewater mixtures, microalgae removed >99 % of ammonium (NH_4^+) and 82-98 % of total phosphorus (TP). The growth of microalgae was higher in the industrial wastewater mixtures with higher DOC concentration (>285 mgL^{-1}) than in municipal wastewater alone (DOC<32 mgL^{-1}). Both species of microalgae achieved the highest growth (dry weight biomass of 0.72-0.76 gL^{-1}) in the industrial wastewater mixture of pulp and paper and dairy wastewater with the addition of flue gas. Mixotrophic growth

produces the highest lipid content of the three growth types which may mean that continuous illumination, which is expensive, is not necessary for productive algae biomass production (Lin and Wu 2015).

2.6.10 Photoheterotrophic cultivation

Microalgae engaged in photoheterotrophic cultivation obtain their energy from light and carbon from organic substances. Photoheterotrophic and mixotrophic cultivation vary primarily in that the former uses light as its energy source, while the latter uses organic chemicals as its energy source. Accordingly, light and sugars are both necessary for the photoheterotrophic state (Lin and Wu 2015).

2.7 Microalgae Biomass Harvesting

Algal oil yields (litre/hectare) have the potential to be much greater than oilseed crop yields (about 20 times higher than soybean yields). Therefore, compared to other forms of biomass, microalgae may require less space to generate triglyceride-rich oil. However, one of the biggest obstacles is harvesting microalgae in an economically viable way. The most energy-intensive phases in the synthesis of biofuel from microalgae are dewatering and drying, which offer the largest room for optimisation. Centrifugation, evaporation, filtration, precipitation by flocculation, sedimentation, and dissolved air flotation (DAF) are now the most widely used methods for harvesting microalgae (Saeid & Chojnacka 2015; Rupiper 2016). Low-density microalgae are cultivated in open pond lagoon environments, and specialised harvesting techniques are applied to achieve appropriate biomass yields. Microalgae are harvested from open pond lagoon systems using a rotating algal biofilm reactor (RABR), filtration, sedimentation, and dissolved air flotation (DAF) devices.

2.7.1 Flocculation

Because microalgae have small cells, they are challenging to dewater. Cells come together during flocculation to form bigger particles. This is frequently suggested as a pretreatment measure before flotation, sedimentation, or filtering. Cells aggregate either directly onto one another or through a bridging surface when cell repulsion decreases. This process is known as flocculation. Research in this area over time has shown that a variety of variables, including pH, temperature, density, hydrophobicity, surface charge, and culture age, influence the degree of flocculation (Asadi et al. 2021). Positively charged ions or polymers include minerals like lime, metal salts like ferric chloride and aluminium sulphate, and naturally occurring flocculants such as tannins and starch derivatives that can cause flocculation.

The usage of chemical flocculants has necessitated pH adjustment in addition to huge dosages. In the absence of chemical removal, the media becomes unrecyclable due to the contamination of the biomass and medium with flocculants. Auto-flocculation can result from bacterial and microalgal aggregation, macromolecule excretion, pH modification, or dietary restriction. Because the density of microalgae is so similar to that of water, separation is challenging. Low-energy methods like flocculation and physical precipitation can only concentrate the microalgal broth to 10 wt. % microalgae. One of the advantages is the removal of biological materials in the form of flocs. According to Czemierska, Szcze, and Jarosz-Wilkołazka (2021), flocculation eliminates almost 90 % of the biomass of algal blooms. Over 90 % of the biomass was recovered in jar tests using natural flocculants Ecotan and Tanfloc at doses of 10 and 50 mg/L, respectively. Gutiérrez *et al*. (2017) observed that Ecotan and Tanfloc both boosted microalgae settling velocity, leading to a quick and effective biomass recovery

of over 90 % in 10–20 minutes, based on column settling trials. Consequently, both flocculants would increase microalgal biomass while lowering settler volume and hydraulic retention time (HRT).

2.7.2 Filtration

Filtration by conventional means works only on bigger (more than 70 μm) or filamentous organisms, such as *Spirulina* and *Coelastrum*. Microfiltration, ultra-filtration, and membrane filtration are acceptable options for smaller cells, but they are typically limited to tiny quantities. One of the main issues is fouling, which is the build-up of particles on the membrane's surface that slows down filtering. Microstraining, or filtration by natural gravity using low-speed spinning drum filters, is a promising approach since it is easy to use and uses minimal energy. To avoid clogging the filter with cells, crossflow membrane filtration uses a turbulent, tangential flow of liquid across the membrane. Air pressure, vacuum, centrifugal force, and gravity are some of the driving forces that propel algal suspension through the filtration process. Membranes used for microfiltration and ultrafiltration can undergo crossflow filtration. Transmembrane pressure and cell shape have a major impact on the process' efficiency. Ultrafiltration membranes can retain materials with molecular weights ranging from 1 K to 1000 K. Their method of particle isolation is based on molecular size. Depending on the chosen membrane filter, microfiltration membranes can eliminate particles and organisms ranging from 0.025 μm to 10.0 μm in size. Magnetic filtering is a less common method. In this case, the incorporation of magnetic metals, which algae cells may absorb or employ to flocculate them, may enable the employment of a magnetic field for capture.

2.7.3 Centrifugation

This is a mechanical method, which is the most reliable and rapid process. It is used to recover suspended algae. Centrifugation can concentrate the algae solution to 20 % by mass, but this requires so much energy input. For a wet extraction process, the precipitate from centrifugation can be used directly and the oil extracted in an organic phase leaving behind the algal biomass and aqueous phase.

2.7.4 Sedimentation

Gravity sedimentation is another type of mechanical separation technique that can recover supernatant and 1.5 % of solids under the influence of gravity with the help of sedimentation tanks and lamella separators. In addition, some of the other advantages include lower operational costs. However, it takes a while for the algae to settle. In addition, a large amount of space is required for constructing sedimentation tanks for large-scale production.

2.7.5 Flotation

Air flotation is a separation technique that involves air or gas being bubbled in an algal suspension. The air or gas molecules attach to algal solid particles and float to the top of the surface. These floated algal solid particles can be removed easily. In dissolved air flotation, 80-90 % of algae can be removed. Some of the drawbacks include the probability and correct timing of algal cells to interact with the bubbles. For example, solid particles and bubbles float upward only if the interaction takes place between bubbles and solid particles at the same time. For air flotation, sometimes chemical flocculants are also used at a large scale; however, these chemical flocculants pose difficulties in downstream processing.

2.7.6 Electrophoresis

In the electrophoresis separation technique, algae get moved by the electric field. Algae are negatively charged; hence they get attached to hydrogen ions because the opposite ions attract. Once algae are bound in aggregates, they can be easily removed in the electrophoresis separation technique. The advantages related to this method include cost efficiency and environmental compatibility. However, this separation method uses up lots of energy and causes system fouling due to high temperature and power usage.

2.8 Microalgae Lipid Extraction

The main task after harvesting is to extract the lipids from their intracellular site as cheaply and efficiently as possible. It's necessary to separate the microalgal lipids from the remaining biomass, which includes water and other components like proteins, carbs, nucleic acids, and pigments. Typically, common harvesting techniques yield a paste or slurry with five to twenty-five per cent solids. The research suggests that removing the remaining water can cost anywhere from 20 to 75 % of the entire processing cost, making it one of the most costly processes in the process. Spray drying, freeze-drying, toroidal driers, flash drying, rotary driers, and sun drying are a few potential methods for drying biomass. Because of the high water content, spray-drying is not economically viable for low-value products, and sun-drying is not an effective approach either. The size of the operation, the needed speed, and the downstream extraction process all influence the drying technique choice.

There exist numerous methods for extracting lipids. The use of solvent extraction techniques is widespread, but there are drawbacks, such as the solvent's toxicity and cost (hexane, for example), and solvent recovery uses a lot of energy. Alternative techniques entail breaking down the cell wall, typically using enzymatic, chemical, or

physical procedures (such as bead milling, sonication, homogenization, or letting the liberated oil float to the top of the solution). There has been research on extraction techniques using ultrasound and microwave assistance (Bibi *et al.* 2017).

Supercritical CO_2 extraction is an efficient process but is too expensive and energy-intensive for anything but lab-scale production. Direct transesterification (production of biodiesel directly from algal biomass) is also possible. Some of these techniques do not require dry biomass, but the larger the water content of the algal slurry, the greater the energy and solvent input required.

Lipids produced by microalgae generally include neutral lipids, polar lipids, wax esters, sterols and hydrocarbons, as well as prenyl derivatives such as tocopherols, carotenoids, terpenes, quinines and pyrrole derivatives such as the chlorophylls. Lipids produced by microalgae can be grouped into two categories, storage lipids (non-polar lipids) and structural lipids (polar lipids). Storage lipids are mainly in the form of triacylglycerides (TAG) made of predominately saturated FAs and some unsaturated FAs which can be transesterified to produce biodiesel. Structural lipids typically have a high content of polyunsaturated fatty acids (PUFAs), which are also essential nutrients for aquatic animals and humans. Polar lipids (phospholipids) and sterols are important structural components of cell membranes that act as a selectively permeable barrier for cells and organelles.

Typical lipid extraction involves two aspects, cell disruption and lipid extraction. There are multiple ways of breaking open the cells, Potter-Elvehjelm homogenization, microwaves, ultrasonication, liquid nitrogen grinding, autoclaving, bead-beating, and 10 % NaCl solutions are a few of them (Rupiper 2016). Rupiper (2016) found that none of the investigated cell-disruption techniques produced statistically different yields except for microwave and homogenization whose yields were approximately 24

% more than the control and popular sonication method for some microalga species. Other researchers found that the microwave method was the most simple and effective method for lipid extraction. Additionally, heating from microwaves costs two-thirds less than conventional heating resulting in energy and cost savings (Drira *et al*. 2016). Homogenization may also be effective at cell disruption; however, it is the most time-consuming and energetic process involving the manual breaking of the cell wall via blenders or other mechanical means. Overall, for the majority of species, the cell disruption technique selected did not have an impact on the final lipid yield post-extraction as most of the neutral lipids can be extracted across the cell wall of the microalgae and only the remaining lipids requiring cell disruption (Rupiper, 2016).

Without treatment or coupled with one of the cell disruption techniques described above the most common extraction method is done via solvent extraction using a 2:1 or 1:1 by-volume chloroform-methanol mixture (Rupiper 2016). Another extraction method that is emerging is the use of supercritical fluid extraction primarily using CO_2. The benefit of this new method is that it results in a crude oil product free of solvents thus minimizing its environmental impact (Drira *et al*. 2016).

2.8.1 Flash drying

Flash drying, also called pneumatic drying, is the process of drying particulate matter by exposing it briefly (typically a few seconds) to a high-temperature gas stream, resulting in a rapid rate of evaporation without excessive heating of the product. The product is separated using cyclones, and/or bag filters.

2.8.2 Rotary drying

The rotary drier is a cylinder, inclined slightly horizontally, which may be rotated, or the shell may be stationary, and an agitator inside may revolve slowly. In either case,

the wet material is fed in at the upper end, and the rotation, or agitation, advances the material progressively to the lower end, where it is discharged.

2.8.3 Toroid drying

The Rotary Universal Drum Dryer (RUDD), often known as the Jet Dryer, has been designed with a sophisticated single-pass free-flow mechanism. When light particles are introduced into the early hot zone of the drum, they undergo rapid drying due to the short retention duration. Particles that are both large and heavy have a reduced rate of moisture evaporation and tend to be retained in the last section of the drum. The utilization of a lower temperature setting in the terminal section of the dryer facilitates a more delicate drying procedure, resulting in reduced harm to the product. The RUDD dryer employs a feedback system to reintegrate the final product, which possesses a sticky or paste-like consistency with high viscosity, into the incoming material at the input during the drying process. By employing this method, the accumulation of the product within the drum is prevented.

2.8.4 Spray drying

Growth rate and lipid content both affect lipid productivity. Dry weight percentage (% DW) was the standard method of reporting lipid content (P). Growth rates are reported as doubling time (Td) or specific growth rate (μ). These are inter-converted according to Equation (2.35).

$$T_d = \frac{ln2}{\mu} \tag{2.35}$$

Standard units of $g.L^{-1}.day^{-1}$ are chosen for biomass productivity. Specific growth rate (μ, in units of day^{-1}) can be converted to volumetric biomass productivity (Q_V, in $g\ L^{-1}\ day^{-1}$) where the biomass concentration (X, in $g\ L^{-1}$) is known. Biomass productivity

is often reported based on surface area (Q_A), in units of g m^{-2} day^{-1}. This can be converted to Q_V using Equation (2.36.) where the depth (D, in m) of the culture vessel can be calculated from the reactor geometry.

$$Q_v = \mu X \tag{2.36}$$

$$Q_v = \frac{Q_A}{D \text{ x } 1000} \tag{2.37}$$

Lipid productivity (Q_P) was infrequently reported in the literature and was generally reported in g L^{-1} day^{-1} or mg L^{-1} day^{-1}. This parameter could be calculated from volumetric biomass productivity (Q_V, in g L^{-1} day^{-1}) and lipid content (P, in % DW) where appropriate data were available (Equation 2.38).

$$Q_P = Q_V \text{x } P \tag{2.38}$$

Two presumptions were required to calculate the lipid productivity for most species:

i. Using an average depth of 0.1 m and the best fit of the data, convert areal productivities (in g m^{-2} day^{-1}) to volumetric productivities (g L^{-1} day^{-1}).

ii. Based on typical experimental results, conversion of a given growth rate to biomass productivity using an average biomass concentration of 0.15 g L^{-1}.

2.8.5 Freeze-drying

The low-temperature dehydration method of freeze-drying, sometimes referred to as lyophilization or cryodesiccation, entails freezing the product, reducing pressure, and finally sublimating the ice to remove it. Freeze drying also called sublimation drying is the drying of a product in a frozen state. The ice evaporates without passing through the liquid state i.e., it sublimes. Conditions of sublimation of pure ice, therefore, exist below the triple point (0.01 ºC and 610.8 Pa) at which all three states of matter can exist. Freeze-drying is always done under a vacuum. Freeze-drying is often reserved

for materials that are heat-sensitive, such as proteins, enzymes, microorganisms, and blood plasma (Basso *et al.* 2021). The low operating temperature of the process leads to minimal damage to these heat-sensitive products.

The manifold, rotary, and tray-style freeze-dryers are the three types of freeze-dryers that are most commonly utilised. A vacuum pump to lower the ambient gas pressure in a vessel holding the material to be dried and a condenser to remove moisture through condensation on a surface cooled to -40 to -80 °C (-40 to -112 °F) are the two parts that all freeze-dryers have in common (Bošnjaković, and Sinaga 2020). The technique used by the tray-type, rotary, and manifold freeze-dryers to interface the dried material with a condenser varies. Manifold freeze-dryers connect several containers containing the dried product to a condenser using a short, typically circular tube. For the dried material, the rotary and tray freeze-dryers each have a single, sizable reservoir. Pellets, cubes, and other pourable materials are often dried using rotary freeze-dryers. Rotating a cylindrical reservoir helps to provide even drying of the material inside the rotary dryers. Typically, tray-style freeze-dryers feature a rectangular reservoir with shelves where goods can be arranged in trays, vials, and other containers. Examples of these items include tissue extracts and medicinal solutions.

When drying liquid materials in tiny containers for immediate use, manifold freeze-dryers are typically utilised in a laboratory setting. The product will be dried to a moisture content of less than 5% using a manifold dryer. Only primary drying, the extraction of the unbound water, is possible in the absence of heat. Secondary drying necessitates the addition of a heater to release the trapped water and reduce moisture content. Compared to manifold dryers, tray-style freeze-dryers are usually larger and more advanced. Many materials are dried using tray-style freeze-dryers. For long-term storage, the driest product is created in a tray freeze-dryer (Ford, and Fox 2017). With

a tray freeze-dryer, you can freeze the product in place while it undergoes primary (removal of unbound water) and secondary (removal of bound water) freeze-drying, resulting in the driest possible final product. It is possible to dry goods in bulk vials or other containers using tray freeze-dryers. To dry in vials, the freeze-drier comes with a mechanism that snaps a stopper into place, sealing the vial before it opens to the air. Long-term storage, like that of vaccines, calls for this (Basso *et al.* 2021). Technological advancements in freeze-drying are underway to broaden the scope of products amenable to this process, enhance product quality, and reduce labour costs while producing the product more rapidly.

2.9 Products from Microalgae

Since every cell in microalgae is photoautotrophic, that is, it absorbs nutrients directly, they do not need a circulatory system to carry nutrients, in contrast to higher plants. According to Kinthong *et al*. (2015), microalgal cells are sunlight-driven cell factories that can transform CO_2 into raw materials for the production of high-value bioactive chemicals like docosahexaenoic acid (DHA), animal food chemical feedstocks, and biofuels (such as biohydrogen, biodiesel, and bioethanol). Chemical and biological processing of microalgal biomass can yield high-value products such as bioacetone, biobutanol, biodiesel, and biomethane.

High concentrations of triacylglycerides, free fatty acids, and carbohydrates (mostly glucose units) are provided by microalgae feedstock, which can be utilised to create biofuels and biodiesel. The four steps involved in producing biofuel from algae are cultivation, harvesting, extraction, and processing (Rupiper 2016). Numerous culturing factors, including a carbon supply, nitrogen deprivation, phosphate limitation, light intensities, iron content, and rising salinity, control the

amount of lipids produced by algae. Thus, each of these variables affects how quickly algae grow and produce lipids.

2.9.1 Microalgae oil conversion to hydrocarbons

The development of motor fuel synthesis techniques based on potential plant oils has been the subject of extensive research. The literature has techniques for converting oils to aromatics by the use of zeolite-containing catalysts modified with Pd, Zn, Ni-Mo, or Ni-W and Co (Gekhman *et al*. 2018). This strategy, however, is no longer relevant because modern petrol fuels contain fewer aromatics. Potential raw sources for the production of biofuel include leftover edible fats and the fatty acids extracted from different oil crops. Research is still ongoing; however, fatty acid methyl esters (FAME), a form of biodiesel made by trans-esterifying fats and oils, are still in use in industry.

However, FAME has some disadvantages over petroleum-based diesel, such as greater cloud points, higher viscosity, and higher boiling points of the C_{16}–C_{18} fractions. To prevent surfactants from forming, the typically homogeneously catalysed procedure requires very pure triglycerides and competes with the human food chain. There are various applications for non-edible raw materials. Typically, "second-generation biofuels" refer to fuels produced from this feedstock. The hydrocarbons used to make them have the same characteristics as fuels derived from petroleum. Non-edible biomasses such as cellulosic material, woody biomass, crop wastes, algae, and free fatty acids, which are often extracted as oils and fats, are the raw materials used to make all of these fuels. However, even if the fuels produced by second-generation biofuels are identical to diesel, they are nevertheless, made using conventional feedstock such as oils and fats.

The first commercial technique to produce biodiesel from trash is the NExBTL process. The UK developed it (Neste Oil). The improved cetane number of NExBTL biodiesel over fossil fuel-derived diesel adds to its excellent blend status. Furthermore, three examples of industrialised biomass-to-liquids (BTL) processes include the Sun Diesel process by Choren and Volkswagen, the H-oil process by Petrobas, and Green Diesel by UOP and Honeywell. These are second-generation biofuels. First-stage gasification of carbonaceous material or biomass, with or without oxygen, occurs at high temperatures in BTL processes. Either oxygen is present or not when this happens. The final result of the gasification process, which includes the conversion steps of steam gasification and partial oxidation, is frequently syngas. After being generated, the syngas are used in Fischer-Tropsch (FT) synthesis to produce liquid fuels or methanol, which is subsequently converted into olefins (MTO-process) or petrol (MTG-process). The process of breaking molecular bonds and accumulating hydrocarbons in FT or MTG yields the necessary biomass-derived fuels. Another way to produce fuels from biomass is by selectively defunctionalizing biomass and biomass platform molecules while preserving a naturally occurring hydrocarbon framework. This process eliminates the need for energy-intensive gasification and FT synthesis. The process of converting triglycerides and their derivatives into hydrocarbons has been the subject of extensive investigation in the last several years.

The scientific literature generally addresses two types of metal-supported catalysts for the removal of oxygen from biomass feedstock: first, supported noble metal catalysts, and second, sulphided transition metal catalysts, which are commonly used as hydro-treating catalysts in the petroleum industry, such as NiS/NiMo/-Al_2O_3 and CoMo/-Al_2O_3. One way to characterise these two kinds of catalysts is as metal-supported catalysts. Immer *et al*. (2017) reported on the chemical processes that happened during

the liquid phase deoxygenation of stearic acid (SA), oleic acid (OA), and linoleic acid. To deoxygenate OA, it underwent sequential hydrogenation and decarboxylation in the presence of hydrogen; however, decarbonylation occurred more successfully in the presence of inert helium at much slower reaction rates.

$$C_{17}H_{33}COOH + H_2 \rightarrow C_{17}H_{35}COOH \quad (2.39)$$

$$C_{17}H_{35}COOH \rightarrow CO_2 + n\text{-}C_{17}H_{36} \quad (2.40)$$

$$C_{17}H_{33}COOH \rightarrow CO + H_2O + C_{17}H_{32} \quad (2.41)$$

Furthermore, the catalyst exhibited enhanced stability upon exposure to an environment comprising 10 vol.-% hydrogen in the form of helium. Likely, this impeded the creation of unsaturated hydrocarbon compounds that would have adhered to the catalyst surface, obstructing the active centres and preventing additional reactions from taking place. Snare *et al*. (2016) conducted liquid-phase deoxygenation studies in a continuous-flow reactor without solvents and in an argon environment using a Pd/C catalyst. The primary by-product was stearic acid; hydrocarbons, mostly olefins and aromatics, formed at a rate of less than 10 mol %. Lestari *et al*. (2015) reported that a mesoporous carbon (Sub-unit) based Pd catalyst was used to continuously deoxygenate pure stearic acid in the liquid phase. With n-heptadecane serving as the principal product, a stable 15 % stearic acid conversion was achieved. The idea posited that CO is generated from CO_2 and H_2 via the decarbonylation of stearic acid and the reverse water-gas shift reaction, as supported by gas phase investigations. In addition to the metal-supported catalysts, zeolites were also investigated for their potential to valorise vegetable oils into biofuels.

Lestari *et al*. (2015) reported that pure stearic acid was continuously deoxygenated in the liquid phase over a Pd catalyst supported by a mesoporous carbon sub-unit. The main product produced was n-heptadecane, but stearic acid was also stabilised at a rate

of about 15%. The idea, which was based on ongoing gas phase investigations, states that stearic acid decarbonylation and the reverse water-gas shift reaction produce carbon monoxide (CO) from carbon dioxide (CO_2) and hydrogen (H_2). It was believed that these two processes were responsible for creating CO. Apart from the catalysts supported on metals that were just covered, zeolites were also looked into as a possible technique to turn vegetable oils into biofuels. The H–ZSM5 zeolite was discovered to be the most effective catalyst for the upgrading of vegetable oils. As a result, it has been the zeolite that has been exposed to the highest amount of research for the breaking of triglycerides. Katikaneni *et al*. (2015) found that potassium-impregnated ZSM5 (K–ZSM5) had a poorer yield of hydrocarbons, especially aromatics, than H–ZSM5. This was because the latter had a substantially lower density of strong Brønsted acidic sites. Despite the hydrogenation of H–ZSM5, this remained the case. This led to the conclusion that the catalyst's acidity level plays a crucial part in the aromatization process, which is the reaction that happens after deoxygenation. However, it had no initial effect on the blood's oxygenation level. Adding steam-suppressed hydride transfer increased the amount of gaseous products produced and extended catalyst life. Hossain *et al*.'s (2019) utilisation of leftover palm oil and conversion rose by 20 % in the presence of composites of H–ZSM5 and MCM–41. Although mesoporous material demonstrated a lower conversion rate, 44 wt. % of petrol was produced overall. The first cracking catalysts employed in the petrochemical sector were amorphous silica-alumina catalysts. Compared to silica-aluminates with a high aluminium content, those with a low content are less active. The most acidic catalyst, Al_2O_3, with a weight percentage of 30 % is required for the catalytic cracking reactions of long-chain hydrocarbons. To create diesel fuel and fuel blends, Hengst *et al.* (2015) described the single-step conversion and deoxygenation

of free fatty acids over acidic catalysts. At a conversion rate of 94 %, a mixture containing 20 % weight of H–ZSM5 and 80 % weight of aluminium oxide produced a C_{17} selectivity of 62 %. The catalyst containing 20 % zeolite had an average pore diameter of 48.3 Å, whereas the pure aluminium oxide had an average pore diameter of 34.4 Å. The zeolite-containing catalyst's bigger pore size improved the catalytic performance by reducing diffusion barriers for the large oleic acid molecules.

Ballotin *et al.* (2016) developed a novel biodiesel synthesis catalyst based on K_2MgSiO_4, derived from the mineral serpentinite. TG, SEM, XRD, AA, and BET investigations demonstrated the ability to convert serpentinite $Mg_3Si_2O_5(OH)_4$ to the primary crystalline phase K_2MgSiO_4 by impregnating it with KOH (5, 10, and 20 wt. %) and thermally treating it at 500, 700, and 900 degrees Celsius. The results of titration and TPD-MS (CO_2) analyses indicated the presence of weak/medium basic sites at comparatively high amounts. With the catalyst at a 10 wt. %, biodiesel production using soybean oil (methanol: soybean oil ratio of 1:12, 1:9, 1:6, 60 ^oC) demonstrated yields exceeding 95 %; this catalyst may be reused three times without significantly lowering the reaction yield.

The observed results are addressed in terms of a novel catalytic phase based on negatively charged oxygen basic sites (K^+ ions) trapped in the cavities of the $MgSiO_4^{2-}$ structure.

Hengst *et al*. (2015) used acidic catalysts containing palladium to deoxygenate oleic acid in the gas phase. Aluminium oxide catalysts were created using three different kinds of boehmite, and they were calcined at temperatures ranging from 500 to 1100 degrees Celsius. Before undergoing deoxygenation experiments in autoclaves, fixed bed plug flow reactors, and trickling bed reactors, each catalyst was impregnated with 1 wt. % palladium. It was possible to construct many combinations of boehmite, the

best alumina precursor, and zeolites to increase the acidity of the catalyst and, as a result, the deoxygenation performance. To find the optimum composite catalyst, hydrogen was tested both with and without the addition of nitrogen, water, and catalyst regeneration through thermal treatment. The researchers also synthesised and assessed silica aluminates doped with 1 wt. % Pd. Utilised techniques included nitrogen adsorption isotherms (BET), field emission scanning electron microscopy (FESEM), thermogravimetric analysis, and X-ray particle diffraction.

Gekhman *et al*. (2018) converted a mixture of fatty acids using catalysts comprising Pt and Sn. Compared to monometallic Pt and Sn precursors, heterometallic precursors have metal-metal linkages, which enables the synthesis of more active and selective catalysts. Catalyst structural characteristics were characterised using TEM, EDS, and XAS methods. According to Sorigue et al. (2016), microalgae may use a unique, light-dependent process to convert C_{16} and C_{18} fatty acids into alkanes and alkenes. Compared to oil accumulation methods, the processes by which microalgae convert fatty acids into alkanes and alkenes have received far less research. The headspace and cell pellet of liquid cultures of *Chlamydomonas reinhardtii* (Chlorophyceae) contained the C_{17} alkene n-heptadecene. It is believed that the alkene 7-heptadecene seen in Chlamydomonas arises from the decarboxylation of cis-vaccenic acid. Deuterated $D_{31\text{-}16:0}$ (palmitic acid) yielded $D_{31\text{-}18:0}$ (stearic acid), $D_{29\text{-}18:1}$ (oleic and cis-vaccenic) acids, and D_{29}-heptadecene when treated with intact Chlamydomonas cells. These findings suggest that the removal of the carboxyl group from a C_{18} monounsaturated fatty acid forms heptadecene. Phase, temperature, and light all had an impact on the synthesis of 7-heptadecene; photosystem II inhibitors had no such effect. The chloroplast contains 80 % of the alkene, according to the cell's fractionation. Numerous Nannochloropsis species including Chlorella variabilis NC64A (Trebouxiophyceae) were reported to

possess pentadecane, heptadecane, and 7- and 8-heptadecene (Eustigmatophyceae). Notwithstanding, the absence of C_{15}–C_{19} hydrocarbons, the diatom *Phaeodactylum tricornutum* and the cyanobacterium *Ostreococcus tauri* (Mamiellophyceae) produced C_{21} hexane. The genomes of *Nannochloropsis*, *Chlorella*, and *Chlamydomonas* were examined for hydrocarbon production genes, but none were found.

Gani *et al.* (2017) evaluated the efficacy of Botryococcus sp. in the phycoremediation of household wastewater and examined the variety of hydrocarbons recovered from microalgal oil. All pollutant loads decreased statistically significantly, with improvements seen in COD, BOD_5, TN, TOC, and TP. Each litre of wastewater generated 0.1 g of dry biomass on average. Additionally, the dry-weight biomass of Botryococcus sp. contained 72.5 % of crude oil. 2-ethyl hexyl tridecyl ester of phthalic acid ($C_{29}H_{48}O_4$) accounted for 71.6 % of the total hydrocarbon components in the extracted algal oil, according to an analysis of the chemical composition of the oil using Gas Chromatography-Mass Spectrometry (GC-MS). According to the study's conclusions, Botryococcus sp. is a potential choice for effective phycoremediation and a consistent source of hydrocarbons for the bio-based plastics sector. Researchers Maltsev *et al*. (2023), Su *et al*. (2022), and Ferreira *et al*. (2019) used batch cultivation techniques to track the growth of microalgae in huge volumes. The main goal of this study was to extract all of the lipids and hydrocarbons using a method based on thermodynamics and kinetics. Growing the algae in a batch manner produced the highest possible amount of dry biomass (23 g m^{-2} d^{-1}). With less than 1 % moisture content, the dry biomass underwent many pre-treatment techniques, solvent systems, and extraction parameter optimisations. This shows that utilising ultrasonication in combination with chloroform: methanol can extract up to 24.2 % of total lipids and hydrocarbons. The study examined the impact of temperature (308-338 K) on kinetics.

Using first-order kinetics, the extraction's rate constants and activation energies were determined to be 3.0431 s^{-1} and 36.7214 kJ mol^{-1}, respectively.

Measuring the thermodynamic activation parameters ΔG, ΔH, and ΔS revealed that the process was endothermic, irreversible, and spontaneous. Microalgae retain hydrocarbons and fatty acids, which are crucial components of biofuels. It is crucial to identify the microalgal strains with the greatest precursor profiles for fuel production during bioprospecting investigations. In this regard, Vidyashankar *et al*. (2015) investigated the biomass production, fatty acid and hydrocarbon composition, and growth mechanism of 32 freshwater green microalgae. *Oocystis pusilla* CFR 6-01/FW, *Scenedesmus dimorphus* CFR 1-05/FW, and *Quadrigula lacustris* CFR 7-01/FW all produced a lot of biomass and multiplied more quickly. To check for lipid accumulation, microalgal cells were treated with a small amount of acetic acid (7 mmol L^{-1}) and then stained with Nile-red. Six strains (*S. dimorphus* CFR 1-05/FW, *Scenedesmus obtusus* CFR 1-09/FW, *Chlorococum sp.* CFR 2-01/FW, *C. humicola* CFR 2-03/FW, *Chlorella sorokiniana* CFR 3-01/FW, and *Dictyosphaerium* CFR 5-01/FW) showed lipid accumulation of >20 wt. % during the stationary phase. All species of chlorophycean included large levels of oleic, palmitic, and alpha-linolenic acids. They found hydrocarbons acceptable for direct blending with fuels derived from petroleum that are of fuel grade. Hydrocarbons accounted for more than 10 % of the dry biomass in 14 strains. There were several n-paraffins with chain lengths ranging from C_{15} to C_{20} in all of the strains. Branching isoprenoid hydrocarbons accounted for 49 % of the total hydrocarbon content of *Scenedesmus sp*. CFR 1- 13/FW in the study. We discovered that 40 % of *Kirchneriella cornuta* CFR 8-01/FW contained n-tetradecane. Because the microalgal hydrocarbon profiles mimic a paraffinic and isoparaffinic component of petroleum diesel and because FAME-based biodiesel

complies with international regulations, it is feasible to blend algae-derived biofuels with conventional petroleum fuels.

2.10 Airlift Reactors (ALR)

In airlift reactors, a reaction broth circulates between a riser and a corresponding downcomer compartment with a minimal gas phase because of the injection of a gas stream into a designated reactor compartment (the riser). These bioreactors are pneumatically mixed. For mass transfer and gaseous and liquid phase mixing, ALR has an internal draft tube. Figure 2.11 presents a general flowchart for the design of bioreactor systems. The unique and well-defined cyclic pattern of fluid circulation through channels that form a loop for liquid recycling is what distinguishes ALR. Numerous specific uses, including the production of fuel ethanol, single-cell protein, and wastewater treatment, have led to the development and construction of large-scale ALR.

2.10.1 The basic parts of airlift reactors

The components of an airlift reactor are the base, downcomer, gas separator, riser, and sparger. Each component is essential to the reactor's basic operation.

2.10.1.1 The Riser

The Riser is similar to a bubble column, where sparged gas moves upward randomly and haphazardly and decreases the density of the riser making the liquid move upward.

2.10.1.2 The Downcomer

The downcomer does not receive the gas, but the degassed medium flows down toward the bottom and circulates within the riser and downcomer. Degassed media and cells.

2.10.1.3 The Base

Connected to Perforated nozzle bank/ plate/Sparger to pump pressurized air.

2.10.1.4 Headspace

Gas release region, flocculation, foam accumulation etc.

2.10.1.5 Gas separator

Facilitates gas/liquid recirculation and maximizes gas residence time, reducing gas friction in the downcomer.

2.10.2 Types of airlift reactors

Airlift reactors have a novel design that allows them to remove products and deliver substrate with energy-efficient mass transfer without appreciably changing the culture broth's shear profile. The three types of driving forces for the airlift loop reactor (ALR-loop) are hydrostatic, hydromechanics propeller (or pump), and hydrodynamic jet flow powered. With fluid or fluidized systems, a propeller or jet drive can power the directed circulation flow of loop reactors, but with gas-liquid (G-L) systems, airlift-drive is the primary source of power. They are particularly well suited for fluid systems in biotechnology that need strong dispersion effects, exact flow conditions across the reaction zone, and a high specific cooling capacity.

2.10.2.1 Internal-loop split airlift reactor

Strategically positioned baffles within a single vessel create the channels required for circulation. A straight line linking the riser and downcomer of a bubble is the shortest path between them.

2.10.2.2 Internal-loop concentric airlift reactor

Numerous chemical and biological processes have adopted the standard reactor configuration for the internal-loop concentric airlift reactor.

2.10.2.3 External loop airlift reactor

Circulation for the External Loop Airlift Reactor occurs via discrete pipes. It is typically necessary to travel a minimum horizontal distance to allow the bubbles to separate.

2.10.3 The features of an airlift reactor

2.10.3.1 Driving force circulation

Airlift reactor utilizes gas (usually air) to create a density difference that drives liquid circulation. It provides good mixing without mechanical agitation. Sheer stress in Equation (2.42) is fundamental in a fluid.

$$Shear\ stress, \tau = \left(\frac{du}{dy}\right) \mu \qquad (2.42)$$

where τ is sheer stress (Pa), μ is the dynamic viscosity of the fluid (Pa.s), and $\left(\frac{du}{dy}\right)$ is the velocity gradient (s^{-1}), representing the rate of change of velocity u with respect to the perpendicular distance y.

Shear stress in airlift reactors is typically low due to gentle mixing caused by gas flow, which is suitable for shear-sensitive biological systems like cell cultures and enzyme reactions. This prevents damage to delicate microorganisms and suspended particles. The shear rate depends on the fluid dynamics within the reactor, especially in the riser and downcomer regions.

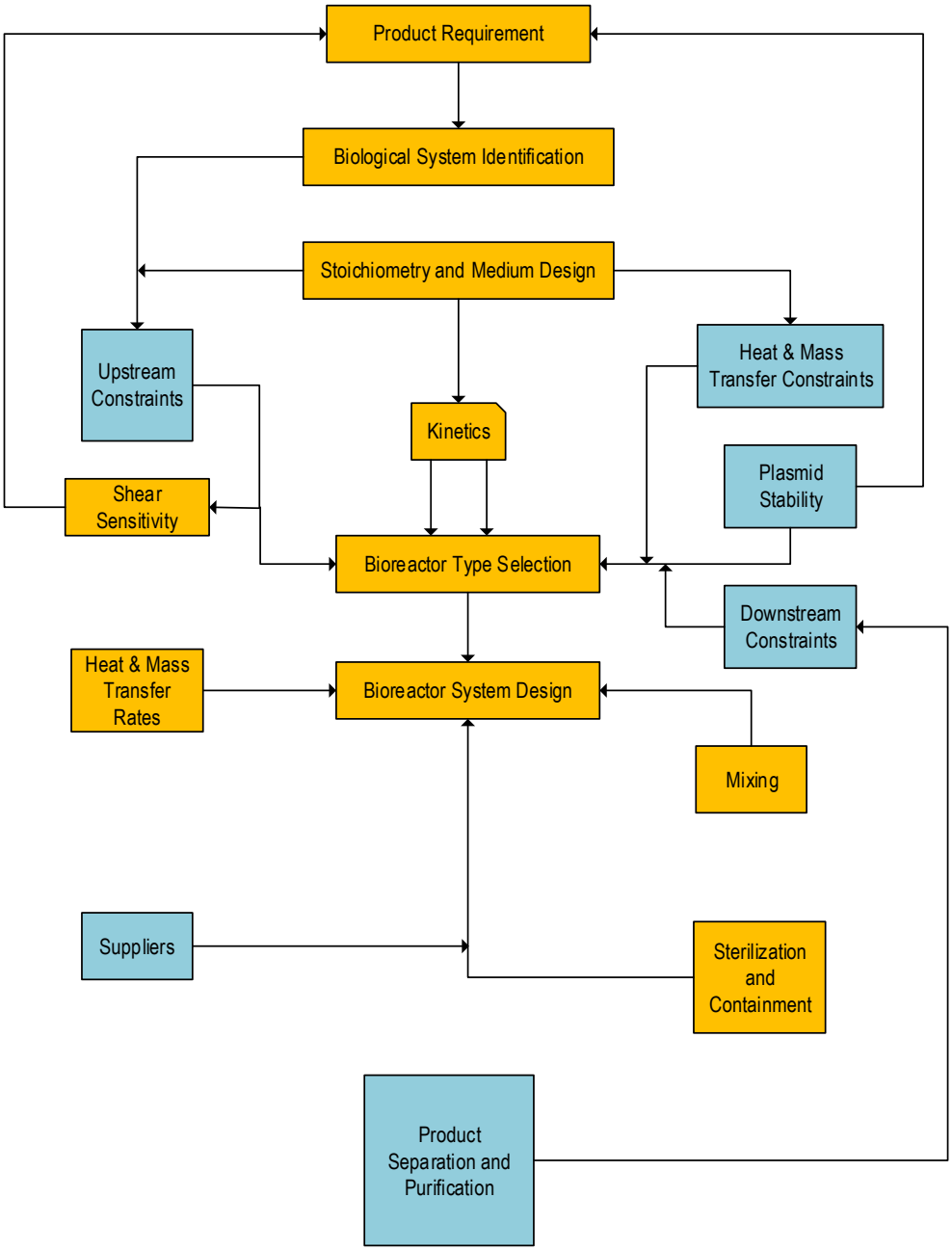

Figure 2.11 Flowchart for bioreactor system design

2.10.3.2 Disengagement of bubbles

Enhances mass transfer between gas and liquid, improving reaction efficiency. Used in processes requiring oxygen or other gases, such as fermentation and bioprocessing.

2.10.3.3 Measuring the liquid velocity

In an airlift reactor, the liquid velocity in the riser section is influenced by factors such as gas holdup and the density difference between the riser and the downcomer. A commonly used empirical correlation to estimate the liquid circulation velocity (U_L) is shown in Equation (2.43).

$$u_L = C\left(\frac{gD_H\Delta\rho}{\rho}\right)^{0.5} \quad (2.43)$$

Where C is an empirical constant, typically determined by experiment, g is the acceleration due to gravity (9.81 m/s^2), D_H is the hydraulic diameter of the reactor, Δρ is the density difference between the liquid in the riser and downcomer, and ρ is the average density of the liquid.

2.10.4 The characteristics of an airlift reactor

An airlift reactor is characterised by the following parametric behaviours:

Liquid Mixing

Mass Transfer

Rate of gas transfer across the gas

Liquid interface per unit of driving force

Energy Dissipation

2.10.5 Modifications of airlift reactors

Modification of reactor targets to improve some specific characteristic behaviours. A mechanical stirring airlift reactor (MS-ALR) combines the airlift benefits of airlift circulation with mechanical agitation to enhance mixing and mass transfer. On the other hand, a static airlift reactor (S-ALR) is without mechanical agitation but relies solely on gas injection to drive liquid circulation, and finds application mostly in

wastewater treatment, fermentation, and chemical processes. A perforated draft tube airlift reactor (PDT-ALR) is a modification of the traditional airlift reactor, where the draft tube has perforations such as holes or slots to enhance mixing and mass transfer. This design improves fluid circulation and gas dispersion, making it suitable for various biotechnological and chemical processes. Table 2.13 lists the benefits of modifying ALR, while Table 2.14 presents the challenges of ALR modification.

Table 2.13 Benefits of mechanical stirred, static and perforated draft tube airlift reactors

Property	MS-ALR	S-ALR	PDT-ALR
Enhanced mixing/energy efficiency	Improves liquid circulation, reducing dead zones and ensuring better nutrient distribution.	Operates with minimal energy input since mixing is achieved through gas sparging, reducing operational costs.	Allows fluid exchange between the riser and downcomer, reducing dead zones.
	Prevents stratification in large reactors	More economical for large-scale applications	Improves circulation, leading to better nutrient and O_2 distribution.
			Mixing is achieved using airlift principles, making it more energy-efficient than traditional stirred reactors.
Increased mass transfer rates	Stirring enhances gas-liquid contact, improving O_2		Enhances O_2 transfer rates, making it ideal for

	transfer in aerobic systems. Beneficial for bioreactors handling high-velocity fluids or non-Newtonian liquids.		aerobic fermentation and wastewater treatment.
Better control over shear conditions.	Can be optimised for shear-sensitive microbes by adjusting impeller speed and airflow.	Gentle circulation makes it ideal for shear-sensitive microbes (biofilms, mammalian cells, filamentous fungi).	Gentle circulation minimises damage to shear-sensitive microbes, such as mammalian cells and biofilms.
	Provides more uniform shear stress distribution compared to traditional airlift reactors.	Reduces cell damage, improving bioprocess yields.	Suitable for bioprocesses requiring controlled hydrodynamics.
Higher gas holdup	Promotes finer bubble dispersion, increasing gas residence time. Better CO_2 removal and O_2 transfer efficiency		Gas bubbles pass through the perforations, increasing gas-liquid contact time.
Flexibility of operation	Can handle a wider range of liquid viscosities and reactor scales.		

	Suitable for bioprocessing, wastewater treatment, and chemical synthesis.		
Solid suspension			The improved circulation enhances the suspension of solid particles, making it useful for solid-state fermentation and multipurpose reactions. Reduces particles settling at the bottom of the reactor.
Maintenance and scalability		Fewer moving parts result in lower maintenance costs and reduced mechanical failure risks. Can be easily scaled up for industrial applications. Works well in large-volume reactors for wastewater treatment.	Fewer moving parts lead to lower maintenance costs and operational downtime. Can be easily scaled up for industrial applications, while maintaining efficient fluid dynamics.

Table 2.14 Challenges of mechanical stirred, static and perforated draft tube airlift reactors

Property	MS-ALR	S-ALR	PDT-ALR
Mixing efficiency		Relies on gas injection for circulation, which may result in poor mixing in high-viscosity liquids or non-Newtonian fluids. This may lead to stagnant zones in large reactors.	Flow patterns can become unpredictable due to interaction between the riser and downcomer, and perforations. Requires careful design optimisation to ensure proper liquid circulation.
Energy consumption	Requires additional power for mechanical agitation, increasing operational costs. Less energy-efficient compared to conventional ALR.		
Mass transfer		Gas holdup and circulation velocity depend on reactor geometry and gas flow rate. In low-density media, O_2 transfer efficiency might be	

		lower than in MS-ALR.	
Mechanical complexity	More moving parts (impellers, shafts, seals) lead to higher maintenance requirements. Potential for mechanical failure, especially in large-scale systems		
Shear damage/control over shear conditions	Some microbes are shear-sensitive and may be damaged by impeller forces. Requires careful optimization of stirring speed to balance mixing and cell viability.		Shear stress is generally low but may be higher than in traditional ALR due to local turbulence near perforations. Not suitable for extremely shear–sensitive cell cultures.
Bubble coalescence issues and uneven gas distribution	Excessive stirring may cause bubbles to merge, reducing the effective surface area of gas transfer. May require additional sparging strategies to maintain fine bubble distribution	Inconsistent gas dispersion can lead to uneven mass transfer, requiring optimised sperger design. Large bubbles can form, reducing gas-liquid contact efficiency.	Large bubbles may form near the perforations, reducing effective gas dispersion. May require optimised perforation size and distribution to

			maintain fine bubble distribution.
Reaction kinetics		May not be suitable for reactions requiring intense mixing, such as some chemical synthesis and crystallization processes. Residence time distribution can be broader, potentially affecting product yield and consistency.	
Handling of high solid concentrations		Can struggle with high solid suspensions, as particles may settle in low-flow zones. May require modification, such as internal baffles to improve solid suspension.	
Potential fouling and blockage			
Scale-up considerations	Designing a large-scale MS-ALR requires careful integration of AL		Requires careful control of perforation size, spacing and gas flow rates to

	and mechanical stirring effects.	maintain efficient hydrodynamics.
	Scale-up must consider fluid dynamics, mass transfer limitations, and potential mechanical stress.	Improper design may lead to uneven mixing and gas maldistribution.

Figure 2.12 shows the layout of the mechanical stirring airlift reactor, static airlift reactor, and perforated draft tube airlift reactor.

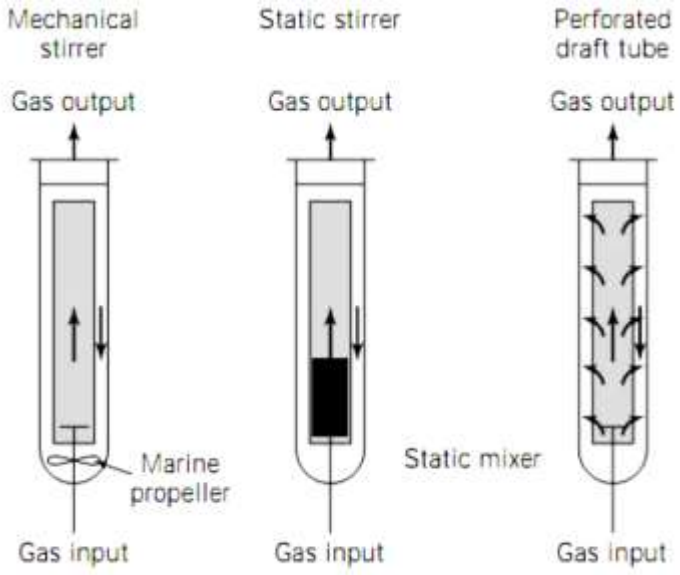

*Figure 2.12 Flowchart for airlift bioreactor system design (*Huang *et al.* 2016*)*

2.10.6 Sparger design

Sparger sizing is based on the superficial gas exit velocity from the porous sparger surface, expressed in feet per minute (FPM), calculated from actual cubic feet per minute per square foot of sparger surface area (ACFM/Ft.^{2}). ACFM is calculated at the liquid pressure and temperature at the sparger, it is not based on gas pressure.

2.10.6.1 Sizing Procedure for In-Tank Spargers

A. The gas flow required is determined in standard cubic feet per minute (SCFM). Then the liquid pressure at the sparger, in PSIG (P). For open or vented tanks,

liquid head in feet x 0.433 x specific gravity = PSIG. (2.44)

(Specific Gravity of water = 1.0)

B. For closed tanks or vessels with pressurized headspace, headspace pressure is added to the liquid head pressure to obtain P.

C. The liquid temperature °F, (T) is determined. ACFM is determined from SCFM using the standard gas formula in Equation (2.45).

ACFM = SCFM x 14.7 x (460 + T) (14.7 + P) 520 5. (2.45)

Select Gas Exit Velocity, FPM.

D. Appropriate Mott sparger element is added or elements and the best in-tank arrangement is determined based on process requirements. Mott in-tank spargers increase gas absorption by as much as 300% over traditional sparging technologies, resulting in faster throughput and less gas usage In agitated tanks, reinforced elements are used or provide support as required.

Smaller bubbles will result from lower exit velocities. Exit velocities could be lower than the stated design values. Sometimes, it is necessary to test and validate the real application.

2.10.7 Product requirement

Microalgae biomass production involves cell growth propagation through the utilization of inorganic carbon, exogenous carbon (soluble organic compounds found in wastewater due to decay or biodegradation of organic materials), nitrogen and

phosphorus in the presence of light. It is indirectly the production of microalgal lipids during the utilization of the stated materials by the hydrodynamic modelling of a named photobioreactor.

2.11 Advancements in Wastewater Treatment Using Microalgae

Beyond hydrocarbon production, microalgae have been explored for various applications in wastewater treatment: Microalgae have a wide range of applications in wastewater treatment beyond hydrocarbon production. Their ability to remove pollutants, recover valuable resources, and contribute to circular bioeconomy solutions makes them an essential tool for sustainable wastewater management. The integration of microalgae into industrial wastewater treatment processes offers a promising avenue for sustainable biofuel production and environmental remediation (Zhou *et al.*, 2012). Ongoing research continues to optimize these systems, aiming to enhance efficiency and economic viability.

2.11.1 Membrane bioreactors (MBRs)

Membrane Bioreactors (MBRs) integrate biological treatment with membrane filtration, significantly improving water quality by removing suspended solids, pathogens, and organic matter (Judd and Jefferson, 2003). They **p**roduces near-drinking water standards, and require less space than conventional activated sludge systems, with enhanced sustainability. However, membranes require regular maintenance, and they have fouling issues, such as clogging, which affects efficiency. Membrane bioreactors find applications municipal wastewater treatment aimed at reuse; and industrial effluent treatment in food and pharmaceutical industries.

2.11.2 Advanced oxidation processes (AOPs)

AOPs use hydroxyl radicals (•OH) to degrade organic pollutants, including pharmaceutical residues, pesticides, and endocrine disruptors (Oturan and Aaron, 2014). The Fenton's process uses iron and hydrogen peroxide; Ozone-based treatment utilizes O_3 effectively degrading micropollutants, while photocatalysis uses UV light with TiO_2 for oxidative degradation. The AOPs bear dual advantages, removing emerging contaminants efficiently and does not produce secondary waste. However, AOPs pose challenges in high energy utilization and the possible formation of toxic by-products. Applications of this technology have been in treating hospital wastewater, and removing persistent organic pollutants (POPs).

2.11.3. Constructed wetlands (CWs)

Constructed wetlands use natural filtration via plants, soil, and microbial communities to treat wastewater in an eco-friendly manner (Vymazal, 2011). Constructed wetlands can take the Surface-Flow configuration, which has open water areas with floating vegetation or the Subsurface-Flow configuration in which wastewater flows through soil media, enhancing microbial degradation. CWs have Low operational costs and are very effective in nitrogen and phosphorus removal. Unfortunately, CWs require large land area to construct and operate, and their efficiency depends on the climatic zone of their location. They are used mainly to decentralize rural wastewater treatment, and agricultural runoff management.

2.11.4 Microbial fuel cells (MFCs)

MFCs use electrogenic bacteria to generate electricity while treating organic waste in wastewater (Logan *et al.,* 2006), exhibiting simultaneous wastewater treatment and energy recovery and reduction in sludge generation. However, power output is low,

and electrode fouling challenges are encountered. MFCs are energy-neutral wastewater treatment plants used to power sensors in remote water treatment facilities.

2.11.5 Electrocoagulation (EC)

EC uses an electric current to induce the aggregation of contaminants, facilitating their removal (Moussa *et al.*, 2017). Electrocoagulation is an effective technique in removing heavy metals and dyes requiring only minimal chemical addition. However, the process consumes high energy, and electrode corrosion reduces long-term efficiency. EC is used to treat textile and tannery wastewater, and to remove heavy metals in mining effluents.

2.11.6 Anaerobic digestion for biogas recovery

Anaerobic digestion converts organic waste into biogas (methane + CO_2) through microbial degradation in oxygen-free conditions (Angelidaki *et al.*, 2018), thus generating renewable energy with reduction in sludge volume. The process requires temperature control, which poses a challenge of slow operation the risk of methane leakages. Anaerobic digestion is applied in wastewater treatment plants with energy recovery, and in industrial organic waste treatment.

2.12 Emerging Trends in Wastewater Treatment

2.12.1 Smart monitoring with AI and Internet of Things (IoT)

AI-driven predictive maintenance for early detection of failures (Zhou *et al.*, 2020). IoT-enabled sensors optimize chemical dosing and aeration in treatment plants.

2.12.2 Nanotechnology in water purification

Nanomaterials (graphene, carbon nanotubes) for heavy metal removal (Qu *et al.*, 2013). Antibacterial nanofilters ar deployed for decentralized drinking water treatment.

2.12.3 Zero liquid discharge (ZLD) Systems

Complete wastewater recovery via evaporation and crystallization, minimizing discharge (Mickley, 2019).

2.13 Future Perspectives and Innovations in Microalgae-Based Wastewater Treatment

Emerging technologies, such as photobioreactors, biofilm reactors, and genetic engineering, are improving the efficiency of microalgae-based wastewater treatment. Additionally, coupling microalgae with bacterial consortia is being explored to enhance pollutant degradation. The field of microalgae-based wastewater treatment is evolving rapidly, with new technologies and approaches aimed at improving efficiency, scalability, and economic viability. The integration of advanced bioreactors, genetic engineering, AI-driven optimization, and industrial circular economy models are pushing microalgae-based wastewater treatment toward large-scale commercial applications. These innovations have the potential to enhance water quality, recover valuable resources, and contribute to climate change mitigation. The following sub-sections speak to the promising future directions and innovations:

2.13.1 Advanced photobioreactors for wastewater treatment

While open pond systems are widely used, advanced photobioreactors (PBRs) are gaining traction due to their ability to enhance algal growth and pollutant removal

efficiency. Key Advancements are in (i) Vertical and Tubular PBRs. These increase light penetration, optimize CO_2 utilization, and improve biomass production. (ii) Membrane-based PBRs: Integrating membranes allows for improved separation of microalgal biomass, reducing harvesting costs. (iii) Hybrid Systems: Combining open ponds with PBRs can improve nutrient uptake efficiency while keeping costs manageable. A hybrid PBR system was recently developed to treat textile wastewater, effectively removing dyes and heavy metals while producing algal biomass for biofuel.

2.13.2 Biofilm-based wastewater treatment systems

Instead of free-floating algae, algal biofilms grown on surfaces are being explored to improve wastewater treatment efficiency and facilitate easier biomass harvesting. Advantages of Biofilm Systems: Reduces water loss and contamination. Requires less energy compared to suspended culture systems. Facilitates continuous wastewater treatment without frequent harvesting. A study on *Chlorella vulgaris* biofilms showed a 90% removal of nitrates and phosphates from agricultural wastewater.

2.13.3 Genetic engineering and synthetic biology

Researchers are engineering genetically modified (GM) microalgae with enhanced wastewater treatment capabilities. Current Innovations in Genetic Engineering are in the areas of (i) Enhancing the expression of genes responsible for heavy metal uptake (e.g., mercury, cadmium), (ii) Increasing the production of lipids and biofuels from wastewater-grown microalgae, and (iii) Modifying algae to degrade complex organic pollutants such as pharmaceuticals and pesticides. Genetically modified Chlamydomonas reinhardtii has been engineered to remove pharmaceutical residues from hospital wastewater.

2.13.4 Microalgae-bacteria consortia for enhanced pollutant removal

Instead of using microalgae alone, researchers are co-cultivating microalgae with bacteria to create more efficient wastewater treatment systems. Microalgae produce oxygen, which supports bacterial degradation of organic pollutants. Bacteria break down complex organic matter, making nutrients more accessible for algal growth. A *Chlorella-Bacillus* system was recently tested in municipal wastewater treatment and showed improved nitrogen removal (92%) and increased algal biomass yield.

2.13.5 Artificial intelligence (AI) and machine learning for process optimization

Artificial intelligence (AI) and machine learning are being used to optimize algal wastewater treatment systems by predicting growth patterns, adjusting nutrient levels, and controlling environmental conditions. AI applications in microalgae wastewater treatment cover (i) Real-time monitoring of pH, CO_2 levels, and light intensity for optimal growth. (ii) Predictive modelling to determine the best harvesting time, and (iii) Automated control of photobioreactors and nutrient dosing. A machine-learning model was successfully used to optimize microalgae-based removal of ammonia and phosphates from dairy wastewater.

2.13.6 High-value product recovery from microalgal biomass

Beyond biofuels, researchers are exploring value-added products from microalgae grown in wastewater, making the process more economically viable. Potential High-Value Products: Bioplastics: Algal biomass can be used to produce biodegradable plastics. Nutraceuticals & Pharmaceuticals: Extracting antioxidants, omega-3 fatty acids, and pigments. Biofertilizers: Converting algal biomass into organic fertilizers for sustainable agriculture. Spirulina cultivated in food-processing wastewater has

been used for phycocyanin pigment extraction, a high-value product in the food industry.

2.13.7 Industrial integration and circular bioeconomy models

Companies are exploring ways to integrate microalgae-based wastewater treatment directly into industrial processes to create closed-loop systems. Circular Economy Approaches: Breweries & Distilleries: Using microalgae to treat wastewater while producing bioethanol. Dairy & Livestock Farms: Treating manure wastewater and converting algal biomass into animal feed. Power Plants: Capturing CO_2 from emissions to fuel algal growth while cleaning wastewater. A cement factory in India integrated microalgae cultivation with its wastewater treatment process, capturing CO_2 emissions and producing biofertilizers from algal biomass.

2.13.8 Decentralized and small-scale algal wastewater systems

In rural and remote areas, low-cost algal wastewater treatment units are being developed as an alternative to expensive infrastructure. Key Features of Decentralized Systems: Can be set up in small ponds or modular units. Uses low-energy input, making it sustainable. Can be adapted for community wastewater treatment. A low-tech algae pond system was recently tested in Africa to treat domestic wastewater while generating biofertilizer for local farmers.

CHAPTER 3

Materials and Methods

3.1 Background

This section seeks to probe the distinctive nature of industrial wastewater and the nature of microalgae biomass before and after microalgal oil extraction. The elements of characterisation are stated and addressed in the sub-sections that follow, not leaving out sampling and sample pre-treatment. It also describes the techniques adopted to characterise the samples.

3.2 Wastewater Sampling, Preservation and Storage

The standard methods for the analysis of water and wastewater (APHA 1999c) were adopted. Wastewater effluent was obtained from the following industries:

(a) Sugar industry (SWW)

(b) Brewing industry (BWW)

(c) Dairy industry (DWW)

Sterilized chemical-resistant bottles were used to collect wastewater samples. Wastewater samples were collected in glass bottles to analyse the solids content. Wastewater samples were collected in plastic bottles for their metallic composition determination. The pH may change significantly in a matter of minutes: dissolved gases (oxygen, carbon dioxide) may be lost. Because changes in such basic water quality properties may occur so quickly, temperature, pH, dissolved oxygen (DO) and conductivity (CD) were measured in the field immediately after taking the sample using a calibrated Aqua Lytic (AL 15) MultiMeter, Germany. Sampling was done

following method 1060 as contained in the standard procedure (APHA 1999a). BOD and COD analyses were carried out immediately upon arrival at the laboratory, which was 30±10 minutes' drive from the sampling site, while the rest of the sample was stored in the cold room at 4 ^{o}C for further analysis.

3.2.1 Wastewater pre-treatment

The work presented in this thesis is focused on the use of microfiltration (MF) as a pre-treatment step of industrial wastewater. Microfiltration is a physical process where a contaminated fluid is passed through a special pore-sized membrane to separate suspended particles and microorganisms from the working liquid. MF is a pressure-driven or vacuum-driven membrane separation process that separates particulate matter from a fluid (water, wastewater, or industrial process fluid) by physical straining.

Direct flow (or "dead end") filtration was applied where all the wastewater to be filtered was driven to supply pressure, in a direction perpendicular to a filtering surface; suspended particles and/or contaminants were captured within the filtration media or built upon the microfilter surface, causing the differential pressure across the filter to rise as it blocks throughout the filtration process. The filtrate exited the filter on the downstream side. Once a certain differential pressure had been reached, after which the fluid flow rate decreased and/or the filter reached its terminal differential pressure, filtration was stopped, and the filter was either discarded or regenerated for re-use. The treatment of the wastewater with 0.2 μm ceramic MF membranes reduced the initial chemical oxygen demand of 5000–10,000 mg/L below 250 mg/L. The filtrate was mixed with reference water (RW) of low and medium contamination and then submitted to biological treatment.

3.3 Wastewater Characterisation

Wastewater from the selected industries was characterised as follows:

Physical characteristics

Inorganic chemical characteristics

Metallic (mineral) composition

Organic constituents

Biological characteristics

3.3.1 Physical characteristics

A physical attribute of a substance is a trait that can be viewed or measured without changing the substance's identity. It has nothing to do with a change in its chemical makeup. The physical qualities of a material are its identifying characteristics or properties. These are physical characteristics that are visible to others even when no further information about the material is available. Colour (intensive), density (intensive), volume (extensive), mass (extensive), boiling point (intensive), melting point (intensive), texture (intensive), smell (intensive), solubility (intensive), polarity (intensive), solids, temperature, and many other characteristics are all physical features of wastewater. Wastewater characterisation gives a plethora of data about the types and concentrations of pollutants present.

3.3.1.1 Solids

The sample was evaporated in a weighted dish over a steam bath and dried to a consistent mass in an oven at 105°C. At 550±1°C, the residue was ignited to a constant weight. The total fixed solids are represented by the surviving solids, while the total volatile solids are represented by the weight lost during ignition.

(i) Total solids (TS)

For this determination, EPA Method 2540 B (EPA 2000) was modified and adapted. A clean porcelain dish that had been washed and dried was maintained in a hot-air oven at 105±1°C for 1 hour and cooled in a silica gel desiccator in this modified procedure. In the analytical balance, the empty warmed and cooled porcelain dish was weighed, and the measured weight was marked as W_1. A 100 mL quantity of the well-mixed wastewater sample was pipetted into a porcelain dish that had been preweighed, preheated, and chilled. The charged porcelain dish was then placed on a hotplate to dry out before being transported to a 105±1°C hot air oven. After 30 minutes in the oven, the sample was transferred to the silica gel desiccator to chill for 2 hours before being weighed. The new weight was denoted as W_2 (EPA 2001; American Public Health Association 1999a). The computations for TS are shown in Appendix A(i), applying Equation (3.1).

$$Total\ solids, TS = \frac{(W_2 - W_1)\ \text{x}\ 1000}{volume\ of\ sample\ (mL)}\ \frac{mg}{L} \tag{3.1}$$

here

W_2 = weight of dried residue + dish, mg,

W_1 = weight of dish, mg.

(ii) Total volatile solids (TVS)

The dried residues in section 3.3.1.1(i) were transferred to a cool muffle furnace in a porcelain dish, after which the furnace was heated to 550±1°C and fired for 2 hours. In a silica gel desiccator, the residue was cooled to an equilibrium temperature. The leftovers were weighed. The residue was re-ignited for 30 minutes before cooling in a desiccator and weighed till the weight difference was less than 4%. The ultimate

weight was noted as W_3. The computations for TVS were done using Equation (3.2) and are shown in Appendix A(ii).

$$Total\ volatile\ solids, TVS = \frac{(W_2 - W_3)\ \text{x}\ 1000}{volume\ of\ sample\ (mL)}\ \frac{mg}{L} \quad (3.2)$$

W_3 = weight of ignited residue + porcelain dish, mg

W_2 = weight of dried residue + porcelain dish, mg,

(iii) Total suspended solids (TSS)

This determination was made using standard procedure 2540 D. A well-mixed wastewater sample was filtered through a weighted 47 mm diameter, 0.45 μm pore glass-fibre filter medium (Macherey-Nagel, Germany) and the residue retained on the filter was dried to a constant weight at 105$\pm$1 °C in this way. The total suspended particles were represented by the increase in the weight of the filter.

The wrinkled side of the filter material was placed into the filtration device first. The disk was vacuumed and then washed three times with 20 mL pieces of de-ionized water. Suction was kept going to get rid of any remaining water. The vacuum cleaner was switched off, and the laundry was thrown away. The filter was taken from the filtering device and placed in a weighing dish made of inert aluminium. It was dried for 1 hour at 105°C in an oven, then cooled to equilibrium temperature in a silica gel desiccator before being weighed. The drying, desiccating, cooling, and weighing cycle was repeated until the weight remained constant. The desiccator was then used to store it until it was needed.

It was time to set up the suction filter assembly device. To seat the filter in place, a tiny amount of de-ionized water was used to wet it. A magnetic stirrer was used to agitate the wastewater sample at a high enough speed to shear bigger particles, resulting in

more uniform particle size. A 100 mL amount of the sample was pipetted onto the seated glass fibre filter while stirring. The filter was washed three times with 10 mL de-ionized water each time, allowing for complete drainage between washings, and suction was maintained for around 3 minutes after filtration was completed. The filter was carefully removed from the filtration system and placed on the support of an aluminium weighing dish. It was dried for 1 hour at 105°C in an oven, cooled to equilibrium temperature in a silica gel desiccator, and weighed. The drying, desiccating, cooling, and weighing cycle was repeated until the weight remained constant. Duplicate weight determinations were made, and they agreed within 5% of their average weight. The computation for TSS was executed using Equation (3.3), which is demonstrated in Appendix A(iii).

$$Total\ suspended\ solids, TSS = \frac{(A - B)\ \text{x}\ 1000}{volume\ of\ sample\ (mL)}\ \frac{mg}{L} \qquad (3.3)$$

where

A = weight of glass fibre filter + dried residue, mg,

B = weight of glass fibre filter, mg.

(iv) Volatile soluble solids (VSS) and fixed solids (FS)

This determination was made using standard procedure 2540 E (EPA 2000). The muffle furnace was heated to and stabilized at 550 for this experiment. Method 2540 C residue was fed into a preheated furnace and fired to constant weight at 550 °C. For 15 minutes, a blank glass-fibre filter was ignited with samples (although, more than one sample and/or heavier residues may overwork the furnace, necessitating longer ignition times). After cooling partially in the air to disperse the majority of the heat, the filter disk was transported to a silica gel desiccator for complete cooling in a dry environment.

As soon as the filter disk had reached room temperature, it was weighed. The process of burning, cooling, desiccating, and weighing was repeated until the weight remained constant. Duplicate weight determinations were made, and they agreed within 5 % of their average weight. Computations for VSS and FS were carried out using Equations (3.4 and 3.5), which is demonstrated in Appendix A(iv).

$$Volatile\ soluble\ solids, VSS = \frac{(A - B)\ \text{x}\ 1000}{volume\ of\ sample\ (mL)}\ \frac{mg}{L} \tag{3.4}$$

$$Fixed\ solids, FS = \frac{(B - C)\ \text{x}\ 1000}{volume\ of\ sample\ (mL)}\ \frac{mg}{L} \tag{3.5}$$

where A = weight of residue + crucible before ignition, mg; B = weight of residue + crucible after ignition, mg; C = weight of crucible, mg.

(v) Total dissolved solids (TDS)

TDS stands for total dissolved solids, which include both inorganic and organic compounds. 2540 C was selected as the standard procedure (EPA 2000). A well-mixed wastewater sample was filtered through a 47 mm diameter, 0.45 μm glass-fibre filter, and the filtrate was evaporated to dryness in a weighted crucible and dried at 180°C to a consistent weight. Total dissolved solids were represented by a rise in the crucible's weight. A hot-air oven was used to heat the empty crucible to 180$\pm$2°C for 1 hour. It was then chilled and stored in a silica gel desiccator until needed. Before use, it was weighed right away. It was decided to employ a suction filtration system. Using a magnetic stirrer, the wastewater sample was mixed. With a vacuum applied to the glass-fibre filter, a 100 mL amount of the well-mixed material was pipetted onto it. It was washed three times with reagent-grade (deionized, 18.2 μmho) water, allowing complete drainage between washings, and suction was maintained for about 3 minutes

after filtration was completed. On a thermostatic hotplate, the total filtrate (including washings) was weighed and evaporated to dryness. The evaporated sample was dried for 1 hour at 180±2°C in a prepared hot-air oven and then weighed after cooling to equilibrium in a silica gel desiccator. The drying, desiccating, and weighing cycle was repeated until a constant weight was reached. Duplicate weight measurements were taken, and they were all within 5 % of each other. The computations of the outcome employed Equation (3.6), which is presented in Appendix A(v).

$$Total\ dissolved\ solids, TDS = \frac{(A - B)\ \text{x}\ 1000}{volume\ of\ sample\ (mL)}\ \frac{mg}{L} \qquad (3.6)$$

where

A = weight of crucible + dried residue, mg

B = weight of the crucible

3.3.1.2 Turbidity

The Hach 2100P Turbidity Meter manual was consulted for specific procedures regarding calibration, maintenance and use. The instrument calibration was conducted and/or verified before each use. The representative sample was collected and poured off enough to fill the cell to the fill line (about 15 mL) and the cap was replaced. Gently, excess water was cleaned, ensuring that any streaks from the surface of the sampling vial were cleaned using a paper towel. The instrument was turned on, placing the meter on a flat, sturdy surface. As a precaution, the meter was not held while making measurements. The sample cell was inserted in the instrument, so the diamond or orientation mark aligned with the raised orientation mark in the front of the cell

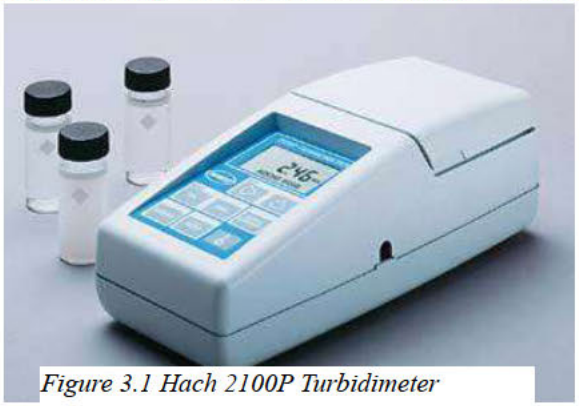

Figure 3.1 Hach 2100P Turbidimeter

compartment. The lid was closed. The range key was pressed to select the manual or automatic range, and the read key was pressed. The turbidity value was displayed in NTU. The Reading was recorded to the correct range-dependent significant digits as required by EPA Method 180.1. The sample cell was rinsed with de-ionized water before the next reading.

3.3.1.3 Temperature

Aqualytic Sensodirect AL15 Multi Set pH/Con 4724210, Germany was used to measure and monitor the temperature of the wastewater samples and the microalgal broth.

3.3.1.4 Electrical conductivity (EC)

Aqualytic Sensodirect AL15 Multi Set pH/Con 4724210 Germany, was used to measure the conductivity decreased and/or the filter reached its terminal differential pressure. The Filter was stopped, and the filter was either discarded or regenerated for re-use.

Figure 3.2 AL15 Multi Set pH/Con

The treatment of the wastewater with 0.2 µm ceramic MF membranes reduced the initial chemical oxygen demand of 5000–10,000 mg/L below 250 mg/L. The produced permeate was mixed with reference water of low and medium contamination and then submitted to biological treatment.

M(V) was engraved on the bottle. Equation (3.7) was used to compute the density (ρ).

$$Density\ (\rho) = \frac{(m_2 - m_1)}{volume\ of\ sample\ (mL)} = \frac{kg}{m^3} \qquad (3.7)$$

where m_2 = mass of density bottle + sample, mg; m_1 = mass of empty density bottle, mg.

The buoyancy of the air was considered for weighing. The specific gravity (SG) is the ratio of the density of the substance (ρ) to the density of water (ρH_2O), and is given in Equation (3.8), while the specific weight is expressed in Equation (3.9).

$$Specific\ gravity\ (SG) = \frac{\rho}{\rho H_2O} \tag{3.8}$$

Specific weight (γ) is the weight (w) of the fluid per unit volume (V)

$$Specific\ weight\ (\gamma) = \frac{w}{V} = \frac{m.g}{V} = \rho g\ \frac{N}{m^3} \tag{3.9}$$

where g = acceleration due to gravity.

3.3.2 Inorganic chemical characteristics

3.3.2.1 Hydrogen ion potential (pH)

The pH of the sample was measured with a digital Aqualytic Sensodirect AL15 Multi Set pH/Con 4724210, Germany. The meter was calibrated using pH 4.0, 7.0 and 9.0 buffer solutions as prescribed by the manufacturers. The sample wastewater was stirred vigorously using a clean glass stirring rod. A 40 mL ± 5 mL sample was poured into the glass beaker using the watch glass for a cover. The sample was allowed to stand for a minimum of one hour to allow the temperature to stabilize, stirring it occasionally while waiting. The temperature of the sample was measured, and the temperature controller of the pH meter was adjusted to that of the sample temperature. The electrode of the pH meter was immersed into the wastewater sample making sure there was good contact between the wastewater and the electrode, and the meter reading was allowed to stabilize. The stable pH value was read and recorded. The electrode was then rinsed well with distilled water and dabbed lightly with a paper towel to remove any film formed on the electrode before the next reading.

3.3.2.2 Alkalinity

Exactly 20 mL portion of the sample of the wastewater was pipetted into a 100 mL conical flask and 2 drops of phenolphthalein indicator were added and titrated against (N/10) HCl until the colour of the solution changed from pink to colourless. The corresponding burette reading indicates the phenolphthalein endpoint (V_1). Again 20 mL portion of the water sample was pipetted into a conical flask, and 2 drops of methyl orange indicator were added. This solution was titrated against the (N/10) HCl solution until the colour changed from yellow to red. This burette reading corresponds to the methyl orange endpoint (V_2). Equation (3.10) was used to compute the alkalinity due to phenolphthalein, while total alkalinity was computed using Equation (3.11)

$$Phenolphthalein\ Alkalinity\ (as\ CaCO_3) = \frac{V_1 \text{ x } N \text{ x } 50{,}000}{mL\ of\ sample} \qquad (3.10)$$

Where:

V_1 = Volume of 0.1N HCl used (mL, phenolphthalein endpoint)

N = Normality of HCl (0.1N)

50,000 = Equivalent weight of $CaCO_3$ (50 mg per meq)

mL of sample = 20 mL (actual sample volume used)

$$Total\ Alkalinity\ (as\ CaCO_3) = \frac{V_2 \text{ x } N \text{ x } 50{,}000}{mL\ of\ sample} \qquad (3.11)$$

Where:

V_2 = Total volume of 0.1N HCl used (mL, methyl orange endpoint)

mL of sample = 20 mL (or actual sample volume used)

3.3.2.3 Chlorine (Cl_2) and Chloride (Cl^-)

Wastewater samples were collected in clean glass bottles. Plastic containers were not used for these tests because they can have a large chlorine demand. The samples were analysed immediately upon arrival at the laboratory. The samples could not be preserved for later analysis because chlorine is a strong oxidizing agent and is unstable in natural waters. Chlorine reacts quickly with various inorganic compounds and more slowly with organic compounds (Mazur and Lebedev 2022). Many factors, including reactant concentrations, sunlight, pH, temperature and salinity influence the decomposition of chlorine in the water. The glass sample containers were preheated to remove chlorine demand and soaked in a weak bleach solution (1 mL commercial bleach to 1 litre of deionized water) for 1 hour. Thereafter, the containers were rinsed fully with deionized water. The sample was taken from a spigot with the wastewater flowing for 5 minutes after the container overflowed with the sample and then the cap was put on the sample container so that there was no headspace (air) above the sample.

3.3.2.4 Total nitrogen (TN), Total Kjeldahl nitrogen (TKN) and Nitrate (NO_3^-)

The Hach Method 10242, also known as TNTplus 880 was adapted for these determinations. It is a simplified green chemistry alternative to other methods approved at 40 CFR 136 for regulatory reporting of TKN (US EPA, 2023). In the simplified total Kjeldahl nitrogen (s-TKN) method, inorganic (NH_3, NH_4^+, NO_2^-) and organic nitrogen are oxidized to nitrate by digestion with peroxodisulphate. The nitrate ions react with 2,6-dimethylphenol in a solution of sulphuric and phosphoric acid to form a nitrophenol. Oxidised forms of nitrogen in the original sample (nitrite + nitrate) are determined in a second test vial and then subtracted, resulting in TKN.

In this method, the DRB200 thermoreactor was set to power on and the temperature was set to 100 °C for preheating. A 1.3 mL portion of the sample, 1.3 mL portion of Solution A and 1 Reagent B tablet were added in quick succession to a dry 20-mm reaction tube. The reaction tube was closed immediately and without inverting, it was inserted in the preheated DRB200 thermoreactor. The lid was closed, and the reaction tube was kept in the reactor for 1 hour. When the timer expired, the reaction tube was removed carefully from the reactor and placed in the test tube rack to cool to room temperature**.** On cooling, 1 MicroCap C was added to the reaction tube. The cap was tightened on the reaction tube and inverted until completely mixed. A dropping pipet was used to add 0.5 mL of the digested sample from the 20-mm reaction tube into a test vial 1 (red label). A micropipette was used to add a 0.2 mL portion of Solution D to the test vial and **q**uickly, the cap was tightened on the vial and inverted until completely mixed. A pipet was used to add a 1.0 mL portion of the undigested sample to test vial 2 (green label). A micropipette was used to add a 0.2 mL portion of Solution D to the test vial. 2 and quickly, the cap was tightened on the vial and inverted until completely mixed. Using a timer, a reaction time of 15 minutes was observed. When the timer expired, the vials were cleaned with a paper towel. The DR3900 UV-vis spectrophotometer was started and after stabilising, the barcode program was selected. Test vial 1 (red label) was inserted into the cell holder. The READ1 button was tapped and quickly, test vial 2 (green label) was inserted into the cell holder. The READ2 button was tapped, and the results were displayed in mg/L Total N, mg/L NO_3–N + NO_2–N and mg/L TKN.

3.3.2.5 Ammonium (NH_4^+)

Nitrogen, Ammonia ULR TNTplus Reagent Set

Pipet, adjustable volume, 1.0-5.0 mL

Pipet tips, for 1.0-5.0 mL pipet

Samples were collected in clean plastic bottles; and analysis was conducted before, during and after treatment.

In this method, the lid from the DosiCap™ Zip cap was carefully removed. The cap of the test vial was removed. A pipet was used to add 5.0 mL of sample to the test vial. Immediately, the DosiCap Zip was turned over so that the reagent side was on the test vial. The cap was tightened on the vial. The vial was shaken until the reagent in the cap dissolved. This was ascertained by looking through the open end of the DosiCap to make sure that the reagent dissolved. The timer was activated, and a reaction time of 15 minutes was allowed, after which the vial was cleaned with a paper towel. The vial was then inserted into the cell holder of the DR 3900 UV-vis spectrophotometer to scan and read the barcoded vial and display the reading in mg/L NH_3–N. The reagent blank correction was not necessary by this method.

3.3.2.6 Orthophosphate (PO_4^{3-})

The ascorbic acid Method 10209/10210 utilising TNTplus™ 845 vials (6 to 60 mg/L PO_4^{3-} was used. In this method, the DRB200 thermoreactor power was set to on. The temperature was set to 100 °C. Carefully, the lid on the DosiCap™ Zip cap was removed. The cap on the test vial was then removed. A dropping pipet was used to add 0.4 mL of sample to the test vial. The DosiCap Zip was turned over so that the reagent side was on the test vial and the cap was tightened on the vial. The vial was inverted several times until the reagent in the cap dissolved, which was confirmed by looking through the open end of the DosiCap. The vial was inserted in the preheated DRB200 thermoreactor and the lid was closed. The vial was maintained at 100 ºC in the reactor

for 1 hour. On the expiry of the 1 hour, the vial was carefully removed from the reactor and set in a test tube rack to cool to room temperature. The vial was shaken 2-3 times. A dropping pipet was used to add 0.5 mL of Solution B to the test vial, and the cap on the Solution B container was immediately tightened. The grey DosiCap C was put on the vial, tightened and the vial was inverted 2–3 times after which the reaction time of 10 minutes was kept. On the timer expiry, the vial was inverted 2–3 times and wiped using a paper towel. The DR 3900 UV-vis spectrophotometer was started and stabilised. The barcode program was selected, and the vial was inserted into the cell holder. The READ button was tapped and the results were displayed in mg/L PO_4^{3-}.

3.3.2.7 Dissolved oxygen (DO)

An Aqualytic Sensodirect AL15 Multi Set pH/Con 4724210 was used to measure the DO of wastewater at all the stages that DO needs to be noted in the course of the experimentation in this research. The oxygen probe was filled with the electrolyte, and its terminal was then inserted into the DO socket of the instrument. The meter was powered ON by pressing the POWER button once. The MODE button was toggled until the display showed '% O_2'. Calibration of the meter was done as follows: The display of '% O_2' was allowed 5 minutes to stabilize with no fluctuations. The REC button was pressed at the same time as the HOLD button and released after the value 20.9 was displayed. The ENTER button was pressed twice to save the calibration data, which completed the calibration procedure with a lower display of "O_2 CAL. OK".

The FUNCTION button was pressed once for the right display to show 'mg/L'. The protective cover was removed from the probe and the probe was immersed in the wastewater sample to a depth of about 10 cm with constant swirling/stirring to achieve thermal equilibrium. A magnetic stirrer was used to sustain the constant and steady

velocity of the solution over the probe and a steady display of DO values (mg/L) was achieved. The temperature value of the measured solution was also displayed and recorded. The probe was rinsed carefully with normal tap water after each series of measurements.

3.3.2.8 Metals analysis

To reduce interference by organic matter and to convert metals associated with particulates to a form (usually the free metal) that can be determined by atomic absorption spectrometry or inductively coupled plasma spectroscopy, digestion techniques presented hereunder provide acceptable and consistent recovery compatible with the analytical method and the metal being analysed.

Method 3030 E was adapted for this determination. A 100 mL portion of a well-mixed (magnetic stirred), glass fibre-filtered wastewater sample was measured into a 125 mL beaker. In a hood, a 5 mL portion of concentrated HNO_3 was added, followed by a few boiling chips. The beaker was covered with a watch glass and the sample was slowly boiled on a hot plate and evaporated to about 20 mL. While still heating, a 3 mL portion of the concentrated HNO_3 was added to complete the digestion, which was indicated by a clear solution. The beaker's inner walls and watch glass cover were washed with deionised water and then filtered using a glass fibre filter. The filtrate and washings were transferred into a 100 mL volumetric flask and rinsed with two 5 mL portions of deionised water. It was cooled, diluted with deionised water to the mark, and mixed thoroughly. Portions of this solution were taken for the required metal determinations, using a microwave plasma atomic emission spectrophotometer (MP-AES, MY18379001, Agilent USA)

3.3.3 Organic chemical characteristics

3.3.3.1 Carbohydrates

The carbohydrate content of algae biomass was determined by employing the procedure published by Wychen and Laurens (2015) and adopted by the National Renewable Energy Laboratory (NREL).

3.3.3.2 Lipids

Centrifugation at 10,000 rpm (Sorvall Legend XTR with an F14S-6x250LE rotor, 15, 2449g) was used to generate the microalgal pellets in triplicate. After that, they were washed in distilled water and heated to 60 °C in 25 mL of solvent for 30 minutes while being constantly stirred. After filtering the suspension via a 0.45 μm PTFE membrane, the separated cell solids were extracted once again using a second 25 mL volume of solvent. A third extraction of the samples was performed to guarantee total lipid removal (Fazal *et al.* 2018). The leftover particles from the second extraction were gathered, dried in a vacuum oven and weighed. When the filtrates were combined, the solvent was extracted using rotary evaporation (60 °C), and a vacuum pump (10-1 Torr) was then used to further dry the mixture to a consistent weight. At a final concentration of 2–10 mg/mL, extracts were re-suspended in 2:2:1:1 isooctane:toluene:acetone:methanol (v/v/v/v), filtered (0.2 μm PTFE), and then subjected to HPLC/ELSD analysis at gain six.

The lipid extraction efficiency of 2-EE was heated in the solvent and compared to 2:1 chloroform:methanol (as previously mentioned). We performed three duplicates of each analysis. Using a Dounce homogenizer, the concentrated algal pellet (200 mg) was broken up in 20 volumes of 2:1 chloroform:methanol for the Folch extraction. A 0.45 μm PTFE membrane filter was used to extract particles from the homogenate.

After the filtrate had been cleared, it was put into a separatory funnel along with 0.25 times the volume of chloroform in distilled water and methanol to make the final composition 8:4:3 (v/v/v) of chloroform, methanol, and water. Following phase separation and shaking, the lower organic phase was collected into a flask that had been previously weighed, the solvent was eliminated (per the previous description), and the extract's weight was ascertained. Before analysis, the extract was diluted in a solution of 2:1:1:1 isooctane:toluene:acetone:methanol (v/v/v/v) and filtered.

We also compared the lipid extraction efficiency of 2-EE with hexane for algal pellets that were both wet and dried. In this case, 12 algal pellets (88 mg each) were split into two groups, with half remaining wet and the other half lyophilized (12 h, 10^{-1} Torr). Refluxing in n-hexane at 68-72 °C or using 2-EE twice to extract three wet and three dried samples.

3.3.3.3 Proteins

Using the Standard Protein Solution, protein standards were prepared at concentrations of 10 mg/L, 100 mg/L, 500 mg/L, 1,000 mg/L, 2,500 mg/L, 5,000 mg/L, 10,000 mg/L, and 30,000 mg/L. Stock Protein Solution was prepared by weighing 1.00 g gelatine (or bovine) dissolving the protein in distilled water and diluting the solution to l,000 mL. 1.00 g of pure gelatine was corrected to 1.14 g to compensate for 86 % protein in the commercial KNOX unflavoured gelatine (supplied by Knox Gelatine Inc., Johnstown, NY 12095, U.S.A.). The protein (gelatine or bovine) and distilled water mixture were heated on low heat with slow stirring to dissolve the protein and obtained 1 mL of solution = 1 mg active ingredient of protein.

Standard Protein Solution was prepared by diluting 10 mL Stock Protein Solution to 1000 mL with distilled water to obtain 1 mL of the solution to be equivalent to 10 μg

active substance. In addition, 50 mL Stock Protein Solution was diluted to 1000 mL with distilled water to obtain 1 mL of the solution to be equivalent to 50 μg active ingredient protein.

Test Tubes were each charged with 2 mL of each Protein Standard and 8 mL of distilled water. 10 mL measure of sodium hydroxide solution (see Appendix) was added to each Protein Sample and capped with a glass marble. It was boiled for 5 minutes and left to cool to room temperature. 2 mL portion each of carbonate tartrate reagent (see Appendix), and copper sulphate solution (see Appendix) was added to each protein sample and mixed thoroughly and left to stand for 15 minutes at room temperature. 2 mL portion of phosphomolybdic phosphotungstic reagent (see Appendix) was added to the sample and mixed immediately. The reaction mixture was left to stand for 30 minutes at room temperature during which there was colour development. It was filtered through a glass-fibre 0.45 μm filter to remove any precipitate. Using distilled water as blank, the DR3900 spectrophotometer was used to determine the optical density at 400-700 nm, which gave readings between 0.4 and 1.8. Plots of Absorbance vs. Concentration at different wavelengths were done to obtain the calibration curves. A 10 mL portion of the wastewater sample was placed in a Test Tube and was treated in the same manner as the protein standard solution described earlier. After colour development, the absorbance was read on the DR3900 spectrophotometer using distilled water as blank. The calibration curves from the protein standards were used to determine the concentration of protein in the wastewater sample. Where the absorbance from one calibration curve exceeded 1.8 for a sample, another wavelength was selected (alternatively, the wastewater sample was diluted as necessary).

3.3.3.4 Biochemical oxygen demand (BOD)

The Standard Methods for the Examination of Water and Wastewater (APHA, AWWA and WEF. 2017) method 5210B was utilized. To obtain BOD5, the concentrations of dissolved oxygen (DO) in a sample were measured before and after the incubation period, and the sample matching dilution factor was appropriately adjusted. To avoid DO production via photosynthesis, this study used 300 mL incubation bottles in which seed microorganisms were dosed with buffered dilution water and held for 5 days in the darkroom at 20 °C. This process necessitates the dilution of water blanks, glucose glutamic acid (GGA) controls, and seed microbe controls in addition to the numerous dilutions of BOD samples. The dilution water blank was used to ensure that the dilution water used to dilute the other samples was of good quality. The GGA control is a standardized solution used to test the seed's quality, with a BOD5 content of 198 mg/L to 30.5 mg/L. After the dilution water has been added to the sample, a nitrification inhibitor is added to detect carbonaceous BOD (cBOD). The inhibitor prevents ammonia-nitrogen from being oxidized, which is the source of nitrogenous BOD (nBOD). Because nitrogenous demand does not reflect the oxygen demand from organic matter, it is common practice to assess only cBOD when performing the BOD5 test. This is because nBOD is produced when proteins are broken down, but cBOD is produced when organic molecules are broken down. BOD_5 is calculated by:

Unseeded: $BOD_5 = \frac{D_0 - D_5}{P}$ (3.10)

Seeded: $BOD_5 = \frac{(D_0 - D_5) - (B_0 - B_5)f}{P}$ (3.11)

where:

D_0 is the dissolved oxygen (DO) of the diluted solution after preparation (mg/L)

D_5 is the DO of the diluted solution after 5 days of incubation (mg/L)

P is the decimal dilution factor

B_0 is the DO of the diluted seed sample after preparation (mg/L)

B_5 is the DO of the diluted seed sample after 5 days of incubation (mg/L)

is the ratio of seed volume in dilution solution to seed volume in the BOD test on seed

3.3.3.5 Chemical oxygen demand (COD)

In 1 L glass bottles, industrial effluent samples were collected for COD determination. The suction filter assembly was used to filter the effluent samples. In the suction filter assembly depicted in Figure 3.3, fibreglass filter paper with a diameter of 47 mm and a pore size of 1.2 m was utilized. COD was determined using a HACH DR 3900 spectrophotometer at 620 nm for a wide range (up to 1500 mg/L). The following procedure was adopted:

The HACH DRB 200 Thermoreactor was preheated to 150°C. The cap of the COD digestion reagent vial was removed. The first vial was marked with the effluent sample ID and the other blank. The vial marked blank was held at a 45-degree angle. With the aid of a micro-pipette, 2 mL in the case of low range and 0.2 mL for a high range of deionized water was transferred into the vial and swirled. The dilution factor, on the other hand, can be applied when necessary. The deionized water was replaced with the effluent sample in step 4 to prepare the effluent sample. To remove stains from the vials, the vial caps

Figure 3-3 Filter Assembly

were tightly closed, rinsed with water, and cleaned with a clean paper towel. The vials were then held in place by the caps and were gently flipped two to three times to ensure appropriate mixing of the contents. The vials were inserted in the preheated HACH DRB 200 thermoreactor, closed properly, and left to heat for 2 hours. The reactor was turned off and allowed to cool to a temperature of 120°C after the heating. While the vials were still heated, they were inverted and placed in a rack until they cooled to room temperature. On the HACH DR 3900 spectrophotometer, the COD HR program was selected, and the proper range was established. A clean paper towel was used to wipe the vials once more. The blank vial was placed into the cell holder and the instrument was zeroed. The effluent sample vial was then inserted, and a reading was obtained, yielding the COD in mg/L directly.

3.3.3.6 Total organic carbon (TOC)

During the collection and handling of the wastewater samples, losses of organic compounds or matter probably occurred due to microbial degradation, sample drying, oxidation, volatilization, and sample processing biases (e.g., selective removal of carbon-bearing components). The samples were stored in an icebox during transportation to the laboratory to reduce microbial degradation but not completely stopped leading to some potential loss of organic matter.

The thermoreactor DRB 200 was set at 105 ^{o}C and was set to running. A 10 mL portion of the sample was added to a 50-mL Erlenmeyer flask. A magnetic stirring bar was put in the Erlenmeyer flask. A 0.4 mL portion of the Buffer Solution (pH 2.0) was added to the Erlenmeyer flask. The pH paper was used to make sure that the sample pH was 2.0. The flask was then put on a stir plate. The sample was stirred at a moderate speed for 10 minutes. The contents of one TOC Persulfate Powder Pillow were added to each

Acid Digestion Vial. One Mid-Range Acid Digestion vial was labelled "Reagent Blank", and the second Mid-Range Acid Digestion vial was labelled "Sample". The sample vial was prepared by adding a 1.0 mL portion of the sample from the Erlenmeyer flask to the sample vial. The blank vial was prepared by adding a 1.0 mL portion of organic-free (de-ionised) water to the blank vial. Two blue Mid/High-Range Indicator Ampules were rinsed with de-ionised water and were cleaned with a wipe. Touching the sides of the ampules was avoided after they were wiped. The ampules were held at the top and one unopened ampule was put into each Acid Digestion Vial. The top of the ampule was snapped off when the score aligned with the top of the vial and the ampules dropped into the vials. No tilting of the vials after the ampule was inside. The vials were closed tightly. They were Inserted into the already heated thermoreactor, and the vials were maintained at 105 ^{o}C for 2 hours. After two hours, the vials were removed from the reactor and placed in a test tube rack to cool for one hour. The liquid in the blank turned to a dark blue colour. The DR3900 UV-vis spectrophotometer was switched on and allowed to stabilise. The stored program 425 for Organic Carbon MR was selected and started. The blank vial was cleaned using a paper towel and inserted into the 6-mm cell holder. The ZERO button was pressed for the display to show 0 mg/L C. The sample vial was cleaned using a paper towel and the sample vial was inserted into the 6-mm cell holder. The READ button was pressed to display the results in mg/L C.

3.3.4 Biological characteristics

Microbiological analysis of wastewater samples commenced as soon as the samples arrived at the laboratory after collection to avoid unpredictable changes in the

microbial population. During transport to the laboratory, the sample was placed in an icebox to maintain its integrity.

3.4 Microalgae Strains

The Institute of Water and Wastewater Technology (IWWT) provided the strains of microalgae that were used in this research. Various strains of microalgae have different combinations of chlorophyll molecules - some have only Chlorophyll-*a*, some *a* and *b*, while other strains have chlorophyll-*a* and Chlorophyll-*c* (Xie *et al.* 2020). The biomass of microalgae contains three main components viz, proteins, carbohydrates and lipids. The collaborative selection skewed towards the strain with high lipid content.

3.4.1 Microalgae cultivation

Three types of photobioreactors were used with the benefit of scale-up operations. Three-litre capacity bubble column photobioreactors were used in a batch process to preliminarily culture the microalgae strains as they passed through the lag phase and the exponential growth, during which the pH, DO, CO_2 flow rate, temperature, nutrient uptake and time (in days) were noted. Already characterised industrial wastewater was used as the culture medium. The mixotrophic culture process derived its light energy from an artificial incandescent fluorescent source.

The use of exponentially expanding seed cultures for inoculation shortened the time required for upscaling and minimised the length of the lag phase. With the reactor's working volume of 2.5 L, the seed culture of 2.182 optical density at 680 nm ($OD_{680\ nm}$) was mixed with the wastewater in the ratio of 1:5 which gave the initial $OD_{680\ nm}$ as 0.321.

On establishing the optimum operating conditions, the second reactor, a 30-L bubble column, was used in a first-step scale-up operation to adjust the parameters for higher volume algal growth. Thereafter, an airlift-raceway reactor was used in a scale-up operation. The operating parameters were monitored and adjusted at set time intervals. The scale-up operation of the 240-L airlift-raceway reactor was based on the adjusted variables of the 30-L bubble column reactor.

3.4.1.1 The algal culture calibration curve

Using a spectrophotometric approach, the biomass density (ρ) and optical density (OD) of the microalgae samples were compared. The culture absorbance was measured at a wavelength of 680 nm. Equation (3.12) illustrates the link between the cell dry biomass density (ρ, g L^{-1}) and optical density (OD_{680}) in calibration curves (Martonen 2017).

$$\rho \text{ (alga species)} = (y \times OD_{680}) + b \quad (3.12)$$

where *y* and *b,* are factors that are specific to the alga species used.

Utilising an optical microscope and hemocytometer, the number of cells per litre of culture was also measured. Equation (3.13) established the dependency of the optical density (OD680) on the cell concentration (Cc, g L^{-1}).

$$Cc \text{ (alga species)} = (X \times OD_{680}) + w \quad (3.13)$$

where *X* and *w,* are factors that are specific to the microalga species under investigation

3.4.1.2 Biomass production

Scotch bottles (500 mL) were used to culture microalgae to acceptable optical density. Figure 3.4 shows the Scotch bottles set up to culture microalgae. Brewing wastewater was utilised for cultivating the microalga Scenedesmus sp. in a 3-L bubble-column reactor with a working volume of 2.5 L. After sparging the broth with CO2 gas at a

rate of 2 L/min, the broth's optical density (OD) rose over time, allowing for the measurement of microalgal biomass production at 680 nm.

Figure 3.5 is the setup for the 3-L bubble column reactor system that was used for microalgal biomass production. The 30-L bubble-column photoreactor was set up as shown in Figure 3.6.

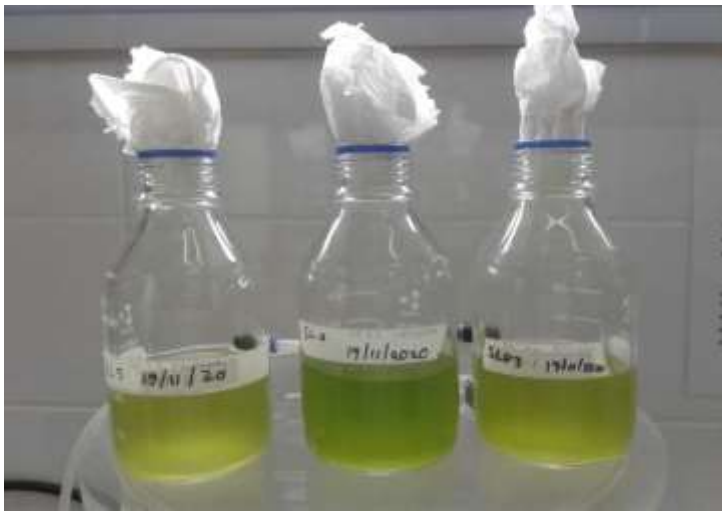

Figure 3.4 Culturing microalgae in Scotch bottles

Figure 3.5 The 3-L Bubble-column reactor

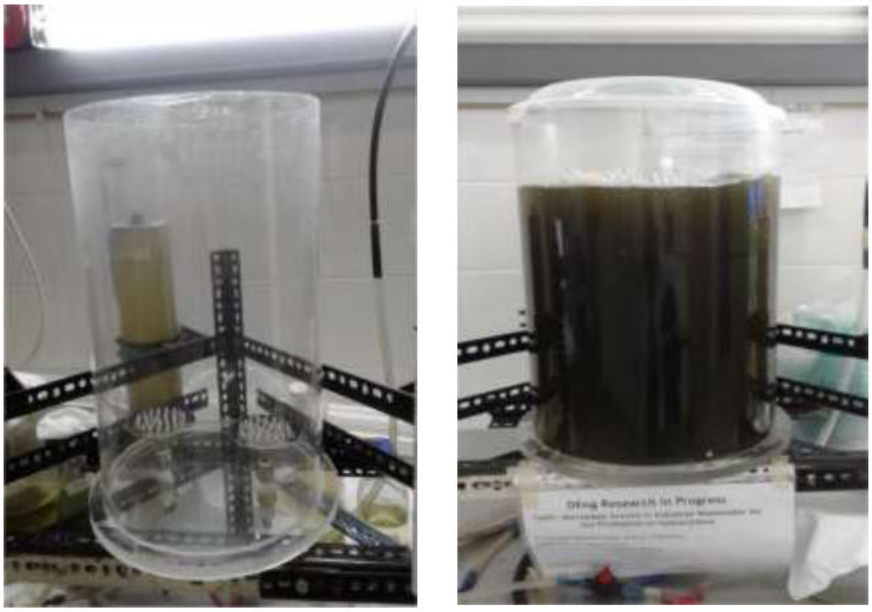

(a) (b)

Figure 3.6 The 30-L Bubble-column reactor: (a)displaying spargers (b)in operation

Airlift-raceway photobioreactor was used for microalgae biomass production. The airlift-raceway photobioreactor was filled with industrial wastewater to the prescribed level and the prescribed amount of microalgae seed volume was added. The setup of the airlift-raceway photbioreactor is shown in Figure 3.7.

The most common method for determining the dry weight of microalgae cells directly is by gravimetric estimate. The following are the steps taken to determine biomass density using this technique, also referred to as total suspended solids (e Silva and Montegia 2015): The air vacuum, suction flask and filter holder were all part of the filtering apparatus that had Whatman GF/C (2.5 cm) filters on it. Three repeated 20 mL amounts of deionized water were used to wash the filters. The filters were taken out and dried in an oven at 70 ℃ for 24 hours after the maximum quantity of liquid was extracted by suction. They were then kept in a vacuum desiccator over silica gel until needed. We next used an analytical balance to weigh the filters to four decimal places.

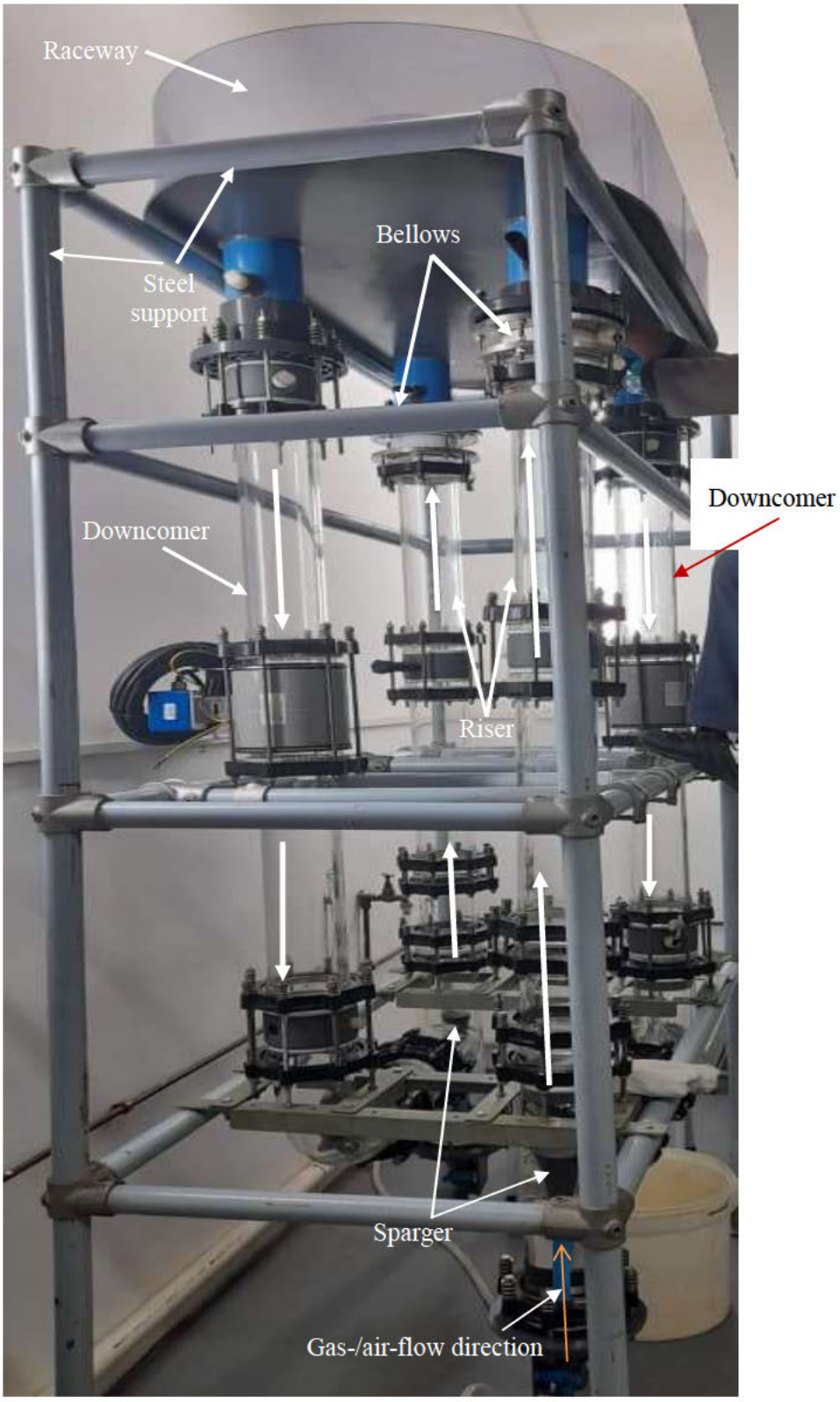

Figure 3:7 Labelled Airlift-raceway photobioreactor

After filtering 10 millilitres of microalgae culture, they were placed in an oven, set at 90 degrees Celsius, for four hours to dry. After allowing the filters to acclimatise to room temperature in a desiccator, they were weighed. Equation (3.14) was utilised to compute the biomass concentration.

$$Biomass\ \left(\frac{mg}{L}\right) = (A - B)\frac{1000}{Sample\ volume\ (mL)} \tag{3.14}$$

where A is the filter's weight plus the dried algae residue (in mg), and B is the filter's weight (in mg) (e Silva and Montegia, 2015).

3.5 Microalgal Growth Kinetics

Data on cell concentration or biomass density were used to determine growth patterns once or twice a day. In the following plotting, the biomass productivity and specific growth rate were computed. A first-order dynamic equation (3.15) was used to simulate the growth of microalgae:

$$\frac{dX}{dt} = \mu X \tag{3.15}$$

where t is the number of days, μ is the specific growth rate (day-1), and X is the biomass concentration (g L^{-1}). Equation (3.16) was used to get the cultures' specific growth rates.

$$\mu = \frac{\left[ln\left({}^{X_t}/_{X_0}\right)\right]}{(t - t_0)} \tag{3.16}$$

For the microalgal cell count per unit volume, samples were serially diluted, which was followed by counting cells using a hemocytometer (Marienfeld, Lauda-Königshofen, Germany).

A 10 mL portion of algal culture was filtered through a pre-weighed filter paper and then washed with distilled water, which was followed by drying in an oven at 100 °C

until there was no change in the weight. The dry weight (DW) per 10 mL was determined as the total weight minus the weight of the filter paper.

Equation (3.17) was used to estimate the linear growth rate, or biomass productivity rate (g $L^{-1}d^{-1}$).

$$p = \frac{(X_t - X_0)}{(t - t_0)} \tag{3.17}$$

Thus, during the exponential growth phase, *P* represents the biomass productivity rate. To achieve the optima for growth parameters, a growth rate specific to each parameter was calculated. A series of media, containing various amounts of target parameters, were prepared. Each culture, representing only one variable, was grown at a particular rate. The highest growth rate determined the optimum amount of that particular parameter. The growth rate, *k*, expressed as the number of doublings per day was calculated using Equation (3.18).

$$k = \frac{\log\left({}^{N_2}/_{N_1}\right)}{t} \tag{3.18}$$

Where N_2 and N_1 are biomass densities at the beginning and end of a time interval (*t*) in the logarithmic growth phase.

3.6 Illumination Sources

Cool white, fluorescent lights emit radiation in the visible region (400-700 nm). The percentage of total light between 400 - 500 nm is 25 % and between 600–700 nm is 20.65 % with a combined percentage of 45.65 %. Since emitted radiance by cool white fluorescent is closer to the light spectrum of daylight, it is used extensively for testing different plant and algae biomass production rates. Four white, fluorescent tubes were used in the open lab already lit by white, fluorescent tubes. Also, blue light-emitting diodes (LED) were used.

3.7 CO_2 Sequestration Rate

Compressed CO_2 was used as the influent gas, and the aeration rate was maintained at 0.5 litres per minute. Measurements were made three times during 21 days, every 12 to 48 hours. Calculating the CO_2 fixation rate required knowledge of the microalgae mass balance. Based on dry weight, microalgal biomass has a carbon content of about 50 %. The primary source of this carbon is carbon dioxide, which can be found in the air or factory waste streams. Twelve grams of carbon make up the 44 g mass of a mole of CO_2. Equation (3.19) yielded the theoretical carbon dioxide consumption per gram of microalgae based on these assumptions.

$$\frac{44\ (\frac{gCO_2}{mol})}{12\ (\frac{gC}{mol})} \text{x}\ \frac{50\ (gC)}{(100\ g\ alga\ biomass)} = 1.83\ (\frac{gCO_2}{g\ alga\ biomass}) \qquad (3.19)$$

An algal dry cell weight of one gramme can theoretically repair 1.83 grammes of carbon dioxide, according to equation (3.19). However, depending on the species and growing circumstances, the carbon content of microalgae varies in the experimental works. The rate of carbon dioxide consumption is dependent on biomass production and experimental carbon content determined by elemental analysis. Equation (3.20) illustrates how these elements relate to one another:

$$CO_2\ fixation\ rate\ (mg\ L^{-1}\ day^{-1}) = P \times C_{carbon} \times \left(\frac{M_{CO_2}}{M_C}\right) \qquad (3.20)$$

where M_{CO2} and M_C stand for the molar masses of CO_2 and carbon, respectively, and P is the biomass productivity (mg) and C_{carbon} is the experimental carbon content.

3.8 The Thermodynamic Model of Microalgal Growth

The microalgal growth process is dependent upon the changes in free energy. The specific growth rate (μ) is related to the growth-limiting nutrient-substrate concentration (C_A) in the broth according to the Monod Equation (3.21).

$$\mu = \mu_{max} \frac{C_A}{K_A + C_A} \tag{3.21}$$

where μ_{max} is the maximum specific growth rate and K_A is the Monod constant.

For a substrate-limiting microalgal culture, the microalgal growth response can be seen simply as a change in the concentration of a nutrient substrate such that, as in Equation (3.22),

$$C_A = C_{Ai}\Delta G^{0*} \tag{3.22}$$

where C_A is the growth-limiting nutrient-substrate concentration in the broth, C_{Ai} is the apparent nutrient-substrate concentration that has been abstracted from the nutrient broth to produce a yield in the algal biomass. When C_A increases, microalgal growth becomes more favourable and the free energy changes, ΔG^{0*}, would decrease. Hence, it can be assumed in Equation (3.23) that

$$\Delta G^{0*} = \Delta G^0 - RTlnC_A \tag{3.23}$$

where ΔG^0 is the change in the standard free energy of the microalgal system.

Analogous to a chemical reaction, the overall change in the free energy (ΔG) of the microalgal growth reaction can be expressed as a function of C_A and C_{Ai} as shown in Equation (3.24).

$$\Delta G = \Delta G^{0*} + RTln\frac{C_{Ai}}{C_A} \tag{3.24}$$

Assume that the carbon dioxide catabolism is negligible, so that, by definition,

$$C_{Ai} = C_{A0} - C_A \tag{3.25}$$

where C_{A0} is the initial nutrient-substrate concentration. Substituting Equation (3.23) in Equation (3.24) gives Equation (3.26).

$$\Delta G = \Delta G^{0*} + RTln\frac{C_{A0} - C_A}{C_A} \tag{3.26}$$

The specific nutrient-substrate utilization rate (q) could be expressed in Equation (3.27).

$$q = \frac{C_{A0} - C_A}{Xt} \tag{3.27}$$

While for the total biomass concentration *X*, the rate of substrate utilization,r_{su}, is related to the specific growth rate as expressed in Equation (3.28).

$$r_{su} = -\frac{\mu X}{Y} \tag{3.28}$$

where Y is the yield coefficient, r_{su} is conventionally negative since it is the rate of depletion of the substrate. Equation (3.26) translates to Equations (3.29) and (3.30).

$$\Delta G = \Delta G^{0*} + RTln\frac{q}{\left(\frac{C_{A0}}{Xt} - q\right)} \tag{3.29}$$

$$\Delta G = \Delta G^{0*} + RTln\frac{\mu}{Y\left(\frac{C_{A0}}{Xt}\right) - \mu} \tag{3.30}$$

So that

$$\Delta G = \Delta G^{0*} + RTln\frac{\mu}{\mu_{max} - \mu} \tag{3.31}$$

Substituting Equation (3.23) in Equation (3.31) gives Equation (3.32).

$$\Delta G = \Delta G^{0} - RTlnC_A + RTln\frac{\mu}{\mu_{max} - \mu} \tag{3.32}$$

When microalgal growth reaches its equilibrium, energy balance must be maintained around the energy carrier at a steady state, for which $\Delta G = 0$; So that Equation (3.32) is reduced to Equation (3.33).

$$\frac{\mu}{\mu_{max} - \mu} = C_A e^{-\frac{\Delta G^o}{RT}} \tag{3.33}$$

When solved for μ, Equation (3.33) translates to Equation (3.34)

$$\mu = \mu_{max} \frac{C_A}{K_A + C_A} - \tag{3.34}$$

where

$$K_A = e^{\frac{\Delta G^o}{RT}} \tag{3.35}$$

K_A is the thermodynamic equilibrium constant for the growth process and is referred to as the Monod constant. Analogous to a chemical reaction, the thermodynamic equilibrium constant *K* of a balanced microalgal growth response is defined as

$$K = e^{-\frac{\Delta G^o}{RT}} \tag{3.36}$$

By inspection, Equations (3.35) and (3.36) are related through Equation (3.37).

$$K_A = \frac{1}{K} \tag{3.37}$$

Equation (3.37) signifies that K_A is a function of the equilibrium constant of the overall microalgal growth process. When the equilibrium constant *K* is very large (i.e., K_A is very small), the microalgal growth process proceeds far towards completion, and the position of equilibrium lies far toward the growth of biomass. In this case, μ would approach μ_{max}. On the other hand, when the equilibrium constant in Equation (3.36) is very small (i.e., K_A is very large), an extremely small amount of biomass is formed, and the position of equilibrium lies far towards the nutrient substrate. The value of K_A is determined by both microalgal species and limiting nutrient-substrate of reference

in the broth. Consequently, the magnitude of the K_A −value represents the equilibrium position of the microalgal growth process, while μ_{max} reflects the limiting extent to which the microalgae species would grow in the prevailing environment. Taking the reciprocal of Equation (3.34) and rearranging it, gives the linearized form of the Monod equation, which is expressed in Equation (3.38).

$$\frac{1}{\mu} = \frac{K_A}{\mu_{max}}\left(\frac{1}{C_A}\right) + \frac{1}{\mu_{max}} \tag{3.38}$$

A plot of $\frac{1}{\mu}$ vs $\frac{1}{C_A}$ gives a Lineweaver-Burk plot, which is a straight line of slope $\frac{K_A}{\mu_{max}}$ and intercept $\frac{1}{\mu_{max}}$ on the $\frac{1}{\mu}$ axis with the potential of extrapolating in the $\frac{1}{C_A} < 0$ regions and striking the $\frac{1}{C_A}$ axis at $-\frac{1}{K_A}$, when $\frac{1}{\mu} = 0$

Solving the natural log in Equation (3.36) gives Equation (3.39).

$$lnK = -\frac{\Delta G^o}{RT} \tag{3.39}$$

For any given temperature, T, the change in Gibbs free energy of a reacting system is defined as in Equation (3.40).

$$\Delta G^o = \Delta H^o - T\Delta S^o \tag{3.40}$$

So that,

$$lnK = -\frac{\Delta H^o - T\Delta S^o}{RT}$$

Or

$$lnK = -\frac{\Delta H^o}{R}\left(\frac{1}{T}\right) + \frac{\Delta S^o}{R} \tag{3.41}$$

Equation (3.41) is the linear form of the Van't Hoff equation, and this equation indicates that a plot with lnK on the y-axis and $\frac{1}{T}$ on the x-axis has a slope given by $-\frac{\Delta H^o}{R}$ and an intercept is given by $\frac{\Delta S^o}{R}$. The optimal cultivation temperature range for

the microalgae species is within that of their native habitat. The most often researched species can grow at 16-27 ºC (Nielsen 2015). Certain species can only survive at temperatures over 35 °C, while others can only grow slowly at temperatures below 16 °C. The way that microalgae react to temperature variations in their culture can have an impact on their rate of metabolism, nutritional requirements, and cell composition. The Van't Hoff analysis was used to determine the favoured product in a reaction as temperature conditions are manipulated since chemical reactions may undergo different reaction mechanisms under different temperatures. The Van't Hoff equation provides information about the temperature dependence of the equilibrium constant (Fogler, 2012). Equation (3.42) is the integrated form of the Van't Hoff equation.

$$ln\left(\frac{K_2}{K_1}\right) = -\frac{\Delta H^o}{R}\left(\frac{1}{T_2} - \frac{1}{T_1}\right) \tag{3.42}$$

Equation (3.43) is the linear form of the Van't Hoff equation.

$$lnK_{eq} = -\frac{\Delta H^o}{RT} + \frac{\Delta S^o}{R} \tag{3.43}$$

where K_1 and K_2 are equilibrium constants at temperatures T_1 and T_2 respectively, K_{eq} is the equilibrium constant at any given temperature T, ΔH^o is the change in enthalpy of photosynthetic reaction, ΔS^o is the change in entropy of the reaction, and R is the universal gas constant.

3.9 Kinetics of Nutrient Depletion During The Cultivation Of Microalga *Scenedesmus sp.*

The demand for constant water and necessary nutrient supply (such as C, N, P, and trace elements) for optimal growth is the fundamental difficulty in the operation of long-term large-scale microalgae production systems. Therefore, a key element in the

operation of pilot- and large-scale microalgae productions is, understanding the nutrient removal kinetics. The kinetic constants needed to produce microalgae on a big scale were calculated using a variety of kinetic models. The most effective model for modelling substrate removal in continuously operating photobioreactors is thought to be the Stover-Kincannon, Equation (3.44) (Okoli, and Okonkwo 2016).

$$S_t = S_0 - \frac{R_{max} S_0}{K_B + \left(Q \frac{S_0}{V}\right)} \tag{3.44}$$

where S_t (mg/L) represents the effluent substrate concentrations at any time t, and S_0 (mg/L) represents the influent substrate concentrations. R_{max} is the maximum substrate removal rate and K_B is a saturation value constant. Michaelis-Menten kinetic model was used to determine the kinetic coefficients, K_m, saturation constant, k, and the reaction rate constant (Equation (3.45)). The substrate concentration corresponds to half the reaction rate giving the saturation constant.

$$R = \frac{R_{max} X}{K_m + X} \tag{3.45}$$

where R stands for the removal rate of the substrate, R_{max} is the rate at which the substrate can be removed at its maximum rate, X is the concentration of the substrate in the effluent, and K_m is the half-saturation constant. When doing a batch operation, both the initial substrate concentrations and the initial substrate removal rates are taken into consideration. In this case, Equation (3.45) should be rewritten in the format given in Equation (3.46).

$$R_{S0} = \frac{R_{m0} X_0}{K_m + X_0} \tag{3.46}$$

where $R_{mo} = k \cdot C_0$ is the maximum initial rate of substrate removal. Therefore, Equation (3.46) can be written as expressed in Equation (3.47).

$$R_{S0} = \frac{k \cdot C_0 X_0}{K_m + X_0} \tag{3.47}$$

where k is the reaction rate constant (time^{-1}), C_0 is the initial algal biomass concentration. The specific rate of substrate removal (R_{Ci}) can be calculated by dividing both terms of Equation (3.47) by the initial biomass concentration in Equation (3.48).

$$R_{Ci} = \frac{R_{S0}}{C_0} = \frac{k \cdot X_0}{K_m + X_0} \tag{3.48}$$

Equation (3.48) can be linearized in double reciprocal form as in Equation (3.49)

$$\frac{1}{R_{Ci}} = \frac{1}{k} + \frac{K_m}{k}\frac{1}{X_0} \tag{3.49}$$

and a plot of $\frac{1}{R_{Ci}}$ versus $\frac{1}{X_0}$ yields a linear regression with a slope of $\frac{K_m}{k}$ with an intercept of $\frac{1}{k}$ on the *y*-axis.

3.10 Lipid and Volatile Fatty Acids (VFA) Contents

A modified chloroform-methanol solvent-based technique was used to evaluate lipid content. The optimised analytical approach for lipid extraction, which employed a 1:1 solvent mixture of chloroform and methanol, did not require pre-treating biomass or including antioxidants(Rohit *et al.* 2018). Weighed 100 mg of lyophilized algae and put them in solvent-resistant tubes, and then we added 4 mL methanol. Add 2 mL chloroform and 0.4 mL distilled water to the liquid, vortex it for 30 seconds, and then immerse it in an ultrasonic bath for 10 minutes. After that, the mixture was centrifuged for 10 minutes at 3300 rpm after adding 2 mL of water and 2 mL of chloroform. After centrifugation, the upper layer containing water and methanol was removed, and the bottom layer was placed in a transparent tube and filtered through a layer of anhydrous sodium sulphate using a Whatman no. 1 filter in a funnel. The remaining solid was

extracted again using 4 mL of a 1:1 chloroform-methanol solution. After the solvents were eliminated using a rotary evaporator, an algal lipid green layer was the result of the extraction. Using Equation (3.50), the total lipid content was determined gravimetrically.

$$Total\ lipid\ content\ (\%) = \frac{algae\ lipid\ (g)}{algae\ biomass\ (g)} \text{ x } 100 \quad (3.50)$$

3.10.1 Microalgae crude oil extraction

A Soxhlet extraction procedure based on EPA Method 9071B (n-hexane extractable material) was employed. This method applies to the extraction of non-volatile hydrocarbons, vegetable oils, animal fats, waxes, soaps, grease, biological lipids, and related materials (EPA Method 9071B).

3.10.2 Determination of FFA in crude microalgal oil

The extracted oil was transferred into a 250 mL Erlenmeyer flask, added with 50 mL reagent grade methanol, and mixed. Then, 2 mL of 1 % phenolphthalein indicator was added, titrated with standardized 0.1562 M of NaOH and swirled until a faint permanent pink appeared. The initial and final volumes of standardized NaOH used were recorded. The total volume of NaOH used was calculated using Equation (3.51).

$$V_{NaOH} = V_{NaOH_f} - V_{NaOH_i} \quad (3.51)$$

Free fatty acid % (FFA %) expressed as oleic acid and the acid number (AN) were determined following the equation below. (AOAC Official Method 940.28, 2010).

$$\%\ FFA = 0.1637M * \left(V_f - V_i\right) * 0.2826\ wt\ sample\ (g) \quad (3.52)$$

$$AN = 1.99 \times \%\ FFA \quad (3.53)$$

3.11 Elemental Analysis

The elemental analyzer (Exeter CE440 CHN-O/S, Control Equipment Corporation, Lowell, MA, USA) was used to determine the biomass of freeze-dried microalgae, including its total carbon, nitrogen, and hydrogen content. The biomass samples were placed into a tiny tin capsule and precisely weighed to the nearest millionth of a gramme. The capsule was then heated to 950 ºC and filled with pure oxygen in a combustion tube to create tin oxide. The samples vaporised to complete combustion when the temperature within the tube was raised well over 1800 ºC. To eliminate any excess oxygen, the samples were now in gas form and had been through a reduction tube. The sample's various gases were then combined at the ambient pressure, temperature, and volume. Small amounts of this mixture were then sent through a series of thermal conductivity cells, allowing the amount of each gas to be measured. These measurements allowed for the calculation of the sample's percentages of carbon, nitrogen, and hydrogen. After that, the data was utilised to calculate the cells' carbon dioxide absorption by determining their carbon content. Additionally, there was a correlation between the nitrogen concentration and the amounts of lipids that the microalgae cells produced.

3.12 Hydrocarbon Compounds Profiling in Microalgal Lipid

Lipid samples extracted from microalgae biomass were subjected to GC-MS analysis. Analyses were carried out on an Agilent 7890A gas chromatographer coupled to an Agilent 5975C mass spectrometer (simple quadrupole) and flame ionization detection (GC-MS/FID). A Zebron 7HG-G007-11 (Phenomenex) polar capillary column (length 30 m, internal diameter 0.25 mm, film thickness 0.25 µm) was used.

The hydrogen carrier gas was at 1 mL. min^{-1}. The oven temperature was programmed with an initial 2-minute hold time at 60 °C, a first ramp from 0 °C to 151°C at 20 °C min^{-1} with a 5-minute hold time at 151 °C, then a second ramp from 151 °C to 240 °C at 6 °C min^{-1} and a final 3 minute hold time at 240 °C. Samples were injected in splitless mode (1 min) at 250 °C. The MS was run in full scan over 40-350 amu (electron impact ionization at 70 eV) and peaks were quantified based on the FID signal using the internal standards.

3.13 Process Flow Diagram (PFD)

A process flow diagram (PFD) is a diagram used in chemical and process engineering to show how plant processes and equipment flow together. Minor details such as plumbing details and designations are not included on the PFD, which shows the interaction between important equipment in a plant site. A flowchart is another frequent word for a PFD. Chemical engineering requires the use of a process flow diagram. Process topology, stream information, and equipment information are the three areas that make up this section. It describes a process and the path taken by each of its parts. PFDs are a graphical representation of a process, its constituent tasks, and their arrangement. A PFD can help with process design brainstorming and communication. Figure 3.8 represents the PFD of the process engaged in this research.

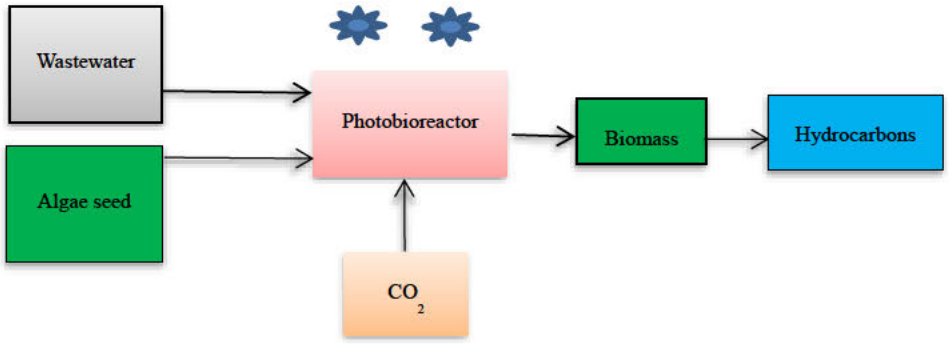

Figure 3.8 Experimental work flowchart

The degree of intricacy is up to the researcher or team to decide. Although it takes longer, more detail reduces the possibility that certain errors may go unnoticed. The most common way to portray it is using a stylized picture that uses symbols from international standards. The international standard for PFD drawing symbols is ISO 10628 (Towler and Sinnott 2012). The block flow diagram (BFD) used in academia is a simplified version of the process flow diagram (PFD), which is rarely used in practice (except on a beermat in a bar debate), though it could be beneficial for presenting ideas to non-technical people who are unfamiliar with PFD symbols (Moran 2019). The PFD is subject to BS 5070, the general British Standard for engineering diagrams, as well as BS EN ISO 10628 in the United Kingdom and Europe. Ideally, the symbols on the PFD should come from BS EN ISO 10628, BS1646, and BS1553. There are equivalent standards in the United States (Moran, 2019)

CHAPTER 4

Characterisation and Screening of Industrial Wastewater

4.1 Background

Process-driven features set apart industrial wastewater across different industries and geographical locations. On the other hand, wastewater normally comprises 25 % soluble materials and 75 % suspended particles, with 40 % of the dissolved elements being organic components; 65 per cent protein, 25 per cent carbohydrate, 9 per cent lipid, and 1 per cent detergent making up the dissolved organic elements (Rezagama, Hibbaan, and Arief-Budihardjo, 2017). Hence, to lower the amounts of pollutants of concern in industrial wastewater, specialised treatment facilities are required. Following the addition of water to a blend of barley, hops, and sugar extracts, yeast fermentation takes place to begin the brewing process. The production and handling of wastewater by the brewing industry is a threat to freshwater ecosystems and human health. Additionally, the continuous release of effluents into rivers, lakes, and streams increases the likelihood of aquatic biota extinction (Abrha and Chen 2017). This chapter presents an examination of wastewater from agro-based enterprises in Durban, South Africa, showing that one of the different sources of industrial wastewater is suitable as a culture medium for producing microalgal biomass. The chapter also discusses the different features of sources of industrial wastewater and the range of applications for which they can be applied.

4.2 Industrial Wastewater Pre-Treatment

The growing of microalgae over an extended time requires a specific environment that is designed to exclude the introduction of other types of microorganisms. The environment of wastewater provides a home for a wide variety of bacteria, some of which can inhibit the growth of algae by competing with it for nutrients and others, which can outcompete it due to their relatively more rapid rate of growth. The majority of the culturing media for microalgae are essentially secondary or tertiary treated wastewater containing significant nutrients like nitrogen and phosphorus. These types of wastewater are supplied from wastewater treatment plants.

Before being used for the production of microalgae, the treated wastewater needs to go through additional pre-treatment steps, such as autoclaving, filtering, UV-irradiation, and dilution. These steps are necessary to remove any remaining contaminants. The pre-treatment gets rid of competing microorganisms, which lowers the toxicity of the wastewater and reduces the number of suspended particulates in it. Filtration is the most reliable of these methods for large-scale applications because it removes (i) the suspended solids that might prevent light penetration in a photobioreactor, which would result in the inhibition of microalgal growth, and (ii) the microorganisms that can compete with microalgae for nutrients. This makes filtration the most effective method for large-scale applications. The microalgal productivity of treated wastewater is increased to a greater extent by filtration as compared to autoclaving and UV treatment. Even while filtering sums up the overall cost of real-scale applications, the economic benefits of high biomass production provide compensation for the costs of operation and maintenance (Yang *et al*., 2016).

4.3 Physical Characteristics of Industrial Wastewater

The total amount of wastewater discharged from a given industry is the sum of the wastewater discharged by each operational unit in the industry. In this context, the term 'Industrial Wastewater,' as used in this thesis, refers to wastewater discharged by an industrial facility. It is a by-product of the manufacturing process. The physical characteristics (of wastewater from sugar refineries (SWW), beer breweries (BWW), and dairy (DWW) are listed in Table 4.1.

Table 4.1 Physical characteristics of virgin industrial wastewater (VIWW)

Parameter	Units	SWW	BWW	DWW	RW	EPA*, 2014	DEA**, 2014
Temperature	°C	31.3±0.2	30.5±0.1	29.8±0.1	27.5±0.2	20-25	25-35
EC	mS/cm	2.9±0.3	85.25±5.83	3.6±0.1	0.4±0.1	250	
TS	mg/L	2687±30	7642.6±9.5	2616±26	547±12		
TSS	mg/L	1263±22	585.8±6.4	863±17	232±8		
TDS	mg/L	1451.±24	7056.7±12.6	1753±19	315±9		
Turbidity	NTU	218±6	319.6±54.1	624±8	2.15±0.6		
Colour	PtCo	551±5	167±21	420±4	18±2		

* Environmental Protection Agency (EPA) of the United States. ** Department of Environmental Affairs (DEA) of South Africa. EC is Electrical Conductivity, TS is Total Solids, TSS is Total suspended Solids, and TDS is Total Dissolved Solids.

4.3.1 Temperature of industrial wastewater

Temperature affects the chemistry of water, so it is important to pay attention to it. Chemical reactions proceed more quickly as the temperature rises. Temperature affects industrial wastewater and influences the effluent treatment systems' efficacy as well. As low as 4 °C, the rates of chemical and biochemical reactions are quite slow, and

biological waste treatment activities can occasionally be severely restricted at these temperatures. During the decomposition of organic matter in wastewater, heat is released thereby causing a temperature rise. Mesophilic-thermophilic transfer may make it difficult for wastewater treatment plants to function at temperatures above 43.3 °C (Cheah *et al*., 2016). Sludge density and settling rate harm waste disposal, as do unstable biological processes and reduced air and oxygen solubility. Temperature increases the number and amount of minerals that can be dissolved from rocks by groundwater. As a result, its electrical conductivity would be improved. When it comes to determining what kinds of organisms can survive in water, thermal energy has a significant impact. The weather had an impact on the temperature range of 22.5-25.6 ^{o}C during the cultivation of *Scenedesmus sp.,* but the microalga's growth was uninterrupted because this temperature range fell within the mesophilic range. Psychrophiles (also known as cryophiles) are a type of extreme-temperature microalgae that can survive in water as cold as 10 ^{o}C, while thermophilic microalgae (or thermophiles) can survive in water as hot as 45 ^{o}C (Hulatt *et al*., 2017). The optimal temperature range for microalgae development is between 25 and 30 °C since higher temperatures have an impact on the amount of saturated fatty acids in algal lipid dispersal.

4.3.2 Odour of industrial wastewater

The odours emitted by wastewater are offensive. Odours can originate from a range of sources, including decomposing organic matter, living algae, microorganisms containing essential oils and other odorous compounds, different organic chemicals like phenols and mercaptans, chlorine and its substituted compounds, and a variety of other chemical species (APHA, AWWA and WEF, 2017). Hydrogen sulphide (H_2S)

and ammonia (NH_3) are the two main inorganic odorous compounds produced by wastewater treatment plants (WWTPs), while many organic malodours are caused by the anaerobic decomposition of nitrogen- or sulphur-containing compounds. These malodourants, such as mercaptans and other nitrogen or sulphur organics, are often unavoidable due to the wastewater's composition. Volatile organic sulphides (VOS) such as methanethiol, carbonyl sulphide (COS), dimethyl sulphide (DMS), carbon disulphide (CS_2), and dimethyl disulphide (DMDS) contribute to the fouling of the atmosphere. They have a very low hedonic value and cause odour pollution even when released in small quantities. Because of their extremely low odour thresholds, high toxicity, and potential corrosive effects, the presence of VOS in the atmosphere should be constantly monitored. The microalga *Scenedesmus sp*. was used to treat the brewery wastewater under investigation, which resulted in the removal of the smell.

4.3.3 Colour of industrial wastewater

Colour is imparted to industrial wastewaters by the presence of metal ions such as chromium, platinum, iron, manganese, conjugated molecules, and dyes, which are simply referred to as "real colour." Conversely, suspended materials can impart colour to wastewater—a phenomenon known as "apparent colour" (APHA, 2017; Kula, Kalaji, and Skoczowski, 2017). The observed colour establishes whether the wastewater sample is clear, brownish, or hazy. The "true colour" principle controls colour assessment. Putrefaction causes effluent from breweries to darken as it breaks down. Over time, when the dissolved oxygen in the effluent stream decreases, changes take place (Sripiboon and Suwannahong, 2018). As shown in Table 4.1, the colour of the brewery wastewater changed from 167 to 61 PtCo during treatment, accounting for 63.5 per cent colour removal.

4.3.4 Solids in industrial wastewater

There are two kinds of total solids (TS) in wastewater: Suspended solids, or non-filterable solids, come first. Before and after treatment, the suspended particles in the brewery wastewater weighed 585.84±6.41 mg/L and 56.75±0.25 mg/L, respectively. This decline could be the result of dissolution or agglomeration, followed by sedimentation. Second, after treating the brewery wastewater with microalgae, the total dissolved solids (TDS) were determined to be 161.55±0.47 mg/L as opposed to 7056.71±12.61 mg/L before treatment. As a result, the TDS reduction was 96.71 %, indicating that *Scenedesmus sp.*, a type of microalga, is a significant biological agent in the TDS extraction process from brewery effluent. This treatment eliminated up to 99.62 % of the total TS, indicating that *Scenedesmus sp.* is a useful biological agent for removing TS from brewery effluent. The first turbidity of 319.62±54.14 NTU decreased by 77.07 % to 73.28±3.82 NTU, suggesting that there were a significant amount of colloidal particles in the wastewater under examination.

4.3.5 Electrical conductivity of industrial wastewater

Equation (4.1) predicts that the conductivity of electrolytes will typically increase with temperature.

$$\varepsilon_T = \varepsilon_{T_{ref}}\left[1 + \theta(T - T_{ref})\right] \quad (4.1)$$

where ε_T is the electrical conductivity at temperature T, T_{ref} is the reference temperature, and T is the sample's temperature. Where θ is the broth's temperature compensation gradient and $\varepsilon_{T_{ref}}$ is the electrical conductivity at the reference temperature $T_{ref.}$ To obtain the temperature coefficient, plot ε_T against (T-T_{ref}). Equation (4.2) can be used to derive theta (θ) by calculating the conductivity of a

sample at two different temperatures, T_1 and T_2, near T_{ref}. The further T is from T_{ref}, the greater the departure from the proper value.

$$\theta = \frac{\left(\varepsilon_{T_2} - \varepsilon_{T_1}\right)}{(T_2 - T_1).\,\varepsilon_{T_1}}.100\ \%/(^{o}\mathrm{C}) \tag{4.2}$$

where ε_{T1} and ε_{T2} are electrical conductivities at T_1 and T_2 temperatures, respectively. The temperature of the empirical sample, T_2, is typically 10°C warmer than T_1. The EC parameter evaluates a solution's capacity to transfer high voltages. The flow of electricity through a solution proves the existence of ions, which are the only carriers of electric current. Therefore, EC is used to detect the concentration of ions in the solution and to examine the mobility of NO_3^- and PO_4^{3-} ions in wastewater as the microalgae cells reproduce. Taking into account the sample's potential for corrosion, EC values are also used to quantify the mineralization of wastewater. This shows that the amount of dissolved solids in a water sample corresponds to its EC. Temperature affects the mobility of ions in a solution. Viscosity reduces with temperature, facilitating greater ion mobility. Therefore, as the temperature rises, EC increases (Musa and Okonkwo, 2017). Based on the above, the EC of the wastewater from the brewery under research was 85.25±5.83 µS/cm before treatment and 1.31±0.42 µS/cm after treatment. *Scenedesmus sp.* removed 98.56 % of the EC from the brewery effluent, indicating that the microalga could draw ions out of the mixture. Because of this, EC is a crucial metric to keep an eye on while assessing the water and wastewater quality.

4.3.6 Turbidity

Turbidity is a measure of wastewater's light-emitting capabilities, and a turbidity test is used to determine the quality of waste discharges in terms of colloidal particles. The turbidity of sewage is determined by its strength.

4.4 Chemical Characteristics of Industrial Wastewater

Chemical parameters routinely evaluated in water and wastewater samples include COD, pH, Cl^-, TKN, NO_3^-, NO_2^-, NH_3, PO_4^{3-}, fats, oil and grease (FOG), S^{2-}, SO_4^{2-}, and dissolved oxygen (DO). Table 4.2 is a list of the chemical properties that this study monitored.

Table 4.2 Chemical characteristics of VIWW and RW***

Parameter	Units	SWW	BWW	DWW	RW
pH		6.54±0.12	7.35±0.21	6.58±0.12	5.81±0.11
Alkalinity, as CO_3^{2-}	mg CO_3^{2-}/L	26.7±0.3	105.1±0.2	18.6±0.8	24.8±0..6
DO	mg/L	6.5±0.3	0.4±0.1	4.5±0.2	7.4±0.2
COD	mg/L	4740±28	5855±15	1642±18	164±7
TOC	mg/L	202±8	200±5	204±9	168±8
TN	mg/L	53.7±3.2	39.1±2.1	48.9±2.3	31.4±2.2
NO_3^-	mg/L	9.9±1.1	4.3±0.2	7.4±1.1	6.8±0.6
NH_3	mg/L	43.6±3.2	34.6±0.2	41.5±3.3	24.6±3.1
Phosphate, PO_4^{3-}	mg/L	0.9±0.2	3.2±0.3	2.4±0.2	1.6±0.3
Chloride, Cl^-	mg/L	988±34	726±12	1082±26	284±8
Residual Cl_2	mg/L	0.01±0.01	0.03±0.01	0.02±0.01	0.01±0.01
FOG	mg/L	4.3±0.1	1.05±0.01	3.74±0.11	0.89±0.04

*Virgin Industrial Wastewater **Raw Water

It is expedient to discuss each of the characteristics listed in Table 4.2.

4.4.1 pH of brewery wastewater

Water dissociates into hydroxonium and hydroxide ions, which are in dynamic equilibrium with the undissociated water molecules, as Equation (4.3) illustrates.

$$2H_2O\ (l) \quad \rightleftharpoons \quad H_3O^+\ (aq) \quad + \quad OH^-\ (aq) \tag{4.3}$$

$$K_w = C_{H_3O^+} * C_{OH^-} \tag{4.4}$$

Empirically, at 25°C, $K_w = 1.008 * 10^{-14}\ mol^2L^{-2}$ (Adeva-Andany *et al.*, 2014)

And at equilibrium, $C_{H_3O^+} = C_{OH^-}$

Therefore, $K_w = C^2{}_{H_3O^+} = 1.008 * 10^{-14}\ mol^2L^{-2}$

$$C_{H_3O^+} = C_{OH^-} = 1.004 * 10^{-7}\ mol\ L^{-1}$$

So, for a neutral solution at 25°C,

$$pH = -log_{10}\, C_{H_3O^+} = 6.998 \approx 7 \tag{4.5}$$

However, as the temperature rises, more water molecules dissolve, increasing the concentration of OH^- and H_3O^+ ions. The pH decreases and the K_w value increases as a result. Empirical evidence indicates that at 37 °C, $K_w = 2.7*10^{-14}$ mol^2L^{-2} yields a neutral pH of 6.784 (Ellis, 2016). Similarly, at 40 °C, $K_w = 2.916*10^{-14}$ mol^2L^{-2}, and pH is 6.767, which is neutral. The pH of a neutral solution falls with increasing temperature, reaching 6.145 at 100 °C. This illustrates how the neutral point of the pH scale moves with temperature, not that the fluid is acidic. K_w decreases as a result of fewer water molecules dissociating at temperatures below 25 °C. Consequently, the pH of neutral solutions is higher than 7.00 at temperatures below 25 °C. The pH value that corresponds to $K_w = 0.681*10^{-14}$ mol^2L^{-2} at 20 °C is 7.083, which is the neutral pH at that temperature.

An imbalance in the hydroxonium to hydroxide ion as well as contamination from foreign materials and certain mineral ions leads to pollution of the water sample. It is, therefore, possible to mislead the pH value to determine the character of the water sample. According to Abrha and Chen (2017), wastewater may then be basic or acidic, and maintaining a pH balance is essential to comply with regulatory bodies' stringent wastewater discharge limitations. Biochemical reactions during microbial organic matter decomposition can cause wastewater's pH to change (Jankowska, Sahu, and Oleskowicz-popiel 2017). In this sample, the optical density rose together with the pH value. This was controlled by sparging CO_2 gas through the broth, which raised the pH to a slightly acidic level. From Table 4.2, the pH of the samples were reported: SWW (6.54±0.20), BWW (7.35±0.21), DWW (6.58±0.12), and RW (5.81±0.11).

4.4.2 Alkalinity of brewery wastewater

Alkalinity is the ability of water to neutralise acid. Some of the ion species that contribute to alkalinity in freshwaters are CO_3^{2-}, HCO_3^-, OH^-, PO_4^{3-}, SiO_4^{4-}, and BO_3^{3-}, according to Martonen (2017). The geography of the soil that the water is running over and through determines which of the aforementioned species is dominant. The five different types of alkalinity include carbonate-phosphate alkalinity, phosphate-hydroxide alkalinity, carbonate-hydroxide alkalinity, and PO_4^{3-}alkalinity. Because the kind of alkalinity in a given study is dependent on the ionic species abundance in the water or wastewater sample, it is crucial to consider this factor. However, alkalinity is typically expressed as total alkalinity or carbonate alkalinity due to protocol constraints (Evans and Sober 2015). Thermal emission from the discharge of industrial effluent into receiving water affects the concentration of H+ ions, which raises the carbonate-to-bicarbonate ratio and lowers pH. If phenolphthalein-alkalinity (P) is

present, it indicates significant carbonate or hydroxide alkalinity. If P = 0, then alkalinity would mainly be due to bicarbonates (HCO_3^-), and total alkalinity (T) would be determined using a methyl orange indicator.

If $P = \frac{1}{2}(T)$, alkalinity is mainly due to carbonate (CO_3^{2-}).

If $P < \frac{1}{2}(T)$, alkalinity is due to bicarbonate (HCO_3^-).

If $P > \frac{1}{2}(T)$, alkalinity is due to hydroxide (OH^-) and carbonate (CO_3^{2-}).

From this study, there was a reduction in alkalinity of the BWW from 105.10±0.20 mg/L to 23.76±2.32 mg/L, or 77.4 %.

4.4.3 Fats, oil, and grease (FOG) in industrial wastewater

Upstream anthropogenic activities include food processing, the manufacture of chemicals based on petroleum, machining, and vehicle maintenance are the sources of FOG in wastewater. FOG, thus, is an indication of a multitude of chemicals extractable by organic solvents rather than an absolute quantity of any one particular substance. According to Udaiyappan *et al.* (2017), fatty acids, lipids, waxes, vegetable oils, soaps, and hydrocarbon oils are among the non-volatile organic compounds found in FOG. Conventional biological wastewater treatment methods, which can be either anaerobic or aerobic, are constrained by FOG. As a measure of the extent of upstream anthropogenic activity, FOG levels in wastewater streams are crucial to understanding the design and upkeep of wastewater treatment facilities (Aniyikaiye *et al*., 2019). Industrial wastewater has significant quantities of FOG, which may be very problematic if they are released into the receiving water system unchecked. This report's untreated brewing wastewater has a FOG level of 1.05±0.20 mg/L, which is less than the 2.5 mg/L recommended by regulatory agencies. See Table 4.2. A

microalgae cultivation procedure that removed up to 73 % of the FOG from the wastewater suggests that the amount of FOG in the brewery wastewater had no discernable effect on the microalgae treatment process.

4.4.4 Chloride ion (Cl^-) in brewery wastewater

Because chloride ions are essential to the survival of water ecosystems, high quantities of them pose a threat to the environment. Because they reproduce at different rates, microalgae and other freshwater plants and animals alter the chemistry of their surroundings and contribute to species extinction. The brewery employs chlorine-based chemicals to remove bacteria from its process water. However, by chlorinating organic compounds, chlorine residues increase the risk to ecosystems and can destroy aquatic life. But keep in mind that Giardia cysts and Cryptosporidium oocysts are resistant to chlorine treatment (Kyser and Doucette 2018). Table 4.2 shows that the study's brewery wastewater had 3.12±0.11 mg Cl^-/L. Following the microalgae treatment procedure, the concentration of Cl^- ions decreased to 1.31±0.04 mg Cl^-/L, signifying a 58 % decrease.

4.4.5 Chemical oxygen demand (COD) of industrial wastewater

When evaluating the pollution levels in residential and commercial wastewater, COD takes into consideration the oxygen required for the chemical oxidation of organic matter using potent chemical oxidants. Wastewater has the necessary amount of oxygen for the oxidation of organic materials to produce carbon dioxide and water. Because it does not account for biodegradability, COD measures the amount of oxygen required to chemically oxidise both organic and inorganic compounds present in water sources. High COD levels indicate significant pollution, which can adversely affect aquatic ecosystems by depleting DO necessary for aquatic life. (Yang *et al*. 2018).

Concentrated sulfuric acid acts as an oxidising agent, releasing the oxygen required for disintegration by providing the acidic medium that dichromate needs. Conversely, the wastewater sample contains straight-chain hydrocarbons, which $AgSO_4$ catalyses the oxidation of. In addition to thermally catalysing the reaction, the digesting block is heated to 150 °C. Digestion processes involve the oxidation of organic carbon material with the hexavalent dichromate ion. Equation (4.6) illustrates how dichromate releases its oxygen (O_2), which then combines with carbon to form CO_2, as Equation (4.8) demonstrates. Equation (4.7) illustrates the dichromate ion's ionic half-reaction, which transfers chromium (VI) to chromium (III).

$$2K_2Cr_2O_7 + 8H_2SO_4 \rightarrow 2K_2SO_4 + 2Cr_2(SO_4)_3 + 8H_2O + 3O_2 \quad (4.6)$$

$$Cr_2O_7^{2-} + 14H^+ + 6e^- \rightarrow 2Cr^{3+} + 7H_2O \quad (4.7)$$

$$C + O_2 \rightarrow CO_2 \quad (4.8)$$

Colourimetric investigation shows that the two chromium ions absorb in the visible spectrum but at different wavelengths. The dichromate ion does not absorb at the wavelength of the Cr^{3+} ion, while the Cr^{3+} ion absorbs a small, correctable portion of the wavelength in the dichromate range. This small interference is zeroed during the calibration process to eliminate its impact on the measurement. The dichromate ion is visible at 420 nm, and the Cr^{3+} ion is visible at 600-620 nm. The low-range COD (150 ppm) study is used to measure the oxidant, $Cr_2O_7^{2-}$. The rapid COD measurement (<1500 ppm) gauges the growth of Cr^{3+}. Chemical oxygen demand (COD) quantifies the amount of organic materials, both biodegradable and nonbiodegradable, in water. Conversely, decomposable organic matter takes up dissolved oxygen, and as Equation (4.9) demonstrates, COD does not distinguish between physiologically degradable organic matter and any other degradable organic matter.

$$\text{Organic matter} + \text{oxidant} \rightarrow CO_2 + H_2O \quad (4.9)$$

Equations (4.10) and (4.11) express the operational half-reactions in the COD vial test if the glucose molecule is used to represent the organic molecule in Equation (4.9).

$$C_6H_{12}O_6 + 6H_2O \rightarrow 6CO_2 + 24e^- + 24H^+ \quad (4.10)$$

$$Cr_2O_7^{2-} + 6e^- + 14H^+ \rightarrow 2Cr^{3+} + 7H_2O \quad (4.11)$$

Equation (4.11) illustrates that starting with electrons, for every mole of oxidised glucose, which releases 24 electrons, there is a corresponding reduction of four moles of dichromate, each of which absorbs six electrons, to produce Cr^{3+} ions. Equation (4.12) then illustrates the entire test.

$$C_6H_{12}O_6 + 4Cr_2O_7^{2-} + 32H^+ \rightarrow 6CO_2 + 8Cr^{3+} + 22H_2O \quad (4.12)$$

In this investigation, the cultivation of microalga *Scenedesmus sp.* in brewery wastewater resulted in a reduction of COD from 5855.0±15.2 mgL^{-1} to 186.0±0.1 mgL^{-1}, indicating a removal rate of more than 96 %.

4.4.6 Nitrogen content of brewery wastewater

Nitrogen is a key component in the construction of biological molecules, and it can assist researchers in better comprehending microalgal growth and biochemical composition change (Chandra *et al*. 2019). The major nitrogen forms of importance in wastewater chemistry are ammonia-nitrogen (NH_3-N), nitrate-nitrogen (NO_3-N), nitrite-nitrogen (NO_2-N), and total Kjeldhal nitrogen (TKN). The initial stage of organic matter breakdown is ammonia-nitrogen, often known as free ammonia. It exists in an aqueous solution as either ammonia or an ammonium ion, depending on the pH. Organic nitrogen in wastewater does not reflect all the nitrogen found in organic matter; rather, it is a small percentage of it, made up of protein, urea, and cell components (like nucleic acids). The approach outlined in "Standard Methods" does

not distinguish between the various forms; rather, organic nitrogen compounds are measured as a group. Total Kjeldhal Nitrogen (TKN) is the sum of organic and ammonia-nitrogen. Albuminoidal nitrogen, which is the amount of nitrogen present in wastewater before organic matter degradation begins, shows how much nitrogenous stuff in the wastewater is under-composed.

Nitrites are a kind of nitrogen that indicates the presence of partially degraded organic materials. Nitrate-nitrogen on the other hand are nitrates that fully oxidised organic matter release. The acidified potassium sulphate digestion of the wastewater with a copper catalyst converts the organic nitrogen in the industrial wastewater sample to NH_3-N in the Kjeldahl test procedure.

The boiling point of the digesting acid is raised by adding potassium sulphate (K_2SO_4), raising the digestion temperature to 395 °C. During acid-catalyzed digestion, however, not all nitrogenous organic molecules contain ammonia; typically, the Kjeldhal test procedure only partially hydrolyzes acrylonitrile and cyanuric acid. But to release NH_3 gas, which is distilled into the acidic cleaning solution and converted back to NH_4^+ as indicated in Equation (4.18), the pH of the acid-digested sample is raised to 9.5 using sodium hydroxide (Barata *et al*. 2018).

While NH_3-N concentrations as high as 1.600 mgL^{-1} immobilise microorganisms and make the environment poisonous to biological wastewater treatment agents like microalgae, concentrations as low as 0.5 mgL^{-1} can be detrimental to aquatic biota like fish (Pang *et al*. 2019). The toxicity of ammonia varies with pH, therefore treated wastewater and streams have low quantities of NO_2-nitrogen. When NH_3 is being nitrified, nitrifying bio-agents rapidly convert the unstable intermediate ion species NO_2^- to NO_3^-. According to Sniffen, Sales, and Olson (2018), fixed nitrogen molecules including NH_3, NO_3^-, NO_2^-, and Organic-N are necessary for biological agents in

wastewater treatment. These compounds are prohibited in wastewater discharge circumstances, thus they need to be treated.

Scenedesmus sp. adapted and grew in all nitrogen sources tested, including NH_4Cl, NH_4HCO_3, $NaNO_2$, $NaNO_3$, NH_4NO_3, yeast extract, and urea. The DCW, biochemical, and fatty acid methyl ester (FAME) makeup differed depending on the nitrogen supply. NH_4HCO_3 had the highest DCW (1.96±0.03) and total lipid content (0.77±0.02), followed by NH_4NO_3 > yeast extract = urea > $NaNO_2$ > $NaNO_3$ > NH_4Cl. The increased biomass and lipid accumulation in ammonium sources (NH_4HCO_3, NH_4NO_3) could be attributed to the direct assimilation of the nitrogen into the microalgae without any preceding redox reaction. In the case of nitrate, it is first converted to nitrite by nitrate reductase, then to ammonia by nitrite reductase and ferredoxin, lowering cellular NADPH levels and placing stress on microalgal cells. Due to the presence of an extra carbon source other than ambient CO_2, the microalgae produced more biomass and lipids in NH_4HCO_3 than in other ammonium sources. The inclusion of bicarbonate in the growth medium has been shown to increase dissolved inorganic carbon (DIC), which boosts microalgal growth and lipid content (Pancha *et al*. 2015). Although NH_4Cl is an ammonium source, there was little biomass and lipid accumulation. When the pH of the medium was measured on day three, it was found to be 4.2, which was lower than in other cultures with a pH ranging from 7.5 to 9. Indeed, when NH_4Cl is broken down, positive NH_4^+ ions are produced, which are taken up in exchange for H^+, culminating in the formation of HCl.

4.4.7 Nitrification

Anaerobic settings destroy nitrifying bacteria because they are obligate aerobes that depend on molecular oxygen for survival. According to Bai (2015), notable

nitrification processes begin from 2.0 to 2.9 mg/L of DO and peak at 3.0 mg/L. Conversely, nitrification would not occur at DO concentrations below 0.5 mg/L. To convert one kilogramme of NH_4^+ ions to NO_3^-, up to 4.6 kg of O_2 are required. The researcher also claimed that if oxygen is supplied once DO is depleted, nitrifying bacteria can survive for up to four hours. Maintaining DO at around 1.5 mgL^{-1} is necessary to guarantee effective nitrification. Within this study, NH_3-N decreased in concentration from 0.382±0.021 mgL^{-1} to 0.064±0.401 mgL^{-1}, signifying 83 % removal; NO_3^--N decreased in concentration from 4.30±0.23 mgL^{-1} to 1.12±0.09 mgL^{-1}, signifying 74 % removal of NO_3^--N; NO_2^--N decreased in concentration from 0.37±0.02 mgL^{-1} to 0.17±0.01 mgL^{-1}, signifying 54 % removal of NO_2^--N; and TKN decreased in concentration from 8.62±1.03 mgL^{-1} to 2.05±0.08 mgL^{-1}, signifying 76 % removal. Equations (4.13) and (4.14) show that two phylogenetically unrelated bacterial strains consecutively oxidise ammonia and/or ammonium to nitrate, which is how the nitrification process starts after 10 to 12 days of cBOD.

$$2NH_3 + O_2 \xrightarrow{\text{Nitrite bacteria (Nitrosomonas)}} 2NO_2^- + 2H^+ + H_2O + \text{new cells} \quad (4.13)$$

$$2NO_2^- + O_2 + 2H^+ \xrightarrow{\text{Nitrate bacteria (Nitrobacter)}} 2NO_3^- + 2H^+ + \text{new cells} \quad (4.14)$$

Equations (4.15) and (4.16) demonstrate how the hydrogen ions produced in Equation (4.13) promote the formation of nitrous acid, which causes the breakdown of carbonate alkalinity.

$$H^+ + NO_2^- \longrightarrow HNO_2 \quad (4.15)$$

$$CaCO_3 + 2H^+ \longrightarrow Ca^{2+} + CO_2 + H_2O \quad (4.16)$$

Nevertheless, nitrifying bacteria use carbonate alkalinity as a carbon source and favour inorganic carbon over organic carbon. In the propagation of biomass synthesis, Summerfelt *et al.* (2015) showed that ammonium ions undergo complete oxidation to

nitrate ions, as Equation (4.17) illustrates; for each mole of ammonium-nitrogen depleted, 4.32 g of dissolved oxygen are consumed and 7.07 g of alkalinity are destroyed by the formation of hydrogen ions.

$$NH_4^+ + 1.89\ O_2 + 0.0805\ CO_2 \xrightarrow{\text{Bacteria}} \quad (4.17)$$

$$0.0161\ C_5H_7O_2N + 0.952\ H_2O + 0.984\ NO_3^- + 1.9833\ H^+$$

An oxidised milligramme of ammonium nitrogen removes 6.0-7.4 mg of alkalinity. A casual look at Equations (4.13) through (4.16) reveals theoretical stoichiometric ratios that point to the loss of 7.14 mg of alkalinity, or $CaCO_3$, for each milligramme of oxidised ammonium ions.

Equation (4.17) illustrates the dynamic equilibrium between soluble molecular ammonia (NH_3) and ammonium ions (NH_4^+), where the equilibrium tilts to the left at higher pH values and temperatures. The relative concentration of each is dependent on the medium's pH and temperature.

$$NH_3\,(g) + H^+\,(aq) \rightleftharpoons NH_4^+\,(aq) \quad (4.18)$$

Because there is not enough alkalinity in the system to provide both the inorganic carbon required by the nitrifying bacteria and buffering pH stability, nitrification activity drastically reduces when the pH drops below 6.7. Therefore, to maintain the appropriate pH range of 7.2 to 8.0 for unimpeded nitrification, residual alkalinity of 50 mg/L is ideal (Rezagama, Hibbaan, and Arief-Budihardjo, 2017). However, this study discovered that more than 77 % of the alkalinity was eliminated, suggesting that nitrification was interfered with when Scenedesmus sp. was cultivated under the given circumstances.

4.4.8 Phosphorus as ortho phosphate ions (PO_4^{3-})

According to Martonen (2017), phosphorus is widely available in a variety of industrial waste streams. These include corrosion inhibitors from the automotive industry, builders from the detergent industry, process chemical reagents from the process sector, and reactive orthophosphate from sanitary waste streams. Waste streams may contain polyphosphates, pyrophosphates, and metaphosphates, depending on the activities carried out in upstream industries. A crucial component of cellular metabolic activities that propel chemical reactions to produce phospholipids and other bioproducts is orthophosphate-phosphorus (Fazal *et al*. 2018). Most biological wastewater treatment systems have a minimum requirement of 100:1 for the BOD:P ratio (Razzak, Ali, and DeLasa 2017). In contrast, this study discovered a BOD:P ratio of 123:1, which dropped to 90:1 upon harvesting the microalgal biomass. Therefore, growing Scenedesmus sp. in brewery wastewater was able to sequester 75 % of the reactive phosphorus.

4.4.9 Mineral characteristics of industrial wastewater

Minerals found in water and wastewater can have impacts that are either useful to the environment and the community that is hosting them, bothersome to the ecosystem, or severely hazardous to the environment: While there are minerals that are necessary for the growth of plants and animals, there are other minerals that can harm water consumers, wastewater treatment systems, and receiving waterways. The levels of certain minerals that can be found in water can either be beneficial or harmful, depending on the situation. The term "dissolved metals" (DM) refers to the metal ions in a sample that are large enough to pass through a membrane filter with a pore size of 0.45 micrometres. They are known as Extractable Metals (EM), and they have very

weak adsorption on particulate materials. Suspended Metals are the metal ions that are present in a sample that has not been acidified and that are captured by a membrane filter with a pore size of 0.45 microns (SM). The Total Metal (TM) ions found in the wastewater system are calculated by adding the DM and SM values together. Despite this, TM can be detected in an unfiltered sample by following the necessary digestion steps.

If dumped into the environment, wastewater that has not been treated but still contains heavy metals can damage aquatic life as well as crops. Heavy metals can eventually make their way into the food chain, where they can be ingested by people and lead to a host of serious health issues due to their toxicity of the metals. Primary sources of heavy metal-containing industrial effluent include iron and steel production, mines and quarries, electric power plants, the production of electronic components and organic chemicals, as well as electroplating and metal surface treatment.

MP – AES (MY 18379001, Agilent, USA) was used to determine the mineral content of three industrial effluents namely, sugar wastewater (SWW), brewery wastewater (BWW) and dairy wastewater (DWW). The outcome is listed in Table 4.3. The concentration of heavy metals such as Mn, Zn, Pb and Ni in the environment is increasing mainly as a result of human activities. Zn is an essential element for several biochemical processes in plants. High concentrations of any of these metals in the soil can trigger no reversal damage to the physiological and biochemical activities in plants. The scarcity of freshwater for irrigation led to the application of industrial and domestic wastewater for agricultural purposes.

Since metal ions in water typically take the cationic form, they adsorb on the surface of substrates. Algae have polyphosphate bodies, which act as a repository for metals. Krishnan *et al*. (2021) averred that green algae store heavy metals like Cd, Co, Hg, Ni, Cu, Ti, Pb, Mg, and Zn in their polyphosphate bodies. Metal ions that have accumulated inside algal cells may be bound to proteins like metallothionein and localised preferentially in certain organelles (Chugh *et al*. 2022).

Table 4.3 Minerals in VIWW and RW using MP-AES (MY 18379001, Agilent, USA)

Parameter (wavelength of measurement)	Units	SWW	BWW	DWW	RW	WHO
Aluminium, Al (394.401 nm)	mg/L	3.98±0.02	7.49±0.01	1.45±0.02	0.45±0.01	
Arsenic, As (188.979 nm)	mg/L	0.53±0.01	0.32±0.01	0.42±0.02	0.35±0.02	
Calcium, Ca (396.847 nm)	mg/L	153.74±0.53	76.35±0.21	95.16±0.25	68.68±0.12	
Copper, Cu (510.554 nm)	mg/L	0.58±0.01	1.12±0.01	0.57±0.01	0.04±0.01	
Iron, Fe (259.940 nm)	mg/L	23.82±0.23	6.61±0.02	18.60±0.12	14.50±0.04	
Magnesium, Mg (383.829 nm)	mg/L	22.91±0.31	21.28±0.13	18.99±0.23	14.38±0.05	
Manganese, Mn (403.076 nm)	mg/L	0.72±0.01	0.28±0.03	0.51±0.03	0.34±0.02	
Nickel, Ni (346.165 nm)	mg/L	0.25±0.03	0.33±0.01	0.11±0.02	00	0.07
Lead, Pb (283.305 nm)	mg/L	0.15±0.02	0.13±0.01	0.12±0.01	0.18±0.01	0.01
Zinc, Zn (202.548 nm)	mg/L	18.75±1.01	17.83±0.02	14.92±0.01	11.23±0.01	

Permissible limits for minerals in IWW discharges are established by environmental regulatory agencies and can vary by country, region, and specific industry. These limits are designed to protect water quality and public health. While specific permissible limits for heavy metals in industrial wastewater are not provided in the avaible sources, it is pertinent to note that these standards are designed to minimize environmental pollution and health risks. Permissible limits can vary based on factors such as type of industry, the characteristics of the receiving water body, and local environmental policies.

4.5 Biological Characteristics of Industrial Wastewater

Dissolved Oxygen (DO), which refers to the quantity of oxygen present in a dissolved form inside water or wastewater, is infrequently observed in wastewater samples. The detection of dissolved oxygen (DO) in untreated wastewater serves as an indicator of its freshness. The occurrence of microorganisms, including aquatic plants, aquatic animals, and aquatic bacteria and viruses, is associated with the biological characteristics of wastewater. Putrefaction refers to the process of organic matter decomposition, whereas liquefaction occurs as a result of the enzymatic dissolution of solid organic substances. Anaerobic bacteria employ alternative electron acceptors, distinct from oxygen, to oxidize organic substances.

Each microorganism has inherent limitations in its capacity to metabolise organic molecules. Certain microorganisms can exclusively use specific organic substances. In a natural environment, when a water channel is exposed to specific organic compounds, microorganisms with the ability to break down that organic matter will thrive. Nevertheless, the culture employed in the BOD test may contain only a minute proportion of microorganisms capable of breaking down the specific organic

compounds present in the waste. Nature contains several organic substances with varying chemical compositions. Not all organic stuff exhibits uniform rates of deterioration. Monosaccharides and polysaccharides undergo fast degradation, resulting in a significantly high rate constant for biochemical oxygen demand (BOD). Table 4.4 showcases microbial prpfile in both IWW and RW. Cellulose exhibits a significantly slower degradation rate, while hairs are indestructible during BOD testing or biological treatment of wastewater (Osman *et al.,* 2023).

As part of their metabolic process, these organisms generate carbon dioxide (CO_2), water (H_2O), hydrogen sulphide (H_2S), methane (CH_4), ammonia (NH_3), nitrogen gas (N_2), reduced organic compounds, and various bacterial species.

Table 4.4 Microbial characteristics of IWW and RW

Parameter	Units	SWW	BWW	DWW	RW
*BOD_5	mg O_2/L	868±26	678±23	538±18	230±10
E.coli	cfu/100 mL	2.02 x 10^6	1.71 x 10^6	1.62 x 10^6	0.12 x 10^6
Faecal coliforms	cfu/100 mL	0.11 x 10^6	0.0	0.16 x 10^6	0.05 x 10^6
Total coliforms	cfu/100 mL	2.5 x 10^6	1.8 x 10^6	2.01 x 10^6	0.18 x 10^6

*Biochemical oxygen demand

Throughout the sampling period, the BOD profile typically ranged from 3.7 to 14 mg/L, while the COD profiles varied from 17 to 394 mg/L. High concentrations of organic matter (such as leaves, dead plants, animals, industrial effluents, sewage treatment plants, food processing plants, woody debris, animal manure, and urban stormwater runoff) are the primary cause of BOD in aquatic systems. Heavy discharge of industrial effluents, home sewage, crops, and animal waste all contribute to high BOD concentrations.

4.6 Wastewater Source Suitability for Microalgae Growth

Different wastewater sources were employed to grow the microalga *Scenedesmus sp*. The wastewater sources were the sugar, dairy and brewery industries. The change in optical density was used as the growth indicator. Figure 4.1 shows the growth response of *Scenedesmus sp.* in the different wastewater sources. The patterns indicate that brewery wastewater (BWW) gave the most vertical displacement of the growth response. This was followed by the dairy wastewater (DWW), which had a dismal response to the growth stimulus of the microalga *Scenedesmus sp.* as shown in the vertical displacement. Sugar wastewater (SWW) did not give any marked response, which had a very poor response to the growth stimulus of the microalga *Scenedesmus sp*.

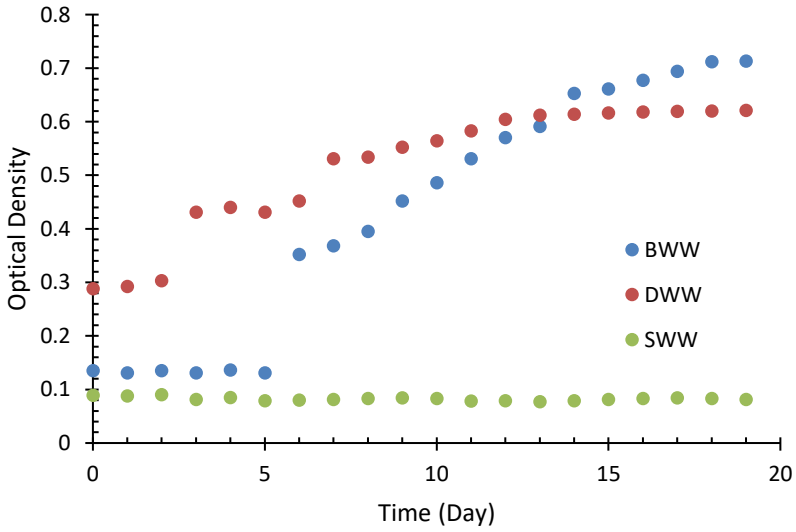

Fugure 4.1 Growth performance of Scenedesmus sp. in dairy, sugar and brewery wastewater sources

BWW gave a good response to the growth stimulus of the microalga *Scenedesmus sp*. by having the most vertical displacement. Consequently, brewery wastewater was best suited to grow *Scenedesmus sp.* in the course of this research.

4.6.1 Nutrient availability in industrial wastewater

Nutrients are the essential components present in the medium that microalgae utilise to support their growth and cellular development. To classify a substance as a "media," the nutrient availability must reach certain concentrations. The three main nutritional factors that microalgae need are vitamins, trace metals, and macronutrients. Nitrogen, as well as phosphorus, are essential macronutrients that play a critical role in promoting algal growth and regulating metabolic activities when supplied appropriately. More than 80 % of nitrogen may be removed by some microalgae species, which can flourish in wastewater.

Figures 4.2a, 4.2b and 4.2c show the nutrient factors in brewery wastewater, sugar wastewater and dairy wastewater. The figures are distinguished for their scale of values. Figure 4.2a highlights total dissolved solids (TDS) and chemical oxygen demand (COD). Wastewater from these industries is heavily loaded with these two factors. TDS is mostly expressed in SWW, followed closely by BWW and DWW. Microalgae can use both organic and inorganic nutrients to promote the growth of their

cells, while simultaneously eliminating TDS and COD in wastewater.

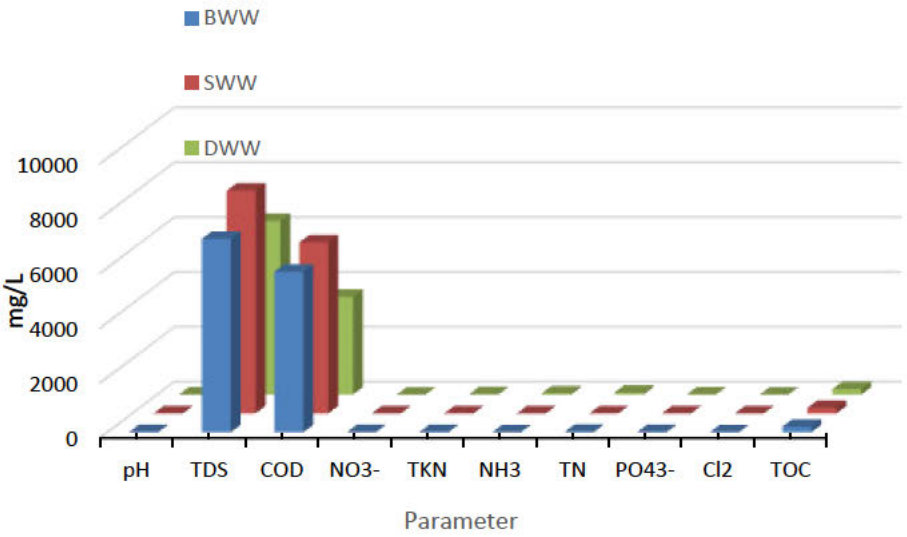

Figure 4.2a. Nutrient factors in industrial wastewater (BWW, SWW and DWW)

Figure 4.2b highlights TKN, NH_3, TN and TOC. The trend of expression of COD.

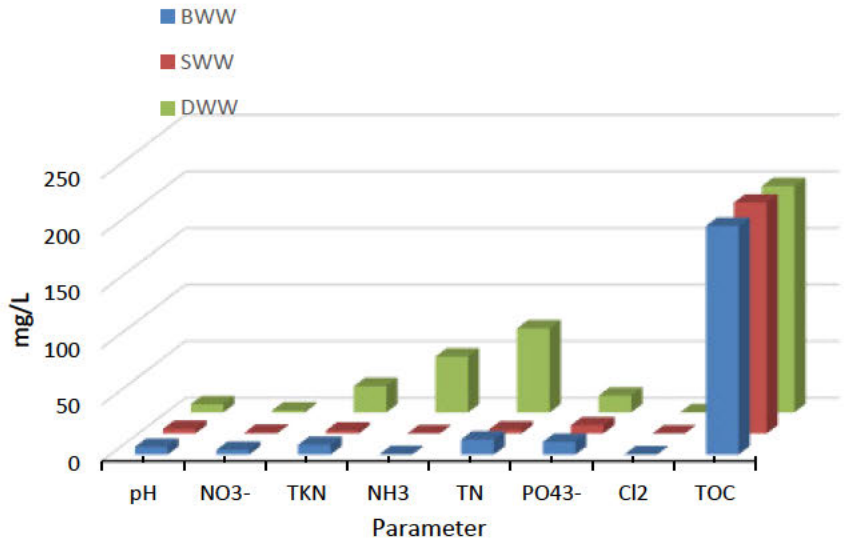

Figure 4.2b. Nutrient factors in industrial wastewater (BWW, SWW and DWW)

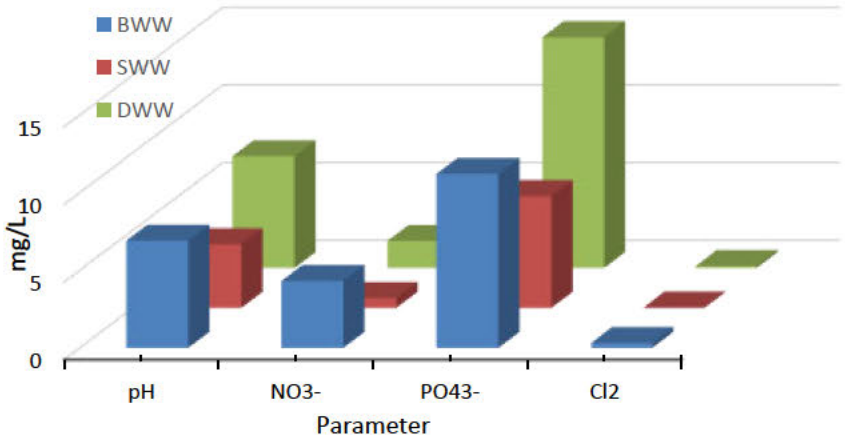

Figure 4.2c. Nutrient factors in industrial wastewater (BWW, SWW and DWW

4.7 Nutrient Enrichment

The product that exits the brewing process lines determines the type of effluent that the plant releases. However, brewery effluent frequently has lower levels of phosphate and nitrogen than municipal wastewater streams (Bakare, Shabangu & Chetty, 2017). On the other hand, when brewery wastewater is stored in an open reservoir, called an oxidation pond, microbial activity encourages nitration and phosphating by breaking down macromolecules. The brewing business is responsible for the production of beer and malt beverages. Malt effluent, as reported by *Enitan et al.* (2015), has a higher BOD than beer effluent. This could lead to a spike in bacterial burdens, which in turn would slow the rate at which bacteria are eliminated from the oxidation pond. Raw brewery waste and brewery effluent were tested, and neither contained faecal coliforms, suggesting that they were not being put into the same sewer as faecal wastes. Dissolved oxygen concentrations in the effluent were consistently lower than those in the influent wastewater throughout the study. Table 4.5 bears the report from monitoring the characteristics of BWW influent to the oxidation pond used in this

study, while Table 4.6 reports on the characteristics of the BWW effluent from the oxidation pond.

The levels of biochemical oxygen demand (BOD) in the entering wastewater showed a range of 20 to 80 mg/L. However, the effluent produced showed a notable increase in BOD levels, ranging from 80 to 280 mg/L. The observed elevation in BOD levels surpassed the established threshold of 30 mg/L, as stipulated by the Department of Water Affairs and Forestry (DWAF; WRC 2010). The observed discrepancy in biochemical oxygen demand (BOD) levels between the incoming wastewater and the effluent discharged from the oxidation ponds indicates the potential build-up of dissolved organic materials within the ponds.

The ensuing accumulation of substances leads to an increase in microbial activity, which in turn causes a significant reduction in levels of dissolved oxygen. This implies that the oxidation pond has shown limited efficacy in the removal of biochemical oxygen demand (BOD). The high level of total solids is probably due to the presence of spent grains and the high dissolved organic matter content of the wastewater from the brewery. The investigation verified that the average concentration of dissolved particles in the discharged wastewater fell within the designated limit of 2000 mg/L, as specified by DWAF (2010).

Table 4.5 Oxidation pond influent characteristics

Parameter	Influent				Sum	Mean	StDev
	a	b	c	d			
NO_3^-, mg/L	5.14	4.84	5.01	4.94	19.93	4.98	0.13
PO_4^{3-}, mg/L	13.94	12.8	13.44	13.18	53.36	13.34	0.48
Fe, mg/L	0.67	0.85	0.73	0.72	2.97	0.74	0.08
Hg, mg/L	1.2	1.53	1.46	1.47	5.66	1.42	0.15
Cd, mg/L	0.06	0.08	0.07	0.05	0.26	0.07	0.01
Cr, mg/L	0.12	0.13	0.12	0.15	0.52	0.13	0.01
Cl_2, mg/L	0.02	0.02	0.03	0.01	0.08	0.02	0.01
As, mg/L	0.72	0.8	0.71	0.67	2.90	0.73	0.05
Pb, mg/L	0.45	0.55	0.58	0.56	2.14	0.54	0.06
T (^oC)	25.3	24.8	24.9	25.1	100.1	25.03	0.22
DO, mg/L	10.6	10.2	11.4	10.4	42.6	10.65	0.53
COD, mg/L	3981	3975	3980	3980	15916	3979	3
BOD, mg/L	20	20	40	60	140	35	19
DOM, mg/L	22.4	24.36	21.8	20.6	89.16	22.29	1.57
TS, mg/L	564	540	480	558	2142	535.5	38.4
TDS, mg/L	240	280	250	260	1030	257.5	17.1
TSS, mg/L	50	60	60	40	210	52.5	9.6
Total coliform, cfu/100 mL	540	620	530	550	2240	560	41
Faecal coliform, cfu/100 mL	0	0	0	0	0	0	0

Table 4.6 Oxidation pond effluent characteristics

Parameter	Effluent				Sum	Mean	StDev
	a	b	c	d			
NO_3^-, mg/L	15.21	17.16	16.24	15.32	63.93	15.98	0.91
PO_4^{3-}, mg/L	38.01	40.23	42.31	39.15	159.7	39.93	1.83
Fe, mg/L	3.21	3.11	2.96	3.18	12.46	3.12	0.11
Hg, mg/L	0.88	0.93	0.84	0.84	3.49	0.87	0.04
Cd, mg/L	0.06	0.88	0.92	0.024	1.88	0.47	0.49
Cr, mg/L	0.03	0.04	0.3	0.21	0.58	0.15	0.13
Cl_2, mg/L	0.02	0.02	0.01	0.01	0.06	0.02	0.01
As, mg/L	0.68	0.72	0.23	0.52	2.15	0.54	0.22
Pb, mg/L	0.12	0.16	0.23	0.18	0.69	0.17	0.05
T (^oC)	22.4	23.5	23.4	23.6	92.9	23.2	0. 6
DO, mg/L	4.2	4.8	4.1	4.3	17.4	4.35	0.31
COD, mg/L	5860	5850	5856	5854	23420	5855	4
BOD, mg/L	284	266	288	278	1116	279	10
DOM, mg/L	57.69	54.4	55.6	54.53	222.22	55.56	1.52
TS, mg/L	620	580	586	578	2364	591	19
TDS, mg/L	310	302	312	308	1232	308	4
TSS, mg/L	60	80	78	81	299	74.75	9.91
Total coliform, cfu/100 mL	15080	14890	15120	14980	60070	15018	103
Faecal coliform, cfu/100 mL	0	0	0	0	0	0	0

Nonetheless, the effluent's suspended particle concentration was far higher than the prescribed level. The elimination of suspended solids is achieved through the process of physical sedimentation of particles, which was subsequently succeeded by the

biological degradation and mineralization of compounds. The measured efficacy of total solids removal in this oxidation pond was found to be less than initially anticipated. The observed phenomena can potentially be accounted for by the limited duration of retention, which hinders the significant sedimentation of suspended substances. Furthermore, it is crucial to recognize that a significant component of this study was the absence of a pre-treatment tank, which was specifically intended for regular desludging to eliminate accumulated sludge. As a result, there were no activities conducted to remove sludge. The elevated concentration of total solids in the effluent being released has the potential to significantly enhance the total solids content of any receiving stream. The increase in total solids concentration has the potential to negatively affect freshwater organisms, particularly aquatic species, by inducing osmotic stress and disrupting their osmoregulatory mechanisms (Bal *et al.* 2022). Additionally, this phenomenon results in the contamination of water, making it unsuitable for human consumption, industrial use, and agricultural purposes.

4.8 Summary and Conclusion of Characterisation and Screening

4.8.1 Summary

The established temperature range of 25 to 30 °C for optimal microalgae growth is due to the effect that high temperatures have on the concentration of saturated fatty acids in the distribution of microalgal lipids. The application of treatment with the microalga Scenedesmus sp. eliminated the odour from the brewery effluent that was the subject of this study. Putrefaction causes the colour of effluent from breweries to deepen during the decomposition process. These changes occur as the dissolved oxygen content of the effluent stream gradually decreases over time. Moreover, the wastewater

from the brewery changes colour during the treatment process, going from 167 to 61 PtCo, which results in a 63.5 % decrease in colouration.

Jankowska, Sahu, and Oleskowicz-Popiel (2017) have posited that the biochemical mechanisms implicated in the degradation of microbial organic matter possess the capacity to either diminish or elevate the acidity levels of wastewater. A positive correlation was observed between the pH value and the optical density in the provided sample. The injection of carbon dioxide (CO_2) gas into the broth led to a reduction in pH, resulting in a mildly acidic environment, which aided in the management of this particular process.

The discharge of industrial wastewater into receiving water bodies leads to thermal emission, which in turn affects the concentration of H^+ ions. This results in a decrease in pH values and a rise in the carbonate-to-bicarbonate ratio. Martonen (2017) found some ion species, such as CO_3^{2-}, HCO_3^-, OH^-, PO_4^{3-}, SiO_4^{4-}, and BO_3^{3-}, that contribute to alkalinity in freshwaters.

The dominance of any of the aforementioned species is contingent upon the topographical characteristics of the soil through which the water is flowing. There are five unique kinds of alkalinity, namely CO_3^{2-} alkalinity, PO_4^{3-} alkalinity, carbonate-phosphate alkalinity, phosphate-hydroxide alkalinity, and carbonate-hydroxide alkalinity. The significance of alkalinity in a specific study is contingent upon the relative abundance of the ionic species present in the water sample.

High amounts of fats, oils, and grease (FOG) are present in industrial wastewater, and if released without proper treatment into the receiving water system, they have the potential to give rise to significant environmental issues. According to the findings presented in this report, the concentration of FOG in untreated brewing wastewater was measured to be 1.05±0.2 mg/L. This value falls below the required limit of 2.5

mg/L set by regulatory authorities. A significant proportion, specifically 73 %, of the fat, oil, and grease (FOG) present in the brewery wastewater was successfully eliminated by the culture of microalgae. This outcome indicates that the initial quantity of FOG in the wastewater did not have any noticeable influence on the efficacy of the microalgae treatment procedure.

The measurement of Chemical Oxygen Demand (COD) in freshwater and wastewater samples provides an indirect assessment of the organic matter content. However, it is important to note that COD does not account for the biodegradability of the organic matter. Consequently, COD measurements may not correctly reflect the possible impact on the receiving stream or river. Additionally, COD considers organic compounds that are physiologically inactive. In this study, it was shown that the culture of *Scenedesmus sp.,* a type of microalga, in brewery wastewater resulted in a significant reduction of chemical oxygen demand (COD). Specifically, the COD levels decreased from an initial concentration of 5855.0±15.2 mgL^{-1} to a final concentration of 186.0±0.1 mgL^{-1}. This reduction indicates a removal efficiency of over 96 %.

The presence of nitrogen in an aqueous solution can be observed in two distinct forms, namely the ammonium ion or ammonia, depending on the pH level. The presence of organic nitrogen in wastewater does not encompass the entirety of the nitrogen content present in organic substances. Instead, it constitutes a minor proportion, primarily composed of protein, urea, and cellular constituents such as nucleic acids.

4.8.2 Conclusion

The results of the study indicate that brewery wastewater exhibits the most potential among the three wastewater sources investigated in promoting the growth and

development of *Scenedesmus sp.* The oxidation pond technique proved to exhibit viability to enrich the nutrients in the brewery wastewater employed.

CHAPTER 5

Cultivation of Microalgae in Brewery Wastewater

5.1 Background

Microalgae were cultivated at the laboratory scale using various vessels, including scotch bottles, Erlenmeyer flasks, and three-litre bubble-column photobioreactors. Figure 5.1 illustrates the cultivation of microalgae in Erlenmeyer flasks on a small scale at a laboratory workstation.

Figure 5.1 Desktop culture of microalgae in Erlenmeyer flasks

The experiment was conducted by utilizing the statistical program Design-Expert version 11. The Design of the Experiment (DOE) was utilized to ascertain the optimal number of experimental trials needed to adequately evaluate the conditions essential for attaining maximum microalgal biomass output in a scale-up setting. This chapter provides further insights into the effects of the rate of CO_2 gas sparging and the initial concentration of nutrients on the development of biomass. The experiment was carried out based on the underlying assumptions that:

(i) Algal blooms occur in downstream regions that are situated at a certain distance from the location where industrial effluent is discharged into the receiving waterbody. (ii) In the case of a receiving environment characterized by a dynamic water body, such as a stream or river, the process of wastewater dilution occurs, leading to an intensified impact as one progresses downstream.

The research was designed to make use of brewery effluent in a diluted state, as per the assumptions outlined in Section 4.2 of this thesis. The dilution procedure was conducted by employing water obtained from the creek situated at the Durban Botanic Garden. Within the context of this thesis, the water in question is commonly denoted as the reference water (RW).

5.2 Useful Terms

The subsequent sub-sections provide explanations for the terms deemed significant in this study.

5.2.1 Variables

The numerical values function as quantifiable indicators and hence represent inherent characteristics of the dataset. Dependent and independent variables are distinct types of variables. Independent variables, denoted as X, are exogenous variables that are unaffected by other values. When evaluating the nutritional content of a substance, it is important to consider factors such as the concentration of nutrients and the dosage of individual components. Dependent variables, denoted as Y, refer to the outcome variables that are influenced by the independent variables. Illustrative instances encompass biomass productivity and the velocity of dissolution (Abiodun-Oyebanji 2017; Marudhar 2019).

5.2.2 Factors

A factor refers to a pre-established variable, such as concentration, temperature, light intensity, nutrient ratio, or the ratio of a nutrient to a combination of nutrients. Factors can be evaluated using either quantitative or qualitative factors. An illustration of a quantitative factor is the concentration, denoted as a percentage (e.g., 1 %, 2 %, etc.), or the nutrient-to-chemical oxygen demand ratio, expressed as 1:30, 1:40, and so forth. Conversely, qualitative elements encompass attributes that cannot be quantified numerically. Qualitative parameters encompass several aspects such as the specific equipment utilized, the polymer grade employed, the prevailing humidity levels, and similar considerations. The variables in question are distinct from one another (Ghanad 2023).

5.2.3 Levels

The levels of a factor refer to the specific designations or values that have been assigned to it. As an illustration, one level of concentration (factor) is denoted by the numerical value of 1 %, whereas another level is denoted by the numerical value of 2 %. With the grading aspect, there exist two distinct levels of plasticizers. Levels are commonly classified as low, moderate, or high based on their degree of intensity. To enhance the simplicity of calculations, discrete and numeric levels are frequently assigned the values of -1 (representing low level) and +1 (representing high level). The general formula for this conversion is expressed in Equation (5.1).

$$Level = \frac{X - Average\ of\ the\ two\ levels}{\frac{1}{2}(Difference\ of\ levels)} \tag{5.1}$$

where *'X'* is the numeric value of the independent variable.

5.2.4 Response

A response is the outcome or outcome variable that is observed or measured from experimental operations. The outcomes are assessed and examined based on many parameters such as biomass productivity, pH variation, nutrient concentration, optical density alteration, and other relevant factors.

5.2.5 Effect of a factor

The term "effect" pertains to the modification in reaction that occurs when the magnitude of a factor is changed. The concept of interaction refers to the dynamic interrelationship among various levels and variables.

5.2.6 Interaction

The idea of interaction can be likened to that of effect, which pertains to the collective influence exerted by numerous variables on a given response.

5.3 The Design of The Experiment (DOE)

The main objective of experiment planning is to identify the most optimal and cost-effective method for testing the hypothesis. The analysis of variance approach allows for testing the null hypothesis that the means of normally distributed populations with identical variances are equal. These methods rely on assumptions derived from statistical analysis: if specific assumptions are not satisfied, the analysis of the data may lack significance, and the results of the hypothesis test may be inaccurate. The main challenge lies in devising a methodology for gathering data that facilitates the use of statistical techniques such as analysis of variance, while ensuring that the underlying assumptions are met. The experimental design permits the creation of a data collection system of this type.

Response surface methodology (RSM) is a type of experimental design that applies a variety of statistical and mathematical techniques to empirically simulate the relationship between observed responses and independent input factors (Datri *et al.*, 2023). RSM permits the separation and combination of independent components' effects on the production procedures that are being studied. Response surface design (RSD), which benefits from precision, was chosen for the study because it aimed to optimise the process. To produce predictions while trying to identify the best possible combinations of components, a comprehensive model is required. Scheffé mixing models have a list of design attributes in Table 5.1. Scheffé mixing models are a subtype of RSMs. When all of the mixture components move from 0 to the total for the design, mixture models are easy to understand because of their simplicity.

5.3.1 Mixture components

In an experiment involving a combination, the quantity of a single component is not important; the quantity of a given component relative to the other components is. If there are no constant mixture elements, the sum of all the components yields a constant total T, which is 100 %. It is necessary to have the constant total, T, for mixed experiments. This constraint requires that every mixing ingredient be separate from the others. Consequently, this independence impacts the experimental zone and presents unique modelling issues that need the development of hybrid solutions. Every component was measured using consistent units during the integration process, and the sum of all iterations was added up to a consistent value. The purpose of this technique was to ensure that the final product would have the same characteristics. The anticipation that the reaction would change depending on the relative proportions of the components and subsequent exposure to the experimental setting led to the

selection of the mixed design. Table 5.1 contains a list of the mixture model's constituent parts. The freshwater volume range, shown in the table, is 0.00 mL to 2500.00 mL. Likewise, the wastewater volume range covers 0.00 mL to 2500.00 mL. Table 5.2 lists all of the model's process variables. The light source's luminance fluctuated between 440 and 1600 lumens, and the CO_2 gas flow rate varied between 2 and 6 litres per minute.

5.3.2 Process factors

The term "factor" may also be employed to denote a manipulated independent variable when describing certain features of experimental studies. The comprehensive definition of the term "factor" encompasses both the phrases "treatment" and "treatment group" in its broadest interpretation. The attainment of each subsequent level of a component is accomplished using multiple iterations of the approach. The factors that influence a given process are a subset of the numerous elements that interact with one another and have effects on said process. Factors can be defined as a subset of elements. The initial stage commonly employed in various projects, including response surface modelling, is referred to as the starting point. As evidenced by the data presented in Table 5.2, the researchers considered a diverse range of factors and variables.

Table 5.1 Components of the mixture model

Component	Name	Units	Type	Minimum	Maximum	Coded Low	Coded High	Mean	StDev.
A	Freshwater	mL	Mixture	0	2500	+0 ↔ 0	+1 ↔ 2500	1241.99	963.72
B	Wastewater	mL	Mixture	0	2500	+0 ↔ 0	+1 ↔ 2500	1258.01	963.72
				Total =	2500.00				

Table 5.2 Process factors

Factor	Name	Units	Type	Minimum	Maximum	Coded Low	Coded High	Mean	StDev.
C	Luminous Intensity	Lumens	Numeric	440.00	1600.00	-1 ↔ 440.00	+1 ↔ 1600.00	1046.03	425.82
D	CO_2 gas	L/min	Numeric	2.00	6.00	-1 ↔ 2.00	+1 ↔ 6.00	4.08	1.57

The luminance of the light was consistently monitored in Lumens throughout the experiment to monitor its impact. In the context of the combination experiment, modifications were made to the quantities of the process factors, commonly known as the formulation factors. These elements are believed to exert influence on the overall outcome of the procedure. Instead of summing up to 1, Equation (5.2), which is applicable in the presence of constant mixing components such as water, computes the aggregate temperature of the mixture.

$$T = 1 - \sum(constant\ mixture\ factors) \tag{5.2}$$

5.3.3 Response surface methodology (RSM)

Response surface methods can improve a system's or process's efficacy and efficiency. One way to investigate the link between variables, or operational circumstances, and the response variable, or y, is to use Response Surface Methodology (RSM). Additionally, it appears that this method will help to illustrate how various experimental factors affect the test results. It is only possible to find an ideal value by using a polynomial function that contains quadratic terms. The response surface experiment can be carried out following the conclusion of the screening procedure and the determination of the important factors. A standard polynomial Equation (5.3) clarifies the connection between the process component (x) and the response variable (y). (He *et al.* 2019; Datri *et al.* 2023)

$$y = \beta_o + \sum_{i=1}^{k} \beta_i x_i + \sum_{i=1}^{k} \beta_{ii} x_i^2 + \sum_{i \neq j} \sum \beta_{ij}\, x_i x_j + \varepsilon \tag{5.3}$$

where β_o is the overall mean response; β_i is the main effects for each factor (i = 1, 2, 3, …..k); β_{ii} is the quadratic effect of the ith factor; β_{ij} is the two-way interaction between the ith and jth factors; ε represents the error associated with the response, y.

Table 5.3 presents the design information based on the mixture model as the output of the Design Expert version 11 software. Twenty-two runs of the experiment were recommended for this study.

Table 5.3 Design information

File Version	11.1.2.0			
Study Type	Combined		Subtype	Randomized
Design Type	I-optimal Point Exchange		Runs	22
Design Model	Quadratic x Quadratic		Blocks	No Blocks
Build Time (ms)	179			
Mixture Components		A B		
Process Factors		C D		

A = Freshwater; B = Wastewater; C = Luminous flux (Lumen); D = CO_2 flowrate (L/min).

When doing a screening experiment with many components using a factorial design, it is of utmost importance to avoid utilising the same combination of factors more than once. Designs that use factorials, particularly fractional factorials, have the intrinsic quality of replication (Datri *et al.* 2023). Having more design points is preferable to using the same ones over and over again. An experimental design, also known as a design point and denoted "Run" in Tables 5.3, 5.4a, and 5.4b, is a matrix of pluses and minuses with one column for each factor and one row for each set of factor combinations (see Tables 5.1 and 5.2). For each run of the experiment, a design point serves as the beginning point. For each design point, there are two mixture components and two process factors. The responses of each run are presented in Tables 5.4a and 5.4b.

With RSM one can determine the values of the controllable parameters that lead to the response's optimisation or determine the values of x in Equation (5.3) that lead to a process or product that satisfies some requirements or specifications. As an alternative, the RSM can be used to identify values for the controllable variables that optimise the response.

5.3.4 Effects of different initial growth stimuli on microalgae

BWW was combined with RW in different ratios to mimic the downstream conditions, coupled with prescribed light intensity and CO_2 gas flow rate and microalgae biomass was cultivated in it using the 3-L bubble column bioreactor.

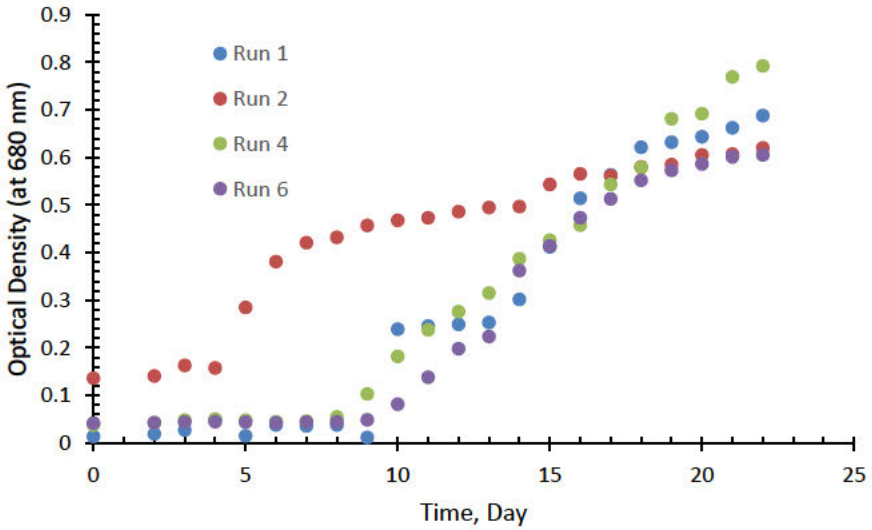

Figure 5.2 Effect of combining BWW with RW (Runs 1, 2, 4 and 6)

As shown in Figure 5.2, Run 1 represents *Scenedesmus sp.* growth output from the initial mixture of 1.25 L of brewery wastewater with 1.25 L of the reference water. This was coupled with the use of fluorescent tubes with a luminous flux of 1100 Lumen and a CO_2 sparging rate of 4 L/min. Run 2 (Figure 5.2) is the result of *Scenedesmus sp.* growth output from the initial BWW and RW mixture of 0.625 L and 1.875 L

respectively coupled with the luminous intensity of 800 Lumen and CO_2 sparging rate of 6 L/min. Run 4 (Figure 5.2) is the output of the *Scenedesmus sp.* growth from the use of 2.5 L of RW with a luminous flux of 1100 Lumen and CO_2 gas sparging rate of 4 L/min. Run 6, on the other hand, displays the *Scenedesmus sp.* growth response to 2.5 L of RW with a luminous flux of 1200 and a CO_2 gas sparging rate of 2 L/min. Consequently, Run 4 gave the most vertical displacement within the period of this study.

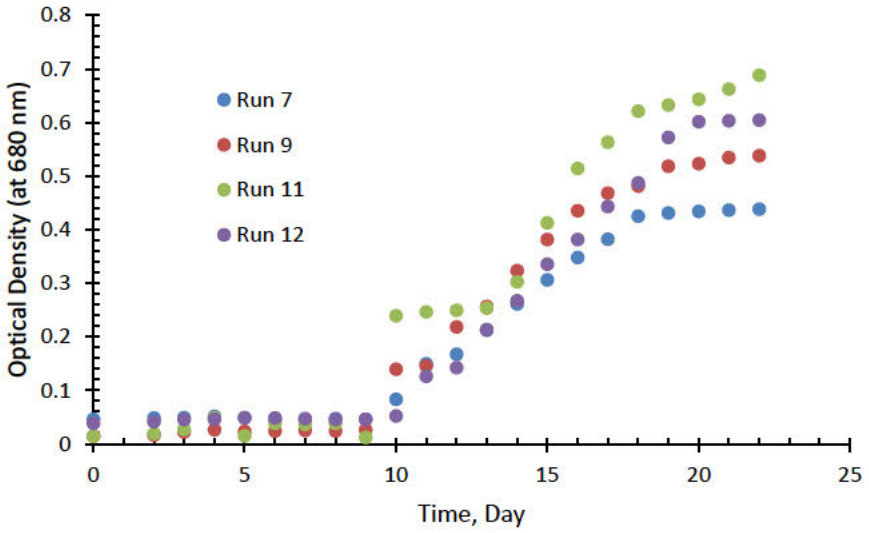

Figure 5.3 Effect of mixing BWW with RW (Runs 7, 9, 11, and 12)

Run 7, in Figure 5.3, is the outcome of the growth response of *Scenedesmus sp.* to the use of 2.5 L of BWW coupled with the luminous intensity of 1100 Lumens and CO_2 gas sparging rate of 4 L/min. Run 9 is the growth response of *Scenedesmus sp.* in a mixture of 1.25 L BWW and 1.25 L RW coupled with exposure to fluorescent light of luminous intensity of 450 Lumen and CO_2 gas sparging rate of 4 L/min. Run 11 shows *Scenedesmus sp.* growth response to the mixture of 1.25 L BWW and 1.25 L RW exposed to fluorescent light of intensity 1100 Lumen and 4 L/min CO_2 gas sparging. Run 12 is the outcome of *Scenedesmus sp.* response to growth stimuli resulting from

the use of 2.5 L of RW with a luminous flux of 1100 Lumen and 6 L/min CO_2 gas sparging rate.

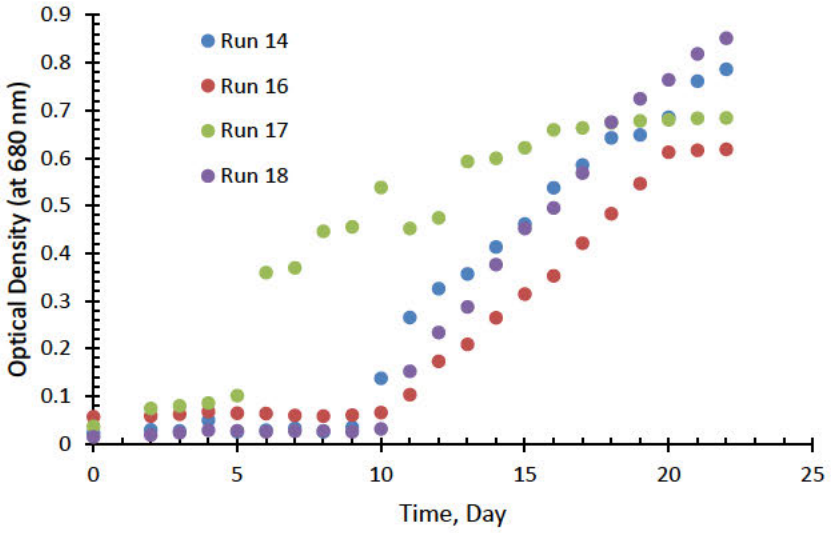

Figure 5.4 Effect of mixing BWW with RW (Runs 14, 16, 17 and 18)

In Figure 5.4, Run 14 represents the growth response of *Scenedesmus sp.* from the use of 2.5 L BWW with 450 Lumens and 5 L/min CO_2 gas sparging. Run 16, on the other hand, is the outcome of *Scenedesmus sp.* response to growth stimuli from 2.5 L RW, 450 Lumens and CO_2gas sparging rate of 5 L/min. Run 17 is the outcome of *Scenedesmus sp.* growth response to 2.5 L BWW, 450 Lumens and CO_2 gas sparging rate of 2 L/min. Run 18 gives the *Scenedesmus sp.* growth response to a mixture of 1.25 L BWW and 1.25 L RW and exposure to 1200 Lumens and 2 L/min CO_2 gas sparging.

In Figure 5.5, Runs 3, 5, 13 and 15 showed very poor responses of *Scenedesmus sp.* to growth stimuli, while Run 8 gave a relatively dismal response.

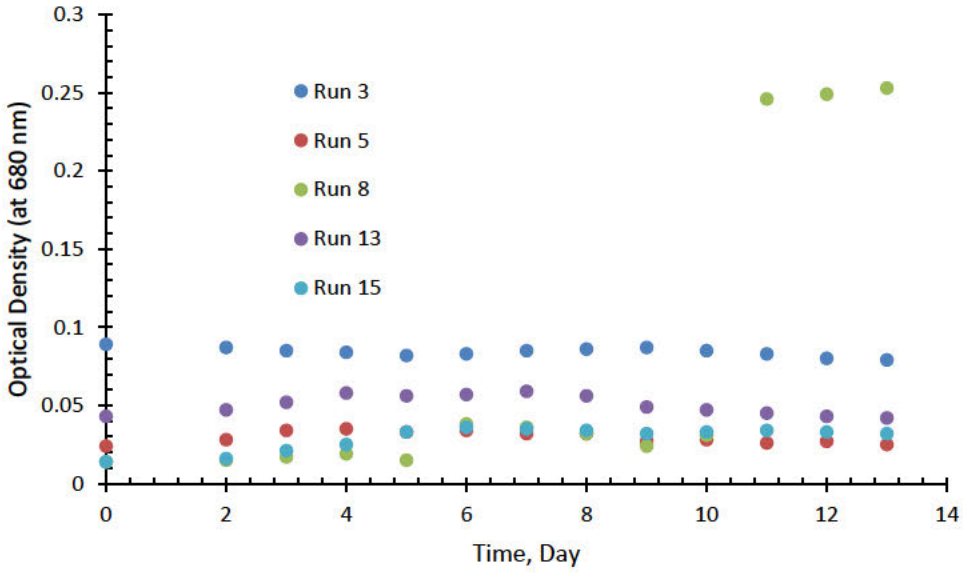

Figure 5.5 Effect of mixing BWW with RW (Runs 3, 5, 8, 13, and 15)

Run 3 in Figure 5.5 was born from the use of 2.5 L BWW under the exposure to light of intensity 1600 Lumen and CO_2 gas sparging rate of 4 L/min. Failure of *Scenedesmus sp.* to respond on the path of growth could be that more light is absorbed that could be utilized for cell growth. The excess excitation energy could be passed off to oxygen, and the resulting highly reactive oxygen has the potential to destroy the photosynthetic system, leading to the death of cells. Since Runs 5, 13 and 15 were exposed to the same light intensity, the same reason for their failure could suffice. However, Run 8 gave an unsustained initial response, which could be attributed to nutrient factors in the media. Figure 5.6 shows Runs 19, 20, 21 and 22. Run 19 is the growth response outcome of *Scenedesmus sp.*, which is the product of the mixture of RW (1.875 L) and BWW (0.625 L). The luminous intensity was 800 Lumen and the CO_2 gas sparging rate was 3 L/min. Run 20, on the other hand, is the outcome of *Scenedesmus sp.* growth response in 2.5 L BWW with a luminous intensity of 1200 Lumen and CO_2 sparging rate of 2 L/min. Run 21 gives a *Scenedesmus sp.* growth response in a mixture of RW

(1.25 L) and BWW (1.25 L) under a luminous intensity of 450 Lumen and 2 L/min CO_2 gas sparging rate.

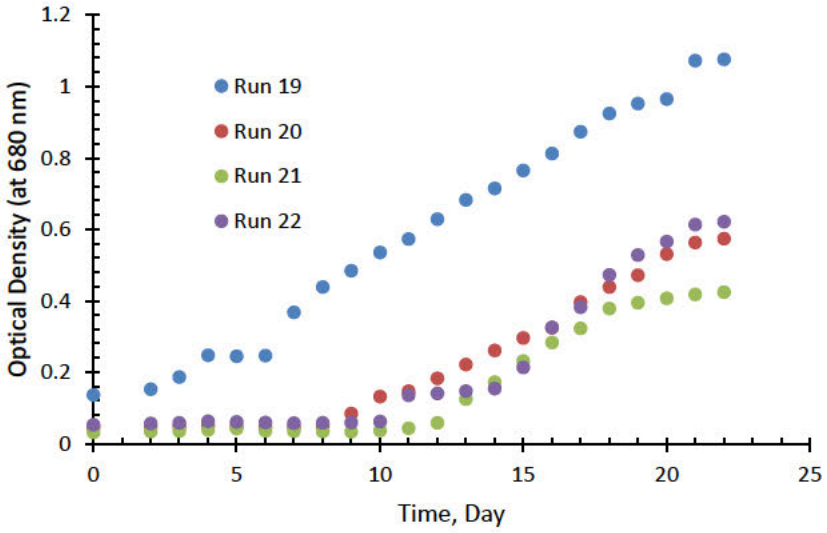

Figure 5.6 Effect of mixing BWW with RW (Runs 19, 20, 21 and 22)

Run 22 gives the response of *Scenedesmus sp.* growth in 2.5 L RW under 450 Lumen and 2 L/min CO_2 gas sparging rate. Consequently, Run 19 exhibited the most vertical displacement.

5.3.5 Optimised solutions and desirability

When an experiment is done at random, the results will also be random. The goal of optimisation is to come up with a list of requirements or priorities for the "best" design. Some ways to do this are to maximise inputs, production, strength, dependability, lifespan, efficiency, and use. Researchers use methods like experimental design and optimisation to precisely measure and analyse a wide range of factors. Every optimisation problem is made up of three parts: an objective function, choice variables, and constraints. The main goal of optimisation is to find the least (or most) value of an objective function given user preferences and/or limits imposed by the nature of the

situation at hand. The optimisation module searches for a set of combinations at the factor level that concurrently fulfil the prerequisites specified for each of the responses and the factors. The replies that were optimised for each of the possible combinations are presented in Tables 5.5, 5.5b, and 5.5c respectively.

Table 5.4a Response surface design with the responses shown in Columns 6-17

	Component 1	Component 2	Factor 3	Factor 4	1	2	3	4	5	6	7	8	9	10	11	12
Run	A: Water	B:Wastewater	C:Luminous Intensity	D:CO_2 gas	pH	Alkalinity	Turbidity	EC	TDS	DO	COD	TN	NH_3-N	NO_3-N	TKN	PO_4^{3-}
	mL	mL	Lumens	L/min		mg $CaCO_3$/L	NTU	mS/cm	mg/L	mg O_2/L	mg/L	mg/L	mg/L	mg/L	mg/L	mg/L
1	1250	1250	1310	4	6.58	56.34±0.04	162±3	5.82±0.02	1902	6.9±0.4	2408	21.7	0.257	2.69	19	11.2
2	2500	0	1600	6	6.78	29.13±0.03	63.62±0.23	5.16±0.01	1273	5.8±0.2	1040	62	27.1	6.41	18.5	10.4
3	0	2500	440	2	6.54	26.71±0.01	463±2	4.86±0.01	1451	6.5±0.3	2192	56.29	49.35	5.25	1.05	3.4
4	0	2500	440	6	7.5	63.62±0.02	131±2	4.84±0.01	2386	5.2±0.2	5602	50.68	41.13	4.41	5.35	9.63
5	1250	1250	1310	4	7.35	63.62±0.02	131±2	4.84±0.01	2386	5.2±0.2	53	50.44	40.062	2.57	8.166	10.4
6	1250	1250	440	3	7.35	63.62±0.02	131±2	4.84±0.01	2386	5.2±0.2	5602	50.68	41.13	4.41	5.35	9.63
7	2500	0	827	2	7.35	26.71±0.01	463±2	4.86±0.01	1451	6.5±0.3	2192	56.29	43.6	9.9	2.79	3.4
8	1875	625	440	6	6.54	56.34±0.04	162±3	5.82±0.02	1902	6.9±0.4	2408	21.7	0.257	2.69	18.75	5.26
9	0	2500	1213	2	6.58	56.34±0.04	162±3	5.82±0.02	1902	6.9±0.4	2408	21.7	0.257	2.69	18.75	5.26
10	0	2500	1213	6	6.58	26.71±0.01	463±2	4.86±0.01	1451	6.5±0.3	2192	56.29	43.6	9.9	2.79	3.4
11	2500	0	1310	4	7.5	56.34±0.04	162±3	5.82±0.02	1902	6.9±0.4	2408	21.7	0.257	2.69	18.75	5.26

Table 5.4b Response surface design with the responses shown in Columns 6-17

	Component 1	Component 2	Factor 3	Factor 4	1	2	3	4	5	6	7	8	9	10	11	12
Run	A:Water	B:Wastewater	C:Luminous Intensity	D:CO_2 gas	pH	Alkalinity	Turbidity	EC	TDS	DO	COD	TN	NH_3-N	NO_3-N	TKN	PO_4^{3-}
	mL	mL	Lumens	L/min		mg $CaCO_3$/L	NTU	mS/cm	mg/L	mg O_2/L	mg/L	mg/L	mg/L	mg/L	mg/L	mg/L
12	1250	1250	827	6	6.58	63.62±0.02	131±2	4.84±0.01	2386	5.2±0.2	5602	50.68	43.6	4.41	2.67	9.63
13	2500	0	440	4	6.54	56.34±0.04	162±3	5.82±0.02	1902	6.9±0.4	2408	21.7	0.257	2.69	19	11.2
14	1250	1250	1310	4	6.58	26.71±0.01	463±2	4.86±0.01	1451	6.5±0.3	2192	56.29	19.89	9.9	26.5	3.4
15	0	2500	730	4	7.5	56.34±0.04	162±2	5.82±0.02	1902	6.9±0.4	2408	21.7	0.257	2.69	19	11.2
16	1250	1250	1600	2	6.54	63.62±0.02	131±2	4.84±0.01	2386	5.2±0.2	5602	50.68	41.13	4.41	5.14	10.4
17	1250	1250	1600	6	6.58	26.71±0.01	463±2	4.86±0.01	1451	6.5±0.3	4508	56.29	43.6	9.9	2.79	3.4
18	2500	0	827	6	7.25	56.34±0.04	162±2	5.82±0.02	1902	6.9±0.4	2408	21.7	0.257	2.69	18.75	5.26
19	0	2500	1600	4	7.25	60.21±0.02	281±3	4.85±0.01	1434	5.4±0.2	810	43.91	22.8	4.26	16.85	9.52
20	1250	1250	827	2	6.54	26.71±0.01	463±2	4.86±0.01	1451	6.5±0.3	2192	56.29	43.6	9.9	2.79	3.4
21	1875	625	1213	2	6.58	56.34±0.04	162±3	5.82±0.02	1902	6.9±0.4	2408	47.1	37.6	7.4	2.1	11.4
22	2500	0	1600	2	7.45	21.73±0.01	131±2	4.84±0.01	958	5.2±0.2	5602	39.7	34.6	4.6	0.5	3.2

An estimated answer is transformed into a scale-free value called Desirability using the desirability function technique (Apandi *et al.* 2021). The desired response value may be minimised, maximised, or some combination of these. Many desirability functions can be utilised, depending on the objective. According to Equation (5.4), the overall desirability, D, is the geometric average of the distinct desirability functions for each response, di(yi).

$$D = \left(\prod_{i=1}^{n} d_i(y_i) \right)^{1/n} \tag{5.4}$$

where *n* is the number of responses

The range of D's numerical value is 0 (beyond the boundaries) to 1. (at the goal). The qualities of a goal can be altered by adjusting its priority or weight. A higher D rating is preferred. Tables 5.5a, 5.5b, and 5.5c contain a list of the desirable properties of each optimised solution. But, given the desirability rating, Table 5-5a, serial number 1, contains the suggested optimised solution. *Scenedesmus sp*. was cultivated in 3-L bubble column photobioreactors with a working volume of 2.5 L using this reaction setup.

Table 5.5a Optimised solutions and desirability

Number	Freshwater (mL)	Wastewater (mL)	Luminous Intensity (Lumens)	CO_2 gas (L/min)	pH	Alkalinity	Turbidity	EC	TDS	DO	COD	TN	NH_3-N	NO_3-N	TKN	PO_4^{3-}	Desirability	Remark
1	**1347.849**	**1152.151**	**1599.999**	**2.743**	**6.930**	**37.738**	**181.134**	**5.253**	**1289.222**	**6.020**	**1314.862**	**37.928**	**0.932**	**3.858**	**1.081**	**3.531**	**0.537**	**Selected**
2	1191.573	1308.427	517.901	2.000	6.902	49.048	193.637	4.840	1130.513	5.984	3456.760	35.396	1.094	4.113	0.673	3.304	0.536	
3	1191.592	1308.408	517.814	2.000	6.902	49.049	193.632	4.840	1130.362	5.984	3456.534	35.398	1.094	4.113	0.673	3.304	0.536	
4	1196.572	1303.428	530.124	2.000	6.903	48.886	194.391	4.840	1145.467	6.003	3478.483	35.292	1.074	4.117	0.697	3.289	0.536	
5	1182.643	1317.357	509.450	2.000	6.901	49.177	193.116	4.843	1125.016	5.971	3449.736	35.412	1.098	4.105	0.658	3.316	0.536	
6	1334.934	1165.066	1600.000	2.711	6.928	37.647	183.098	5.245	1248.970	6.039	1348.777	37.798	0.933	3.883	1.103	3.532	0.536	
7	1183.815	1316.185	498.149	2.000	6.901	49.311	192.420	4.840	1106.576	5.952	3421.247	35.583	1.129	4.108	0.638	3.335	0.536	
8	1345.504	1154.496	1600.000	2.694	6.930	37.640	184.214	5.245	1289.534	6.049	1347.177	37.402	0.908	3.852	1.116	3.533	0.536	
9	1348.296	1151.704	1594.879	2.748	6.930	37.807	180.661	5.251	1298.753	6.020	1323.059	38.009	0.938	3.865	1.092	3.580	0.534	
10	1335.779	1164.221	1600.000	2.593	6.928	37.426	191.204	5.228	1272.686	6.112	1424.522	36.396	0.864	3.851	1.201	3.546	0.532	
11	2500.000	0.000	1600.000	2.552	7.141	40.201	194.307	5.567	2220.680	6.139	637.806	23.314	0.336	2.238	1.242	3.555	0.525	
12	1013.071	1486.929	618.402	2.155	6.870	48.558	184.442	4.958	1401.083	6.020	3489.941	33.840	0.910	3.915	1.020	3.375	0.512	
13	1483.726	1016.274	1599.995	3.042	6.955	38.614	166.200	5.319	1836.581	5.868	1003.278	38.558	0.884	3.585	0.929	3.562	0.512	

Table 5.5b Optimised solutions and desirability

Number	Freshwater (mL)	Wastewater (mL)	Luminous Intensity (Lumens)	CO_2 gas (L/min)	pH	Alkalinity	Turbidity	EC	TDS	DO	COD	TN	NH_3-N	NO_3-N	TKN	PO_4^{3-}	Desirability	Remark
14	1562.795	937.205	440.004	2.000	6.969	48.784	188.850	4.611	766.621	5.855	2605.650	40.344	3.585	4.382	0.547	3.492	0.501	
15	476.812	2023.188	810.698	2.000	6.775	46.489	211.783	5.264	1469.376	6.373	3481.216	25.156	0.350	3.021	1.890	3.679	0.500	
16	513.030	1986.970	815.935	2.000	6.781	46.358	212.110	5.239	1450.455	6.379	3483.599	25.424	0.360	3.059	1.936	3.698	0.500	
17	383.338	2116.662	816.738	2.000	6.758	46.521	212.160	5.323	1495.445	6.379	3415.647	24.414	0.324	2.920	1.943	3.701	0.497	
18	1480.141	1019.859	1599.999	4.347	6.954	41.015	151.761	5.486	1528.273	5.666	874.564	46.449	0.751	3.930	0.825	4.364	0.476	
19	1487.904	1012.096	1600.000	4.595	6.956	41.486	156.637	5.517	1527.468	5.712	923.820	46.026	0.650	4.007	0.876	4.572	0.475	
20	1489.746	1010.254	1599.999	4.672	6.956	41.631	158.718	5.527	1526.055	5.731	946.518	45.782	0.620	4.036	0.898	4.634	0.474	
21	1503.693	996.307	1599.999	5.001	6.959	42.263	171.093	5.566	1543.194	5.844	1078.583	44.058	0.504	4.164	1.041	4.850	0.473	
22	1494.883	1005.117	1599.999	5.069	6.957	42.372	174.437	5.577	1512.544	5.874	1131.099	43.756	0.482	4.221	1.084	4.881	0.473	
23	1527.199	972.801	1600.000	5.156	6.963	42.589	179.244	5.579	1603.693	5.915	1149.451	42.779	0.458	4.205	1.150	4.912	0.471	
24	1545.062	954.938	1600.000	5.097	6.966	42.511	175.907	5.566	1665.771	5.886	1085.790	42.948	0.477	4.132	1.104	4.892	0.471	
25	1481.735	1018.265	1600.000	5.211	6.955	42.611	182.546	5.599	1469.619	5.942	1248.666	42.901	0.440	4.330	1.198	4.925	0.471	

Table 5.5c Optimised solutions and desirability

Number	Freshwater (mL)	Wastewater (mL)	Luminous Intensity (Lumens)	CO_2 gas (L/min)	pH	Alkalinity	Turbidity	EC	TDS	DO	COD	TN	NH_3-N	NO_3-N	TKN	PO_4^{3-}	Desirability	Remark
26	1517.314	982.686	1599.998	5.316	6.961	42.864	189.576	5.602	1564.263	5.998	1291.788	41.719	0.414	4.327	1.308	4.937	0.469	
27	176.681	2323.319	944.910	2.000	6.722	44.590	220.086	5.386	1479.765	6.497	2860.087	22.957	0.278	2.726	3.828	4.308	0.462	
28	1571.191	928.809	1599.999	5.405	6.971	43.118	196.394	5.592	1715.929	6.050	1315.239	40.554	0.397	4.298	1.429	4.932	0.462	
29	2500.000	0.000	1600.000	4.793	7.141	43.703	162.575	4.973	2196.092	5.767	261.970	33.052	3.639	2.566	0.940	4.723	0.460	
30	2218.453	281.547	440.002	6.000	7.089	53.211	213.094	5.156	698.770	6.429	1844.374	26.708	0.458	3.173	4.951	6.498	0.458	
31	2242.748	257.252	440.003	5.959	7.094	53.037	207.764	5.176	735.206	6.386	1710.270	26.956	0.452	3.133	5.393	6.816	0.455	
32	0.000	2500.000	788.607	2.000	6.691	47.550	210.414	5.640	1888.093	6.349	3369.354	21.959	0.248	2.591	1.715	3.603	0.445	
33	2378.409	121.591	1600.000	5.811	7.119	45.106	239.934	4.885	2043.425	6.336	1339.911	34.650	1.639	4.066	2.806	4.712	0.400	
34	0.000	2500.000	1393.644	5.846	6.691	45.247	238.008	5.196	1721.153	6.546	2359.900	28.670	0.587	3.671	4.703	7.153	0.350	
35	1495.980	1004.020	785.168	6.000	6.957	52.711	232.661	4.958	1442.294	6.735	2682.658	32.313	0.854	4.457	15.684	4.357	0.327	
36	0.000	2500.000	804.824	6.000	6.691	56.275	233.733	5.708	1894.473	6.745	947.958	23.136	0.249	2.699	16.512	4.389	0.298	
37	2453.223	46.777	484.057	4.089	7.133	48.922	122.295	4.904	1869.775	5.345	204.970	46.773	6.781	2.728	7.803	9.752	0.261	

Optimisation based on the design of experiments (DOE) is a methodology that has been effectively employed in solving engineering problems. Data presented in Table 5.6 were used to model the optimised set up for *Scenedesmus sp.* cultivation.

Table 5.6 Model terms

S/No	Term	Standard Error	VIF	R_i^2	Power
1	A	0.998825	9.103568	0.890153	0.194898
2	B	1.006109	8.224582	0.878413	0.194898
3	AB	3.82818	8.357909	0.880353	0.36044
4	AC	0.620559	1.960231	0.489856	0.238279
5	AD	0.550692	1.8996	0.473574	0.287801
6	BC	0.627064	1.783092	0.439176	0.234441
7	BD	0.557713	1.602737	0.376067	0.282041
8	ABC	2.711753	2.112885	0.526713	0.207977
9	ABD	2.508715	2.059642	0.514479	0.234374
10	ACD	0.739406	1.936306	0.483553	0.182802
11	BCD	0.748343	1.61005	0.378901	0.179639
12	ACÂ²	1.030512	4.73598	0.78885	0.320152
13	ADÂ²	0.968777	5.762971	0.826478	0.353483
14	BCÂ²	1.031939	4.210086	0.762475	0.319442
15	BDÂ²	0.951967	4.647285	0.784821	0.363517
16	ABCD	3.372148	2.102521	0.52438	0.151999
17	ABCÂ²	4.600754	5.002853	0.800114	0.2686
18	ABDÂ²	3.975475	5.074543	0.802938	0.339295

i = áµ¢Â

Standard errors should be similar to each other in a balanced design. Lower standard errors are better. VIF is the Variance Inflation Factor, which is a measure of the amount of multi-collinearity in a set of multiple regression variables. The ideal VIF value is 1.0. VIFs above 10 are cause for concern. VIFs above 100 are cause for alarm, indicating coefficients are poorly estimated due to multi-collinearity.

Ideal R_i^2 is 0.0. High R_i^2 means terms correlate with each other, possibly leading to poor models. For mixture designs, the proportions of components must sum to one. This is a constraint on the system and causes multi-collinearity to exist. This inflates the VIFs and the R_i^2, rendering these statistics useless. The Fraction of Design Space (FDS) statistics uses prediction-based metrics instead.

Power is inappropriate for determining the usefulness of a design involving a mixture of components. Figure 5.7 shows the optimised positions of the various factors.

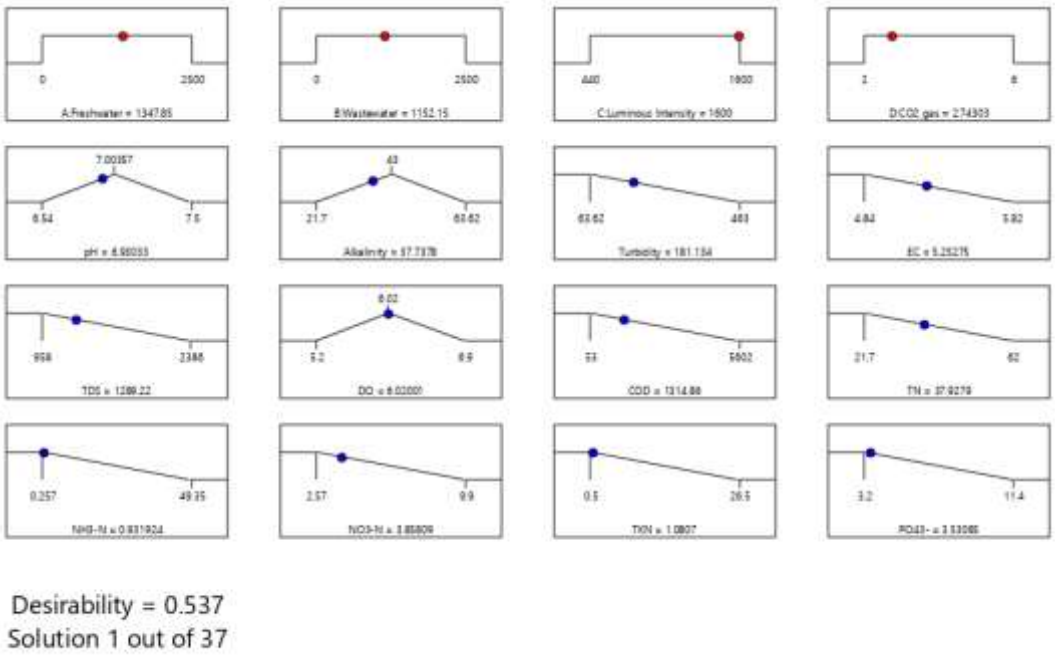

Figure 5.7 Optimised set-up for Scenedesmus sp. cultivation in BWW using 2.5-L working volume

5.4 Bubble-Column Photobioreactor Optimised Brewery Wastewater Microalgae Culture

To assess the accuracy of the optimised conditions, a control experiment was conducted using the reference water (RW). Furthermore, the wastewater discharged from the brewery was employed, wherein it was diluted with the RW. The specific

segment of the examination was designated as the "untreated" trial. The enhanced setup was designated as "Optimised" when compared to both the control and untreated experiments. The optimization of *Scenedesmus sp.* biomass output is seen in Figure 5.8.

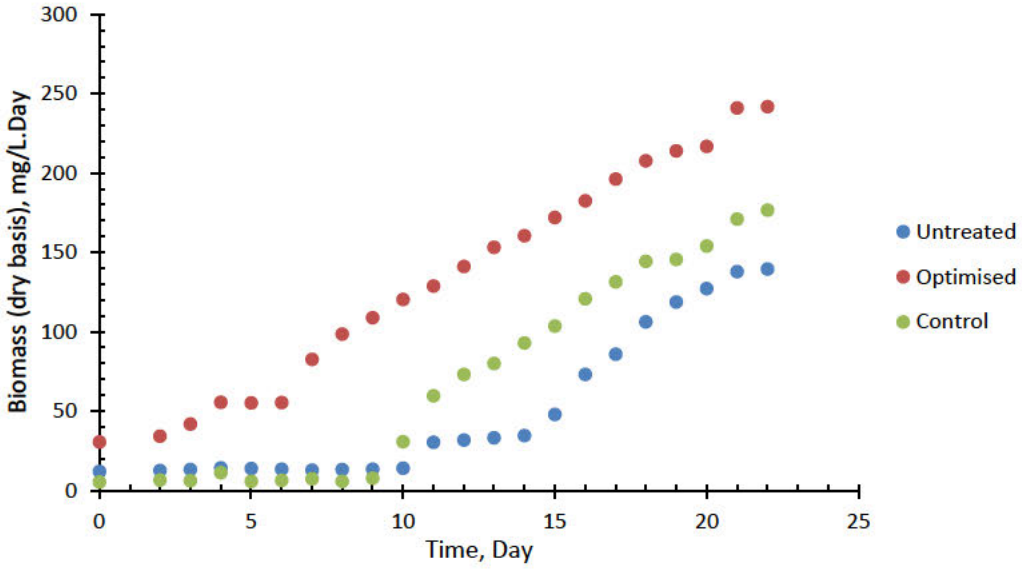

Figure 5.8 Biomass production (dry-basis) of the optimised, untreated and controlled Scenedesmus sp. cultivation conditions

In comparison to the untreated control, the optimised experimental run of the *Scenedesmus sp.* culture (Figure 5.8) exhibited a significant upward shift, suggesting that the derived and optimised conditions were conducive to the growth of *Scenedesmus sp.*

The primary determinant of microalgae development in vertical photobioreactors (PBRs) is the light utilization's restricted efficiency. Cellular proliferation is influenced by the amount and quality of light that reaches cellular structures, which is why light delivery is so crucial. Because of the mutual shadowing between cells, light penetration is noticeably reduced in high-cell-density cultures, where the cell density can reach 10^9 cells (Osman *et al.*, 2023).

5.5 The Kinetics of Nutrient Removal from Culture Media

The growth of microalgae is not influenced by the enlargement of individual microalgal cells but rather pertains to an augmentation in the number of microalgal cells. The process of microorganism growth initially entails an augmentation in cellular mass and ribosome count, followed by replication of the chromosome, production of the fresh cell wall and plasma membrane, segregation of the two chromosomes, construction of a septum, and ultimately, cellular division. The method of reproduction in which two genetically identical daughter cells are produced is referred to as binary fission. This asexual mechanism is responsible for the generation of offspring (Rolfe *et al.,* 2012).

The kinetic model accounts for four main microalgal development stages in the batch cultivation mode, namely the lag, exponential (log), stationary, and death phases. The updated Contois model (Schediwy *et al.,* 2019) gave the microalgal growth rate constant K_c that is represented in Equation (5.1).

$$K_c = \frac{C_A}{x}\left(\frac{\mu_{max}}{\mu} - 1\right) \tag{5.1}$$

This encompasses biomass growth and accumulation of the extractives including lipids, hydrocarbons and hydrocarbon derivatives.

Microalgae biomass is structured on a carbon backbone, and microalgal growth is thus premised on the fixing of carbon to the backbone. However, the mechanistic microalgal boom can be explained by the significant cell multiplication, with each cell acting as a bioreactor for multiple processes, which results in diverse incorporated extractive bio-products including, among others, lipids and hydrocarbons. The cultivation of microalgae in a given culture media exhibits responses to the dynamic

changes in the indicator nutrient substrates; and the highly diverse microalgae can be photoautotrophic, heterotrophic, or mixotrophic as they engage in cell multiplication. Microalgal bloom can be explained by significant cell multiplication: each cell acts as a bioreactor for multiple processes, resulting in diverse incorporation of extractive bio-products such as lipids, hydrocarbons, fatty acids, proteins, and carbohydrates.

5.5.1 The lag phase of microalgae cultivation

Following the introduction of microalgae cells into a newly prepared culture medium, the population experiences a temporary period of stability without any significant changes. Despite the absence of observable cell division, Rolfe *et al.* (2012) documented that the cells may undergo growth in terms of volume or mass, as well as engage in the synthesis of enzymes, proteins, RNA, and other molecules, thereby enhancing their metabolic activity. The cells are capable of adapting and acclimating to the given media and growth conditions, leading to the activation of various genes involved in metabolising distinct substrates. In addition to ongoing repair operations, the cell is engaged in the re-synthesis of damaged cell constituents in anticipation of binary fission. The duration of the lag phase is influenced by several factors, such as the initial size of the inoculum, the time needed for recovery from physical damage or shock during transfer, the synthesis time for essential coenzymes or division factors, and the synthesis time for new (inducible) enzymes required for metabolising the substrates in the medium. Additionally, the age of the inoculum, referring to a microbial population introduced into a culture medium to initiate growth, can also impact the lag phase. For instance, an older culture may contain a higher proportion of dead or aged cells, which could result in a longer adjustment period to the new medium.

5.5.2 Log (exponential) phase of microalgae cultivation

The exponential growth phase is characterised by a state of balanced growth, where cells undergo regular division through binary fission and experience geometric development in their overall growth. Cell division occurs at a consistent rate, which is contingent upon the specific composition of the growth medium and the incubation circumstances.

The duration of this phase is often of relatively brief duration within the context of the overall growth trajectory. Cells in this particular phase exhibit heightened metabolic activity and are particularly favoured for industrial applications, especially when there is a requirement for efficient production of a certain product. Cells that exhibit exponential growth are generally in a state of optimal health, making them highly appealing for investigations on their enzymes or other cellular constituents. The constancy of the generation time results in a linear relationship when growth during the logarithmic phase is represented on a logarithmic plot. The phenomenon of exponential growth in a batch culture is inherently limited and cannot be sustained indefinitely.

5.5.3 The stationary phase of biomass development

Over time, the exponential increase in population observed during the logarithmic phase gradually diminishes due to the exhaustion of available nutrients and the accumulation of waste products. The proliferation of microalgal cells achieves a state of equilibrium, commonly referred to as the stationary phase, wherein the rate of cell division is balanced by the rate of cell death. Consequently, there is a lack of total population increase. In less advantageous circumstances, Hamill *et al.* (2020) averred that there is an escalation in competition for nutrients, resulting in a decrease in cellular

metabolic activity. During this phase, spore-forming microorganisms undergo the process of endospore production, while pathogenic bacteria initiate the synthesis of virulence factors that aid their survival under adverse circumstances, hence leading to the onset of disease.

5.5.4 The death phase of microalgae biomass cultivation

The increasing scarcity of nutrients and accumulation of waste products contribute to a progressive escalation in the mortality rate of microalgal cells. During the death phase, there is an exponential drop in the number of living cells, accompanied by a significant decline in population increase. When cells undergo lysis or rupture, their internal contents are released into the surrounding environment, rendering these nutrients accessible to other microorganisms. This mechanism facilitates the survival of spore-producing microbes by ensuring their longevity until spore production occurs. The ability of spores to withstand adverse conditions during the death phase enables their subsequent transformation into viable bacteria upon exposure to a conducive environment for growth.

5.6 Thermodynamics of Biomass Production

The microalgal growth process is dependent upon the changes in free energy. The specific growth rate (μ) is related to the growth-limiting nutrient-substrate concentration (C_A) in the broth.

The Monod equation provides the lead to determining the specific growth rate of microalgae in terms of the nutrient substrate as given in Equation (5.2).

$$\mu = \mu_{max}\left(\frac{C_A}{K_A + C_A}\right) \tag{5.2}$$

where μ_{max} is the maximum growth rate; K_A is the half-saturation constant.

The microalgal growth thermodynamic equilibrium constant $K_A$whose value represents the position of the microalgal growth process is expressed in Equation (5.3).

$$K_A = e^{\frac{\Delta G}{RT}} \tag{5.3}$$

$$lnK_A = \frac{\Delta G}{R}\left(\frac{1}{T}\right) \tag{5.4}$$

This thermodynamic model was tested with data from this study (Figure 5.9). It gave a straight line passing through the origin with a slope of $\frac{\Delta G}{R}$.

The Monod equation is rewritten by solving for K_A : Equations (5.5), (5.6), and 5.7) seek to position the rearrangement of Equation (5.2) with feasible assumptions.

First, divide both sides by μ_{max} :

$$\frac{\mu}{\mu_{max}} = \frac{C_A}{K_A + C_A} \tag{5.5}$$

Then, solve for K_A:

$$K_A + C_A = \frac{C_A \mu_{max}}{\mu} \tag{5.6}$$

$$K_A = \frac{C_A \mu_{max}}{\mu} - C_A \tag{5.7}$$

Low substrate concentration approximation: If C_A is small compared to K_A, then $K_A + C_A \approx K_A$, leading to a simplified form.

Neglecting the -C_A term: If the substrate concentration C_A is relatively small or if the equation is approximated under conditions where $C_A \ll K_A$, the $-C_A$ term is often ignored, simplifying to:

$$K_A \approx \left(\frac{C_A}{\mu}\right)\mu_{max} \tag{5.8}$$

Thus, the key assumptions are:

(a) The substrate concentration C_A is relatively small.

(b) The term $-C_A$ is negligible compared to the other terms.

(c) Equation (5.8) is approximated in a regime where $C_A \ll K_A$.

Equation (5.8) enables the computation of K_A for every change in the nutrient concentration. From Equation (5.4), data was generated as defined in Equation (5.8) and tabulated in Table 5.7. These thermodynamic data were transformed into a plot in Figure 5.9, which pave the way for the determination of change in free energy, ΔG, a vital thermodynamic property that speaks to the growth response of organisms.

Table 5.7 Thermodynamic data for Scenedesmus sp. growth index for NO_3^- stimulus.

$C_A(\frac{mg}{L})$	$K_A = \frac{C_A}{\mu}(\mu_{max})$	lnK_A	T (°C)	$^1/_T$
2.69±0.03	3.6778±0.0121	1.3023±0.0112	22±1	0.0454±0.0011
2.24±0.02	54.3069±1.2131	3.9946±0.0213	23±1	0.0435±0.0010
1.87±0.02	7.5487±0.0252	2.0214±0.0132	24±1	0.0417±0.0009
1.33±0.01	2.3002±0.0213	0.8329±0.0023	25±1	0.0400±0.0008
0.38±0.01	0.6126±0.0032	-0.4900±0.0016	26±1	0.0385±0.0007

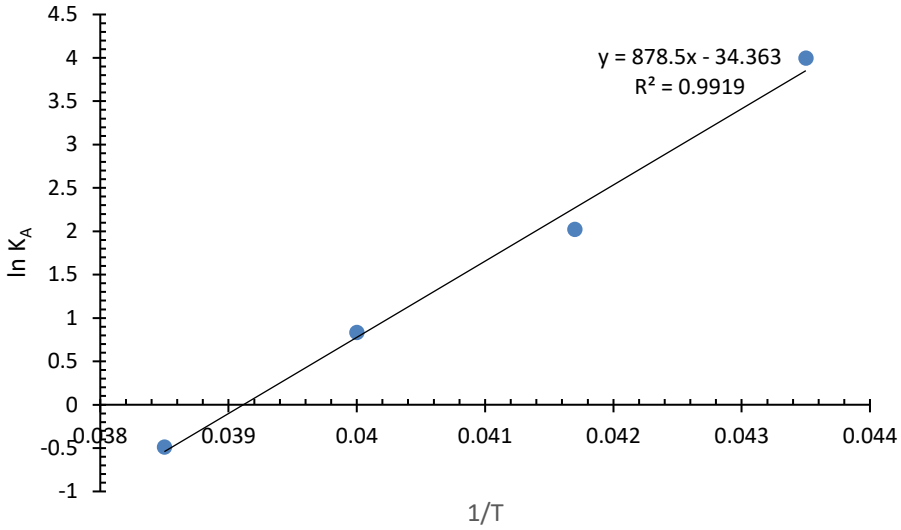

Figure 5.9 Thermodynamic Scenedesmus sp. growth index for nitrate substrate

From the plot in Figure 5.9, the regression line is given in Equation (5.9) with a coefficient R^2 of 0.9919.

$$y = 878.5x - 34.363 \tag{5.9}$$

This implies that

$$\frac{\Delta G}{R} = 878.5 \tag{5.10}$$

And

$$\Delta G = 878.5R = 878.5 * (8.314\ J\ mol^{-1}K^{-1}) = 7303.85\ J\ mol^{-1}K^{-1} \tag{5.11}$$

Or

$$\Delta G = 7.304\ kJ\ mol^{-1}K^{-1} \tag{5.12}$$

This indicates that *Scenedesmus sp.* would not spontaneously respond to the NO_3^- - growth stimulus unless other factors are involved.

5.8 Summary and Conclusion

5.8.1 Summary

To grow biomass for the 3-L bubble column photobioreactors, microalgae were raised at the nursery level using Erlenmeyer flasks and Scotch bottles. Using the Design of Experiment (DOE) to ascertain the number of experimental runs that might average sufficiently and the parameters that would generate the best yield of microalgal biomass under a scale-up scenario, the experiment was modelled using the statistical programme Design-Expert version 11. After that, the Response Surface Methodology (RSM) was utilised to enhance the growth conditions for microalgae using three-litre bubble column photobioreactors. We tracked the growth of microalgae using the lag phase, log (or exponential) phase, stationary phase, and death phase.

Several factors interacted to influence the development of *Scenedesmus sp.* in brewery wastewater. These variables, which include brightness, nutrients like nitrate and phosphate, organic carbon from the decaying brewery wastewater, and carbon sources like CO_2 all work together to exert an influence on these aspects. The initial size of the inoculum, the amount of time required for recovery from physical damage or shock during transfer, the synthesis time for division factors or essential coenzymes, and the synthesis time for new (inducible) enzymes needed for metabolising the substrates in the medium are some of the factors that affect how long the lag phase lasts. In this experiment, the lag phase varied from 4 to 8 days.

In relation to the overall growth trajectory, the log phase's duration is frequently somewhat short. This phase of the cell development has increased metabolic activity and is extremely useful for industrial applications, especially when efficient synthesis of a specific product is required. There is no overall population growth during the

stationary period since the rate of cell division and death are equal. In this stage, bacteria that cause disease begin to synthesise virulence factors, which help them survive in unfavourable conditions. Spore-forming microorganisms go through the process of producing endospores during this time.

The growth of *Scenedesmus sp.* in brewery wastewater was shown to be driven by free energy to the extent that $\Delta G = 7.304$ kJ mol^{-1} K^{-1}, indicating that it is not spontaneous, according to the thermodynamic model. Microalgal growth requires the application of certain growth stimulants or ingredients to be sustainable.

5.8.2 Conclusion

The microalga *Scenedesmus sp.* was successfully cultivated in brewery wastewater. From the table-top Scotch bottle and Erlenmeyer culture, biomass was developed to the extent of feeding the 3-L bubble column reactor with the seed microalgae, which in turn supplied the feed to the 30-L bubble column reactor. The microalgae broth in the 30-L reactor suffered performance (Table E-1) due to poor luminance due to the wide diameter poor lighting arrangement . However, cell growth was significant to feed the 240-L airlift-raceway bioreactor (Table F-1).

CHAPTER 6

Hydrocarbons and Lipid Profiling of *Scenedesmus sp.* Grown in Brewery Wastewater Using a Novel Airlift-raceway Photobioreactor

6.1 Background

The present chapter provides a detailed account of the cultivation of microalgal biomass within an innovative airlift-raceway photobioreactor. The monitoring system observed the flow regime of the broth within the airlift-raceway bioreactor, as well as the rate at which CO_2 was introduced through sparging. The chapter additionally emphasizes the accumulation of hydrocarbons and hydrocarbon derivatives within the biomass of *Scenedesmus sp.*, as well as the subsequent extraction of bio-oil that is rich in these compounds. This chapter includes reports on the Gas Chromatography-Mass Spectroscopy (GC-MS) investigations conducted on the microalgal bio-oil, as well as the Scanning Electron Microscopy (SEM) analysis performed on the biomass.

6.2 Airlift-Raceway Photobioreactor

The airlift-raceway bioreactor is an integrated arrangement of two reactor systems (airlift and raceway) to form a single hybrid reactor whose flow regime is controlled by a pneumatic fluid flow, which is initiated by gas sparging. Investigation of microalgae growth in the novel airlift-raceway reactor was carried out at a culture flow velocity of 10 cms^{-1} under continuous illumination provided by fluorescent lights. The average light intensity at the free surface of the raceway was 4000 lux. The culture broth volume was 240 L and the air flow rate to the riser column was 600 mL/min.

During these tests, carbon dioxide gas was supplemented with nitrogen gas and the pH was measured every 24 hours using standard pH probes.

6.3. The Novel Airlift-Raceway Photobioreactor Configuration

A schematic diagram of the airlift-raceway photobioreactor is shown in Figure 6.1. The external-loop airlift system was fabricated out of borosilicate glass pipe sections ps100/500 piping (100 mm inner diameter) using perspex connectors 100/75 fitted with DN 100 piping gasket. Two risers and two downcomers were positioned to enhance the adequate flow regime in the hybrid reactor. The raceway section was constructed using a 15 mm PVC sheet as the floor; while transparent 6 mm PVC sheets were used to construct the walls 200 mm high, 1500 mm long and 700 mm wide.

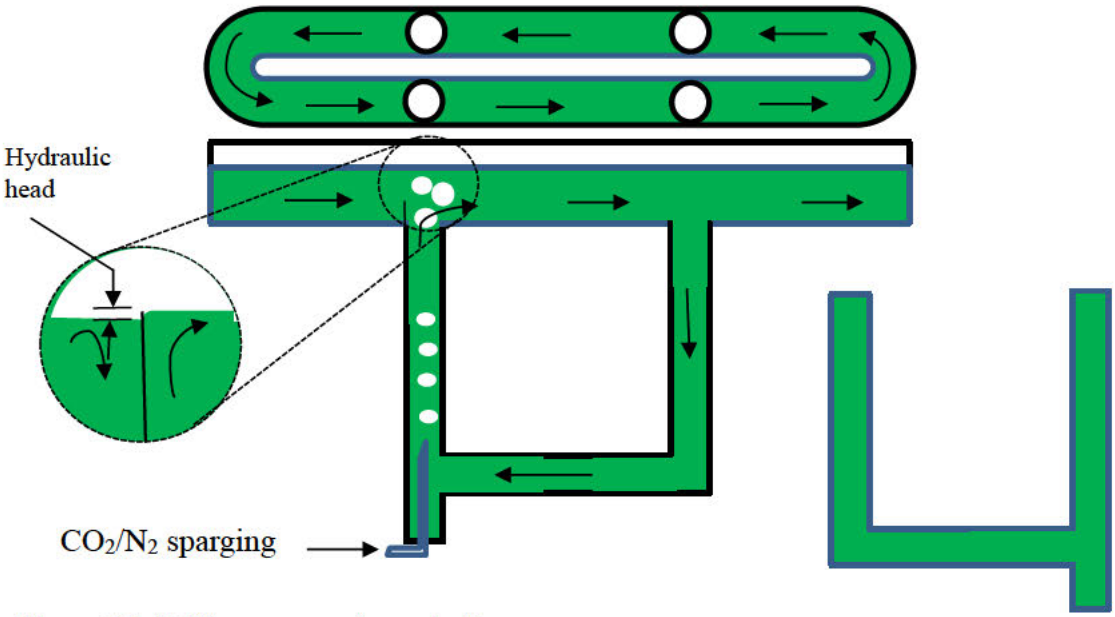

Figure 6.1 Airlift-raceway schematic diagram

The sparger is located at the bottom of the riser to create fine N_2/CO_2 gas bubbles causing the density of the gas-broth mixture on the riser side to be less than that in the down-comer. The difference in the broth density creates a hydraulic head at the top of the riser, driving the fluid flow around the raceway.

Figure 6.2 is the schematic diagram of the sparger, which was constructed and fitted to the riser-end of the airlift-raceway photobioreactor.

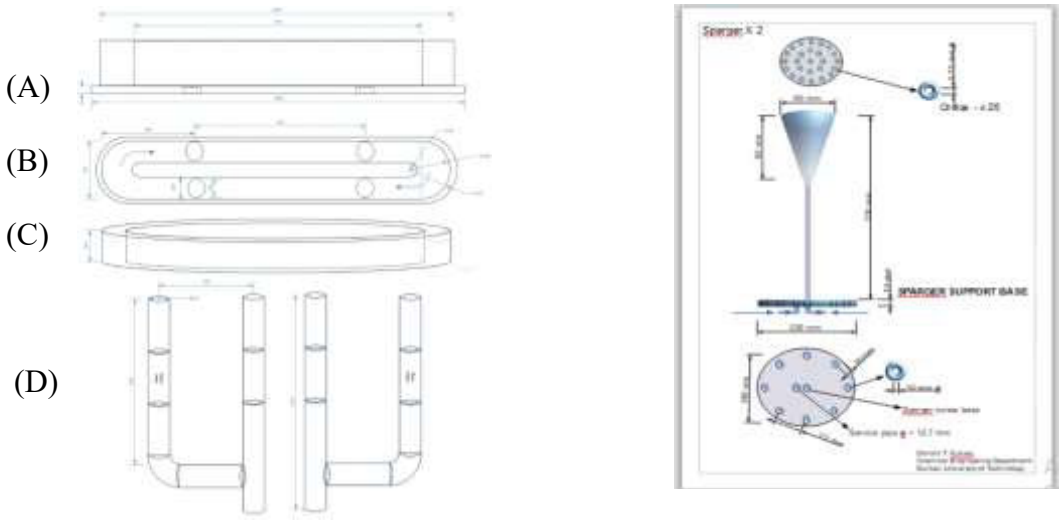

Figure 6.2 Airlift-raceway graphics with sparger: (i) Airlift-raceway (A = sectional view of the raceway tank; B = aerial view of the raceway tank; C = side view of the raceway tank; D = airlift external loop configuration (ii) Sparger

By the design of the airlift-raceway photobioreactor, two spargers were used, each of which has a shower-type orifice arrangement with twenty-five 3.5 mm diameter orifices. This was aimed at enhancing effective CO_2 gas distribution, and pH control for microalgae biomass production and mass transfer.

(a)

(b)

(c)

(d)

Figure 6.3 Novel airlift-raceway photobioreactor assemblage: (a) Sparger inspection (b) Raceway tank inspection (c) airlift-raceway assembly (d) Complete airlift-raceway ready to run.

Adding gases to the airlift and bubble column reactors is one of the expenses associated with cultivating microalgal cultures. These gases are necessary to start the broth's

pneumatic flow through the reactor. Aquaculture currently uses airlift photobioreactors and bubble column photobioreactors to produce microalgae (Merchuk *et al.* 2019).

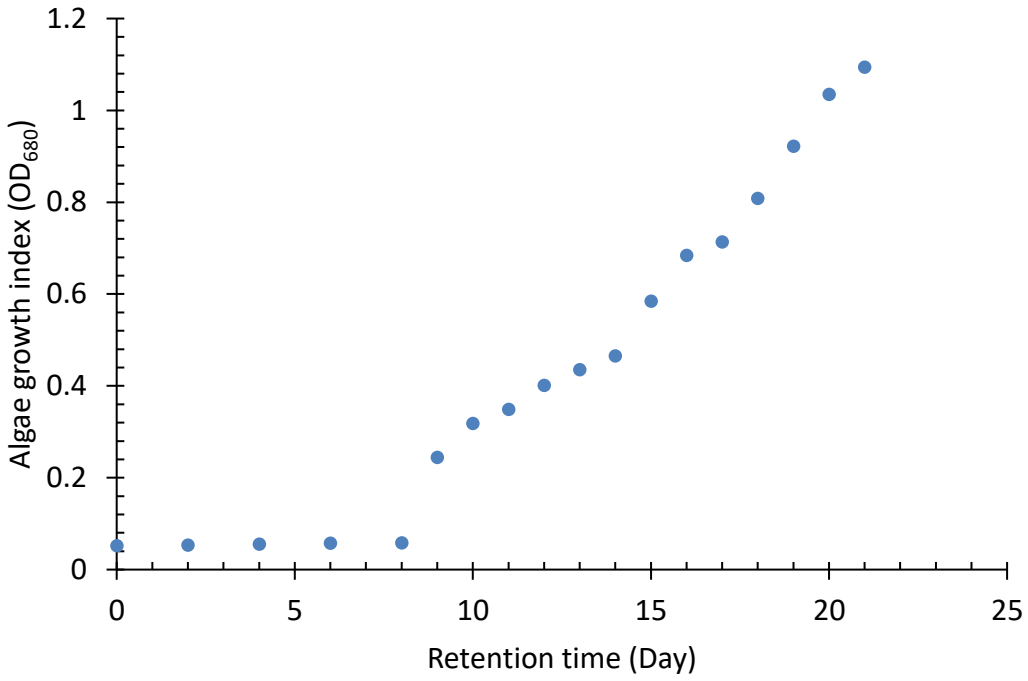

Figure 6.4 Microalgal growth index in BWW using 240-L airlift-raceway photobioreactor

For continuous microalgal generation, a photobioreactor system with an external loop airlift and swirl flow was reported. A series of modules, each made up of two vertically connected columns (a riser column and a downcomer column), make up this system. Utilising a capillary sparger, this method produced a swirling motion that reduced cell adhesion to the wall, emulating the previously mentioned helical flow promoter in an airlift reactor. This modular design made operation simple and long-term; a 120-L version was used in a commercial hatchery to produce microalgae. Certain bubble column photobioreactors use two spargers or a rubber membrane diffuser to enhance the mass transfer of gases, removing O_2 and providing CO_2. This is because of the high mass transfer, low energy costs, and extremely minimal physical stress.

Compared to conventional sparging, the efficiency of CO_2 transfer increased fivefold in the case of dual sparging. However, it also seems that bubble size is important for reducing shear damage to cells. Because of light scattering, bubbles created by sparging Scenedesmus sp. seemed to boost light penetration into a culture by as much as 20 %. Thus, it makes sense to assess how bubbles affect each type of algae being cultivated in air-sparged reactors. Considerations of shear sensitivity limit the aeration rate. Because the effects of hydrodynamic stress on various microalgal species vary, there is an upper limit to the tolerable level of turbulence. In bubble columns and airlift reactors, increasing the aeration rate generally results in increased mixing, liquid circulation, and gas-liquid mass transfer. High surface gas velocities in photobioreactors enhance mixing and gas-liquid mass transfer, facilitating efficient CO_2 utilization and preventing oxygen accumulation. However, elevated aeration rates can also increase shear stress, adversely affecting certain microalgae species. (Michiel *et al.,* 2010). A study investigated the impact of shear stress on the marine microalga *Chaetoceros muelleri* by applying varying shear rates and medium viscosities . The findings revealed that shear stress levels between 1 and 1.3 pascals (Pa) significantly reduced cell viability, dropping to 52–66% beyond this threshold. Notably, the primary detrimental effects occurred within the first minute of exposure, with minor additional impacts up to eight minutes (Michels *et al.,* 2016).

In photobioreactor operations, achieving optimal mixing and gas exchange must be balanced against the shear sensitivity of the cultivated microalgae species. For instance, while *Tetraselmis suecica* can tolerate shear stresses up to 80 Pa, species like *Isochrysis galbana*, *Skeletonema costatum*, and *Chaetoceros muelleri* exhibit growth inhibition or cell damage at much lower shear stress levels (Michels *et al.*, 2010; Wang and Lan, 2018).

Therefore, when increasing surface gas velocities to improve mass transfer, it's crucial to consider the specific shear tolerance of the microalgae species in use. Adjusting aeration rates and employing reactor designs that minimize shear stress can help mitigate adverse effects, ensuring both efficient gas exchange and the viability of sensitive microalgal cultures.

Shear stress was seen to be relatively consistent and significantly lower in the downcomer, although it varied with the radius of the culture column in the airlift and increased with the surface gas velocity in the riser. The airlift bioreactor's top and bottom sections were also found to have high shear stress, and adjusting the clearance in these areas significantly changed the flow structure and shear stress. These modifications could have a substantial impact on the performance of airlift-raceway bioreactors, especially when stress-sensitive microalgae are involved.

For the cultivation of microalgae, vertical column photobioreactors, particularly the airlift photobioreactor, offer some benefits. These include the absence of moving parts, low power consumption, high mass transfer rate, good solids suspension, homogeneous shear, quick mixing, and the requirement for less land due to the vertical orientation. One potential issue with scaling up these bioreactors, though, is that light penetration into the reactor diminishes exponentially with increasing distance from the light source. There are restrictions on expanding the column's diameter, just like with tubular reactors.

6.4 Variation of Biomass Production with Sparger Orifice Size

The size of the sparger orifice plays a crucial role in microalgae biomass production as it directly affects CO_2 mass transfer, mixing efficiency, and bubble size distribution in photobioreactors. A comprehensive review by Tan *et al.*, (2020) discussed various

photobioreactor designs, including vertical column bioreactors that utilize spargers to introduce air bubbles. The review highlighted that the size of these bubbles, influenced by the sparger's orifice size, played a critical role in homogenising the culture and facilitating gas exchange, thereby impacting microalgae growth rates. Granata (2017) statistically analysed 317 photobioreactor studies equipped with dual spargers: one with single orifice spargers producing large bubbles for mixing, and another with a perforated membrane sparger generating smaller bubbles for efficient CO_2 mass transfer.

6.4.1 Effects of small orifice size on biomass production

Small orifice size produces finer bubbles, increasing the gas-liquid interfacial area and improving CO_2 dissolution into the culture medium. This can enhance microalgae growth, provided that CO_2 levels do not become excessive, leading to acidification. Smaller orifices lead to a more uniform bubble distribution and better turbulence, improving light exposure by reducing cell sedimentation. This can enhance photosynthetic efficiency. Smaller orifices generate high bubble shear forces, which can damage fragile microalgae species. However, some strains tolerate this well and benefit from increased CO_2 availability (Holdt *et al.*, 2014).

6.4.2 Effects of large orifice size on biomass production

Large orifice size generates larger bubbles, reducing the gas-liquid interfacial area and potentially leading to lower CO_2 utilization efficiency. However, it may prevent CO_2 oversaturation and excessive acidification. Larger orifices result in larger bubbles that rise quickly, leading to poor mixing and potential CO_2 stratification, which can create localized CO_2 depletion zones. Larger orifices produce lower shear forces, making

them more suitable for shear-sensitive strains but potentially leading to lower CO_2 transfer efficiency (Holdt *et al.*, 2014).

6.4.3 Biomass productivity trends

There is an ideal orifice size range where CO_2 dissolution is maximised without excessive shear stress or acidification, leading to peak biomass productivity. Optimising the sparger orifice size is crucial for maximising microalgae biomass production. Figure 6.5 shows the performance of five different orifice sizes (1.5 mm, 2.5 mm, 3.5 mm, 4.5 mm and 6.0 mm) concerning microalgae biomass productivity. In this study, a reference study was carried out, without sparging, for microalgae biomass production.

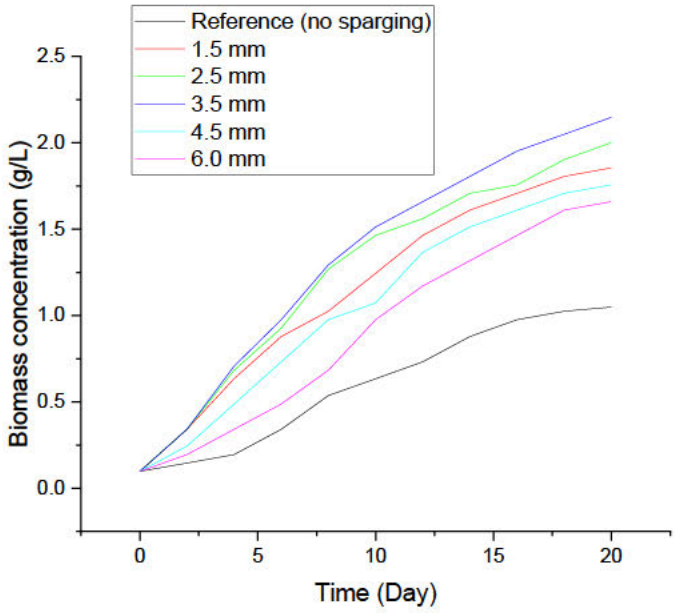

Figure 6.5 Microalgal biomass concentration with sparging orifice size

Where there was no sparging was used as a reference experimental run. Vertical microalgae growth displacement was used to assess the performance of biomass

concentration. Consequently, sparger orifice performance in this study can be graded as: 3.5 mm > 2.5 mm > 1.5 mm > 4.5 mm > 6.0 mm. This implies that the sparger orifice of 3.5 mm diameter, as shown in Figure 6.5, gave the most biomass concentration.

6.4.4 Strategies for Optimization

Using multiple small orifices instead of one large orifice to create finer bubbles and improve gas distribution. Adjusting gas flow rates in conjunction with sparger size to avoid excessive turbulence. Implementing oscillating spargers or diffusers that vary bubble size dynamically based on real-time CO_2 demand.

For maximizing algal biomass production, sparger orifice size should be optimized based on the reactor type and algae strain. Table 6.1 shows the recommended sparger orifice size based on the type of reactor. The expected effect is also presented.

Table 6.1 Sparger orifice size based on reactor type and the expected effect

Photobioreactor Type	Recommended Orifice Size (mm)	Expected Effect
Airlift Photobioreactor	0.5–1	Good CO_2 utilization, moderate turbulence
Bubble Column	0.5–1.5	Enhanced mass transfer, reduced shear stress
Raceway Pond	>2	Requires additional mixing to compensate for poor dispersion
Stirred-Tank	1–2	Moderate mixing, avoids excessive turbulence

The variation of algal biomass production with sparger orifice size follows a nonlinear trend, where intermediate-sized orifices (0.5–1 mm) generally yield the highest

biomass productivity. This is due to the balance between CO_2 mass transfer, mixing efficiency, shear stress, and light penetration. Fine bubbles (0.5–1 mm) optimize CO_2 dissolution and biomass growth. Coarse bubbles (>2 mm) may lead to CO_2 loss, poor distribution, and excessive turbulence. Too-small bubbles (<0.2 mm) can cause foam formation and mechanical stress. Thus, sparger design should be carefully tailored based on bioreactor type, microalgae species, and process goals to ensure maximum efficiency in algal biomass production.

Biomass availability and supply are geographically spread, but there is a limit to the supply. Integrating process steps leads to the most effective use of the available biomass for the production of food, non-food and energy resources (Velichkova *et al.,* 2016). Furthermore, integration is essential to maximise economic potential and to simultaneously minimise the environmental impacts. Integration should be done on several levels: (1) using the interactions between resource supply, algae growth and processing in the process chain design, (2) combining the processing of biomass to several products, and (3) considering various performance indices.

6.5 The Microalgae Biomass Production Using Airlift-Raceway Photobioreactor

Figure 6.3 shows the photobioreactor used to produce microalgae biomass. This research's innovative design served as the foundation for building the photobioreactor. With a 220 L total working space, the vertical photobioreactor was conceived and built utilising clear acrylic materials. After degreasing, the airlift-raceway photobioreactor's surface with liquid detergent, three tap water washes were conducted. There was one more rinse with reference water (RW).

The airlift-raceway photobioreactor was filled with 120 L of the RW, followed by 80 L of BWW and 20 L of the *Scenedesmus sp.* seed-broth, resulting in an initial optical density of 0.052 and microalga cell density of 8.9×10^6 mL^{-1}. The photobioreactors were placed indoors at an average temperature of 23.4±2.1 ºC. Harvesting took place after 22 days of allowing the microalgae, *Scenedesmus sp*., and microalgae consortium to grow.

Using Design-Expert version 11 software, the effects of independent variables (BWW concentrations and aeration rate) on dependent variables (biomass productivity and growth rate) of *Scenedesmus sp*. were evaluated. RSM was utilised to build a geometrical model for factor prediction, which allowed for the independent assessment of each factor and its interaction within the proposed model. The extremely substantial statistical analysis that RSM provided demonstrated this. Equation (6.1) shows how a second-order model in the form of a quadratic polynomial equation fits the experimental result as a function of the independent process variables.

$$y = \beta_o + \sum_{i=1}^{k} \beta_i x_i + \sum_{i=1}^{k} \beta_{ii} x_i^2 + \sum_{i \neq j} \sum \beta_{ij}\, x_i x_j + \varepsilon \qquad (6.1)$$

In this equation, *y* is the predicted response for the reduction percentage β0, βi, βii and βij represent the regression coefficients, x_i is the coded variable, and x_j is the independent variable in coded form, while k is the number of n dependent variables. The relationship between the natural variable ε_i and coded variable x_i is:

$$x_i = \frac{\varepsilon_i - \frac{[V_{max} - V_{min}]}{2}}{\frac{[V_{max} - V_{min}]}{2}} \qquad (6.2)$$

Vmax and Vmin are the maximum and minimum values of the independent variables, respectively, in Equation 6.2. The labels -1, 0 and +1 denoted the minimum,

intermediate and maximum values of each variable, respectively. Table 6.2 lists the independent variables' levels and ranges.

Table 6.2 Experimental factors and their levels set up for microalgal growth

Independent Variable	Symbol	Levels		
		-1 (Minimum)	0 (Medium)	+1 (Maximum)
Brewery Wastewater (L)	BWW	0	1250	2500
CO_2 gas flow rate (L/min)	F_{CO2}	2.00	4.00	6.00

To investigate the linear and quadratic model of independent variables and determine the relationship between the variables coded in Equation 6.3, where x_i is the coded and real value, x_o is the real value at the centre point of the investigated area, and δ is the value of step change, experimental runs were conducted with BWW concentrations (10 % to 75 %) and an average carbon dioxide flow rate of (0.02 L/min to 4.0 L/min).

$$x_i = \frac{x_i - x_0}{\delta x} \tag{6.3}$$

Table 6.2, which displays the experimental design and findings, provides the response in terms of biomass productivity and maximum growth rate at each of the 22 experimental runs. A hemocytometer was used to determine the concentration of Scenedesmus sp. grown in the airlift-raceway photobioreactor. On the other hand, the productivity of microalgae biomass was assessed using the DR-3900 UV-Vis Spectrophotometer (Hach-USA) to measure the OD680 (optical density of microalgae culture at 680 nm) every 24 hours. We used the linear equations (6.4) and (6.5) to estimate the connection between the concentrations of dry biomass and the optical density.

Biomass concentration (dry weight) $\left(\frac{mg}{L}\right)$ = 456.8 (OD_{680}) + 278.02 (6.4)

The biomass productivity $\left(\frac{\frac{mg}{L}}{day}\right)$ was calculated using Equation (6.5).

$$\text{Biomass Productivity } P_{max} = \frac{x_2 - x_1}{t_x - t_0} \quad (6.5)$$

where x_1 is the starting biomass concentration at t_o (day), and x_2 is the biomass concentration in mg/L after the culture phase (t_x). Equation (6.6) provided the particular growth rate (μ_{max}).

$$\mu_{max} = \frac{lnN_2 - lnN_1}{t_2 - t_1} \quad (6.6)$$

where N_1 and N_2 represent, respectively, the concentrations of microalgae cells at the start (t_1) and finish (t_2) of the exponential development phase.

6.6 Lipid Extraction and Fatty Acid Composition Analysis

We used a chloroform:methanol (2:1) solvent mixture for lipid extraction and quantification, following the methodology of Zielinsky *et al*. (2023). Equations (6.7) and (6.8) were used to compute the lipid productivity (P_L, mgL^{-1} day^{-1}) and the lipid content (C_L, % mass fraction).

$$C_L = \frac{W_L}{W_B} \quad (6.7)$$

where W_L and W_B stand for the weights of the biomass of lyophilized algae and extracted lipids, respectively.

$$P_L = \frac{C_L}{t} \quad (6.8)$$

where t is the run's duration and C_L is the lipid concentration at the end of the batch run. The process of transforming crude lipid extracts into fatty acid methyl esters allowed for the determination of the fatty acid composition of the microalgal biomass. Table 6.3 displays the relative percentage content of the fatty acids.

One of the significant concerns of microalgal biomass harvesting is to use it as feedstock for the production of value products. The fatty acid profile of microalgae oil is depicted in Table 6.3. The content of various fatty acids of microalgal lipids ranged from C_{12}-C_{20}. The Palmitic acid ($C_{16:0}$) was the most abundant (24.54±2.1 %) fatty acid, followed by oleic acid ($C_{18:1}$) and linolenic acid ($C_{18:3}$) with weight per cent of 16.21±1.1 % and 12.32±1.3 %, respectively. While the other fatty acids, such as stearic acid ($_{C18:0}$), linoleic acid ($C_{18:2}$), palmitoleic acid ($C_{16:1}$), and myristic acid ($C_{14:0}$), were less than 12 % of total fatty acids. Simultaneously, arachidic acid ($C_{20:0}$) was the least abundant, accounting for 0.98 ± 0.58 % of total fatty acid. Various biofuel properties such as oxidative properties, cold flow properties, and cetane number solely depend on the chain length and degree of unsaturation of the biofuel constituents. Biodiesel with a higher amount of monounsaturated fatty acid (MUFA) and higher chain length have better oxidative stability, while polyunsaturated fatty acids (PUFA) content enhances the cold flow properties.

However, the content of monounsaturated (18.55 %), polyunsaturated (22.74 %), as well as saturated fatty acid (35.15 %) corroborates the compatibility towards biodiesel production as these fatty acids have better stability to fluidity and oxidation properties of biodiesel (Kukwa and Chetty, 2022). Moreover, the high content of oleic acid is the most favoured quality of biodiesel as it provides a better balance between cold flow properties and the stability of oxidation. Moreover, several polyunsaturated fatty acids like linolenic acid linoleic acids are essential omega fatty acids, a vital dietary supplement for humans and animals. Hence, the present study reflects that the *Scenedesmus sp.* biomass has the potential as a promising nutrient supplement resource and feedstock for biodiesel production.

Table 6.3 Fatty acid composition of microalgae oil.

Variable	Composition (% w/w)	
	Scenedesmus sp.	Microalgae consortium
Myristic (Tetradecanoic) acid (C14:0)	1.36±1.71	0.22±0.03
Palmitic (Hexadecanoic) acid (C16:0)	24.54±2.11	0.29±0.07
Palmitoleic (cis-9-Hexadecenoic) acid (C16:1)	2.34±0.21	ND
Stearic (Octadecanoic) acid (C18:0)	8.27±0.57	ND
Oleic (cis-9-Octadecenoic) acid (C18:1)	16.21±1.12	0.06±0.01
Linoleic (cis,cis-9,12-Octadecadienoic) acid (C18:2)	10.42±1.15	ND
Linolenic (alpha-Linolenic) acid (C18:3)	12.32±1.31	ND
Arachidic (Eicosanoic) acid (20:0)	0.98±0.58	0.06±0.01
Dodecanoic (Lauric) acid (C12:0)	ND	0.04±0.01
Pentadecanoic (Pentadecylic) acid (C15:0)	ND	0.04±0.01
Heptadecanoic acid (C17:0)	ND	6.10±0.34
Docosanoic (Behenic) acid (C22:0)	ND	0.19±0.07
9-Octadecanoic (Ricinoleic) acid (C18:0)	ND	0.81±0.13
22-Tricosenoic acid (C23:0)	ND	0.81±0.11
Trans-13-Octadecenoic acid (C18:1)	ND	0.81±0.12
Tridecanoic acid (C13:0)	ND	1.55±0.16

ND = Not detected.

Table 6.4 Physicochemical properties of microalgae oil

Variable	Value as defined		Reference
	Scenedesmus sp.	Microalgae consortium	
Density (g/cm^3)	0.87±0.03	0.88±0.04	This work
Percentage yield (%)	5.49±1.02	3.45±0.06	This work
Free fatty acid (%)	0.85±0.12	4.79±1.08	This work
Acid value (mg KOH/g)	2.47±0.22	9.58±1.21	This work
Iodine value (g I_2/100 g)	108.15±1.31	81.22±1.42	This work
Saponification value (mg KOH/g)	203.16±2.01	213.18±2.03	This work

6.6.1 Density of microalgae oil

The density of the microalgal oil falls within the standard range of 0.85-0.9 g/cm^3 at room temperature, as commonly observed in most oils. The observed density of 0.87±0.03 g/cm^3 for *Scenedesmus sp.* and 0.88±0.04 g/cm^3 for the microalgae consortium are consistent with the findings of Ejim and Kamem (2013), who reported a density of 0.893 g/cm^3, and Konga *et al*. (2016), who reported a density of 0.864 g/cm^3. Given that oils with higher density have a larger energy content, the utilization of oil as a biofuel is justified based on its ability to meet the energy requirements. The density of oils is subject to multiple parameters, such as their composition of fatty acids, presence of minor components, species of microalgae, extraction method, and temperature (Elgharbawy *et al*., 2021).

Udayan *et al.*, (2022) explored lipid production capabilities of various microalgae species and reported that microalgae oils rich in polyunsaturated fatty acids (PUFAs)

tend to have lower densities compared to oils with more saturated fats. The presence of docosahexaenoic acid (DHA) and eicosapentaenoic acid (EPA), commonly found in microalgae, can influence the oil's density. Oils extracted using solvent-based methods, such as hexane or supercritical CO_2, may retain different levels of impurities, slightly affecting density. Crude microalgae oil might have a slightly higher density due to residual biomass or moisture. Like most oils, microalgae oil becomes less dense at higher temperatures due to thermal expansion. In comparison with other oil sources, olive oil has a density range of 0.91-0.92 g/mL, soybean oil has a density of about 0.91 g/mL, petroleum diesel has a density of about 0.85 g/mL, and biodiesel has a density ranging from about 0.86 g/mL to 0.90 g/mL (Xue *et al.*, 2020).

6.6.2 Percentage of oil yield

A total of 90.5 grams of algal biomass was employed in the extraction process, yielding 4.97 grams of microalgae oil from *Scenedesmus sp.* In contrast, the identical quantity of biomass yielded 3.12 grams of microalgae oil from the microalgae consortium as presented in Table 6.4. Consequently, the determined percentage yield of algal oil was observed to be 5.49% and 3.45% for *Scenedesmus sp.* and the consortium of algae, respectively. The efficiency of biofuel production is adversely affected by the limited oil output generated by the consortium of algae. The presented situation bears resemblance to the phenomenon of algae strains within a consortium that have a reduced ability to produce oil. Therefore, it is essential to cultivate specific strains of algae that can produce a greater amount of lipids (Adeniyi *et al*., 2018). The transition from biomass growth to lipid accumulation can be enhanced by optimization (D'Mello & Chemburkar, 2018).

6.6.3 Acid value of microalgae oil

The acid value of *Scenedesmus sp*. oil is recorded as 2.47, while the consortium of microalgae oil has an acid value of 9.58, presented in Table 6.4. This demonstrates the comparative impact of solvent extraction versus mechanical extraction on the acid content of microalgal oil since the solvent extraction process has resulted in a reduction of acidity. The acid values presented in this study indicate the degree to which the constituent glycerides can undergo decomposition as a result of lipase activity.

The measurement provided pertains to the estimation of the content of free fatty acids within the microalgae oils. Triglycerides are a prevalent form in which fatty acids are typically found. The hydrolysis process involves the cleavage of ester bonds found in fatty acids, leading to the production of free fatty acids (FFA) (Aremu *et al.,* 2015). The measurement in question is a comparative assessment of the degree of rancidity, as free fatty acids (FFA) are often generated during the degradation process of triglycerides. The acid values of 2.47 and 9.58 mg KOH/g observed in this study are comparatively higher than the acid values reported by Su *et al.* (2022) (1.9 mg KOH/g) and Oluogun *et al*. (2021) (0.59 mg KOH/g). As previously mentioned, the elevated acidity of the wastewater utilized throughout the cultivation phase can facilitate the generation of organic acids, which can have a collective influence on the resultant oil. The higher acid readings in this case indicate that the oil is unstable, which leads to the production of free fatty acids. This condition is deemed unfavourable for the manufacture of biofuels. According to Sakthivela *et al*. (2018), the utilization of these oils in an untreated state can lead to severe corrosion in an engine's fuel tanks and supply lines.

6.6.4 Free fatty acids (FFA) in microalgae oil

The term "free fatty acid" pertains to fatty acids that are not esterified and can exist in a complex state with proteins or membranes, or a free state within a solution. The quantification is denoted as a weight percentage, of a certain fatty acid. The formation of these substances occurs through the process of hydrolysing oils and fats. The aforementioned observation provides empirical support for the presence and extent of hydrolysis assisted by lipolytic enzymes and oxidation, as documented by Aremu *et al.* (2015). The presence of a high free fatty acid (FFA) content in the feedstock leads to catalyst consumption during the transesterification process. The recorded FFA values of 0.85 % and 4.79 % exhibit a significant level of elevation, rendering both the *Scenedesmus sp.* and the consortium of algae oils unsuitable for direct implementation in the synthesis of biofuels (Su *et al.* 2022). Because of the need for a catalyst, earlier research by Elgharbawy *et al*. (2021) has shown that oils with free fatty acid concentrations higher than 1% cannot perform a direct base-catalysed transesterification reaction for the synthesis of biofuel. Free fatty acid (FFA) reduction in crude oil can be accomplished in many ways. One method is to treat the crude oil with an alkaline solution to neutralise the FFA before moving on to transesterification. One further approach uses a two-step processing strategy. The FFA is converted into an ester during the initial step, which is called acid esterification. Alkaline transesterification is then completed in the second stage.

6.6.5 Saponification value of microalgae oil

The saponification value is a quantitative measure that represents the quantity of alkali needed to completely saponify a specific quantity of a given sample. High saponification levels are suggestive of a substantial amount of short-chain fatty acids,

which could lead to the production of soap. Consequently, the separation of products will pose considerable challenges. The low output of biofuel (specifically biodiesel) could perhaps be attributed to this factor.

The triglycerides of the microalgae oil contain low molecular weight fatty acids, both saturated and unsaturated, according to the saponification values of 203.16 for Scenedesmus sp. and 213.18 for the microalgae consortium, respectively, as stated in Table 6.4. The outcome was superior when compared to other oils, including palm (208-213), moringa (185-205), laurel berries (198-206) and laurel wax (210-240) (Ivanova *et al.,*2022). With the FFA values of 0.85 and 4.79, the microalgae oils are unstable and can easily degrade and form soap when reacted with alkali and form a stable emulsion thus preventing separation of biodiesel from glycerol during transesterification.

According to Konga *et al.* (2016), samples with low saponification values are indicative of longer fatty acid chains and greater molecular weights. This study recorded the saponification values of 203.16 mg KOH/g microalgae oil for *Scenedesmus sp.* and 213.18 mg KOH/g microalgae oil for the consortium, which compare favourably with the value reported by Ejim and Kamem (2013) of 200 mg KOH/g. However, it is important to note that this value is also lower than the value reported by Konga *et al.* (2016). In their study, they reported a saponification value that was not specified. Nonetheless, the saponification values obtained in this study were significantly lower compared to the value reported by Oluogun *et al.* (2021) of 245.44 mg KOH/g.

6.6.6 Iodine value of microalgae oil

The assessment of the chemical stability of different oils against oxidation is commonly conducted using the iodine value (IV). Iodine numbers are employed for the quantification of unsaturation levels in fatty acids through the formal addition of iodine to the double bonds. The iodine content of the microalgae oil in this study was 108.15 g I_2/100 g for *Scenedesmus sp.* and 81.22 g I_2/100 g for the microalgae consortium, which is within the acceptable limit of 120 g I_2/100 g. This indicates that the oils bear unsaturated fatty acids. Unsaturated fatty acids, particularly monounsaturated fatty acid chains found in triglycerides, are highly favoured for the formation of biofuels, specifically biodiesel. This preference stems from their ability to undergo a more rapid conversion reaction into fatty acid methyl esters, which serve as biofuel. The values agree with the findings of Su *et al.* (2022) (100–120 g I_2/100 g) and Konga *et al*. (2016) (65 g I_2/100 g). According to Konga *et al.* (2016), biofuels possessing elevated iodine values have a propensity to undergo polymerization, resulting in the formation of deposits on injector nozzles and piston rings.

6.7 Proximate and Elemental Composition of Microalgal Biomass

Proximate analysis of biomass indicates the composition of the biomass regarding the moisture content, volatile matter, ash content, and fixed carbon. The type of biomass regarding storage capacity, energy content, and biomass is graded based on the outcome of this analysis. The proximate composition of algae includes proteins, carbohydrates, lipids, and proteins, in varying proportions. Table 6.5 presents the elemental composition of microalgae on a dry-weight basis.

Table 6.5 Elemental composition of microalgae biomass (% dry-weight basis)

Element	*Scenedesmus sp.*	Microalgae consortium
Carbon, C (%)	36.30±1.15	50.12±2.72
Hydrogen, H (%)	6.87±0.07	8.54±0.05
Nitrogen, N (%)	8.71±0.02	10.32±0.12
Oxygen, O (%)	48.12±0.31	28.99±0.98
Phosphorus, P (%)	-	2.03±0.07

The microalgae consortium and *Scenedesmus sp*. were both grown in nutrient-replete BWW under consistent growth conditions for this study. When the stationary phase was reached after twenty-two days, the biomasses were harvested. collected lipids on the eighteenth day of incubation during the early stationary phase. Staining revealed the intracellular lipids as golden yellow droplets. Generally, the mass fraction of dry biomass expressed as a percentage indicates the lipid content. In Scenedesmus sp., the lipid content ranged from 8.9 % to 40.9 % of the dry biomass mass fraction within the consortium. According to Griffiths and Harrison (2018) and Talebi *et al*. (2020), the range of 11 % to 31 % mass fraction of dry biomass corresponded with the average lipid content of the microalgal strains. As a high lipid-producing strain in the current investigation, Scenedesmus sp. displayed lipid accumulation greater than 20 % mass fraction at the stationary phase. High lipid content has the potential to increase biomass processing efficiency, raising the yield of the final product (bioproduct) and sharply lowering production costs. The average biomass productivity of the strains will have a major impact on the viability of microalgal biodiesel production, and lipid content may not be the only deciding criterion. There is an inverse link between biomass

productivity and fat buildup, according to several experts. Botryococcus sp. accumulate high lipid/hydrocarbon content (>25 % mass fraction), however their low growth rate and biomass output (34 mg L^{-1} day^{-1}) limit their applicability in the industrial setting, according to Vidyashankar *et al.* (2015). The current study's findings with a consortium of microalgae high in lipids were similar. To choose viable strains, one might use a balanced criterion that takes into account both biomass productivity and lipid content, such as volumetric lipid productivity (mg L^{-1} day^{-1}). Based on their greater lipid productivity (>15 mg L^{-1} day^{-1}) and high biomass yield, Scenedesmus sp. satisfied the requirements for both stationary phase lipid content and the current investigation.

The primary composition of algae includes proteins, carbohydrates, lipids, and proteins, in varying proportions. Depending on the kind of algae, the proportion of fatty acids in their mass might range from 40 % to 60 %. This fatty acid from the algae can be extracted and converted into biodiesel. Microalgal oil is very high in unsaturated fatty acids (UFA), which include Arachidonic acid (AA), Eicosapentaenoic acid (EPA), Docosahexaenoic acid (DHA), Gamma-linolenic acid (GLA), Linoleic acid (LA), etc.

The lipid contents reported in the present study are obtained under nutrient-replete conditions which can be further enhanced by altering the culture conditions mainly nutritional regime such as nutrient deprivation (nitrate, phosphate). Therefore, a two-phase cultivation system could be suggested for improved lipid accumulation. The first stage comprises biomass-enhancing nutrient-replete conditions followed by the incubation of obtained biomass under nutrient-deplete conditions for lipid enhancement. Higher lipid content and volumetric lipid productivity are crucial factors to consider when choosing microalgae to produce lipids boosted by biofuel (Brennan

and Owende, 2010). Table 6.6 shows the proximate composition of microalgae biomass on dry weight basis.

Table 6.6 Proximate composition of microalgae biomass (% dry weight basis)

Parameter	*Scenedesmus sp.*	Microalgae consortium
Moisture	6.41±0.26	7.52±0.31
Carbohydrates	34.60±1.02	42.31±1.13
Lipid	14.72±0.17	5.76±0.69
Protein	41.15±0.23	19.65±0.12
Ash	3.12±0.04	24.76±0.09

What makes a lipid suitable as a substrate for the synthesis of biofuel is its fatty acid content or lipid quality.

6.8 Hydrocarbons Profiling of Microalgae Oil

Dayananda *et al*. (2020) explained the process of extracting hydrocarbons from 100 mg of dry algal biomass using n-hexane. To purify the crude extracts, a glass column of 10 mm in diameter and 150 mm in height was filled with silica gel (60-120 mesh, SRL, Mumbai) and n-hexane. All other polar components, including pigments and lipids, were left in the column while pure hydrocarbons were extracted using n-hexane. The extracts were vacuum-dried and then measured using gravimetric analysis. Using Equation (6.8), the biomass's hydrocarbon content (C_H, % mass fraction) was determined.

$$C_H = \frac{W_H}{W_B} \tag{6.8}$$

where W_H and W_B stand for the relative weights of the dry algal biomass collected and the extracted hydrocarbons respectively.

Lipid samples extracted from microalgae biomass were subjected to GC-MS analysis. Analyses were carried out on an Agilent 7890A gas chromatographer coupled to an Agilent 5975C mass spectrometer (simple quadrupole) and flame ionization detection (GC-MS/FID). A Zebron 7HG-G007-11 (Phenomenex) polar capillary column (length 30 m, internal diameter 0.25 mm, film thickness 0.25 µm) was used. The hydrogen carrier gas was at 1 mL min^{-1}. The oven temperature was programmed with an initial 2-minute hold time at 60°C, a first ramp from 0°C to 151°C at 20°C min^{-1} with a 5-minute hold time at 151°C, then a second ramp from 151°C to 240°C at 6°C min^{-1} and a final 3 minute hold time at 240°C. Samples were injected in splitless mode (1 min) at 250°C. The MS was run in full scan over 40-350 amu (electron impact ionization at 70eV) and peaks were quantified based on the FID signal using the internal standards.

The prevalence of fatty acids as primary constituents of triglycerides for biofuel (biodiesel) synthesis is a well-established phenomenon (Mata, Martins and Caetano, 2010). Table 6.3 displays the oil's fatty acid composition, which primarily consists of medium- to long-chain saturated and monounsaturated fatty acids. Table 6.7 on the other hand gives the characteristic chemical composition of *Scenedesmus sp.* oil. Fatty acids serve as the primary determinants for identifying triglycerides within an oil extract.

The oil is mostly composed of several fatty acids, namely oleic acid, eicosanoic acid, decanoic acid, dodecanoic acid, octadecenoic acid, hexadecanoic (palmitic) acid, and hexadecenoic acid. The straight chain characteristic exhibited by oils serves as a reliable indicator of their favourable reactivity and suitability for efficient processing

in refineries (Saad *et al.* 2019). A promising fuel source that can lower greenhouse gas emissions and enhance engine performance is fatty acid alkyl esters, generally referred to as biodiesel (Chuah *et al*. 2022). The oil extract contains a significant amount of fatty acid esters. These esters include heptadecanoic acid (heptadecyl ester), methoxyacetic acid (tridecyl ester), tetradecanoic acid (2-hydroxy-methyl ester), methoxyacetic acid (decyl ester), and methoxyacetic acid (3-pentadecyl ester). By breaking down triglycerides (TAGs) into fatty acids and glycerol and then re-esterifying the fatty acids to produce different kinds of fatty acid esters, a process known as transesterification produces fatty acid esters in algae. The enzymes lipases and acyltransferases are responsible for catalysing this reaction (Sahoo *et al.* 2020). Due to the high material load and low oxygen penetration, the alcoholic component of the algae required for the reaction originates from brewery wastewater. The availability of nutrients, light, temperature, and other environmental conditions can all have an impact on this (Tan *et al.* 2017). However, it is important to highlight that the production of fatty acid esters in algae is a complicated process that can be influenced by some variables. To completely understand the underlying mechanisms, more research is required.

Table 6.7 Characteristic chemical composition of Scenedesmus sp. oil by GC-MS

Peak	Retention Time (min)	Area (%)	Chemical Identity	Molecular Formula	MW (g/mol)
1	2.595	3.84	5-methyl-2-heptanamine	$C_8H_{19}N$	129.24
2	8.539	0.06	Eicosanoic acid	$C_{20}H_{40}O_2$	312.53
3	8.848	0.04	Tetradecanoic acid	$C_{14}H_{28}O_2$	228.37
4	9.384	0.19	Tridecanoic acid	$C_{13}H_{26}O_2$	214.34
5	9.693	0.07	Z-11-Hexadecenoic acid	$C_{16}H_{30}O_2$	254.41
6	9.891	0.06	Docosanoic acid	$C_{22}H_{44}O_2$	340.60
7	10.257	0.04	Decanoic acid, silver (1+) salt	$C_{10}H_{19}AgO_2$	279.12
8	10.482	0.01	Dodecanoic acid,	$C_{12}H_{24}O_2$	200.32
9	10.989	0.13	l-(+)-Ascorbic acid 2,6-dihexadecanoate	$C_{38}H_{68}O_2$	652.9
10	11.496	0.22	n-Hexadecanoic acid	$C_{16}H_{32}O_2$	256.42
11	13.384	0.81	trans-13-Octadecenoic acid	$C_{18}H_{34}O_2$	282.50
12	14.567	1.55	Methoxyacetic acid, tetradecyl ester	$C_{17}H_{34}O_3$	286.40
13	14.989	12.06	3-trifluoroacetoxypentadecane	$C_{17}H_{31}F_3O_2$	324.40
14	15.384	3.33	Hexadecanoic acid, 2-hydroxy-, methyl ester	$C_{17}H_{34}O_3$	286.45
15	15.863	1.92	4-Trifluoroacetoxytetradecane	$C_{16}H_{29}F_3O_2$	310.39
16	16.173	5.94	Tetradecanoic acid, 2-hydroxy-methyl ester	$C_{15}H_{30}O_3$	258.39
17	16.792	9.19	Methoxyacetic acid, decyl ester	$C_{13}H_{26}O_3$	230.34
18	16.933	5.67	Methoxyacetic acid, 3-pentadecyl ester	$C_{18}H_{36}O_3$	300.50
19	17.130	12.07	1-bromo-octadecane	$C_{18}H_{37}Br$	333.4
20	17.412	4.02	Methyl 21-methyl-hexacosanoate	$C_{17}H_{34}O_2$	270.45
21	17.694	12.18	Eicosane, 1,20-dibromo-	$C_{20}H_{40}Br_2$	440.30
22	17.863	6.10	Heptadecanoic acid, heptadecyl ester	$C_{34}H_{68}O_2$	508.90
23	18.004	13.26	Methoxyacetic acid, decyl ester	$C_{13}H_{26}O_3$	230.34
24	18.454	4.03	Methoxyacetic acid, tridecyl ester	$C_{16}H_{32}O_3$	272.42
25	18.708	1.88	Cyclobutanone, oxime	C_4H_7NO	85.10
26	19.018	2.94	4-Trifluoroacetoxytetradecane	$C_{16}H_{29}F_3O_2$	310.39

The compound 2-pentadecanol has been documented to exhibit antibacterial, antifungal, and antiviral properties. Alkyl halides such as 1-bromo-octadecane, serve as intermediates in the chemical manufacturing process of various organic compounds, including octane and carbon nanotubes (Daneshvar *et al.* 2022). Another example is 1, 20-dibromo-eicosane, which functions as a starting material in the synthesis of eicosane, a compound used in the production of antifungal substances. Additionally, 4-trifluoroacetoxytetradecane has been identified as an antimicrobial compound with potential applications (Manaa and Kim 2018). Amines, particularly 5-methyl-2-heptanamine, exhibit significant relevance due to the presence of cyclobutanone oxime. This compound finds diverse applications in various fields, including the synthesis of amides, aziridines, hydrazones, cyclobutane, and oximes (Li and Wang 2016). Additionally, it serves as a ligand in transition metal-catalysed reactions (Liu *et al*. 2016) and functions as a reagent in chemical analysis for the detection and quantification of carbonyl compounds (Wiczkowski and Szawara-Nowak 2017).

These properties of oil extracted from cultured algae are evidence of its versatile uses and relevance to science and technology development.

6.9 Factor Removal Efficiency Using Different Reactor Systems and Sizes

Nutrient utilization by microalgae can be influenced by the type of reactor deployed for the operation, reactor size and substrate circulation.

The bar charts in Figure 6.6 demonstrate that *Scenedesmus sp.*'s removal efficiency of alkalinity was 85.83±12.13 % when the 3-L bubble column bioreactor was deployed. However, when the 30-L bubble column bioreactor was deployed, alkalinity removal efficiency dropped to 77.22±14.35 %.

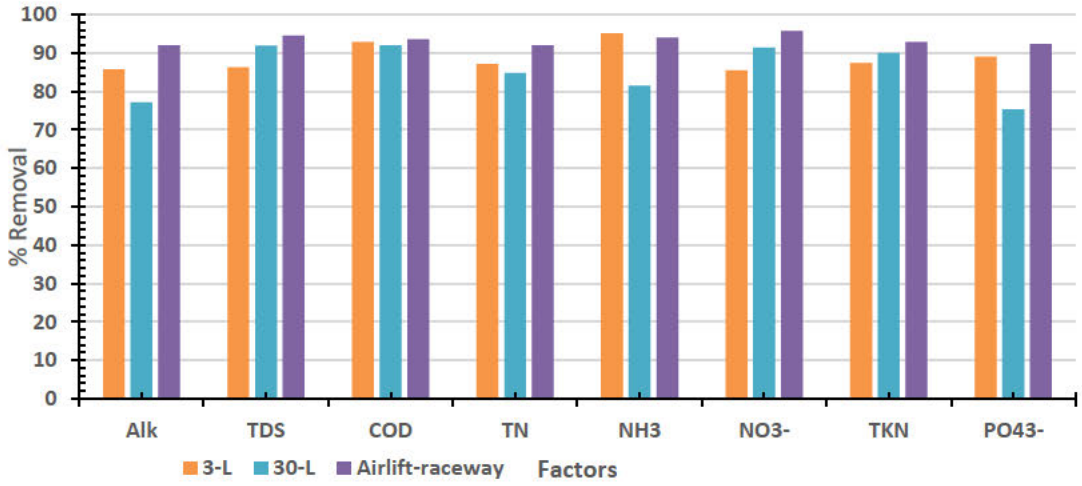

Figure 6.6 Factor removal efficiency by reactor basis

Deploying the 240-L airlift-raceway reactor (ALRR) boosted the alkalinity removal efficiency to 92.07±3.28 %. This trend may be due to the improved circulation of the media in the ALRR, thereby enhancing continuous fresh contact of microalgae cells with the factors (Table 6.8).

Table 6.8 Percentage factor sequestration efficiency

Factor	Reactor		
	3-L BCR	30-L BCR	240-L ALRR
Alkalinity, %	85.83±12.13	77.22±14.35	92.07±3.28
TDS, %	86.25±12.76	91.92±1.55	94.54±1.02
COD, %	92.87±2.61	92.06±7.54	93.53±1.68
TN, %	87.14±10.82	84.75±2.11	92.02±5.35
NH_3, %	95.13±0.27	81.56±6.98	94.06±1.01
NO_3^-, %	85.57±12.72	85.57±12.72	95.72±1.21
TKN, %	87.39±10.53	90.02±2.84	92.84±1.41
PO_4^{3-}, %	89.06±9.28	75.39±15.79	92.39±5.98

The ALRR stood out in the factor removal efficiencies. Relative to the 3-L BCR, the 30-L BCR showed superior removal efficiency of TDS (91.92±1.55 %), and TKN (90.02±2.84 %). This selective factor removal efficiency of the 30-L BCR may be due to the effective sparging system but to its large diameter, which limited light penetration through the broth.

CHAPTER 7

Techno-economic and Life Cycle Analyses of Microalgae-based Hydrocarbon Production

7.1 Introduction

Microalgae-based hydrocarbon production from brewery wastewater treatment is an emerging approach that integrates wastewater bioremediation with sustainable biofuel generation. A techno-economic analysis (TEA) of this system typically evaluates the feasibility, costs, and potential profitability of the process. The dominance of fatty acid methyl esters (FAMEs) in the microalgae-oil extracts suggests that the traditional transesterification step could be bypassed in favour of a purification step. This modification reduces chemical and processing costs while simplifying the biodiesel production process.

Life Cycle Analysis (LCA), on the other hand, is a systematic approach to evaluating the environmental impact of a process from raw material extraction to final disposal. This LCA assesses the use of *Scenedesmus sp.* for brewery wastewater treatment and biodiesel production in a hybrid airlift-raceway photobioreactor (HARPBR) with blue light manipulation.

7.2 Technical Analysis

7.2.1 Microalgae cultivation and wastewater treatment

Brewery wastewater, which has undergone nutrient enrichment, is rich in organic matter, nitrogen, and phosphorus, and supports *Scenedesmus sp*. growth. The HARPBR combines efficient mixing (airlift) and large surface area exposure

(raceway) to improve CO_2 utilization and light penetration. It reduces contamination risks compared to open systems. Blue Light Manipulation enhances lipid metabolism favouring FAME production, thus reducing the need for further chemical modification (transesterification).

7.2.2 Lipid extraction and purification

Direct FAME extraction uses solvents like hexane or ethanol. Alternative methods include supercritical CO_2 extraction, which is eco-friendly but costly. The purification step skips transesterification since FAMEs are dominant in the oil extract. Purification (e.g., distillation, adsorption, or membrane filtration) is sufficient to meet biodiesel standards. This step removes residual impurities (free fatty acids, pigments, and moisture) and enhances fuel quality. Residual biomass can be repurposed as animal feed, biofertilizer, or biochar. Glycerol content (if available) may be utilized in bioproduct manufacturing (Zhou *et al.*, 2012).

7.2.3 Economic analysis

7.2.3.1 Capital Expenditures (CAPEX) (Couper, James and Smith, 2019)

This has to do with the provision of infrastructure and equipment Hybrid Airlift-Raceway PBR: Estimated cost of $50,000–$150,000 per hectare (dependent on scale and automation). Lipid Extraction System: Solvent-based ($100,000+). Purification Unit: Estimated at $30,000–$70,000 for industrial-scale purification

7.2.3.2 Operational Expenditures (OPEX) (Couper, James and Smith, 2019)

Energy costs for photobioreactor operation: approximately $0.10–$0.30/kWh for aeration, mixing, and lighting; lipid extraction: solvent recovery and drying increase energy demand (~$0.50–$1 per litre); Purification: Adsorption/membrane separation

is energy-efficient, reducing total processing costs by 15-30 % compared to transesterification; labour and maintenance: A skilled labour for monitoring, harvesting, and processing; routine maintenance of reactors, pumps, and purification units; Chemicals and consumables: Solvent costs (if used) are recurrent but mitigated by recycling; Adsorbents or membranes for purification (~$5,000–$20,000 per year).

7.2.3.3 Revenue Streams

Biodiesel Sales: Purified FAME-rich oil can directly replace conventional biodiesel; Market price: $1.20–$1.50 per litre; Carbon Credits and Wastewater Treatment Fees: Industries may pay for effluent treatment (~$0.05–$0.15 per litre of treated wastewater); Byproduct Sales: Residual biomass for animal feed (~$0.30/kg); Glycerol (if present) for pharmaceuticals or cosmetics (Couper, James and Smith, 2019).

7.2.3.4 Economic Feasibility Indicators

Table 2.1 Economic feasibility indicators

Parameter	With Transesterification	With Direct Purification
CAPEX	Higher due to reactors and catalysts	Lower due to reduced chemical processing
OPEX	Higher (chemicals & energy)	Lower (no catalyst, reduced processing)
Energy Consumption	~1.5–2 kWh/L	~1–1.5 kWh/L
Biodiesel Cost	~$0.80–$1.10/L	~$0.60–$0.90/L
Profit Margin	Moderate	Higher due to lower processing costs

Table 7.1 shows economic feasibility indicators of the process. To determine the economic feasibility of biodiesel production from *Scenedesmus* sp. using brewery wastewater and a hybrid airlift-raceway photobioreactor (PBR), several key economic feasibility indicators must be analyzed. These indicators help assess the investment attractiveness, profitability, and financial viability of the process.

a. CAPEX (Initial Investment Costs)

CAPEX includes costs associated with infrastructure, equipment, and installation. Table 7.2 presents the costs associated with infrastructure, equipment and installation.

Table 7.2 Costs associated with infrastructure, equipment and installation

Cost Component	Estimated Cost (USD)	Remarks
Hybrid Airlift-Raceway PBR	$50,000–$150,000 per hectare	More cost-effective than fully enclosed PBRs.
Lipid Extraction System	$20,000–$50,000	Solvent-based or supercritical CO_2 extraction.
Purification Unit	$30,000–$70,000	Adsorption or membrane filtration.
Storage & Processing Equipment	$10,000–$30,000	For oil storage and handling.
Total CAPEX	$110,000–$300,000	Lower than conventional biodiesel setups.

The economic implication of Table 7.2 is that lower CAPEX due to the removal of transesterification reduces financial risks, and Hybrid PBRs provide a cost-effective balance between open ponds and closed PBRs.

b. OPEX (Recurring Costs)

OPEX includes energy, labour, maintenance, and raw material costs. These are given in Table 7.3.

Table 7.3 Costs associated with energy, labour, maintenance and raw materials

Cost Component	Cost per Litre (USD)	Remarks
Energy (Mixing, Aeration, Lighting)	$0.10–$0.30	Hybrid PBRs require moderate energy.
Harvesting & Extraction	$0.15–$0.25	Solvent recovery improves efficiency.
Purification	$0.10–$0.20	Adsorption/membrane filtration is cost-effective.
Labor & Maintenance	$0.20–$0.30	A skilled workforce is required.
Total OPEX per Liter	$0.55–$1.05	Competitive with conventional biodiesel.

The economic implication of Table 7.3 is that lower chemical consumption reduces OPEX and that solvent recovery and purification lower costs compared to traditional transesterification. The cost of production and market price of biodiesel, as estimated, are presented in Table 7.4

Table 7.4 Cost of production against market price of biodiesel and profit margin

Metric	With Transesterification	With Direct Purification
Production Cost per Liter	\$0.80–\$1.30	\$0.55–\$1.05
Market Price of Biodiesel	\$1.20–\$1.50	\$1.20–\$1.50
Profit Margin per Liter	\$0.10–\$0.70	\$0.15–\$0.95

The economic implication of Table 7.4 is that direct purification reduces production costs by up to 40 %, increasing competitiveness, and higher profit margins (\$0.15–\$0.95 per litre) make it more attractive for investors.

7.2.3.5 Net Present Value (NPV)

NPV measures the project's total profitability over time by considering future cash flows discounted to present value. Equation (7.1) gives the expression for the NPV (Couper, James and Smith, 2019).

$$NPV = \sum \frac{R_t}{(1+r)^t} - C_0 \tag{7.1}$$

where

R_t = Net cash inflow in year t

r = Discount rate (e.g., 10 %)

C_0 = Initial investment

If NPV > 0, the project is profitable.

Scenario analysis may ensue where the school of optimism holds onto high biodiesel prices, NPV = \$500,000+ over 10 years. However, for pessimists with low biodiesel demand, NPV = \$100,000+ (still positive). The economic perspective still keeps NPV positive in most scenarios, showing financial sustainability.

7.2.3.6 Internal Rate of Return (IRR)

IRR is the discount rate at which NPV becomes zero. A higher IRR indicates a better investment. Typically, IRR for biofuel projects is 10–18 %. The estimated IRR for this process is 15–25 %. From an economic perspective, the IRR is above 15 %, making the project financially viable for investors. A higher IRR means a faster return on investment.

7.2.3.7 Payback Period

The payback period, Equation (7.2) measures how long it takes to recover the initial investment (Couper, James and Smith, 2019).

$$Payback\ Period = \frac{Initial\ Investment\ (CAPEX)}{Annual\ Net\ Profit} \tag{7.2}$$

Table 7.5 Payback period

Scenario	With Transesterification	With Direct Purification
Payback Period	5–8 years	3–6 years

Table 7.5 shows shorter payback periods, which should encourage investments; and a payback period of 3–6 years increases attractiveness for investors. Faster break-even means quicker financial sustainability.

7.2.3.8 Sensitivity Analysis

Economic feasibility is affected by changes in raw material costs, energy prices, and market demand. For break-even analysis, if energy prices increase by 20 %, OPEX rises by ~$0.10 per litre but remains profitable. If biodiesel prices drop to $1.00 per litre, the profit margin shrinks but remains positive. Large-scale production reduces OPEX per litre by 10–20 % due to economies of scale.

7.2.3.9 Risk Assessment

A detailed risk assessment is crucial in evaluating the economic feasibility of microalgae-based biodiesel production using *Scenedesmus* sp., brewery wastewater, and hybrid airlift-raceway photobioreactors (PBRs). Table 7.6 presents the risk assessment of the process.

Table 7.6 Risk assessment

Risk Factor	Potential Impact	Mitigation Strategy
Biodiesel Market Price Volatility	Profitability fluctuations	Long-term contracts with buyers.
High Energy Costs	Increased OPEX	Use of renewable energy sources (solar, biogas).
Regulatory Changes	Impact on subsidies/tax credits	Diversify revenue streams (wastewater treatment, byproducts).
Scale-Up Challenges	Higher CAPEX	Pilot testing before full-scale deployment.

Below is a structured breakdown of key financial, operational, and environmental risks**,** along with mitigation strategies**.**

1. Financial Risks

a. Market Volatility in Biodiesel Prices: Global biodiesel prices fluctuate due to crude oil prices, supply-demand imbalances, and government policies. A price drop below $1.00 per liter could reduce profitability. This could have medium impact . However, the following mitigation strategies may salvage the threat: (i) Establish long-

term contracts with fuel distributors and government agencies. (ii) Diversify into high-value co-products (e.g., animal feed, biofertilizers). (ii) Leverage carbon credit incentives to offset financial losses (Pittman, Dean and Osundeko, 2011).

b. High Initial Capital Expenditure (CAPEX): Setting up hybrid PBR systems, extraction units, and purification plants requires substantial upfront investment ($110,000–$300,000), delivering a high impact. Mitigation strategies would encourage modular deployment of a pilot-scale plant before full-scale commercialization. Also, seek government grants, subsidies, and venture capital funding for biofuels; and implement phased investment strategies to reduce financial strain (Razzak *et al.*, 2013).

c. Fluctuating Operating Costs (OPEX): Costs for electricity, CO_2 supply, and wastewater treatment can vary significantly. Thus, delivering medium impact. Mitigation strategies would be the use of renewable energy sources (solar panels, anaerobic digestion for biogas), optimize CO_2 injection efficiency to reduce losses, and develop energy-efficient harvesting and extraction methods (Gulde *et al.*, 2017).

2. Operational Risks

a. Biomass Yield Variability: The growth rate and lipid content of *Scenedesmus sp*. may vary due to seasonal temperature changes, nutrient availability in wastewater, and light fluctuations. This could deliver a high impact, but could be mitigated through implementation of real-time monitoring systems to track and adjust culture conditions, supplement controlled LED lighting to stabilize productivity, and maintain a backup freshwater nutrient system for extreme conditions (Sierra *et al.*, 2008)

b. Photobioreactor Performance Limitations: The hybrid airlift-raceway PBR may face inefficiencies in CO_2 mass transfer, light penetration, and biofouling over time. This may deliver a medium impact on the system. The following mitigation strategies

would salvage the situation: (i) Conduct regular cleaning and maintenance to prevent clogging and contamination. (ii) Optimize mixing and aeration strategies to improve CO_2 uptake. (iii) Use anti-biofouling coatings or advanced reactor materials (Morales-Amaral *et al*., 2015)

c. Lipid Extraction and Purification Efficiency: The economic advantage of the process depends on bypassing transesterification; however, purification technologies must achieve high FAME purity (≥98%) at a low cost. Medium impact may be experienced. However, Mitigation strategies may include (i) investment in membrane filtration, adsorption techniques, or fractional distillation to enhance purification; (ii) Develop solvent recovery systems to minimize extraction costs. (iii) Explore green solvents (ionic liquids, supercritical CO_2) to reduce chemical usage (Zhang, Xu and Sun, 2020).

3. Environmental and Regulatory Risks

a. Regulatory Compliance & Policy Uncertainty: Biofuel policies and incentives vary across regions. Regulatory restrictions on wastewater-based biofuels could limit commercialization. This could deliver high impact on the operations, but could have a soft landing by (i) Engaging with government agencies to ensure compliance with ASTM D6751 and EN 14214 fuel standards. (ii) Advocating for carbon credit incentives and biofuel subsidies. (iii) Conducting independent third-party testing to validate product safety (He *et al*., 2015).

b. Environmental Impact and Public Perception: Although wastewater recycling is a sustainability advantage, concerns about microalgae-derived biodiesel emissions, land use, and waste disposal may arise. The impact on the operation may be medium. Mitigation strategies may include (i) Performing a Life Cycle Assessment (LCA) to quantify environmental benefits. (ii) Implement waste valorization strategies for

leftover biomass (biofertilizers, animal feed, or bioplastics). (iii) Educate stakeholders on the sustainability benefits of microalgal biofuels (Laurens *et al*., 2017).

c. Climate Sensitivity and Extreme Weather Events: Outdoor raceway systems may suffer from extreme heat, cold, storms, or droughts, affecting productivity. The setback may be temporal, and mitigation strategies would be to (i) develop climate-resilient hybrid PBR designs with temperature control, (ii) use indoor or semi-covered systems in extreme climate regions, (iii) integrate climate forecasting models to adjust operations proactively (Yap *et al.*, 2014)

4. Supply Chain and Market Risks

a. Feedstock Supply and Brewery Wastewater Availability: Brewery wastewater may not always be consistently available or nutrient-rich, affecting algae growth. This could deliver a medium impact on the operation, but mitigation strategies could be to (i) establish contracts with multiple breweries to ensure stable wastewater supply. (ii) develop an on-site nutrient supplementation system for lean wastewater periods. (iii) optimize wastewater pre-treatment (oxidation ponds for nutrient enrichment) to maintain steady nutrient levels (Quinn and Davis, 2015).

b. Logistics and Distribution Challenges: Transporting, storing, and distributing microalgae-based biodiesel requires specialized infrastructure. This would have medium impact on the system. Mitigation strategies, in this case would be to (i) set up localized biorefineries near breweries to minimize transport costs. (ii) partner with existing fuel distributors to integrate with existing supply chains. (iii) explore on-demand, decentralized production models (e.g., mobile biofuel units) (Beal *et al*., 2018).

5. Summary of Key Risks and Mitigation Strategies

Table 7.7 Key risks and mitigation strategies

Risk Category	Specific Risk	Impact	Mitigation Strategy
Financial	Biodiesel price fluctuations	Medium	Secure long-term contracts, diversify revenue streams
	High CAPEX investment	High	Phased investment, government grants
	OPEX cost variations	Medium	Use renewable energy, optimize CO_2 utilization
Operational	Biomass yield instability	High	Real-time monitoring, LED light supplementation
	PBR efficiency limitations	Medium	Anti-biofouling coatings, optimized aeration
	Lipid purification efficiency	Medium	Membrane filtration, solvent recovery
Regulatory & Environmental	Policy uncertainty	High	Engage policymakers, secure certifications
	Environmental concerns	Medium	LCA studies, public education campaigns
	Climate change impacts	Medium	Climate-resilient reactor designs
Supply Chain & Market	Inconsistent wastewater supply	Medium	Multi-brewery contracts, nutrient supplementation
	Fuel distribution challenges	Medium	Localized biorefineries, industry partnerships

7.2.4 Challenges and Considerations

Biodiesel-grade microalgae oil is purely FAMEs, which must meet ASTM D6751 and EN 14214 biodiesel standards. Hybrid PBR systems require careful optimization for large-scale applications. Competition with fossil fuels and policy incentives would impact profitability. Efficient use of residual biomass enhances economic feasibility.

7.2.5 Conclusion and Recommendations

By eliminating transesterification and integrating a direct purification step, this process achieves: lower processing costs, higher energy efficiency, reduced chemical dependency, and improved economic viability. For commercialization, pilot-scale validation and policy support (such as tax incentives for biofuels) would enhance feasibility.

The process is economically feasible with strong economic indicators: Low CAPEX and OPEX compared to conventional biodiesel production. High profit margins ($0.15–$0.95 per litre) ensure financial viability. The short payback period (3–6 years) makes it attractive for investors. Strong IRR (15–25 %) and positive NPV confirm long-term profitability.

The following recommendations could be deduced: Pilot-scale validation to refine cost estimates. Government incentives or carbon credits can further improve feasibility. Partnering with breweries for wastewater treatment reduces operational costs and enhances revenue streams.

7.3 Life Cycle Analysis (LCA)

7.3.1 Goal and scope definition

The goals of LCA are to (i) assess the environmental impact of a modified process where FAMEs are directly purified from *Scenedesmus sp.* oil extracts, bypassing the transesterification step. (ii) compare this improved process to conventional microalgal biodiesel production and wastewater treatment methods.

The scope of this LCA is limited to and not exceeding 1 m^3 of treated brewery wastewater and 1 kg of biodiesel produced. The process description includes microalgal cultivation, wastewater treatment, biomass harvesting, lipid extraction, FAME purification, and biodiesel utilization. The impact was focused on energy demand, greenhouse gas (GHG) emissions, nutrient recovery, water footprint, and land use. Process modification includes the elimination of the transesterification step (which typically involves methanol and catalysts), and the inclusion of a FAME purification step, which may involve solvent-based fractionation, filtration, or supercritical CO_2 extraction (Alonso-Riaño *et al.,* 2022)

7.3.2 Life cycle inventory (LCI)

The LCI quantifies inputs (resources) and outputs (emissions, waste) throughout the improved process.

7.3.2.1 Inputs

Input materials include brewery wastewater as a nutrient source, microalgal inoculum (*Scenedesmus sp.*), purification chemicals (e.g., hexane, ethanol, or supercritical CO_2), energy sources like blue LED lighting for enhanced lipid production, airlift pump operation (for aeration and circulation), raceway mixing system, harvesting and

dewatering (flocculation, filtration, or centrifugation), FAME purification system (solvent extraction or supercritical CO_2 processing), brewery wastewater as a growth medium, and CO_2 supplementation.

7.3.2.2 Outputs

The desired outputs include treated wastewater with reduced organic load and nutrients; microalgal biomass, rich in directly usable FAMEs; biodiesel (purified FAMEs). By-products include residual biomass (protein-rich for animal feed or fertilizer); gaseous emissions (CO_2 from aeration and biodiesel combustion); waste solvents (for solvent-based purification method).

7.3.3 Life cycle impact assessment (LCIA)

The environmental impact of each stage is evaluated with the process modification in mind.

7.3.3.1 Microalgae cultivation and wastewater treatment

Energy demand is between moderate and high due to LED lighting and airlift-raceway mixing. The GHG emission signature reduced due to CO_2 uptake by microalgae. Nutrient removal efficiency is high (>90% nitrogen and phosphorus removal), while the water footprint is low, as brewery wastewater is recycled.

7.3.3.2 Biomass harvesting and lipid extraction

Energy demand is moderate due to centrifugation or flocculation-based harvesting. Minimal environmental Impact as no chemical transesterification is involved. This process results in 20–30 % lipid content in *Scenedesmus sp.* biomass, with a high proportion of direct FAMEs, giving it an efficient system endorsement.

7.3.3.3 FAME purification (instead of Transesterification)

Energy demand is reduced compared to transesterification, but depends on purification method. For solvent-based FAME purification, environmental impact would be moderate due to solvent recovery needs. For supercritical CO_2 purification, there would be higher energy demand but no chemical waste. GHG emissions from FAME-purified biodiesel are lower than methanol-transesterified since methanol use is avoided.

7.3.3.4 Biodiesel utilization and waste management

The combustion of biodiesel promotes lower CO_2 emissions than conventional diesel. Residual microalgae biomass can be utilized for feed or biofertilizer. Table 7.8 presents the comparative analysis of HARPBR with FAME, transesterification, conventional WW treatment and petroleum diesel regarding energy use, GHG emissions, nutrient recovery, biodiesel yield and water footprint (Rawar *et al.*, 2011).

Table 7.8 Comparative analysis with conventional systems

Parameter	HARPBR with FAME Purification	HARPBR with Transesterification	Conventional WW Treatment	Petroleum Diesel
Energy Use	Lower	Higher	Medium	Very High
GHG Emissions	Lowest	Low	High	Very High
Nutrient Recovery	High	High	Low	N/A
Biodiesel Yield	~30 % lipid as FAMEs	~30 % after transesterification	N/A	N/A
Water Footprint	Low	Low	Medium	High

7.3.4 Interpretation and recommendations for further optimization

Avoiding transesterification drastically lowers the amount of chemicals used and waste produced. Depending on the technique, energy demand is still an issue, particularly in FAME purification. The high rate of nutrient recovery makes wastewater treatment extremely effective (Rawat *et al.*, 2011).

However, solvent extraction may be replaced by energy-efficient purification techniques including (i) membrane filtering and (ii) supercritical CO_2 optimisation for reduced energy consumption. Utilise bio-flocculation rather than centrifugation to lower the energy required for harvesting. Incorporate sustainable energy sources, such airlift pumps and solar panels for LED lighting.

7.3.5 Conclusion

This upgraded process enhances sustainability by eliminating methanol-based transesterification and focusing on direct FAME purification. The key advantages include lower chemical waste, reduced GHG emissions, and a streamlined process. However, energy demand for purification should be minimized to improve overall efficiency. Future research should explore membrane-based and low-energy supercritical CO_2 methods to further optimize this system.

7.4 Implications for Renewable Energy Policies and Environmental Engineering Practices in South Africa and Other Parts of the World

Renewable energy policies and environmental engineering practices play a critical role in addressing climate change, reducing carbon emissions, and ensuring sustainable development. South Africa, like many other countries, faces challenges in transitioning

from fossil fuels to cleaner energy sources while maintaining economic growth and energy security.

7.4.1 Renewable energy policies in South Africa

South Africa's energy sector has historically been dominated by coal, contributing to high greenhouse gas emissions. However, the country has recognized the need to transition to renewable energy, with policies such as:

7.4.1.1 Renewable energy independent power producer procurement programme (REIPPPP)

Launched in 2011, this initiative promotes private sector investment in wind, solar, and biomass energy (Eberhard & Naude, 2016). It has attracted significant investments and improved energy diversification.

7.4.1.2 The integrated resource plan (IRP) 2019

A government strategy that outlines energy transition plans, including the decommissioning of coal-fired power plants and an increase in renewable energy capacity (Department of Mineral Resources and Energy, 2019).

7.4.1.3 Carbon tax act (CTA) (2019)

This policy aims to reduce carbon emissions by penalizing industries for excessive emissions, thus incentivizing the adoption of cleaner technologies (National Treasury, 2019). Despite these efforts, challenges such as grid capacity constraints, political resistance, and financial instability at Eskom (the national power utility) hinder rapid renewable energy expansion (Baker, 2022).

7.4.2 Renewable energy policies in other parts of the world

Globally, countries have implemented diverse policies to transition to renewable energy.

7.4.2.1 European Union (EU)

The EU Green Deal (2019) aims for carbon neutrality by 2050, emphasizing wind, solar, and hydrogen energy (European Commission, 2020).

7.4.2.2 United States

The Inflation Reduction Act (2022) includes tax incentives for renewable energy projects, aiming to reduce emissions by 40% by 2030 (IEA, 2023).

7.4.2.3 China

The world's largest producer of solar panels and wind turbines, China's 14th Five-Year Plan (2021-2025) aims to achieve 33% non-fossil fuel energy consumption by 2025 (IEA, 2022).

7.4.2.4 Implications for environmental engineering practices

Environmental engineering is crucial in implementing renewable energy projects while minimizing ecological impact. Key areas of focus include:

(a). Sustainable infrastructure development

Engineers must design energy projects that integrate with existing infrastructure, reducing environmental degradation. Smart grids and battery storage systems are necessary for handling intermittent renewable energy sources.

(b). Waste management in renewable energy

The disposal of solar panels and wind turbine blades presents a challenge, requiring innovations in recycling and material recovery (IRENA, 2020). Policies should mandate Extended Producer Responsibility (EPR) programs for manufacturers.

(c). Water and land use management

Large-scale renewable projects, such as hydropower and solar farms, can affect ecosystems. Environmental Impact Assessments (EIA) should be mandatory to minimize negative effects.

(d). Climate adaptation and resilience

Engineers should incorporate climate adaptation strategies in energy infrastructure to withstand extreme weather events. Decentralized energy systems, such as microgrids, enhance resilience in disaster-prone regions.

7.4.2.5 Conclusion

Renewable energy policies and environmental engineering practices are essential in achieving sustainability goals. While South Africa has made progress through REIPPPP and the IRP, further efforts are needed to overcome policy and infrastructure challenges. Globally, countries like the EU, U.S., and China are setting ambitious targets, with environmental engineering playing a critical role in ensuring safe and efficient energy transitions. Future success will depend on technological advancements, policy enforcement, and public-private partnerships.

7.5 Comparative Analysis of Existing Photobioreactors versus the Hybrid Airlift-Raceway Reactor

Photobioreactors (PBRs) are specialized systems designed for cultivating microalgae and other photosynthetic organisms for applications in biofuels, pharmaceuticals, wastewater treatment, and CO_2 sequestration. Various types of PBRs exist, including tubular, flat-panel, and raceway reactors. However, recent advancements have led to the development of hybrid systems such as the Hybrid Airlift-Raceway Reactor (HARAR), which combines the advantages of conventional airlift and raceway designs to improve performance and efficiency.

This analysis compares conventional PBRs with the HARAR in terms of design, mass transfer, productivity, scalability, energy efficiency, and operational challenges.

7.5.1 Existing photobioreactor types

7.5.1.1 Tubular photobioreactors

Tubular photobioreactors consist of transparent tubes arranged in vertical or horizontal loops. They have high surface area-to-volume ratio, good light penetration, and efficient gas exchange (Ugwu *et al.*, 2008). However, they are prone to biofouling, high energy consumption for pumping, and difficulty in temperature control.

7.5.1.2 Flat-panel photobioreactors

Flat-panel photobioreactors are thin, vertical, or inclined panels made of transparent materials. They have high light utilization efficiency, better mixing, and low shear stress (Xiao *et al.*, 2020). The construction materials are expensive, they are difficult to scale-up and have limited CO_2 mass transfer.

7.5.1.3 Raceway reactors

Typical raceway reactors are open-pond systems with paddle wheels for circulation. These are low-cost, scalable, and easy to maintain reactors (Chisti, 2013). However, light distribution is poor with high water evaporation, and contamination risks.

7.5.1.4 Airlift photobioreactors

Airlift pgotbioreactors use a central riser and downcomer sections to promote circulation via air injection. They have good gas exchange, reduced shear stress, and efficient mixing (Sánchez Mirón *et al.*, 2000). However their construction is complex and have limited scalability for large-scale operations.

7.5.2 The hybrid airlift-raceway reactor (HARAR)

The Hybrid Airlift-Raceway Reactor (HARAR) integrates the gas exchange efficiency of airlift reactors with the scalability and cost-effectiveness of raceway ponds to improve microalgal productivity (Moreno-García *et al.*, 2017).

7.5.2.1 Design features

A raceway channel for low-energy mixing. An airlift column to enhance gas exchange and reduce oxygen accumulation. A segmented flow system to optimize nutrient and light distribution.

7.5.2.2 Comparative advantages

The comparative analysis of existing photobioreactors with the hybrid airlift-raceway reactor is presented in Table 7.9.

Table 7.3 Comparative analysis of existing photobioreactors versus the hybrid airlift-raceway reactor

Feature	Traditional PBRs	Hybrid Airlift-Raceway Reactor
Mass Transfer Efficiency	Moderate to high (varies by type)	High, due to airlift circulation
Mixing & Shear Stress	Some require mechanical stirring (tubular)	Low shear stress, natural circulation
Light Utilization	High in flat-panel, low in raceway	Optimized due to airlift section
Scalability	Limited (except raceway)	Highly scalable
Contamination Risk	Moderate to high in open systems	Reduced due to controlled sections
Energy Consumption	High in closed systems, low in raceway	Lower than tubular but more efficient than raceway
Cost-Effectiveness	Expensive (tubular, flat-panel)	More cost-effective for large-scale production

7.5.2.3 Key implications and applications

HARAR provides an efficient alternative for large-scale microalgal biofuel production due to its low energy requirements and high biomass yield (Moreno-García *et al.*, 2017). Compared to traditional PBRs, HARAR enhances CO_2 absorption efficiency, making it suitable for industrial carbon sequestration applications (Ugwu *et al.*, 2008). HARAR offers a controlled cultivation environment that minimizes contamination risks, crucial for producing high-value compounds like omega-3 fatty acids and pigments (Xiao *et al.*, 2020).

7.5.2.4 Conclusion

While traditional PBRs like tubular and flat-panel reactors provide high biomass productivity, they suffer from high operational costs and scalability issues. Raceway ponds, though cost-effective, struggle with low efficiency and contamination risks. The Hybrid Airlift-Raceway Reactor (HARAR) emerges as a promising alternative, offering improved gas exchange, energy efficiency, and scalability, making it ideal for industrial-scale microalgae cultivation. Further research is needed to optimize its hydrodynamics, nutrient transport, and automation for commercial deployment.

CHAPTER 8

Summary, Conclusion and Recommendations

This chapter presents the summary of this research and its findings, the conclusion is drawn and highlights the recommendations for future research.

8.1 Summary

Wastewater from the three industrial sources was screened using the best laboratory practices and it was found that brewery wastewater had the most potential to support the growth of the microalga *Scenedesmus sp.*

The study discovered that because of the abundance of saturated fatty acids, microalgae grow best around 25–30°C. *Scenedesmus sp.* treatment caused putrefaction and colour deepening while eliminating the odour from brewery wastewater. The treatment resulted in a 63.5% decrease in colouration from 167 to 61 PtCo.

Biochemical mechanisms in microbial degradation can alter wastewater acidity levels. Carbon dioxide gas injection reduced pH, creating a mildly acidic environment, aiding in wastewater management. Industrial wastewater discharges thermal emissions, affecting H+ ion concentrations, pH, and carbonate-to-bicarbonate ratios. Ion species like CO_3^{2-}, HCO_3^-, OH^-, PO_4^{3-}, SiO_4^{4-}, and BO_3^{3-} contribute to alkalinity in freshwaters. The species dominance depends on soil topography and alkalinity, with five types: CO_3^{2-}, PO_4^{3-}, carbonate-phosphate, phosphate-hydroxide, and carbonate-hydroxide. Alkalinity's significance depends on ionic species abundance.

The report found that industrial wastewater contains high amounts of fats, oils, and grease (FOG), which can cause environmental issues if released untreated. Untreated brewing wastewater had a concentration below the regulatory limit of 2.5 mg/L.

Microalgae culture successfully eliminated 73% of FOG, indicating no significant impact on the treatment process.

The study found that the culture of *Scenedesmus sp.* in brewery wastewater significantly reduced chemical oxygen demand (COD), indicating a removal efficiency of over 96%. This is because COD measurements do not account for the biodegradability of organic matter and consider physiologically inactive compounds. Nitrogen in aqueous solutions can be ammonium ion or ammonia, depending on pH. Organic nitrogen in wastewater is a minor proportion, mainly composed of protein, urea, and nucleic acids.

Utilising response surface methodology (RSM), it was possible to determine the best circumstances for microalgae growth by investigating the correlations between several explanatory variables and one or more response variables. This approach gave the measure of the desirability of the microorganism and/or the system to thrive. The highest desirability of 0.537 was recorded, which was occasioned by the dilution ratio of 1-L BWW to 1.1698-L RW resulting in the composition of TN (37.938), NH_3 (0.932), NO_3^- (3.858), TKN (1.081) and PO_4^{3-} (3.531).

Using the 3-L bubble-column bioreactor, the microalga *Scenedesmus sp.* could remove alkalinity (85.83±12.13 %), TDS (86.25±12.76 %), COD (92.87±2.61 %), TN (87.14±10.82 %), NH_3 (95.13±0.27 %), NO_3^- (85.57±12.72 %), TKN (87.39±10.53 %) and PO_4^{3-} (89.06±9.28 %). However, with the 30-L bubble-column bioreactor, *Scenedesmus sp.* removed alkalinity (77.22±14.35 %), TDS (91.92±1.55 %), COD (92.06±7.54 %), TN (84.75±2.11 %), NH_3 (81.56±6.98 %), NO_3^- (91.39±6.88 %), TKN (90.02±2.84 %) and PO_4^{3-} (75.39±15.79 %). Using the 240-L airlift-raceway bioreactor, on the other hand, *Scenedesmus sp.* removed alkalinity (92.07±3.28 %),

TDS (94.54±1.02 %), COD (93.53±1.68 %), TN (92.02±5.35 %), NH_3 (94.06±1.01 %), NO_3^- (95.72±1.21 %), TKN (92.84±1.41 %), and PO_4^{3-} (92.39±5.98 %).

Microalgae were grown using Erlenmeyer flasks and Scotch bottles for 3-L bubble column photobioreactors. Design-Expert version 11 was used to model experiments and the Response Surface Methodology (RSM) was used to improve growth conditions. The experiment was tracked using various phases: the lag phase, log (or exponential) phase, stationary phase, and death phase.

The development of *Scenedesmus sp.* in brewery wastewater is influenced by brightness, nutrients, organic carbon, and CO_2. Factors such as initial inoculum size, recovery time, and synthesis time affect the lag phase, which ranges from 4 to 8 days in this experiment. The log phase, characterized by short duration and increased metabolic activity, is useful for industrial applications, particularly in product synthesis. During the stationary period, bacteria synthesize virulence factors and endospores, preventing population growth and promoting disease survival. The growth of *Scenedesmus sp.* in brewery wastewater was shown to be driven by free energy to the extent that $\Delta G = 7.304$ kJ mol^{-1} K^{-1}, indicating that it is not spontaneous, according to the thermodynamic model. Microalgal growth requires the application of certain growth stimulants or ingredients to be sustainable.

GC-MS analysis was conducted on lipid samples extracted from microalgae biomass using an Agilent 7890A gas chromatographer coupled to an Agilent 5975C mass spectrometer and flame ionization detection (GC-MS/FID). A Zebron 7HG-G007-11 polar capillary column was used, and the oven temperature was programmed with various ramps. Samples were injected in splitless mode at 250°C, and the MS was run in full scan over 40-350 amu. Species were quantified using internal standards.

Fatty acids are the primary constituents of triglycerides, used in biofuel synthesis. The composition of Scenedesmus sp. oil, primarily composed of saturated and monounsaturated fatty acids, is crucial for identifying triglycerides within an oil extract.

Oils serve as a versatile fuel source, containing fatty acids like oleic acid, eicosanoic acid, decanoic acid, dodecanoic acid, octadecenoic acid, hexadecanoic acid, and hexadecenoic acid. Their straight chain characteristic indicates their reactivity and suitability for refinery processing. Biodiesel, a promising fuel source, can lower greenhouse gas emissions and enhance engine performance through fatty acid esters like heptadecanoic, methoxyacetic, tetradecanoic, and tridecyl.

Algae undergo transesterification, breaking down triglycerides into fatty acids and glycerol. These acids are re-esterified to produce fatty acid esters. Lipases and acyltransferases catalyze this process, requiring alcoholic components from brewery wastewater due to high material load and low oxygen penetration. Environmental conditions like nutrients, light, temperature, and light can influence the production of esters. Understanding the underlying mechanisms is crucial for a comprehensive understanding of this complex process.

Technoeconomic analysis (TEA) of the process described in this research evaluates the feasibility of producing fatty acid methyl esters (FAMEs) from *Scenedesmus sp*. cultivated in brewery wastewater. The study considers a hybrid airlift-raceway photobioreactor (PBR) system, blue light optimization for lipid enhancement, and a direct purification process instead of traditional transesterification**.**

Scenedesmus sp. (with high lipid content, adaptable to wastewater) was used to treat Brewery wastewater (rich in nitrogen & phosphorus) in a hybrid airlift-raceway PBR (improves CO_2 utilization and mixing). A solvent-based lipid extraction was employed

with solvent recovery. The *Scenedesmus sp.* oil was found to be rich in FAMEs, and direct separation and purification of FAMEs (bypassing transesterification). Production scale was aimed at 1-hectare facility operating for 300 days per year, and the target product was biodiesel compliant with ASTM D6751 & EN 14214 standards. LCA assesses the environmental impact of a modified process using Scenedesmus sp. oil extracts, comparing it to conventional biodiesel production and wastewater treatment methods. The LCA focuses on wastewater treatment, biomass harvesting, lipid extraction, FAME purification, and biodiesel utilization in a brewery. The process includes microalgal cultivation, wastewater treatment, and biomass harvesting. The impact is on energy demand, greenhouse gas emissions, nutrient recovery, water footprint, and land use. The process modification includes eliminating transesterification and incorporating FAME purification.

FAME purification is a crucial process for wastewater treatment, reducing chemical usage and waste production. However, energy demand remains a challenge, especially in FAME purification. Energy-efficient techniques like membrane filtering and supercritical CO_2 optimization can reduce energy consumption. Bio-flocculation and sustainable energy sources like airlift pumps can also be used.

8.2 Conclusion

Based on the tests carried out on the three wastewater sources in this research, it was convenient to conclude that BWW had the most potential to support the growth of microalgae. From the RSM, the highest desirability was 0.537, which corresponded to an optimised dilution ratio of 1-L BWW to 1.1698-L RW resulting in the composition of TN (37.938), NH_3 (0.932), NO_3^- (3.858), TKN (1.081) and PO_4^{3-} (3.531).

The culturing of microalgae in BWW using the novel airlift-raceway photo bioreactor recorded good advantages over the 3-L and 30-L bubble-column bioreactors. Factor removal far outshined those in the other bioreactors used in this study and stated earlier. Biomass productivity was far more than that of the other reactors used in this study. Mass transfer of CO_2, nutrients and O_2 were far better than any of the other reactors used in this study. The airlift-raceway bioreactor volume of 240 L registers the first of its kind in the treatment of wastewater by the microalgae method, giving this research a novel approach to enhanced microalgae cultivation.

The morphology of the microalgal biomass before and after lipid extraction confirmed exhaustive extraction. The physicochemical parameters of the microalgal oil compete favourably with the trans-esterified oils, except for its acid value, which points to the necessity to treat before its application.

The presence of hydrocarbons, substituted hydrocarbons, fatty acids and fatty acid esters has given an impetus to the laboratory protocols in this study to advance the suggestion to abrogate the transesterification step in the production of biodiesel from microalgal oil. This advance forms the main contribution to the body of knowledge in this area of research.

By eliminating transesterification and integrating a direct purification step, this process achieves lower processing costs, higher energy efficiency, reduced chemical dependency, and improved economic viability. For commercialization, pilot-scale validation and policy support (such as tax incentives for biofuels) would enhance feasibility.

The process is economically feasible with strong economic indicators such as low CAPEX and OPEX compared to conventional biodiesel production. High profit margins ($0.15–$0.95 per litre) ensure financial viability. The short payback period

(3–6 years) makes it attractive for investors. Strong IRR (15–25 %) and positive NPV confirm long-term profitability.

By concentrating on direct FAME purification and doing away with methanol-based transesterification, this improved method improves sustainability, with reduced GHG emissions, less chemical waste, and a more efficient procedure are the main benefits.

Despite being inexpensive, raceway ponds have low efficiency and contamination issues. The Hybrid Airlift-Raceway Reactor (HARAR) emerges as a promising alternative, delivering enhanced gas exchange, energy efficiency, and scalability, making it perfect for industrial-scale microalgae culture.

8.3 Recommendations

More strains of microalgae should be explored for their competence to produce more fatty acid esters. The airlift-raceway bioreactor should be automated to improve its capabilities.

The production of fatty acid esters in microalgae is a complicated process that can be influenced by some variables. To completely understand the underlying mechanisms, more research is required.

However, in order to increase overall efficiency, the energy required for purification should be lower. To further optimise this system, future studies should investigate membrane-based and low-energy supercritical CO_2 techniques.

Achieving sustainability objectives requires environmental engineering techniques and renewable energy legislation. Even though South Africa has made strides with the IRP and REIPPPP, more work is required to address infrastructure and policy issues. Globally, nations such as the United States, China, and the European Union are

establishing ambitious goals, and environmental engineering is essential to guaranteeing secure and effective energy transitions. Success in the future will be reliant on public-private collaborations, policy enforcement, and technological breakthroughs.

To maximise its automation, nutrient transfer, and hydrodynamics for commercial use, more study is required. Key area to priotise for future research would be to:

(i) Optimize light conditions and reactor design for maximal lipid yield in large-scale hybrid airlift-raceway PBRs.

(ii) Develop cost-effective, scalable lipid extraction & purification methods without transesterification.

(iii) Conduct full life cycle assessments to quantify environmental and economic benefits.

(iv) Strengthen industry-academia collaboration for brewery wastewater integration and process scale-up.

(v) Investigate byproduct valorization to enhance profitability and reduce waste.

Addressing these research gaps can accelerate commercialization, lower costs, and improve sustainability, making microalgae-based biodiesel a viable alternative to fossil fuels.

REFERENCES

Abiodun-Oyebanji, O. J. 2017. Research Variables: Types, Uses and Definition of Terms. In: Jaiyeoba, A. O., Ayeni, A. O. and Atanda, A. I. eds. *Research in Education*. 43-54.

Abramova, A. A., Isakov, V. G., Grakhova, E. V. and Nepogodin, A. M. 2020. Methods for detection of antibiotics in urban wastewater. *IOP Conference Series: Materials Science and Engineering*, 862 (6): 062059.

Acharya, V. V. and Chaudhuri, P. 2021. Modalities of Protein Denaturation and Nature of Denaturants. *International Journal of Pharmaceutical Sciences Review and Research*, 69 (2): 19-24.

Adeniyi, O.M., Azimov, U., Burluka, A. 2018. Algae biofuel: Current status and future applications. *Renewable and Sustainable Energy Reviews*, 90: 316–335.

Agoro, M. A., Okoh, O. O., Adefisoye, M. A. and Okoh, A. I. 2018. Physicochemical Properties of Wastewater in Three Typical South African Sewage Works. *Polish Journal of Environmental Studies,* 27 (2): 1-9.

Alonso-Riaño, P., Sánchez-Bayo, J. M., García, D. R., and González-Delgado, Á. D. 2022. Sustainable biorefinery of *Scenedesmus obliquus*: Supercritical CO_2 extraction and life cycle assessment. *Bioresource Technology, 349*: 126809.

Amenorfenyo, D. K., Huang, X., Zhang, Y., Zeng, Q., Zhang, N., Ren, J. and Huang, Q. 2019. Microalgae Brewery Wastewater Treatment: Potentials, Benefits and the

Challenges. *International Journal of Environmental Research and Public Health*, 16 (11). Doi: 10.3390/ijerph16111910

Angelidaki, I., Treu, L., Tsapekos, P., Luo, G., Campanaro, S., Wenzel, H., and Kougias, P. G. 2018. Biogas upgrading and utilization. *Bioresource Technology, 266*: 575-585.

Apandi, N. M., Muhamad, M. S., Mohamed, R. M. S. R., Sunar, N. M., Al-Gheethi, A., Gani, P. and Rahman, F. A. 2021. Optimizing of Microalgae Scenedesmus sp. Biomass Production in Wet Market Wastewater Using Response Surface Methodology. *Sustainability*, 13: 2216.

APHA. 1999a. Standard Methods for the Examination of Water and Wastewater 1000 - 3000, Methods 1000 - 3000. USA: APHA, AWWA, WEF.

APHA. 1999b. *Standard Methods for the Examination of Water and Wastewater_4000-6000*, Standard. USA: American Public Health Association, American Water Works Association, Water Environment Federation.

APHA. 1999c. *Standard Methods for the Examination of Water and Wastewater_9000-10900a*, Standard. USA: American Public Health Association, American Water Works Association, Water Environment Federation.

Aremu, M. O., Ibrahim, H. and Bamidele, T. O. 2015. Physicochemical Characteristics of the Oils Extracted from Some Nigerian Plant Foods. *Chemical and Process Engineering Research*, 32: 36-52.

Arora, N., Tripathi, S., Pruthi, P. A., Poluri, K. M. and Pruthi, V. 2020. Assessing the robust growth and lipid-accumulating characteristics of Scenedesmus sp. for biodiesel

production. *Environmental Science and Pollution Research International*, 27 (22): 27449-27456.

Asadi, Z., Abdi, H., Nnaji, M., Rajabi, H., Aminzadeh, O., Madadi, K. and Hajhashemi, Y. 2021. Flocculation process and Increasing sedimentation of total suspended solids in a clarifier. *Journal of Chemistry Letters*, 2 (2021): 82-88.

Bakare, B. F., Shabangu, K. and Chetty, M. 2017. Brewery wastewater treatment using laboratory scale aerobic sequencing batch reactor. *South African Journal of Chemical Engineering*, 24: 128-134.

Baker, L. 2022. Renewable Energy in South Africa: Progress and Challenges. *Energy Policy Journal*, 135: 1109-1124.

Bal, A., Panda, F., Pati, S. G., Anwar, T. N., Das, K. and Paital, B. 2022. Influence of Anthropogenic Activities on Redox Regulation and Oxidative Stress Responses in Different Phyla of Animals in Coastal Water via Changing in Salinity. *Water*, 14 (24): 4026

Ballotin, F. C., Cibaka, T. E., Ribeiro-Santos, T. A., Santos, E. M., Teixeira, A. P. D. C. and Lago, R. M. 2016. K_2MgSiO_4: A novel K^+ -trapped biodiesel heterogeneous catalyst produced from serpentinite $Mg_3Si_2O_5(OH)_4$. *Journal of Molecular Catalysis A: Chemical*, 422: 258-265.

Bani-Melhem, K., Bsoul, A. A., Al-Qodah, Z., Al-Ananzeh, N., Al-Kilani, M. R., Al-Shannag, M. and Bani-Salameh, W. 2023. Impact of a Sand Filtration Pretreatment Step on High-Loaded Greywater Treatment by an Electrocoagulation Technique. *Water*, 15 (5): 990.

Basso, T. P., Basso, T. O. and Basso, L. C. eds. 2021. *Biotechnological Applications of Biomass*. London, United Kingdom: IntechOpen. Available: http://dx.doi.org/10.5772/intechopen.89320 (Accessed 13/09/2022).

Beal, C. M., Gerber, L. N., Thongrod, S., Phromkunthong, W., Kiron, V., Granados, J., and Huntley, M. E. 2018. The economics of microalgae oil. *Bioresource Technology,* 267: 493-503.

Bibi, R., Ahmad, Z., Imran, M., Hussain, S., Ditta, A., Mahmood, S. and Khalid, A. 2017. Algal bioethanol production technology: A trend towards sustainable development. *Renewable and Sustainable Energy Reviews*, 71: 976-985.

Bleakley, S. and Hayes, M. 2017. Algal Proteins: Extraction, Application, and Challenges Concerning Production. *Foods*, 6 (5)

Bohleber, P., Hoffmann, H., Kerch, J., Sold, L. and Fischer, A. 2018. Investigating cold-based summit glaciers through direct access to the glacier base: a case study constraining the maximum age of Chli Titlis glacier, Switzerland. *The Cryosphere*, 12 (1): 401-412.

Bošnjaković, M. and Sinaga, N. 2020. The Perspective of Large-Scale Production of Algae Biodiesel. *Applied Sciences*, 10 (22): 8181.

Brennan, L., and Owende, P. 2010. Biofuels from microalgae—A review of technologies for production, processing, and extractions of biofuels and co-products. *Renewable and Sustainable Energy Reviews, 14* (2): 557–577.

Caporgno, M. P., Taleb, A., Olkiewicz, M., Font, J., Pruvost, J., Legrand, J. and Bengoa, C. 2015. Microalgae cultivation in urban wastewater: Nutrient removal and biomass production for biodiesel and methane. *Algal Research*, 10: 232-239.

Castro-Tapia, J. M., Dibildox-Alvarado, E. and Soria-Guerra, R. E. 2022. Effect of temperature on lipid accumulation in three green microalgae species. *African Journal of Biotechnology*, 21 (10): 464-471.

Chaudhry, R. and Varacall, M. 2018. *Biochemistry, Glycolysis*. Treasure Island (FL): StatPearls Publishing.

Chisti, Y. 2013. Raceways-based photobioreactors: Prospects and challenges. *Biotechnology Advances, 31* (7): 1408-1423.

Chuah L. F., Bokhari A., Asif S., Klemeš J. J., Dailin D. J., Enshasy H. E., Yusof A. H. M. 2022. A Review of Performance and Emission Characteristics of Engine Diesel Fuelled by Biodiesel. *Chemical Engineering Transactions*, 94: 1099-1104.

Chugh, M., Kumar, L., Shah, M. P. and Bharadvaja, N. 2022. Algal Bioremediation of heavy metals: An insight into removal mechanisms, recovery of by-products, challenges, and future opportunities. *Energy Nexus* 7: 100129. Available: https://doi.org/10.1016/j.nexus.2022.100129

Cirne, I., Boaventura, J., Guedes, Y. and Lucas, E. 2016. Methods for Determination of Oil and Grease Contents in Wastewater from the Petroleum Industry. *Chemistry & Chemical Technology*, 10 (4): 437-444.

Costa, J. A. V., Freitas, B. C. B., Santos, T. D., Mitchell, B. G. and Morais, M. G. 2019. Open pond systems for microalgal culture. In: *Biofuels from Algae*. Elsevier B.V. , 199-223.

Couper, James R., Darryl W. Hertz, and (Francis) Lee Smith. 2019. "CAPITAL COST ESTIMATION." Chap. 9.3 in *Perry's Chemical Engineers' Handbook*. 9th ed., edited by Don W. Green and Marylee Z. Southard. New York: McGraw-Hill Education. https://www.accessengineeringlibrary.com/content/book/9780071834087/toc-chapter/chapter9/section/section14

Czemierska, M., Szcze´S, A. and Jarosz-Wilkołazka, A. 2021. Physicochemical factors affecting flocculating properties of the proteoglycan isolated from Rhodococcus opacus. *Biophysical Chemistry*, 277 (2021): 106656.

Daneshvar, E., Wicker, R. J., Show, P.-L. and Bhatnagar, A. 2022. Biologically-mediated carbon capture and utilization by microalgae towards sustainable CO2 biofixation and biomass valorization – A review. *Chemical Engineering Journal*, 427: 130888.

Datri, S., Nataraj, K. S. and Lakshmana, R. A. 2023. Response Surface Methodology Statistical Tool for the Optimization of Responses. *Global Journal of Addiction & Rehabilitation Medicine*, 7 (1): 1-7.

Davis, R., Aden, A., and Pienkos, P. T. 2011. Techno-economic analysis of autotrophic microalgae for fuel production. *Applied Energy,* 88 (10): 3524-3531.

De Klein, J. J. M., Overbeek, C. C., Juncher Jørgensen, C. and Veraart, A. J. 2017. Effect of Temperature on Oxygen Profiles and Denitrification Rates in Freshwater Sediments. *Wetlands*, 37 (5): 975-983.

Delrue, F., Alvarez-Diaz, P. D., Fon-Sing, S., Fleury, G. and Sassi, J. F. 2016. The Environmental Biorefinery: Using Microalgae to Remediate Wastewater, a Win-Win Paradigm. *Energies*, 9 (3)

Department of Mineral Resources and Energy 2019. *Integrated Resource Plan 2019*. Government of South Africa.

Department of Water and Sanitation. 2017. *Blue Drop Green Drop Report: Department of Water and Sanitation Briefing*. Republic of South Africa: Department of Water and Sanitation.

Dhanjal, Sinha, A., Zhao, H., Chen, J. and Mugo, S. M. 2019. Water analysis I Determination of Chemical Oxygen Demand. In: Worsfold, P., Poole, C. and Miró, M. eds. *Encyclopedia of Analytical Science*. Third ed. 258-270.

Din, N. A. S., Mohd Alayudin, S., Sofian-Seng, N. S., Rahman, H. A., Mohd Razali, N. S., Lim, S. J. and Wan Mustapha, W. A. 2022. Brown Algae as Functional Food Source of Fucoxanthin: A Review. *Foods*, 11 (15): 2235.

D'Mello, B. R. and Chemburkar, M. S. 2018. Effect of temperature and pH variation on biomass and lipid production of *Auxenochlorella pyrenoidosa. Research Journal of Life Sciences, Bioinformatics, Pharmaceutical and Chemical Sciences* 4(6): 378-387.

Duygu, D. Y. 2019. Growth Kinetics of Scenedesmus obliquus Strains in Different Nutrient Media. LIMNOFISH, *Journal of Limnology and Freshwater Fisheries Research* 5(2): 95-103.

DWAF; WRC. 2010. South African water quality management series. Procedures to Assess Effluent Discharge Impacts. Pretoria: Department of Water Affairs and Forestry and Water Research Commission.

Eberhard, A., and Naude, R. 2016. The South African Renewable Energy Independent Power Producer Procurement Programme: A Review. Energy Research Centre, UCT.

Elgharbawy, A.S., Wagih, A.S., Olfat, M.S., Mosaad, A.K. 2021. A Review on Biodiesel Feedstocks and Production Technologies. *Journal of Chilean Chemical Society*, 66(1): 5098-5109.

Eloka-Eboka, A. C. and Inambao, F. L. 2017. Effects of CO_2 sequestration on lipid and biomass productivity in microalgal biomass production. *Applied Energy*, 195: 1100-1111.

Enitan, A. M., Adeyemo, J., Kumari, S., Swalaha, F. M. and Bux, F. 2015. Characterisation of brewery wastewater composition. *International Journal of Environmental and Ecological Engineering*, 9 (9): 1073-1076.

E. P. A. 2001. Methods for Chemical Analysis of Water and Wastes, METHOD 1684 USA: EPA.

European Commission 2020. *The European Green Deal*. Brussels, Belgium.

Ezechi, E. H., Kutty, S. R. B. M., Isa, M. H., Malakadmad, A., Ude, C. M., Menyechi, E. J. and Olisa, E. 2015. Determination of decay coefficient of biomass through endogenous respiration. *Research Journal of Microbiology*, 10 (8): 355-365.

Fazal, T., Mushtaq, A., Rehman, F., Khan, A. U., Rashid, N., Farooq, W., Rehman, M. S. U. and Xu, J. 2018. Bioremediation of textile wastewater and successive biodiesel production using microalgae. *Renewable and Sustainable Energy Reviews*, 82: 3107-3126.

Ferreira, G. F., Ríos Pinto, L. F., Carvalho, P. O., Coelho, M. B., Eberlin, M. N., Maciel Filho, R. and Fregolente, L. V. 2019. Biomass and lipid characterization of microalgae genera Botryococcus, Chlorella, and Desmodesmus aiming high-value fatty acid production. *Biomass Conversion and Biorefinery*, 10.1007/s13399-019-00566-3

Ford, W. I. and Fox, J. F. 2017. Stabilization of benthic algal biomass in a temperate stream draining agroecosystems. *Water Research*, 108: 432-443.

Gani, P., Sunar, N. M., Matias-Peralta, H. and Latiff, A. A. A. 2016. Screening of Sustainable Hydrocarbon Extracted from Microalgae via Phycoremediation. *ARPN Journal of Engineering and Applied Sciences*, 11 (12): 7431-7436.

Gani, P., Sunar, N. M., Matias-Peralta, H., Mohamed, R., Latiff, A. A. A. and Parjo, U. K. 2017. Extraction of hydrocarbons from freshwater green microalgae (Botryococcus sp.) biomass after phycoremediation of domestic wastewater. *International Journal of Phytoremediation*, 19 (7): 679-685.

Gekhman, A. E., Chistyakov, A. V., Tsodikov, M. V., Zharova, P. A., Shapovalov, S. S. and Pasynskii, A. A. 2018. The Mixture of Fatty Acids Conversion into Hydrocarbons

Over Original Pt-Sn/Al_2O_3 Catalyst. In: Anisimov, K. V., Dub, A. V., Kolpakov, S. K., Lisitsa, A. V., Petrov, A. N., Polukarov, V. P., Popel, O. S. and Vinokurov, V. A. eds. *Proceedings of Scientific-Practical Conference "Research and Development - 2016"*, Springer International Publishing, 297-304. doi:10.1007/978-3-319-62870-7_33

Ghanad, A. 2023. An Overview of Quantitative Research Methods. *International Journal of Multidisciplinary Research and Analysis*, 06 (08): 3794-3803.

Goessling, J. W. 2017. *Biophotonics of diatoms - Linking frustule structure to photobiology* (PhD thesis). PhD, University of Copenhagen.

González, L. E., Díaz, G. C., Aranda, D. a. G., Cruz, Y. R. and Fortes, M. M. 2015. Biodiesel Production Based in Microalgae: A Biorefinery Approach. *Natural Science*, 7: 358-369.

Granata, Tim. 2017. Dependency of Microalgal Production on Biomass and the Relationship to Yield and Bioreactor Scale-up for Biofuels: a Statistical Analysis of 60+ Years of Algal Bioreactor Data. *BioEnergy Research.* 10. 10.1007/s12155-016-9787-2.

Guldhe, A., Singh, B., Rawat, I., and Bux, F. 2017. Synthesis of biodiesel from Scenedesmus sp. by in situ transesterification process. *Fuel,* 187: 180-188.

Guo, W. Q., Zheng, H. S., Li, S., Du, J. S., Feng, X. C., Yin, R. L., . . . Chang, J. S. 2016. Removal of cephalosporin antibiotics 7-ACA from wastewater during the cultivation of lipid-accumulating microalgae. *Bioresource Technology*, 221: 284-290.

He, L., Chen, Y., Wu, X., Chen, S., Liu, J. and Li, Q. 2019. Effect of Physical Factors on the Growth of Chlorella Vulgaris on Enriched Media Using the Methods of Orthogonal Analysis and Response Surface Methodology. *Water*, 12 (1): 34-45.

He, Q., Yang, H., Wu, L., Hu, C., and Li, Y. 2015. Enhancement of lipid accumulation in microalgae by introducing blue light under mixotrophic culture conditions. *Bioresource Technology,* 192: 760-765.

Helliwell, K. E., Lawrence, A. D., Holzer, A., Kudahl, U. J., Sasso, S., Krautler, B., Scanlan, D. J., Warren, M. J. and Smith, A. G. 2016. Cyanobacteria and Eukaryotic Algae Use Different Chemical Variants of Vitamin B12. *Current Biology*, 26 (8): 999-1008.

Hengst, K., Arend, M., Pfützenreuter, R. and Hoelderich, W. F. 2015. Deoxygenation and cracking of free fatty acids over acidic catalysts by single-step conversion for the production of diesel fuel and fuel blends. *Applied Catalysis B: Environmental*, 174-175: 383-394.

Hicks, T. D., Kuns, C. M., Raman, C., Bates, Z. T. and Nagarajan, S. 2022. Simplified Method for the Determination of Total Kjeldhal Nitrogen in Wastewater. *Environments*, 9 (5): 55.

Hodgkinson, A. J., Cakebread, J., Callaghan, M., Harris, P., Brunt, R., Anderson, R. C., Armstrong, K. M. and Haigh, B. 2017. Comparative innate immune interactions of human and bovine secretory IgA with pathogenic and non-pathogenic bacteria. *Developmental and Comparative Immunology*, 68: 21-25.

Holdt, S. L.; Christensen, L.; Iversen, J. J. L. . 2014. A novel closed system bubble column photobioreactor for detailed characterisation of micro- and macroalgal growth. *Journal of Applied Phycology,* 26(2), 825–835. doi:10.1007/s10811-013-0190-5

Huang, J., Ying, J., Fan, F., Yang, Q., Wang, J. and Li, Y. 2016. Development of a novel multi-column airlift photobioreactor with easy scalability using computational fluid dynamics simulations and experiments. *Bioresource Technology*, 222: 399-407

Ibarra, L. G. B. 2015. *Impact of water activity on the mineralogy of hydrated cement* (PhD Thesis). PhD in Cement and Concrete Science, Materials Engineering, Ecole Polytechnique Fédérale de Lausanne.

IEA 2022. *China's Energy Policy Review 2022*. International Energy Agency.

IEA 2023. *The Role of Policy in the U.S. Energy Transition*. International Energy Agency.

IRENA 2020. *End-of-Life Management for Solar Photovoltaic Panels*. International Renewable Energy Agency.

James, E. K. 2017. Nitrogen Fixation. In: Thomas, B., Murray, B. G. and Murphy, D. J. eds. *Encyclopedia of Applied Plant Sciences*. Second ed. Elsevier.

Jebrail, A. 2016. *Wastewater Treatment Pro*cess (Bachelor's thesis). Bachelor's Degree, Hame University of Applied Sciences.

Jubb, A. I. 2015. Determination of Volatile Solids in Wastewater Sample. *Environmental measurement lab*, Journal Article: http://site.iugaza.edu.ps/nkaheil/files/2016/2009/Lab_2071.pdf.

Judd, S., and Jefferson, B. 2003. Membrane bioreactors for wastewater treatment. *Water Science and Technology, 47*(1): 191-200.

Jyothi, K., Krishna, P. M. and Mohan, N. R. G. 2016. Algae in Fresh Water Ecosystem. *Phykos*, 46 (1): 25-31.

Kabdash, I., Tunay, O. and Orhon, D. 2022. Chemically Enhanced Biodegradation of High Organic Matter in Wastewater - Confectionery Plant Effluents. *Biointerface Research in Applied Chemistry*, 12 (5): 6608-6617.

Kainth, G. S. 2015. *Removal of Turbidity from Water using Low-Cost Adsorbents*. Bachelor of Technology, National Institute of Technology.

Karki, B. 2016. *Water quality measurement by a water sensor: Testing a sample from a peat production area by an optical sensor* (Bachelor's thesis). Bachelor in Engineering, Helsinki Metropolia University of Applied Sciences.

Kim, S. Y., Park, J. W., Noh, J. H., Bae, Y. H. and Maeng, S. K. 2022. Potential organic matter management for industrial wastewater guidelines using advanced dissolved organic matter characterization tools. *Journal of Water Process Engineering*, 46: 102604.

Kim, Y., Kim, H., Beuchat, L. R. and Ryu, J.-H. 2018. Development of non-pathogenic bacterial biofilms on the surface of stainless steel which are inhibitory to Salmonella enterica. *Food Microbiology*, 69: 136-142.

Klinthong, W., Yang, Y.-H., Huang, C.-H. and Tan, C.-S. 2015. A Review: Microalgae and Their Applications in CO_2 Capture and Renewable Energy. *Aerosol and Air Quality Research*, 15 (2): 712-742.

Koh, S. H. and Shaw, A. R. 2017. Gaseous Emissions from Wastewater Facilities. *Water Environmental Research*, 89 (10): 1268-1280.

Konga, A. K., Muchandi, A. S. and Ponnaiah, G. P. 2016. Soxhlet extraction of *Spirogyra sp*. algae: an alternative fuel. *Biofuels* 8(1): 29-35.

Krishnan, S., Zulkapli, N. S., Kamyab, H., Taib, S. M., Din, M. F. B. M., Majid, Z. A., Chaiprapat, S., Kenzo, I., Ichikawa, Y., Nasrullah, M., Chelliapan, S. and Othman, N. 2021. Current technologies for recovery of metals from industrial wastes: An overview. *Environmental Technology & Innovation* 22: 101525. Available: https://doi.org/10.1016/j.eti.2021.101525

Krustok, I. 2016. Microbiological analysis of municipal wastewater treating photobioreactors (PhD Thesis). PhD, Mälardalen University.

Kube, M., Jefferson, B., Fan, L. and Roddick, F. 2018. The impact of wastewater characteristics, algal species selection and immobilisation on simultaneous nitrogen and phosphorus removal. *Algal Research* 10.1016/j.algal.2018.01.009. Available: https://doi.org/10.1016/j.algal.2018.01.009

Kukwa, D. T. and Chetty, M. 2022. Biomass Production and Simultaneous Minerals Sequestration from Brewery Wastewater with Concomitant Lipid Accumulation Using Algae. *Chemical Engineering Transactions*, 96: 475-480.

Kukwa, D. T. and Chetty, M. 2020. Microalgae: The Multifaceted Biomass of the 21st Century. In: Basso, T. P., Basso, T. O. and Basso, L. C. eds. *Biotechnological Applications of Biomass* online: IntechOpen, 355-382. Available:

https://www.intechopen.com/online-first/microalgae-the-multifaceted-biomass-of-the-21st-century (Accessed 20/12/2020).

Kulkarni, B., Wanjule, R. V. and Shinde, H. H. 2018. Study On Sewage Quality From Sewage Treatment Plant At Vashi, Navi Mumbai. *Materials Today: Proceedings*, 5 (1): 1859-1863.

Kullberg, R. 2016. Polyphosphate: The impact of polyphosphate on growth and nutrient uptake of Pelargonium x hortorum 'Mårbacka' and Petunia x hybrida 'Origami Watermelon'. (Master's Thesis). Master of Science, Swedish University of Agricultural Science. Available: http://stud.epsilon.slu.se (Accessed

Kumar, A. 2016. *Wastewater Treatment Processes* (online). Available: http://web.iitd.ac.in/~arunku/files/CVL100_Y16/LecSep1220.pdf (Accessed

Kumar, N., Banerjee, C. and Jagadevan, S. 2021. Identification, characterisation, and lipid profiling of microalgae *Scenedesmus sp*. NC1, isolated from coal mine effluent with potential for biofuel production. *Biotechnology Reports*, 30: e00621.

Labconco. 2019. *A guide to freeze-drying for the laboratory: An Industry Service Publication*. Available: https://pim-resources.coleparmer.com/data-sheet/labconco-guide-freeze-dry-in-lab.pdf (Accessed 12/02/2022).

Laurens, L. M. L., Markham, J., Templeton, D. W., Christensen, E. D., Van Wychen, S., Vadelius, M. S., ... and Pienkos, P. T. 2017. Development of algae biorefinery concepts for biofuels and bioproducts: Current status and future research. *Biofuels, Bioproducts and Biorefining,* 11(1): 110-129.

Lee, C.-H., Chae, H.-S., Lee, S.-H. and Kim, H. S. 2015. Growth characteristics and lipid content of three Korean isolates of *Botryococcus braunii* (Trebouxiophyceae). *Journal of Ecology and Environment*, 38 (1): 67-74.

Leitzen, S., Vogel, M., Steffens, M., Zapf, T., Müller, C. E. and Brandl, M. 2021. Quantification of Degradation Products Formed during Heat Sterilization of Glucose Solutions by LC-MS/MS: Impact of Autoclaving Temperature and Duration on Degradation. *Pharmaceuticals*, 14 (11): 1121.

Li, T., and Wang, X. 2016. Recent progress in the Synthesis and Biological Activities of Oxime-containing Heterocycles. *Chemistry Central Journal,* 10(1): 1-18.

Lima, G. M., Teixeira, P. C. N., Teixeira, C. M. L. L., Filócomo, D. and Lage, C. L. S. 2018. Influence of spectral light quality on the pigment concentrations and biomass productivity of Arthrospira platensis. *Algal Research*, 31: 157-166.

Lin, C.-Y., Nguyen, M.-L. T. and Lay, C.-H. 2017. Starch-containing textile wastewater treatment for biogas and microalgae biomass production. *Journal of Cleaner Production*, 168: 331-337.

Lin, S., Mackey, H. R., Hao, T., Guo, G., Van Loosdrecht, M. C. M. and Chen, G. 2018. Biological sulfur oxidation in wastewater treatment: A review of emerging opportunities. *Water Research*, 143: 399-415.

Liu, Y., Zhao, M., Lu, X., Sun, W., and Zhang, X. 2016. Asymmetric allylic alkylation of cyclic ketimines with allylic alcohols catalysed by chiral spiro palladium (II) pyrrolidine-oxime complexes. *Royal Society of Chemistry Advances*, 6(91): 88122-88127.

Liu, X., Hou, W., Dong, H., Wang, S., Jiang, H., Wu, G., Yang, J. and Li, G. 2015. Distribution and Diversity of Cyanobacteria and Eukaryotic Algae in Qinghai–Tibetan Lakes. *Geomicrobiology Journal*, 33 (10): 860-869.

Logan, B. E., Hamelers, B., Rozendal, R., Schröder, U., Keller, J., Freguia, S., and Rabaey, K. 2006. Microbial fuel cells: Methodology and technology. *Environmental Science & Technology, 40*(17): 5181-5192.

Lukubye, B. and Andama, M. 2017. Physico-Chemical Quality of Selected Drinking Water Sources in Mbarara Municipality, Uganda. *Journal of Water Resource and Protection*, 09 (07): 707-722.

Macdonald, R. K. 2015. *Turbidity and Light Attenuation in Coastal Waters of the Great Barrier Reef* (Doctoral Thesis). Doctor of Philosophy Ph.D, James Cook University.

Machín-Sánchez, M., Gil-Rodríguez, M. C. and Haroun, R. 2018. Phylogeography of the Red Algal Laurencia Complex in the Macaronesia Region and Nearby Coastal Areas: Recent Advances and Future Perspectives. *Diversity*, 10 (1): 10-31.

Mahmoud, R. H., Wang, Z. and He, Z. 2022. Production of algal biomass on electrochemically recovered nutrients from anaerobic digestion centrate. *Algal Research*, 67: 102846.

Maltsev, Y., Kulikovskiy, M. and Maltseva, S. 2023. Nitrogen and phosphorus stress as a tool to induce lipid production in microalgae. *Microb Cell Fact*, 22 (1): 239.

Mannaa, M. and Kim, K. D. 2018. Biocontrol Activity of Volatile-Producing *Bacillus megaterium* and *Pseudomonas protegens* against *Aspergillus* and *Penicillium* spp. +Predominant in Stored Rice Grains: Study II, *Mycobiology*, 46 (1): 52-63.

Martonen, K. 2017. *Cultivation of Microalgae in Wastewater - Water treatment and biomass production* (Master's Thesis). Master of Science in Technology, University of Vaasa.

Marudhar. 2019. Identifying Variables. *International Journal of Science and Research*, 8 (3): 865-868.

Mata, T. M., Martins, A. A., and Caetano, N. S. 2010. Microalgae for biodiesel production and other applications: A review. *Renewable and Sustainable Energy Reviews, 14* (1): 217–232.

Maxil, J. A. E. 2015. Heat modelling of wastewater in sewer networks: Determination of thermal energy content from sewage with modelling tools (Master's Thesis). Master in Environmental Engineering, Delft University of Technology.

Mazur, D. M. and Lebedev, A. T. 2022. Transformation of Organic Compounds during Water Chlorination/Bromination: Formation Pathways for Disinfection By-Products (A Review). *Journal of Analytical Chemistry*, 77 (14): 1705–1728.

Mehta, P., Singh, D., Saxena, R., Rani, R., Gupta, R. P., Puri, S. K. and Mathur, A. S. 2018. High-Value Coproducts from Algae - An Innovational Way to Deal with Advance Algal Industry. In: al., R. R. S. e. ed. *Waste to Wealth*. Singapore: Springer Nature, 343-363.

Michels MH, van der Goot AJ, Norsker NH, Wijffels RH. 2010. Effects of shear stress on the microalgae *Chaetoceros muelleri. Bioprocess and Biosystems Engineering.* 33(8):921-7.

Michels MHA, van der Goot AJ, Vermuë MH, Wijffels RH. 2016. Cultivation of shear stress sensitive and tolerant microalgal species in a tubular photobioreactor equipped with a centrifugal pump. *Journal of Applied Phycology*. 28(1): 53-62.

Michiel H. A. Michels; Atze J. van der Goot; Niels-Henrik Norsker; René H. Wijffels. 2010. Effects of shear stress on the microalgae *Chaetoceros muelleri*. , 33(8): 921–927.

Mickley, M. 2019. Review of zero liquid discharge treatment technologies. *Desalination and Water Treatment, 172*: 3-11.

Mohapatra, S., Padhye, L. P. and Mukherji, S. 2018. Challenges in Detection of Antibiotics in Wastewater Matrix. In: Gupta, T., Agarwal, A. K., Agarwal, R. A. and Labhsetwar, N. K. eds. *Environmental Contaminants: Measurement, Modelling and Control*. Singapore: Springer Singapore, 3-20. Available: https://doi.org/10.1007/978-981-10-7332-8_1

Molobela, I. P., and Sinha, P. 2011. Management of water resources in South Africa: A review. *African Journal of Environmental Science and Technology*, 5(12): 993-1002.

Morales-Amaral, M. M., Gomez-Serrano, C., Acién, F. G., Fernández-Sevilla, J. M., and Molina-Grima, E. 2015. Outdoor production of Scenedesmus sp. in raceway reactors: Influence of culture conditions on productivity and biomass composition. *Bioresource Technology,* 187: 184-190.

Morales-Sánchez, D., Schulze, P. S. C., Kiron, V. and Wijffels, R. H. 2020. Production of carbohydrates, lipids and polyunsaturated fatty acids (PUFA) by the polar marine microalga Chlamydomonas malina RCC2488. *Algal Research*, 50: 102016.

Moreno-García, L., Adjallé, K., Barnabé, S., and Raghavan, G. S. V. 2017. Microalgae biomass production for a biorefinery system: Recent advances and the way towards sustainability. *Renewable and Sustainable Energy Reviews, 76*: 493-506.

Mostafa, M. K., Elshafei, M. M. and Peters, R. W. 2015. Improve Water Quality at the El-Rahawy Drain and the Rosetta Branch, Egypt. *Journal of Environmental Protection*, 06 (10): 1139-1148.

Moussa, D. T., El-Naas, M. H., Nasser, M., and Al-Marri, M. J. 2017. A comprehensive review of electrocoagulation for water treatment. *Chemical Engineering Journal, 330*: 414-432.

Mujtaba, G. and Lee, K. 2017. Treatment of real wastewater using co-culture of immobilized *Chlorella vulgaris* and suspended activated sludge. *Water Research*, 120: 174-184.

Naidoo, D. 2018. Day Zero on the back of drought in Southern Africa: Lessons for the future. *The Water Wheel,* 17 (2): 4-5.

Najafabadi, H. A., Malekzadeh, M., Jalilian, F., Vossoughi, M. and Pazuki, G. 2015. Effect of various carbon sources on biomass and lipid production of Chlorella vulgaris during nutrient sufficient and nitrogen starvation conditions. *Bioresource Technology*, 180: 311-317.

National Treasury (2019). *Carbon Tax Act 2019*. Government of South Africa.

Newinger, C. 2015. The Barrier Layer and Ocean Colour in the Amazon and Orinoco Plume: Competing for the Oceanic Control on Tropical Cyclone Intensity (PhD Thesis). PhD, Imperial College London.

Nielsen, A. 2015. Treatment of wastewater with microalgae under mixotrophic growth: A focus on removal of DOC from municipal and industrial wastewater (Degree Thesis in Geoecology). Master of Science in Geoecology, Umeå Universitet.

Nzayisenga, J. C., Farge, X., Groll, S. L. and Sellstedt, A. 2020. Effects of light intensity on growth and lipid production in microalgae grown in wastewater. *Biotechnol Biofuels*, 13: 4.

Ogbonna, I. O., Ikwebe, J., Ogbonna, J. C., Eze, C. N. and Ndrimbula, J. B. 2022. Effects of light intensity and photoperiod on growth, lipid accumulation and fatty acid composition of Desmodesmus subspicatus LC172266 under photoautotrophic cultivation. *Nigerian Journal of Biotechnology*, 38 (2): 1-13.

Oluogun, M. O., Aladeitan, Y., Omolara I. and Atanda, B. 2021. Extraction and Characterisation of Oil from Algae. *International Journal of Science and Research*, 10 (5): 143-147.

Osman, M. E. H., Abo-Shady, A. M., Gheda, S. F., Desoki, S. M. and Elshobary, M. E. 2023. Unlocking the potential of microalgae cultivated on wastewater combined with salinity stress to improve biodiesel production. *Environmental Science and Pollution Research* 30 (53): 114610-114624.

Osuoha, J. O., Anyanwu, B. O. and Ejileugha, C. 2023. Pharmaceuticals and personal care products as emerging contaminants: Need for combined treatment strategy. *Journal of Hazardous Materials Advances*, 9 (2023): 100206.

Oturan, M. A., and Aaron, J. J. 2014. Advanced oxidation processes in water/wastewater treatment. *Environmental Science and Pollution Research, 21* (14): 8493-8524.

Palmer, M. and Hatley, H. 2018. The role of surfactants in wastewater treatment: Impact, removal and future techniques: A critical review. *Water Research*, 147 (4): 60-72.

Patel, A., Arora, N., Sartaj, K., Pruthi, P. A., and Pruthi, V. 2020. Sustainable biodiesel production from oleaginous microbes: A critical review. *Renewable and Sustainable Energy Reviews,* 128: 109876.

Pham, T.-L., Dao, T.-S., Bui, H., Pham, T., Ngo, T. and Bui, H. 2020. Lipid Production Combined with Removal and Bioaccumulation of Pb by Scenedesmus sp. Green Alga. *Polish Journal of Environmental Studies*, 29 (2): 1785-1791.

Phanwilai, S., Noophan, P., Li, C.-W. and Choo, K.-H. 2020. Effect of COD:N ratio on biological nitrogen removal using full-scale step-feed in municipal wastewater treatment plants. *Sustainable Environment Research*, 30 (1): 24.

Piligaev, A. V., Sorokina, K. N., Shashkov, M. V. and Parmon, V. N. 2018. Screening and comparative metabolic profiling of high lipid content microalgae strains for application in wastewater treatment. *Bioresource Technology*, 250: 538–547.

Pittman, J. K., Dean, A. P., and Osundeko, O. 2011. The potential of sustainable algal biofuel production using wastewater resources. *Bioresource Technology,* 102 (1): 17-25.

Qu, X., Alvarez, P. J., and Li, Q. 2013. Applications of nanotechnology in water and wastewater treatment. *Water Research, 47* (12): 3931-3946.

Quinn, J. C., & Davis, R. (2015). The potentials and challenges of algae-based biofuels: A review of techno-economic, life cycle, and resource assessment modeling. *Bioresource Technology, 184, 444-452.*

Qureshimatva, U. M., Maurya, R. R., Gamit, S. B., Patel, R. D. and Solanki, H. A. 2015. Determination of Physico-Chemical Parameters and Water Quality Index (Wqi) of Chandlodia Lake, Ahmedabad, Gujarat, India. *Journal of Environmental & Analytical Toxicology*, 05 (04)

Ramanna, L. 2015. *Lab-scale assessment and adaptation of wastewater for cultivation of microalgal biomass for biodiesel production* (Master Thesis). Master of Applied Science in Biotechnology, Durban University of Technology.

Rashed, A. M., Hetta, A. M. A., Hashem, Z. S., El-Katatny, M. M. H. and 2020. Validation of moist and dry heat processes used for sterilization and depyrogenation during ampoules manufacturing. *Journal of Advanced Biomedical and Pharmaceutical Sciences*, 3: 177-183.

Rashid, N., Park, W.-K. and Selvaratnam, T. 2018. Binary culture of microalgae as an integrated approach for enhanced biomass and metabolites productivity, wastewater treatment, and bioflocculation. *Chemosphere*, 194: 67-75.

Rastogi, R. P., Pandey, A., Larroche, C. and Madamwar, D. 2018. Algal Green Energy – R&D and technological perspectives for biodiesel production. *Renewable and Sustainable Energy Reviews*, 82: 2946-2969.

Rawat, I., Ranjith Kumar, R., Mutanda, T., and Bux, F. 2011. Dual role of microalgae: Phycoremediation of domestic wastewater and biomass production for sustainable biofuels production. *Applied Energy, 88*(10), 3411–3424.

Razzak, S. A., Bahar, K., Islam, K. M. O., Haniffa, A. K., Faruque, M. O., Hossain, S. M. Z. and Hossain, M. M. 2023. Microalgae cultivation in photobioreactors: Sustainable solutions for a greener future. In: *Green Chemical Engineering*.

Razzak, S. A., Hossain, M. M., Lucky, R. A., Bassi, A. S., and De Lasa, H. 2013. Integrated CO_2 capture, wastewater treatment, and biofuel production by microalgae culturing—A review. *Renewable and Sustainable Energy Reviews,* 27: 622-653.

Richardson, M. J. 2017. *The Analysis of Water Availability Indicators And Access to Available Water In The Developing, Semi-Arid, Rural Setting* (Master's Thesis). Master of Science in Natural Resources and Environmental Sciences, University of Illinois at Urbana-Champaign.

Richardson, J. W., Johnson, M. D., Outlaw, J. L., and Holtzapple, M. 2012. A financial assessment of two alternative cellulosic biofuel technologies. *Biomass and Bioenergy,* 46: 287-300.

Rinna, F., Buono, S., Cabanelas, I. T. D., Nascimento, I. A., Sansone, G. and Barone, C. M. A. 2017. Wastewater treatment by microalgae can generate high-quality biodiesel feedstock. *Journal of Water Process Engineering*, 18: 144-149.

Robillard, D., Gabel, D. and Williams, T. O. 2018. FOG Waste receiving and processing facility design considerations. *Water Practice and Technology*, 13 (1): 164-171.

Rohit, M. V. and Venkata Mohan, S. 2018. Quantum Yield and Fatty Acid Profile Variations With Nutritional Mode During Microalgae Cultivation. *Front Bioeng Biotechnology*, 6: 111.

Saad, G. M, Dosoky, S. N., Zoromba,S. M., and Shafik, M. H. 2019. Algal Biofuels: Current Status and Key Challenges. *Energies*, 12 (10): 1-14.

Sahoo, S., Mahapatra, S. R., Das, N., Parida, B. K., Rath, S., Misra, N. and Suar, M. 2020. Functional elucidation of hypothetical proteins associated with lipid accumulation: Prioritizing genetic engineering targets for improved algal biofuel production. *Algal Research*, 47: 101887.

Sakarika, M. and Kornaros, M. 2016. Effect of pH on growth and lipid accumulation kinetics of the microalga Chlorella vulgaris grown heterotrophically under sulfur limitation. *Bioresource Technology*, 219: 694-701.

Sakthivela, R., Ramesh, K., Purnachandrana, R. and Shameera, P. M. 2018. A review of the properties, performance and emission aspects of the third-generation biodiesels. *Renewable and Sustainable Energy Reviews* 82: 2970–2992.

Samy, R., Abdelmonem, N., Ismail, I. and Abdelghany, A. R. 2022. Removal techniques of ammonia from drinking water and wastewater in Egypt and developing countries: a review study. Paper presented at the International Conference on Chemistry and Environmental Engineering (ICEE-11) *Journal of Physics: Conference Series*. Alexandria, Egypt, IOP Publishing, 24

Sánchez Mirón, A., Contreras Gómez, A., García Camacho, F., Molina Grima, E., and Chisti, Y. 2000. Comparative evaluation of compact photobioreactors for large-scale monoculture of microalgae. *Journal of Biotechnology, 70* (1-3): 249-270.

Shrestha, N., Dandinpet, K. K. and Schneegurt, M. A. 2020. Effects of Nitrogen and Phosphorus Limitation on Lipid Accumulation by Chlorella kessleri str. UTEX 263 Grown in Darkness. *Journal of Applied Phycology*, 32 (5): 2795-2805.

Shukla, M. and Kumar, S. 2018. Algal growth in photosynthetic algal microbial fuel cell and its subsequent utilization for biofuels. *Renewable & Sustainable Energy Reviews*, 82: 402-414.

Sierra, E., Acien, F. G., Fernandez, J. M., Garcia, J. L., Gonzalez, C., and Molina, E. 2008. Characterization of a flat-panel photobioreactor for the production of microalgae. *Chemical Engineering Journal,* 138(1-3): 136-147.

Sigdel, B. 2017. *Water Quality Measuring Station pH, Turbidity and temperature measurement* (Bachelor's Thesis). Bachelor's Degree, Helsinki Metropolia University of Applied Sciences.

Singh, P., Guldhe, A., Kumari, S., Rawat, I. and Bux, F. 2015. Investigation of the combined effect of nitrogen, phosphorus and iron on lipid productivity of microalgae Ankistrodesmus falcatus KJ671624 using response surface methodology. *Biochemical Engineering Journal*, 94: 22-29.

Sivaramakrishnan, R., Suresh, S., Pugazhendhi, A., Mercy Nisha Pauline, J. and Incharoensakdi, A. 2020. Response of Scenedesmus sp. to microwave treatment:

Enhancement of lipid, exopolysaccharide and biomass production. *Bioresource Technology,* 312: 123562. Available: https://doi.org/10.1016/j.biortech.2020.123562

Sorigue, D., Legeret, B., Cuine, S., Morales, P., Mirabella, B., Guedeney, G., Li-Beisson, Y., Jetter, R., Peltier, G. and Beisson, F. 2016. Microalgae Synthesize Hydrocarbons from Long-Chain Fatty Acids via a Light-Dependent Pathway. *Plant Physiology*, 171 (4): 2393-2405.

Srirangan, S., Sauer, M.-L., Howard, B., Dvora, M., Dums, J., Backman, P. and Sederoff, H. 2015. Interaction of Temperature and Photoperiod Increases Growth and Oil Content in the Marine Microalgae *Dunaliella viridis. PLOS ONE*, 10 (5): e0127562.

Su, M., Dell'orto, M., Scaglia, B., D'imporzano, G., Bani, A. and Adani, F. 2022. Growth Performance, Biochemical Composition and Nutrient Recovery Ability of Twelve Microalgae Consortia Isolated from Various Local Organic Wastes Grown on Nano-Filtered Pig Slurry. *Molecules*, 27 (2): 422.

Subhash, G. V., Rajvanshi, M., Kumar, B. N., Govindachary, S., Prasad, V. and Dasgupta, S. 2017. Carbon streaming in microalgae: extraction and analysis methods for high-value compounds. *Bioresource Technology*, 244 (Pt 2): 1304-1316.

Sultana, N., Hossain, S. M. Z., Mohammed, M. E., Irfan, M. F., Haq, B., Faruque, M. O., Razzak, S. A. and Hossain, M. M. 2020. Experimental study and parameters optimization of microalgae-based heavy metals removal process using a hybrid response surface methodology-crow search algorithm. *Scientific Reports* 10(1): 15068. Available: https://doi.org/10.1038/s41598-020-72236-8

Sunday, K., Henrietta, O. and Monday, M. 2017. Physicochemical and Mineral Compositions of Wastewater and Soils from Two Selected Abattoirs in Warri, Delta State, Nigeria. *International Journal of Sciences*, 3 (11): 29-33.

Sutherland, D. L., Howard-Williams, C., Turnbull, M. H., Broady, P. A. and Craggs, R. J. 2015. Enhancing microalgal photosynthesis and productivity in wastewater treatment high rate algal ponds for biofuel production. *Bioresource Technology*, 184: 222-229.

Suwarno, S. and Nasir, M. 2020. Effect of Sulphuric Acid Concentration on the Corrosion Rate of ASTM A213-T12 Steel. *Key Engineering Materials*, 867: 213-217.

Tan, Jia Sen; Lee, Sze Ying; Chew, Kit Wayne; Lam, Man Kee; Lim, Jun Wei; Ho, Shih-Hsin; Show, Pau Loke. 2020. A Review on Microalgae Cultivation and Harvesting, and Their Biomass Extraction Processing Using Ionic Liquids. *Bioengineered,* 21655979.2020.1711626–. doi:10.1080/21655979.2020.171162

Tan, Z., Zhang, Z. and Liu, L. 2022. Application of inorganic chemicals in industrial wastewater treatment. *E3S Web of Conferences*, 358: 02058.

Tan, X-B., Zhao, X-C., Zhang, Y-L., Zhou, Y-Y., Yang, L-B., Zhang, W-W. 2017. Enhanced lipid and biomass production using alcohol wastewater as a carbon source for *Chlorella pyrenoidosa* cultivation in anaerobically digested starch wastewater outdoors, *Bioresource Technology,* 247: 784-793

Taylor, M., Elliott, H. A. and Navitsky, L. O. 2018. Relationship between total dissolved solids and electrical conductivity in Marcellus hydraulic fracturing fluids. *Water Science and Technology*, 77 (7-8): 1998-2004.

Turgeon, G., Kutz, S. J., Lejeune, M., St-Laurent, M.-H. and Pelletier, F. 2018. Parasite prevalence, infection intensity and richness in an endangered population, the Atlantic-Gaspesie caribou. *International Journal for Parasitology Parasites and Wildlife*, 7 (1): 90-94.

Udaiyappan, A. F. M., Hasan, H. A., Takriff, M. S. and Abdullah, S. R. S. 2017. A review of the potentials, challenges and current status of microalgae biomass applications in industrial wastewater treatment. *Journal of Water Process Engineering*, 20: 8–21.

Udayan A, Pandey AK, Sirohi R, Sreekumar N, Sang BI, Sim SJ, Kim SH, Pandey A. 2022. Production of microalgae with high lipid content and their potential as sources of nutraceuticals. *Phytochemistry Reviews.* 23:1-28. doi: 10.1007/s11101-021-09784-y.

Ugwu, C. U., Aoyagi, H., and Uchiyama, H. 2008. Photobioreactors for mass cultivation of algae. *Bioresource Technology, 99* (10): 4021-4028.

UKEssays. November 2018. Analysis of Response Surface Methodology (RSM). [online]. Available from: https://www.ukessays.com/essays/sciences/analysis-response-surface-methodology-9308.php?vref=1 [Accessed 28 February 2022].

Unfccc. 2008. Kyoto Protocol Reference Manual on Accounting of Emissions and Assigned Amount. Climate Change Secretariat (UNFCCC): United Nations.

US EPA. 2023. Title 40, Code of Federal Regulations (CFR): Protection of Environment, eCFR: Title 40 of the CFR -- Protection of Environment. Accessed: 26/10/2023.

Van Der Merwe, I. S. W. and Brink, I. C. 2018. Development of a deterministic design model for a high-rate algal pond. *Water South Africa*, 44 (4): 612-623

Van Wagenen, J. M., Angelidaki, I., De Francisci, D. and Holdt, S. L. 2016. *Cultivation of microalgae in industrial wastewaters* (PhD Thesis), Technical University of Denmark.

Vidyashankar, S., Venugopal, K. S., Swarnalatha, G. V., Kavitha, M. D., Chauhan, V. S., Ravi, R., Bansal, A. K., Singh, R., Pande, A., Ravishankar, G. A. and Sarada, R. 2015. Characterisation of fatty acids and hydrocarbons of chlorophycean microalgae towards their use as a biofuel source. *Biomass and Bioenergy*, 77: 75-91.

Vymazal, J. 2011. Constructed wetlands for wastewater treatment: Five decades of experience. *Environmental Science & Technology, 45* (1): 61-69.

Wall, D. M., Dumont, M. and Murphy, J. D. 2018. *Facilitating a future green gas grid through the production of renewable gas* San Francisco, USA: IEA Bioenergy.

Wanda, F. M., Matuha, M., Magezi, G., Nabwire, R. and Amondito, B. 2021. Potential Impacts of Oil and Grease on Algae, Invertebrates and Fish in the Bujagali Hydropower Project Area. *Uganda Journal of Agricultural Sciences*, 20 (2): 23-35.

Wang C, Lan CQ. 2018. Effects of shear stress on microalgae - A review. *Biotechnology Advancements*. 36 (4): 986-1002.

Wang, S., Sirbu, D., Thomsen, L., Kuhnert, N., Ullrich, M. S. and Thomsen, C. 2019. Comparative lipidomic studies of Scenedesmus sp. (Chlorophyceae) and Cylindrotheca closterium (Bacillariophyceae) reveal their differences in lipid production under nitrogen starvation. *Journal of Phycology*, 55 (6): 1246-1257.

Wiczkowski, W., and Szawara-Nowak, D. 2017. Formation of oximes from carbonyl compounds: A Review. *Reviews in Analytical Chemistry*, 47 (30): 207-224

Wu, S., Gu, W., Huang, A., Li, Y., Kumar, M., Lim, P. E., . . . Wang, G. 2019. Elevated CO_2 improves both lipid accumulation and growth rate in the glucose-6-phosphate dehydrogenase-engineered Phaeodactylum tricornutum. *Microbial Cell Factories*, 18 (1): 161.

Wu, Z., Duangmanee, P., Zhao, P., Juntawong, N. and Ma, C. 2016. The Effects of Light, Temperature, and Nutrition on Growth and Pigment Accumulation of Three *Dunaliella salina* Strains Isolated from Saline Soil. *Jundishapur Journal of Microbiology*, 9 (1): e26732.

Wychen, S. V. and Laurens, L. M. L. 2015. *Determination of Total Carbohydrates in Algal Biomass: Laboratory Analytical Procedure (LAP)*. NREL, U.S. Department of Energy. Available: www.nrel.gov/publications (Accessed 17/05/2019).

Xiao, Y., Ruan, C., and Xu, J. 2020. Advances in photobioreactor design for algal biofuel production. *Renewable Energy, 156*: 519-530.

Xie, Z., Pei, H., Zhang, L., Yang, Z., Nie, C., Hou, Q. and Yu, Z. 2020. Accelerating lipid production in freshwater alga *Chlorella sorokiniana* SDEC-18 by seawater and ultrasound during the stationary phase. *Renewable Energy*, 161: 448-456.

Xue, Z., Yu, Y., Yu, W., Gao, X., Zhang, Y., and Kou, X. 2020. Development Prospect and Preparation Technology of Edible Oil From Microalgae. *Frontiers in Marine Science.* 7: 402. doi: 10.3389/fmars.2020.00402

Yaakob, M. A., Mohamed, R. M. S. R., Al-Gheethi, A., Gokare, R. A. and Ambati, R. R. 2021. Influence of Nitrogen and Phosphorus on Microalgal Growth, Biomass, Lipid, and Fatty Acid Production: An Overview. *Cells*, 10 (2): 393.

Yap, Y. H., Lim, P. E., Yusoff, F. M., and Yow, Y. Y. 2014. Direct conversion of wet microalgae to biodiesel using supercritical methanol. *Bioresource Technology,* 155: 330-333.

Yuan, X., Liu, F., Zhou, H., Liu, B., Li, G., Yan, P., . . . Niu, F. 2023. A simulation study on enhancing sterilization efficiency in medical plastics through gamma radiation optimization. *Scientific Reports*, 13 (1): 20289.

Zhang, M., Ning, R., Zheng, Q. and Gao, K. 2023. Microalgae-based biotechnology as a promising strategy for removing antibiotics from wastewater: opportunities, challenges and future directions. *Frontiers of Bioengineering and Biotechnology* 11: 1248765.

Zhang, X., Xu, J., and Sun, S. 2020. Effects of light quality and intensity on the growth and lipid accumulation of microalgae for biofuel production. *Bioresource Technology Reports,* 11: 100499.

Zhimiao, Z., Xinshan, S., Wei, W., Yanping, X., Zhijie, G., Yuhui, W., Yufeng, Z., Yu, C. and Mengyuan, M. 2016. Influences of iron and calcium carbonate on wastewater treatment performances of algae-based reactors. *Bioresource Technology*, 216: 1-11.

Zhou, W., Min, M., Li, Y., Hu, B., Ma, X., Cheng, Y., Liu, Y., Chen, P., & Ruan, R. (2012). A hetero-photoautotrophic two-stage cultivation process to improve

wastewater nutrient removal and enhance algal lipid accumulation. *Bioresource Technology, 110*: 448–455.

Zhou, Y., Tian, Y., Jiang, S., Luo, H., and Li, X. 2020. Application of artificial intelligence in wastewater treatment. *Journal of Environmental Management, 263*: 110402.

Zielinski, M., Debowski, M., Kazimierowicz, J. and ´Swica, I. 2023. Microalgal Carbon Dioxide (CO_2) Capture and Utilization from the European Union Perspective. *Energies* 16: 1446

APPENDICES

A Wastewater Characterisation

(i) Total solids (TS) computation

Initial weight of the Crucible (W_1) = ……..g

Final weight of the Crucible + sample (W_2) = ……..g

Weight of residue (W) = W_2 - W_1 g

Amount of total solids present in the sample $= \frac{1000*1000w}{v}$ g

w = weight of total residue in (mg). (Therefore, multiply *w* with 1000)

v = Volume of the sample (mL) (To convert mL to L)

(ii) Total Volatile Solids TVS) computation

The initial weight of the evaporating dish + sample (W_1) = g

The final weight of the evaporating dish + sample after drying at 105ºC (W_2) = g

The final weight of the evaporating dish + sample after drying at 550ºC (W_3) = g

Weight of volatile substance (W) =$W_2 – W_3$ g

$$\text{TVS present in the sample} = \frac{1000W \times 1000}{V\ (mL)} = \text{mg/L}$$

(iii) Total suspended solids (TSS) computations

$$\text{TSS (mg/L)} = \frac{(A-B)x\ 1000}{Sample\ volume\ (mL)}$$

Where A = mass of filter + dry residue = g

B = mass of filter = g

(iv) Volatile soluble solids (VSS) and Fixed solids (FS) computations

$$\text{VSS (mg/L)} = \frac{(A-B)x\ 1000}{Sample\ volume\ (mL)}$$

and

$$\text{FS (mg/L)} = \frac{(B-C)x\ 1000}{Sample\ volume\ (mL)}$$

Where A = mass (mg) of residue + dish before ignition

B = mass (mg) of residue + filter after ignition and

C = mass (mg) of filter.

Or

$$\text{FS (mg/L) present in the sample} = \frac{1000W}{V\ (mL)}$$

where

W = mass of non-volatile substance = $W_3 - W_1$

W_1 = mass (g) of evaporating dish

W_2 = mass (g) of evaporating dish + sample after drying at 105ºC

W_3 = mass (g) of evaporating dish + sample after drying at 550ºC

V = Volume of the sample (mL)

(v) Total dissolved solids (TDS) computation

$$\text{TDS (mg/L)} = \frac{(A-B)x\ 1000}{Sample\ volume\ (mL)}$$

Where A = mass of evaporating dish + dried residue = mg

B = mass of evaporating dish = mg

(vi) Settleable solids

Settleable solids (mg/L) = A – B

where

A = total suspended solids (mg/L)

B = non-settleable solids (mg/L)

(vii) Alkalinity of a given water or wastewater sample

Alkalinity is a measure of the capability of water to absorb H^+ ions without a significant change in pH. In other words, alkalinity is a measure of the acid-buffering capacity of water. The determination of alkalinity of water is necessary for controlling the corrosion, to calculate the amount of lime and soda needed for water softening; in conditioning the boiler feedwater, etc. The alkalinity of a sample of water is due to the presence of OH^- (hydroxide ion), HCO_3^- (bicarbonate ion) and CO_3^{2-} (carbonate ion) or the mixture of two ions present in water. It is not likely that OH^- and HCO_3^- ions are present at the same time since they combine to form CO_3^{2-} ions.

$$OH^- + HCO_3^- \longrightarrow CO_3^{2-} + H_2O$$

The alkalinity due to different ions can be estimated separately by titration against a standard acid solution, using selective indicators like phenolphthalein and methyl orange.

i) $OH^- + H^+ \longrightarrow H_2O$

ii) $CO_3^{2-} + H^+ \longrightarrow HCO_3^-$

iii) $HCO_3^- + H^+ \longrightarrow H_2O + CO_2$

The neutralization reaction, up to the phenolphthalein endpoint, shows the completion of reactions (i) and (ii) (OH^- and CO_3^{2-}) and (CO_3^{2-} and HCO_3^-) only. The amount of acid used thus corresponds to the complete neutralization of OH^- plus half neutralization of CO_3^{2-}. The titration of a water sample using methyl orange indicator marks the completion of the reactions (i), (ii) and (iii). The amount of acid used after the phenolphthalein endpoint corresponds to one-half of normal carbonate and all the bicarbonates. The total amount of acid used represents the total alkalinity due to all ions present in a water sample.

Table A-1 Standardisation of HCl solution (Strength of Na2CO3 solution (S1)= 0.1N)

Run	Vol. of Na_2CO_3 solution (V_1, mL)	Burette reading (mL)		Vol. of HCl required (mL)	Mean vol. of HCl required (V_2, mL)
		Initial	Final		
1	10				
2	10				
3	10				

Table A-2 Phenolphthalein alkalinity of wastewater (using HCl solution (S2) = _ N)

Run	The volume of Wastewater sample (mL)	Burette reading (mL)		Vol. of HCl required (mL)	Mean volume of HCl required (V_4, mL)
		Initial	Final		
1	20				
2	20				
3	20				

Table A-3 Total (methyl orange) alkalinity of wastewater

Run	The volume of Wastewater sample (mL)	Burette reading (mL)		Vol. of HCl required (mL)	Mean volume of HCl required (V_5, mL)
		Initial	Final		
1	20				
2	20				
3	20				

B Sample Volume For Metal Composition

Liquid samples are atomized into an extremely fine mist and aspirated into a plasma torch. Lesser volumes, to a minimum of 5 mL, are appropriate for graphite furnace, ICP, and ICP-MS. Instead, samples were diluted with elevated analyte concentrations after digestion. If the recommended volume exceeded digestion vessel capacity, sample was added as evaporation proceeded. For samples containing particulates, wide-bore pipets were useful for volume measurement and transfer. When samples are concentrated during digestion (e.g., >100mL sample used) determine metal recovery for each matrix digested, to verify method validity. Using larger samples will require additional acid, which also would increase the concentration of impurities.

Table B-1 A guide on sample preparation for metal determination

Estimated metal concentration (mg/L)	Sample volume (mL)
< 0.1	1000
0.1 - 10	100
10 – 100+	10

For Atomic Emission Spectrometry (AES), results are reported as follows:

$$Metal\ concentration\ \left(\frac{mg}{L}\right) = A\ x\ \frac{B}{C}$$

where

A = instrument measured concentration of metal in the digested solution, mg/L,

B = final volume of digested solution, mL, and

C = sample volume, mL

Although it is always best to eliminate all relevant sources of contamination, a reagent blank prepared with the same acids and subjected to the same digestion procedure as the sample can correct for impurities present in acids and reagent water. However, blank correction is not recommended for any other sources of contamination such as impurities adsorbed on glassware.

C Biological Characteristics

(i) Faecal coliform

Bacteriophage infects and multiplies in sensitive bacteria. This results in lysis of the bacterial cells and a release of phage particles to infect adjacent cells. As the infected coliform bacteria are lysed, visible clear areas known as plaques develop in the lawn of confluent bacterial growth. Count plaques on each plate and record. Obtain the number of plaques/100 mL of the sample by summing the plaques on the four plates and multiplying them by 5. If a diluted sample has been used, additionally multiply by the reciprocal of the dilution factor. Based on coliphage counts, estimate total and faecal coliform numbers as shown below. Independently verify equations for specific types of samples and locations.

Total coliforms: $\log y = 0.627 (\log x) + 1.864$

where

y = total coliforms/100 mL and

x = coliphages/100 mL.

Faecal coliforms: $\log y = 0.805 (\log x) + 0.895$

where

y = faecal coliforms/100 mL and

x = coliphages/100 mL

D Experimental Design

Table D-1, Design expert output for the lab

Run	Variables			
	Reference water* (mL)	BWW (mL)	Luminous flux (Lumen)**	CO_2 gas flowrate (L/min)
1	1250	1250	1100	4
2	625	1875	800	6
3	0	2500	1600	4
4	2500	0	1100	4
5	2500	0	1600	5
6	2500	0	1200	2
7	0	2500	1100	4
8	1250	1250	1600	6
9	1250	1250	450	4
10	0	2500	1200	6
11	1250	1250	1100	4
12	2500	0	1100	6
13	1250	1250	1600	4
14	0	2500	450	5
15	1250	1250	1600	4
16	2500	0	450	5
17	0	2500	450	2
18	1250	1250	1200	2
19	1875	625	800	3
20	0	2500	1200	2
21	1250	1250	450	2
22	2500	0	450	2

*Reference water refers to the natural habitat from where the microalgae were sampled and isolated, which was the Botanic Garden stream, Durban, South Africa; **Lumen

Table D-2. Brewery wastewater analysis before commencement of experimental runs

Run	Parameters											
	pH	Turbidity NTU	Alkalinity $CaCO_3$ mg/L	EC mS/cm	TDS mg/L	DO mg/L	COD mg/L	TN mg/L	NH_3 mg/L	NO_3^- NO_2^- mg/L	TKN mg/L	PO_4^{3-} mg/L
1	6.58	162	56.34	5.82	1902	6.9	2408	21.7	0.257	2.69	19.01	11.2
2	6.78	238	29.1	5.16	1273	5.8	1040	62.0	37.1	6.41	18.50	10.4
3	6.54	463	26.7	4.86	1451	6.5	2192	6.29	0.735	5.25	1.05	3.4
4	7.35	131	63.62	4.84	2386	5.2	5602	50.68	41.13	4.41	5.35	9.63
5	7.35	131	63.62	4.84	2386	5.2	53	2.44	0.062	1.57	0.866	10.4
6	7.35	131	63.62	4.84	2386	5.2	5602	50.68	41.13	4.41	5.35	9.63
7	6.54	463	26.7	4.86	1451	6.5	2192	6.29	0.735	5.25	1.05	3.4
8	6.58	162	56.34	5.82	1902	6.9	2408	21.7	0.257	2.69	19.0	5.26
9	6.58	162	56.34	5.82	1902	6.9	2408	21.7	0.257	2.69	19.0	5.26
10	6.54	463	26.7	4.86	1451	6.5	2192	6.29	0.735	5.25	1.05	3.4
11	6.58	162	56.34	5.82	1902	6.9	2408	21.7	0.257	2.69	19.0	5.26
12	7.50	131	63.62	4.84	2386	5.2	5602	50.68	41.13	4.41	5.35	9.63
13	6.58	162	56.34	5.82	1902	6.9	2408	21.7	0.257	2.69	19.0	11.2
14	6.54	463	26.7	4.86	1451	6.5	2192	6.29	0.735	5.25	1.05	3.4
15	6.58	162	56.34	5.82	1902	6.9	2408	21.7	0.257	2.69	19.0	11.2
16	7.50	131	63.62	4.84	2386	5.2	4508	50.68	41.13	4.41	5.35	10.4
17	6.54	463	26.7	4.86	1451	6.5	2192	6.29	0.735	5.25	1.05	3.4
18	6.58	162	56.34	5.82	1902	6.9	2408	21.7	0.257	2.69	19.0	5.26
19	7.25	281	60.21	4.85	1434	5.4	810	43.91	22.8	4.26	16.85	9.52
20	6.54	463	26.7	4.86	1451	6.5	2192	6.29	0.735	5.25	1.05	3.4
21	6.58	162	56.34	5.82	1902	6.9	2408	21.7	0.257	2.69	19.0	11.2
22	7.45	131	21.7	4.84	958	5.2	3979	39.1	34.6	4.6	0.767	9.26

Table D-3. The growth performance of Scenedesmus sp. during run 1 (CO_2 flowrate, 4 L/min; Luminous flux, 1100 Lumen)

Time (Day)	Parameters												
	pH	Turb NTU	Alk $CaCO_3$ mg/L	EC mS/cm	TDS mg/L	DO mg/L	COD mg/L	TN mg/L	NH_3 mg/L	NO_3 NO_2 mg/L	TKN mg/L	PO_4 mg/L	OD_{680}
0	6.58	162	56.34	5.82	1902	9.9	2408	21.7	0.257	2.69	19.01	11.2	0.014
1													0.019
2													0.027
3													0.049
4	7.2	186	47.21	5.13	1631	10.4	2136	18.3	0.215	2.24	15.85	9.82	0.015
5													0.038
6													0.036
7													0.038
8	6.85	217	44.35	4.83	1523	10.6	1852	8.78	0.19	1.87	6.72	7.51	0.012
9													0.239
10													0.246
11													0.249
12	7.8	265	33.52	3.36	1287	12.4	1254	4.51	0.15	1.33	3.03	5.91	0.253
13													0.302
14													0.412
15													0.514
16	8.4	312	21.93	1.64	853	10.8	667	2.09	0.10	0.38	1.51	4.37	0.563
17													0.621
18													0.632
19													0.643
20													0.662
21	8.6	324	12.85	0.87	255	8.3	72	0.651	0.035	0.35	0.266	2.83	0.688

Table D-4. The growth performance of Scenedesmus sp. during run 2 (CO_2 flowrate, 6 L/min; Luminous flux, 800 Lumen)

Time (Day)	Parameters												
	pH	Turb (NTU)	Alk $CaCO_3$ mg/L	EC mS/cm	TDS mg/L	DO mg/L	COD mg/L	TN mg/L	NH_3 mg/L	NO_3 NO_2 mg/L	TKN mg/L	PO_4 mg/L	OD_{680}
0	6.78	176	29.1	5.16	1273	5.8	1040	62.0	37.1	6.41	18.50	10.4	0.136
1													0.141
2													0.163
3													0.158
4	7.4	196	23.4	4.35	1074		837	50.65	29.74	5.38	15.53	8.79	0.285
5													0.381
6													0.421
7													0.432
8	7.8	232	18.6	3.71	863		529	41.21	24.87	3.84	12.5	6.67	0.457
9													0.468
10													0.473
11													0.486
12	8.1	283	14.2	3.02	736		283	31.62	19.54	2.68	9.4	5.83	0.495
13													0.497
14													0.543
15													0.565
16	8.7	364	9.1	2.43	512		98	17.06	12.38	0.85	3.83	4.16	0.561
17													0.580
18													0.585
19													0.605
20													0.607
21	9.2	415	5.7	0.87	232		27	10.38	8.67	0.24	1.47	3.72	0.620

Table D-5. The growth performance of Scenedesmus sp. during run 3 (CO_2 flowrate, 4 L/min; Luminous flux, 1600 Lumen)

Time (Day)	Parameters												
	pH	Turb NTU	Alk $CaCO_3$ mg/L	EC mS/cm	TDS mg/L	DO mg/L	COD mg/L	TN mg/L	NH_3 mg/L	NO_3 NO_2 mg/L	TKN mg/L	PO_4 mg/L	OD_{680}
0	6.54	463	26.7	4.86	1451	6.5	2192	56.29	49.35	5.25	1.05	3.4	0.089
1													0.087
2													0.085
3													0.084
4	5.92	452	25.8	4.85	1446	8.8	2191	56.21	30.47	3.33	22.41	3.2	0.082
5													0.083
6													0.085
7													0.086
8	5.72	457	25.2	4.85	1441	7.4	1972	50.76	29.06	3.16	17.94	3.3	0.087
9													0.085
10													0.083
11													0.080
12	5.67	435	25.1	4.87	1438	9.1	2063	48.73	28.52	2.89	17.32	3.1	0.079
13													
14	The negative growth trend had to be discontinued												
15													
16													
17													
18													
19													
20													
21													

Table D-6. The growth performance of Scenedesmus sp. during run 4 (CO_2 flowrate, 4 L/min; Luminous flux, 1100 Lumen)

Time (Day)	Parameters												
	pH	Turb NTU	Alk $CaCO_3$ mg/L	EC mS/cm	TDS mg/L	DO mg/L	COD mg/L	TN mg/L	NH_3 mg/L	NO_3 NO_2 mg/L	TKN mg/L	PO_4 mg/L	OD_{680}
0	7.35	131	63.62	4.84	2386	5.2	5602	50.68	41.13	4.41	5.35	9.63	0.038
1		139											0.043
2		157											0.048
3		160											0.050
4	7.58	156	57.17	4.35	2144	6.8	4672	45.31	36.96	3.72	4.63	7.85	0.048
5		146											0.045
6		152											0.046
7		163											0.055
8	7.84	267	48.13	3.66	1805	8.1	3744	38.14	31.14	2.93	3.54	5.26	0.103
9		430											0.182
10		546											0.238
11		625											0.276
12	8.11	705	30.74	2.34	1153	9.7	2814	24.36	20.24	1.74	2.38	3.88	0.315
13		854											0.387
14		935											0.426
15		1001											0.458
16	8.46	1177	16.04	1.22	602	10.5	1879	12.71	10.03	0.92	1.76	2.87	0.543
17		1251											0.579
18		1319											0.681
19		1346											0.692
20		1373											0.769
21	8.71	1386	6.21	0.47	233	12.3	728	3.15	1.92	0.36	0.87	1.47	0.792

Table D-7. The growth performance of Scenedesmus sp. during run 5 (CO_2 flowrate, 5 L/min; Luminous flux, 1600 Lumen)

	Parameters												
Day	pH	Turb NTU	Alk $CaCO_3$ mg/L	EC mS/cm	TDS mg/L	DO mg/L	COD mg/L	TN mg/L	NH_3 mg/L	NO_3 NO_2 mg/L	TKN mg/L	PO_4 mg/L	OD_{680}
0	7.35	28	63.62	4.84	2386	5.2	53	50.44	40.062	2.57	8.166	10.4	0.004
1		53											0.028
2		76											0.040
3		146											0.045
4	4.96	53	25.8	4.85	1446	8.8	2191	56.21	30.47	3.33	22.41	3.2	0.028
5													0.035
6													0.032
7													0.032
8	4.86	55	25.2	4.85	1441	7.4	1972	50.76	29.06	3.16	17.94	3.3	0.027
9													0.028
10													0.030
11													0.029
12	4.84	54	25.1	4.87	1438	9.1	2063	48.73	28.52	2.89	17.32	3.1	0.027
13													
14	The unsteady growth trend observed here had to be discontinued												
15													
16													
17													
18													
19													
20													
21													

Table D-8. The growth performance of Scenedesmus sp. during run 6 (CO_2 flowrate, 2 L/min; Luminous flux, 1200 Lumen)

	Parameters												
Day	pH	Turb NTU	Alk $CaCO_3$ mg/L	EC mS/cm	TDS mg/L	DO mg/L	COD mg/L	TN mg/L	NH_3 mg/L	NO_3 NO_2 mg/L	TKN mg/L	PO_4 mg/L	OD_{680}
0	7.35	131	63.62	4.84	2386	5.2	5602	50.68	41.13	4.41	5.35	3.2	0.042
1		139											0.043
2		157											0.044
3		160											0.045
4	7.23	156	57.17	4.35	2144	6.8	4672	45.31	36.96	3.72	4.63	7.85	0.044
5		146											0.043
6		152											0.044
7		163											0.045
8	7.30	267	48.13	3.66	1805	8.1	3744	38.14	31.14	2.93	3.54	5.26	0.049
9		430											0.082
10		546											0.138
11		625											0.198
12		705	30.74	2.34	1153	9.7	2814	24.36	20.24	1.74	2.38	3.88	0.224
13		854											0.362
14		935											0.414
15		1001											0.473
16		1177	16.04	1.22	602	10.5	1879	12.71	10.03	0.92	1.76	2.87	0.513
17		1251											0.552
18		1319											0.573
19		1346											0.586
20		1373											0.601
21		1386	6.21	0.47	233	12.3	728	3.15	1.92	0.36	0.87	1.47	0.605

Table D-9. The growth performance of Scenedesmus sp. during run 7 (CO_2 flowrate, 4 L/min; Luminous flux, 1100 Lumen)

	Parameters												
Day	pH	Turb NTU	Alk $CaCO_3$ mg/L	EC mS/cm	TDS mg/L	DO mg/L	COD mg/L	TN mg/L	NH_3 mg/L	NO_3 NO_2 mg/L	TKN mg/L	PO_4 mg/L	OD
0	6.54	463	26.7	4.86	1451	6.5	2192	21.7	0.257	2.69	19.0	1.3	0.041
1													0.046
2													0.048
3													0.049
4	6.72						1890	20.12	0.218	2.247	17.65	1.08	0.051
5													0.048
6													0.045
7													0.046
8	6.61						1850	18.77	0.212	2.211	16.35	1.06	0.047
9													0.046
10													0.083
11													0.140
12	7.76						1508	15.59	0.167	1.732	13.70	0.826	0.167
13													0.212
14													0.261
15													0.306
16	8.12						895	9.28	0.077	0.774	8.43	0.352	0.348
17													0.382
18													0.425
19													0.431
20													0.434
21	8.81						482	6.08	0.034	0.296	5.75	0.117	0.436

Table D-10. The growth performance of Scenedesmus sp. during **run 8** (CO_2 flowrate, 6 L/min; Luminous flux, 1600 Lumen)

	Parameters												
Day	pH	Turb NTU	Alk $CaCO_3$ mg/L	EC mS/cm	TDS mg/L	DO mg/L	COD mg/L	TN mg/L	NH_3 mg/L	NO_3 NO_2 mg/L	TKN mg/L	PO_4 mg/L	OD
0	6.58	162	56.34	5.82	162	6.9	2408	21.7	0.257	2.69	19.0	5.26	0.014
1													0.015
2													0.017
3													0.019
4	6.83												0.018
5													0.038
6													0.036
7													0.032
8	7.36												0.024
9													0.031
10													0.246
11													0.249
12													0.253
13													
14													
15													
16													
17													
18													
19													
20													
21													

Table D-11. The growth performance of Scenedesmus sp. during run 9 (CO_2 flowrate, 4 L/min; Luminous flux, 450 Lumen)

Day	Parameters												
	pH	Turb NTU	Alk $CaCO_3$ mg/L	EC mS/cm	TDS mg/L	DO mg/L	COD mg/L	TN mg/L	NH_3 mg/L	NO_3 NO_2 mg/L	TKN mg/L	PO_4 mg/L	OD
0	6.58	162	56.34	5.82	1902	6.9	2408	21.7	0.257	2.69	19.0	5.26	0.014
1													0.016
2													0.022
3													0.026
4	7.01	182	49.44	5.11	1670	8.21	2113	18.9	0.218	2.43	16.25	4.97	0.023
5													0.024
6													0.025
7													0.024
8	7.11	204	36.76	4.33	1414	9.04	1572	14.05	0.162	1.81	12.08	3.69	0.026
9													0.025
10													0.145
11													0.218
12	7.82	338	13.13	1.55	594	11.6	836	7.47	0.086	0.963	6.42	1.96	0.323
13													0.398
14													0.454
15													0.487
16	8.67	523	6.98	0.824	269	8.25	378	3.374	0.039	0.435	2.90	0.89	0.534
17													0.591
18													0.638
19													0.645
20													0.651
21	9.02	870	3.16	0.373	90	10.15	127	1.134	0.013	0.146	0.98	0.23	0.655

Table D-12. The growth performance of Scenedesmus sp. during run 10 (CO_2 flowrate, 6 L/min; Luminous flux, 1200 Lumen)

Day	Parameters												
	pH	Turb NTU	Alk $CaCO_3$ mg/L	EC mS/cm	TDS mg/L	DO mg/L	COD mg/L	TN mg/L	NH_3 mg/L	NO_3 NO_2 mg/L	TKN mg/L	PO_4 mg/L	OD_{680}
0	6.54	463	26.7	4.86	1451	6.5	2192	55.69	43.65	9.25	2.79	3.4	0.046
1													0.048
2													0.049
3													0.051
4	6.83	520	23.43	4.27	1273	8.4	1925	48.87	38.30	8.12	2.45	2.98	0.048
5													0.045
6													0.046
7													0.047
8	6.79	582	19.85	3.63	1265	7.5	1901	48.41	38.06	7.98	2.37	2.62	0.046
9													0.083
10													0.147
11													0.167
12	7.61	761	8.78	1.30	452	9.6	679	17.29	13.59	2.85	0.85	0.94	0.212
13													0.261
14													0.306
15													0.348
16	8.84	1178	4.67	0.69	241	10.3	362	9.19	7.22	1.52	0.45	0.51	0.382
17													0.425
18													0.512
19													0.523
20													0.531
21	9.62	1729	2.12	0.312	109	9.2	164	4.16	3.267	0.69	0.203	0.23	0.538

Table D-13. The growth performance of Scenedesmus sp. during run 11 (CO_2 flowrate, 4 L/min; Luminous flux, 1100 Lumen)

	Parameters												
Day	pH	Turb NTU	Alk $CaCO_3$ mg/L	EC mS/cm	TDS mg/L	DO mg/L	COD mg/L	TN mg/L	NH_3 mg/L	NO_3 NO_2 mg/L	TKN mg/L	PO_4 mg/L	OD
0	6.58	162	56.34	5.82			2408	21.7	0.257	2.69	19.0		0.014
1													0.019
2													0.027
3													0.049
4													0.015
5													0.038
6													0.036
7													0.038
8													0.012
9													0.239
10													0.246
11													0.249
12													0.253
13													0.302
14													0.412
15													0.514
16													0.563
17													0.621
18													0.632
19													0.643
20													0.662
21													0.688

Table D-14. The growth performance of Scenedesmus sp. during run 12 (CO_2 flowrate, 6 L/min; Luminous flux, 1100 Lumen)

	Parameters												
Day	pH	Turb NTU	Alk $CaCO_3$ mg/L	EC mS/cm	TDS mg/L	DO mg/L	COD mg/L	TN mg/L	NH_3 mg/L	NO_3 NO_2 mg/L	TKN mg/L	PO_4 mg/L	OD
0	6.54		63.62	4.84	2386	5.2	5602	50.68	41.13	4.41	5.35	3.2	0.038
1													0.041
2													0.045
3													0.046
4	6.82												0.027
5													0.038
6													0.046
7													0.048
8	6.91												0.051
9													0.052
10													0.126
11													0.142
12	7.41												0.213
13													0.267
14													0.335
15													0.481
16	8.12												0.543
17													0.627
18													0.632
19													0.641
20													0.663
21	9.08												0.684

Table D-15. The growth performance of Scenedesmus sp. during run 13 (CO_2 flowrate, 4 L/min; Luminous flux, 1600 Lumen)

Day	Parameters												
	pH	Turb NTU	Alk $CaCO_3$ mg/L	EC mS/cm	TDS mg/L	DO mg/L	COD mg/L	TN mg/L	NH_3 mg/L	NO_3 NO_2 mg/L	TKN mg/L	PO_4 mg/L	OD
0	6.58	162	56.34	5.82			2408	21.7	0.257	2.69	19.0		0.385
1													0.395
2													0.406
3													0.412
4													0.441
5													0.442
6													0.443
7													0.460
8													0.472
9													0.476
10													
11													
12													
13													
14													
15													
16													
17													
18													
19													
20													
21													

Table D-16. The growth performance of Scenedesmus sp. during run 14 (CO_2 flowrate, 5 L/min; Luminous flux, 450 Lumen)

	Parameters												
Day	pH	Turb NTU	Alk $CaCO_3$ mg/L	EC mS/cm	TDS mg/L	DO mg/L	COD mg/L	TN mg/L	NH_3 mg/L	NO_3 NO_2 mg/L	TKN mg/L	PO_4 mg/L	OD
0	6.54	463	26.7	4.86	1451	6.5	2192	56.29	19.89	9.92	26.05	3.4	0.014
1													0.021
2													0.024
3													0.025
4	6.82	579											0.024
5													0.018
6													0.021
7													0.023
8	6.91												0.022
9													0.025
10													0.267
11													0.352
12	7.41												0.432
13													0.493
14													0.537
15													0.586
16	8.12												0.634
17													0.688
18													0.736
19													0.752
20													0.768
21	9.08												0.772

Table D-17. The growth performance of Scenedesmus sp. during run 15 (CO_2 flowrate, 4 L/min; Luminous flux, 1600 Lumen)

	Parameters												
Day	pH	Turb NTU	Alk $CaCO_3$ mg/L	EC mS/cm	TDS mg/L	DO mg/L	COD mg/L	TN mg/L	NH_3 mg/L	NO_3 NO_2 mg/L	TKN mg/L	PO_4 mg/L	OD
0	6.58	162	56.34	4.84	1902	6.9	2408	21.7	0.257	2.69	19.0	11.2	0.014
1													0.021
2													0.024
3													0.025
4													0.024
5													0.018
6													0.021
7													0.023
8													0.022
9													0.025
10													0.267
11													0.352
12													
13													
14													
15													
16													
17													
18													
19													
20													
21													

Table D-18. The growth performance of Scenedesmus sp. during run 16 (CO_2 flowrate, 5 L/min; Luminous flux, 450 Lumen)

	Parameters												
Day	pH	Turb NTU	Alk $CaCO_3$ mg/L	EC mS/cm	TDS mg/L	DO mg/L	COD mg/L	TN mg/L	NH_3 mg/L	NO_3 NO_2 mg/L	TKN mg/L	PO_4 mg/L	OD
0	7.35	131	63.62	4.84	2386	5.2	4508	50.68	41.13	4.41	5.35	3.2	0.056
1													0.058
2													0.062
3													0.067
4	7.82	112	54.29	4.13	2036	6.2	3805	42.10	34.05	3.57	4.48	2.71	0.064
5													0.063
6													0.059
7													0.058
8	7.78	111	54.25	4.12	2033	5.8	3802	42.04	34.04	3.54	4.46	2.70	0.060
9													0.065
10													0.103
11													0.173
12	8.41			2.70		6.1	3099	33.25	26.96	2.71	3.59	1.73	0.208
13													0.264
14													0.314
15													0.352
16	8.84			2.00			1883	24.47	19.88	1.87	2.72	1.24	0.421
17													0.483
18													0.546
19													0.612
20													0.612
21	9.31			1.28			992	14.23	5.72	0.221	0.98	0.74	0.618

Table D-19. The growth performance of Scenedesmus sp. during run 17 (CO_2 flowrate, 2 L/min; Luminous flux, 450 Lumen)

Day	Parameters												
	pH	Turb NTU	Alk $CaCO_3$ mg/L	EC mS/cm	TDS mg/L	DO mg/L	COD mg/L	TN mg/L	NH_3 mg/L	NO_3 NO_2 mg/L	TKN mg/L	PO_4 mg/L	OD
0	6.54	463	26.7	4.86	1451	6.5	2192	6.29	0.735	5.25	1.05	5.26	0.036
1													0.016
2													0.022
3													0.026
4	7.01	182	49.44	5.11	1670	8.21	2113	18.9	0.218	2.43	16.25	4.97	0.023
5													0.024
6													0.025
7													0.024
8	7.11	204	36.76	4.33	1414	9.04	1572	14.05	0.162	1.81	12.08	3.69	0.026
9													0.025
10													0.145
11													0.218
12	7.82	338	13.13	1.55	594	11.6	836	7.47	0.086	0.963	6.42	1.96	0.323
13													0.398
14													0.454
15													0.487
16	8.67	523	6.98	0.824	269	8.25	378	3.374	0.039	0.435	2.90	0.89	0.534
17													0.591
18													0.638
19													0.645
20													0.651
21	9.02	870	3.16	0.373	90	10.15	127	1.134	0.013	0.146	0.98	0.23	0.655

Table D-20. The growth performance of Scenedesmus sp. during run 18 (CO_2 flowrate, 2 L/min; Luminous flux, 1200 Lumen)

	Parameters												
Day	pH	Turb NTU	Alk $CaCO_3$ mg/L	EC mS/cm	TDS mg/L	DO mg/L	COD mg/L	TN mg/L	NH_3 mg/L	NO_3 NO_2 mg/L	TKN mg/L	PO_4 mg/L	OD
0	6.58	162	56.34	5.82			2408	21.7	0.257	2.69	19.0		0.014
1													0.018
2													0.023
3													0.028
4													0.027
5													0.025
6													0.026
7													0.027
8													0.025
9													0.031
10													0.152
11													0.233
12													0.287
13													0.376
14													0.452
15													0.495
16													0.568
17													0.675
18													0.724
19													0.764
20													0.818
21													0.851

Table D-21. The growth performance of Scenedesmus sp. during run 19 (CO_2 flowrate, 3 L/min; Luminous flux, 800 Lumen)

	Parameters												
Day	pH	Turb NTU	Alk $CaCO_3$ mg/L	EC mS/cm	TDS mg/L	DO mg/L	COD mg/L	TN mg/L	NH_3 mg/L	NO_3 NO_2 mg/L	TKN mg/L	PO_4 mg/L	OD_{680}
0	7.25	281	60.21	4.85	1434	5.4	810	43.91	22-8	4.26	16.85	9.52	0.136
1													0.152
2													0.186
3													0.247
4													0.245
5													0.246
6													0.367
7													0.438
8													0.484
9													0.535
10													0.573
11													0.628
12													0.682
13													0.714
14													0.765
15													0.812
16													0.873
17													0.924
18													0.952
19													0.965
20													1.072
21													1.076

Table D-22. The growth performance of Scenedesmus sp. during run 20 (CO_2 flowrate, 2 L/min; Luminous flux, 1200 Lumen)

	Parameters												
Day	pH	Turb NTU	Alk $CaCO_3$ mg/L	EC mS/cm	TDS mg/L	DO mg/L	COD mg/L	TN mg/L	NH_3 mg/L	NO_3 NO_2 mg/L	TKN mg/L	PO_4 mg/L	OD_{680}
0	6.54	463	26.7	4.86	1451	6.5	2192	6.29	0.735	5.25	1.05	3.4	0.045
1													0.046
2													0.048
3													0.049
4	6.82						2131						0.048
5													0.047
6													0.046
7													0.047
8	7.16						2045						0.084
9													0.132
10													0.147
11													0.183
12	7.83						1288						0.221
13													0.261
14													0.296
15													0.324
16	8.24						569						0.396
17													0.438
18													0.471
19													0.531
20													0.563
21	8.96						393						0.574

Table D-23. The growth performance of Scenedesmus sp. during run 21 (CO_2 flowrate, 2 L/min; Luminous flux, 450 Lumen)

	Parameters												
Day	pH	Turb NTU	Alk $CaCO_3$ mg/L	EC mS/cm	TDS mg/L	DO mg/L	COD mg/L	TN mg/L	NH_3 mg/L	NO_3 NO_2 mg/L	TKN mg/L	PO_4 mg/L	OD_{680}
0	6.58	162	56.34	5.82	1902	6.9	2408	21.7	0.257	2.69	19.0	15.6	0.031
1													0.034
2													0.035
3													0.038
4	6.70	173	52.66	5.44	1778	6.45	1976	18.25	0.188	2.58	15.48	14.1	0.042
5													0.036
6													0.035
7													0.033
8	7.03	172	52.43	5.43	1772	6.43	1820	18.20	0.187	2.17	15.84	13.03	0.037
9													0.043
10													0.058
11													0.231
12	8.46	374	42.40	3.35	1433	5.20	1381	14.72	0.119	1.80	12.80	10.45	0.283
13													0.341
14													0.394
15													0.452
16	8.82	512	26.96	2.76	911	3.31	944	9.36	0.05	1.34	7.97	7.85	0.487
17													0.513
18													0.541
19													0.562
20													0.571
21	9.61	781	12.82	1.32	433	1.57	216	4.45	0.012	0.63	3.81	2.73	0.579

Table D-24. The growth performance of Scenedesmus sp. during run 22 (CO_2 flowrate, 2 L/min; Luminous flux, 450 Lumen)

	Parameters												
Day	pH	Turb NTU	Alk $CaCO_3$ mg/L	EC mS/cm	TDS mg/L	DO mg/L	COD mg/L	TN mg/L	NH_3 mg/L	NO_3 NO_2 mg/L	TKN mg/L	PO_4 mg/L	OD_{680}
0	7.45	131	21.7	4.89	958	5.2	5602	39.7	34.6	4.6	0.767	3.2	0.053
1													0.056
2													0.058
3													0.063
4													0.061
5													0.059
6													0.057
7													0.058
8													0.059
9													0.062
10													0.158
11													0.231
12													0.353
13													0.398
14													0.394
15													0.572
16													0.627
17													0.673
18													0.721
19													0.762
20													0.771
21													0.779

E Thirty-Litre (30-L) Scale-Up Operation

Table E-1: A scale-up operation of algal growth in BWW using a 30-L bubble column reactor

Day	Determinants												
	pH	Turb NTU	Alk $CaCO_3$ mg/L	EC mS/cm	TDS mg/L	DO mg/L	COD mg/L	TN mg/L	NH_3 mg/L	NO_3 NO_2 mg/L	TKN mg/L	PO_4 mg/L	OD_{680}
0	6.9	29.6	21.7	1.9	2386		1040	39.1	34.6	4.6	0.767	1.6	0.052
1	7.0	32.7											0.056
2	7.1	29.8											0.053
3	7.3	28.8											0.051
4	7.5	29.6	21.5	1.8	2386		1031	38.8	33.53	4.5	0.765	1.55	0.053
5	7.63	31.2											0.055
6	7.75	32.8											0.057
7	7.93	32.4											0.056
8	7.81	33.8	20.6	1.6	2317		989	36.5	31.67	4.2	0.626	1.46	0.058
9	7.94	135											0.244
10	8.04	179											0.318
11	8.23	197											0.349
12	8.44	225	9.51		1228		464	20.97	18.20	2.41	0.359	0.839	0.401
13	8.52	242											0.435
14	8.61	258											0.465
15	8.73	321											0.584
16	8.81	377	6.34		926		309	15.59	13.53	1.79	0.267	0.624	0.684
17	8.82	392											0.713
18	8.87	446											0.808
19	8.93	509											0.922
20	9.1	577											1.035
21	9.2	607	2.74		219		138	5.38	4.67	0.62	0.092	0.215	1.094

F 240-L Airlift-Raceway Scale-Up Operation

Table F-1: A scale-up operation of algal growth in BWW using a 240-L airlift-raceway reactor

Day	Determinants												
	pH	Turb NTU	Alk $CaCO_3$ mg/L	EC mS/cm	TDS mg/L	DO mg/L	COD mg/L	TN mg/L	NH_3 mg/L	NO_3 NO_2 mg/L	TKN mg/L	PO_4 mg/L	OD_{680}
0	6.9	29.6	21.7	1.9	2386		1040	39.1	34.6	4.6	0.767	1.6	0.052
1	7.0	32.7											0.056
2	7.1	29.8											0.053
3	7.3	28.8											0.051
4	7.5	29.6	21.5	1.8	2386		1031	38.8	33.53	4.5	0.765	1.55	0.053
5	7.63	31.2											0.055
6	7.75	32.8											0.057
7	7.93	32.4											0.056
8	7.81	33.8	20.6	1.6	2317		989	36.5	31.67	4.2	0.626	1.46	0.058
9	7.94	135											0.244
10	8.04	179											0.318
11	8.23	197											0.349
12	8.44	225	9.51		1228		464	20.97	18.20	2.41	0.359	0.839	0.401
13	8.52	242											0.435
14	8.61	258											0.465
15	8.73	321											0.584
16	8.81	377	6.34		926		309	15.59	13.53	1.79	0.267	0.624	0.684
17	8.82	392											0.713
18	8.87	446											0.808
19	8.93	509											0.922
20	9.1	577											1.035
21	9.2	607	2.74		219		138	5.38	4.67	0.62	0.092	0.215	1.094